U.S. Department of Energy
Office of FreedomCAR and Vehicle Technologies
1000 Independence Avenue S.W.
Washington, DC 20585-0121

FY 2003

Progress Report for High Strength Weight Reduction Materials

Energy Efficiency and Renewable Energy
Office of FreedomCAR and Vehicle Technologies
Advanced Materials Technologies

Edward Wall	**Program Manager, OFCVT**
Rogelio Sullivan	**Materials Technologies Team Leader**
Sidney Diamond	**Technology Development Area Specialist**

April 2004

CONTENTS

1. INTRODUCTION 1

2. MATERIALS DEVELOPMENT 7
A. Integrated Approach for Development of Energy-Efficient Steel Components for Heavy Vehicle and Transportation Applications 7

3. MATERIALS PROCESSING TECHNOLOGIES 15
A. Oxidative Stabilization of PAN Fiber Precursor 15
B. Wrought Magnesium Alloy/Process Development 21
C. Equal Channel Angular Extrusion 29
D. Equal Channel Angular Extrusion Processing of Alloys for Improved Mechanical Properties 39
E. Lightweight High-Strength Steel Alloy Castings for Heavy Vehicle Applications 49
F. Development of an Advanced Squeeze Casting Process for the Production of High-Integrity Truck Components 55
G. Ultra-Large Casting Benchmark Study for Aluminum and Magnesium Alloys: Phase II 61

4. ENABLING TECHNOLOGIES 69
A. Improved Friction Tests for Engine Materials 69
B. Laser Glazing of Railroad Rails to Reduce Friction 73
C. Laser Surface Texturing of Seal Faces 79
D. Joining of Advanced Materials by Plastic Deformation 85
E. Friction Stir Joining and Processing of Advanced Materials, Including Metal Matrix Composites 93
F. Friction Stir Processing of Advanced Materials 101
G. Basic Studies of Ultrasonic Welding for Advanced Transportation Systems 109
H. Attachment Techniques for Heavy Truck Composite Chassis Members 119

5. LIGHTWEIGHT VEHICLE STRUCTURES 127
A. Lightweight Stainless Steel Bus Frame: Phase III 127
B. Large Castings for Advanced Cab Structures 135
C. New-Generation Frame for Pick-Up/Sport Utility Vehicle Application 137

6. APPLICATION OF INNOVATIVE MATERIALS 141
A. Advanced Materials for Friction Brakes 141
B. Advanced Composite Structural Cab Components 145
C. Advanced Composite Structural Chassis Components 149
D. Carbon Fiber Sheet Molding Compound for Class 8 Vehicle Hoods 153
E. Advanced Composite Support Structures 157
F. Hybrid Composite Materials for Weight-Critical Structures 161
G. Application of Carbon Fiber for Large Structural Components 165
H. High-Conductivity Carbon Foam for Thermal Management in Heavy Vehicles 177
I. Lightweight Functional Composite Materials 185

7. MAINTENANCE, REPAIR, RECYCLE 191
A. Effects of Highway Ice-Clearing Treatments on Corrosion of Heavy Vehicle Materials and Components 191

APPENDIX A. ACRONYMS AND ABBREVIATIONS 199

1. INTRODUCTION

As a major component of the U.S. Department of Energy's (DOE's) Office of FreedomCAR and Vehicle Technologies (OFCVT), the High-Strength Weight Reduction (HSWR) Materials Technology Development Area seeks to reduce parasitic energy losses due to the weight of heavy vehicles without reducing vehicle functionality, durability, reliability, or safety, and to do so cost-effectively. The development area is focused on the development of materials and materials processing technologies that can contribute to weight reduction. In addition, it is recognized that improved materials may enable implementation of other technologies that can further improve the fuel efficiency of the vehicles. Through many of its technology development programs, DOE supports the government/industry 21st Century Truck Partnership.

The specific goals of the HSWR Materials Technology Development Area are

- By 2010, reduce the weight of an unloaded tractor-trailer combination from the current 23,000 pounds to 18,000 pounds, a 22% reduction in weight.
- By 2010, develop and validate advanced material technologies needed to meet OFCVT goals.
- Enable significant reductions in the weight of other classes of heavy vehicles (10–33% reduction in vehicle weight, depending on performance requirements and duty cycles).
- Develop materials that exhibit performance, durability, reliability, and safety characteristics comparable to those of conventional vehicle materials and that are cost-competitive on a life-cycle basis.
- Be consistent with the materials regulation requirements to maintain environmental responsibility.

To reach the stated goals, the HSWR Materials Technology Development Area has been developing a broad spectrum of advanced materials technologies that can be applied to a wide array of body, chassis, and suspension components. The research required to develop these technologies is too high-risk to be pursued independently by the heavy vehicle industry because of substantial return-on-investment uncertainties. Research is focused on overcoming barriers to the widespread introduction of lightweight materials in the heavy vehicle industry. Major barriers exist in the following areas: cost; design and simulation technologies; manufacturability; prototyping and tooling; joining and assembly; and maintenance, repair and recycling. Priority materials include advanced high-strength steels, aluminum, magnesium, titanium, and composites such as metal matrix materials and glass- and carbon-fiber-reinforced thermosets and thermoplastics.

Research and development (R&D) activities are being conducted through a variety of contractual mechanisms, including cooperative research and development agreements (CRADAs), university grants, R&D subcontracts, and directed research. Research partners include heavy vehicle manufacturers (including member companies of the 21st Century Truck Partnership), first-tier and materials suppliers, national laboratories, and other non-profit technology organizations. Laboratories include Argonne National Laboratory (ANL), Idaho National Engineering and Environmental Laboratory (INEEL), Los Alamos National Laboratory (LANL), Oak Ridge National Laboratory (ORNL), and Pacific Northwest National Laboratory

(PNNL). Research is coordinated with various organizations—both government and private—as shown in the following table.

Research Coordination

Technology Area	Organization
Production and fabrication of aluminum	The Aluminum Association, DOE-Industrial Technologies Program (ITP), Natural Resources of Canada (NRCAN), Automotive Lightweighting Materials (ALM) Technology Development Area
Production and fabrication of magnesium	International Magnesium Association, NRCAN, ALM Technology Development Area
Fabrication of steel and cast iron	American Iron and Steel Institute, the Auto/Steel Partnership, ALM Technology Development Area
Fundamental materials research	DOE Office of Energy Research, National Science Foundation
High-volume composite processing	Department of Commerce—National Institute of Standards and Technology's Advanced Technology Program, ALM Technology Development Area
Materials research for defense applications	Department of Defense
Materials research for space applications	National Aeronautics and Space Administration
Crashworthiness	Department of Transportation, ALM Technology Development Area
International vehicle material R&D	International Energy Association
Production and fabrication of titanium	The International Titanium Association, ALM Technology Development Area
Production and fabrication of composites	American Plastics Council

FY 2003 Accomplishments

During 2003, ORNL issued a Request for Proposals for "Development of Technologies for Reduction in Weight of Class 7 and 8 Tractor Trailers." After review and ranking by an evaluation team, two proposals were selected to receive awards:

- The Liburndas Project, submitted by Heil Trailer International
- Development of High-Performance Lightweight Class 7–8 Truck Cab Using an Innovative New Formable Aluminum Foam Sandwich (AFS) Material, submitted by International Truck and Engine Corporation.

The use of friction stir processing technology to improve the surface properties of cast aluminum alloys is being investigated in collaboration with the Ford Motor Company and the South Dakota School of Mines. Results of the work demonstrate that friction stir processing can dramatically refine the size of particulate phases in aluminum A319 and distribute them more uniformly. The processing also closes open porosity in the treated volume. The ductility

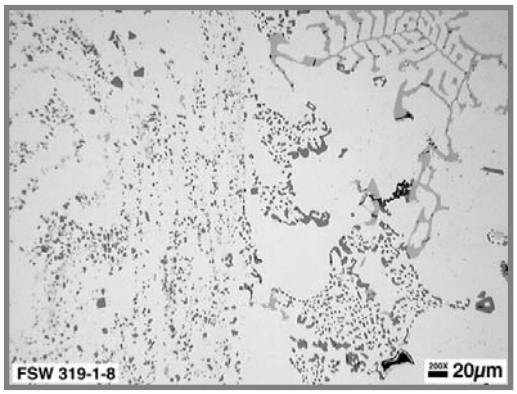

Optical micrograph taken on the surface of a friction stir processing bead on A319 Al casting. The boundary between base metal and stir zone is approximately in the center of the micrograph; the base metal is on the right and the stir zone on the left.

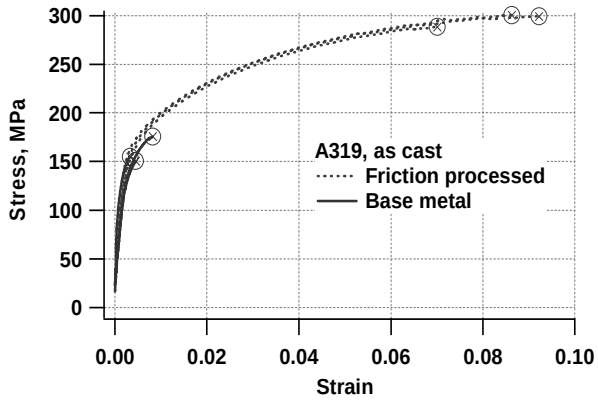

Stress-strain plot from room-temperature tensile tests of A319 base metal and friction stir processing stir zone.

and fatigue life of the cast materials was significantly increased. The surface property improvements could have important implications for the manufacturing of critical cast aluminum components for a wide variety of automotive applications.

The design phases were completed for three subcontracts to develop cab, body, and chassis structures of carbon-fiber-reinforced composites. Those projects have resulted in the early entry of composite tie rods into the commercial market and the development of the first truly low-cost carbon fiber sheet molding compound, which will have wide applicability in a number of applications. One project initially redesigned a component for manufacture using composite materials. The component redesign was accepted but the part was manufactured using aluminum, which saved about half the weight of the original design, was easier to manufacture, and met cost targets.

As part of a project to evaluate the design of an optimized hybrid materials frame that enables significant reduction in the weight of a pickup/sport utility vehicle (PU/SUV frame, DaimlerChrysler completed vehicle testing of the frame of a Durango SUV. The accelerated testing proved that the hybrid frame design had sufficient strength and durability to meet the vehicle performance requirements. Based on these positive results, the team is using a computer-aided engineering-based (CAE) approach and higher-risk manufacturing technologies to produce the next-generation frame, which is lighter than the previously tested frame and requires 35% fewer components.

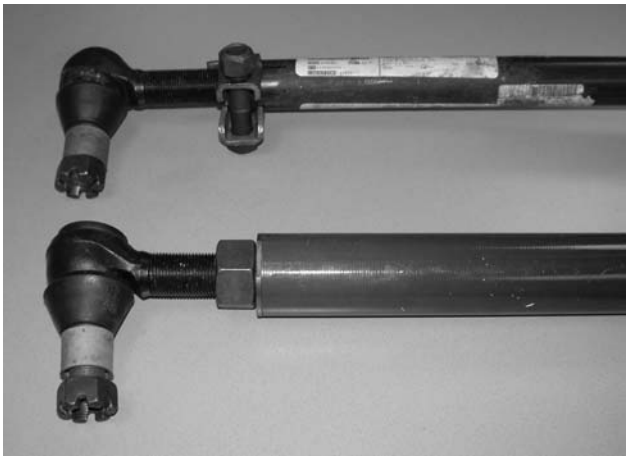

Typical steel (top) and composite lateral link assemblies.

Next-generation frame design.

As advances in aerodynamic design and low rolling resistance tires combine to reduce the effective drag on trucks, demands on braking systems are increased. A project is evaluating the wear characteristics of advanced materials and surface treatments that enable weight reduction in truck brake components while equaling or improving their performance; it has conducted studies of a variety of candidate brake materials. Of these, titanium alloys offer a number of attractive characteristics, but their thermal conductivity and wear behavior must be enhanced. Surface coatings or treatments are expected to enable the materials to perform quite well as brakes. Further work is planned to develop a better understanding of the friction and wear behavior of titanium alloys and to evaluate several alternative coating methods.

PNNL recently completed a project with Freightliner, LLC, and Alcoa to investigate the use of large castings for advanced truck cab structures. A large cast component was developed and analyzed. The final design resulted in a 27% reduction in weight and a 70% reduction in part count. Under typical production assumptions, it appears that a large casting is cost-competitive with the baseline fabricated component.

Candidate brake disc materials after friction testing on the SSBT: commercially-coated titanium (upper left), experimental ceramic composite (upper right), uncoated titanium alloy (bottom).

Future Direction

The HSWR Materials Technology Development Area, for the most part, has addressed the near- and intermediate-term energy efficiency and safety technical needs of the heavy-duty (primarily class 7 and 8 trucks) transport sector in conjunction with the original equipment manufacturers and their suppliers.

Currently, DOE is placing increased emphasis on the identification and evaluation by systematic means of emerging energy-efficient materials, technologies, and processes that may initially be too long-term or too speculative for our industrial partners to explore at this time. If the initial evaluation proves sufficiently cogent technically, DOE will then seek to establish conventional collaborative efforts with one or more industry partners to further develop the technology toward maturity and eventual commercialization by industry.

Several materials thrust areas have been identified, and exploratory scoping efforts have been initiated within them. They are

1. advanced joining technologies,
2. titanium use in heavy duty structural and component applications, and
3. advanced surface modification technologies to tailor friction and wear characteristics and other surface-sensitive properties of materials.

In area 1, advanced joining, DOE seeks to develop effective joining technologies that can enable the increased use of attractive advanced materials such as metal matrix composites without the severe alteration of microstructure and degradation of properties that are attendant upon conventional joining methods. The latter generally involve heating the materials adjacent to the joint into the liquid state. This technique results in significant phase redistribution, among other modifications that are deleterious to the properties of the resulting joint.

In area 2, vigorous efforts are under way around the world that may result in the delivery of titanium feedstock at considerably lower costs than have prevailed up to this time. Anticipating this achievement, DOE has initiated activities to identify and develop applications of titanium and titanium alloys in various structural, engine, and transmission components for heavy vehicles because of their attractive lightweighting, high-strength, and high-temperature characteristics.

In area 3, advanced surface modification, a number of innovative technologies have been identified that can significantly reduce the friction coefficients and wear rates of many engine and transmission components of heavy vehicles. These can contribute to appreciable increases in the energy efficiency of the vehicles. In addition, optimizing lubricant-surface interactions through formulation modifications may enable a total increase in energy efficiency of up to 5% in addition to improvements that may be gained in the combustion process.

It is anticipated that collaborative efforts with the Automotive Lightweighting Materials Technology Development Area will be pursued where appropriate so that energy-efficient technologies may be developed expeditiously without duplication and introduced into both the heavy-duty and light-duty sectors to maximize the impact on reducing fuel consumption. The conventional near-term and intermediate-term R&D activities performed in conjunction with DOE's industrial partners will, however, continue to make up the bulk of the next year's project portfolio.

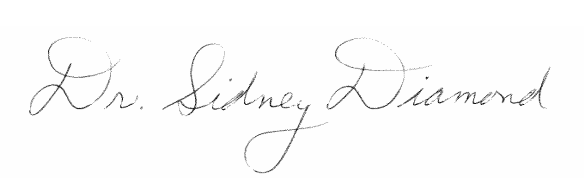

Sidney Diamond
Technology Development Area Specialist
Office of FreedomCAR and Vehicle Technologies
Energy Efficiency and Renewable Energy

2. MATERIALS DEVELOPMENT

A. Integrated Approach for Development of Energy-Efficient Steel Components for Heavy Vehicle and Transportation Applications

Co-Principal Investigator: Leo Chuzhoy
Caterpillar, Inc.
P.O. Box 1875, Peoria, IL 61656-1875
(309) 578-6621; fax: (309) 578-2953; email: Chuzhoy_Leo@cat.com

Co-Principal Investigator: Gerard Ludtka
Oak Ridge National Laboratory
P.O. Box 2008, Oak Ridge, TN 37831-6064
(865) 574-5098; fax: (865) 574-3940; email: ludtkagm1@ornl.gov

Co-Principal Investigator: Clyde Briant
Brown University
Box D, Brown University, Providence, RI 02912-D
(401) 863-1422; fax: 401-863-1157; email : Clyde_Briant@Brown.EDU

Technology Development Area Specialist: Sidney Diamond
(202) 586-8032; fax: (202) 586-1600; email: sid.diamond@ee.doe.gov
Field Technical Manager: Philip S. Sklad
(865) 574-5069; fax: (865) 576-4963; email: skladps@ornl.gov

Contractor: Caterpillar Inc.
Contract No.: DE-AC05-00OR22726

Objective

- This project focuses on development of methods and tools to achieve energy-efficient and environmentally benign steel components. The primary objective of this four-year project is to develop microstructure-level (often called mesoscale) simulation tools to capture the formation and influence of nonhomogeneous (real life) microstructures in steel processing. The tools will be used to understand and predict microstructure evolution during processing and ultimately to predict the resultant component performance. This information will then be used to design steel microstructures and develop process roadmaps. The developed techniques will be demonstrated on a pilot project at Caterpillar involving a defined structural component, namely a track roller shaft, which represents a steel component with high production volume that can potentially benefit from microstructure-level improvements. These goals will be achieved through the four tasks described in the technical task section.

Approach

To apply an integrated approach to development of energy-efficient steel components, three major areas of research needs will be pursued:

- Develop microstructure-level models to accurately predict the evolution and behavior of steel microstructures during component processing and performance.
- Characterize thermo-mechanical properties of microstructural constituents as a function of temperature and composition for exact chemistries.
- Develop the tools to assess required environmental resources and integrate them into the modeling simulation endeavor.

Accomplishments

- Reviewed project objectives and task responsibilities of each participating organization at the project kick-off meeting in September 2003.
- Distributed the two alloys to be investigated to the project team members so that machining of the test specimens required for the microstructural characterization, machining experiments, and strain rate dependent mechanical property determination tasks could be initiated during the first quarter of FY 2004.

Future Direction

During the first year, work will begin on all of the tasks described in the technical tasks section in this report; the project participants will also demonstrate that the approach and methods are valid. To this end the project will focus on Task 2, Machining Processing, and Task 4, Pilot Project, and will use parts of the work described in these tasks as a proof of concept. More specifically, our first year deliverables will be the following:

- Select a 1500-series steel and a micro-alloyed steel that are typical of track roller shaft applications, identifying the microstructures that are most commonly used for these applications.
- Produce and characterize the microstructures in the laboratory for both types of steel.
- Perform all mechanical tests on these microstructures that are required for inputs and validation of the mechanical models. These tests will include the temperature and strain rate dependence of mechanical properties. In addition, fracture toughness will be measured for these microstructures.
- Model the mechanical tests all the way through plastic deformation and fracture to determine actual material response. The simulation results will be validated using measured stress-strain curves and fracture toughness for the selected microstructures.
- Create a basic machining model from these models and demonstrate its applicability to one machining process of a 1500-series steel and a micro-alloyed steel for a track roller shaft. The orthogonal machining tests will be conducted using two cutting speeds and two depths of cut for a 1500-series steel and a micro-alloyed steel. The chip morphologies will be characterized and used for model validation.

Introduction

Product cost and performance are two major pressures influencing the acceptance of energy savings technologies by the manufacturers, suppliers, and users in the heavy vehicle and transportation industries. Energy cost has become a significant portion of total product cost for steel applications. Major reductions in energy use are

potentially achievable for the transportation and heavy vehicle industries through development and optimization of cost-effective fabrication processes and enhanced product performance. The key enabling technologies to achieve these benefits are improved materials and realistic, microstructure-level simulations to predict manufacturability and life-cycle performance. Over the past two decades, steel mills and forge shops have successfully implemented numerous energy-efficient processes. The next logical step is to focus on the development of steel microstructures that are produced in such a way that they are energy efficient and environmentally benign over the entire manufacturing cycle.

Structural materials used in critical steel components of machines have evolved to the point where further improvements in the performance can be achieved only through a fundamental understanding of the mechanisms driving material behavior during processing and service. Microstructural elements such as grain size, inclusion and precipitate distributions, and chemistry control the performance of engineering materials. Variation in these microstructural elements leads to variation in such critical properties as fatigue life, toughness, and wear resistance. Therefore, understanding and developing the capability to control the formation of steel microstructures and predicting its functional and environmental performance is critical to moving the industry closer to its energy-efficiency, resource-efficiency, and pollution-prevention goals. The full realization of these benefits, however, requires a design tool that optimizes the microstructure with respect to the mechanical and environmental performance throughout the life cycle of a particular steel component.

To apply an integrated approach to development of energy-efficient steel components, the development of three major areas of research needs to be completed:

- microstructure-level models to accurately predict evolution and behavior of steel microstructures during component processing and performance,
- thermomechanical properties of microstructural constituents as a function of temperature and composition for exact chemistries, and
- tools to assess required environmental resources.

This project addresses activities required for the first of these three areas. The second and third tasks are either supported by current funding through the National Science Foundation or are expected to be funded through the DOE Initiative for Proliferation Prevention. Through these integrated efforts, a design tool will be developed that optimizes the microstructure, manufacturability, and performance of components with respect to the mechanical and environmental performance required throughout the components' life cycles. The overall benefit of this research will be the development and demonstration of a design methodology that will enable the domestic transportation and heavy vehicle industries to compete effectively in future worldwide markets through improved product performance and energy savings. Furthermore, the proposed design tool can be extended to other materials, i.e., cast iron, aluminum, titanium, magnesium, nickel-based alloys, ceramics, and composites, thus impacting virtually all industries.

In addition to the transportation and steel industries receiving significant energy and cost savings benefit through microstructure-level modeling, virtually all industries will be impacted. Examples of such industries include aerospace (engines, transmissions, structural), marine (engines and drives), agricultural and construction equipment, oil and chemical processing (pumps and gear boxes), military vehicles, mining machinery, appliances (compressors,

motors, gear boxes, shafts), power tools, and automotive aftermarket.

Deliverables

The deliverables for the project will be the following:

- Microstructure-level methods for simulating the manufacturing cycle of steel products coupled with material performance computations (Tasks 1, 2, and 3).
- A specific chemical composition and processing map for a 1500-series steel and a micro-alloyed steel suitable for the application under consideration (Task 4).
- Energy and environmental resources required to produce the selected steel component using at least two steels and processing schemes (Task 4).

The project tasks will focus on three critical areas in the development of these models: heat treatment processing, machining, and materials performance in specific applications. These three processes have been chosen because they are critical steps in reaching the goal of being able to develop a specific steel for a particular application with a heavy reliance on modeling and with energy requirements optimized as an integral part of the development process. Modeling of casting and forming processing has been performed under other programs, and Caterpillar has shown successful application and commercialization of these models. These existing models will be used along with the heat treatment, machining, and specific applications models described below to complete a suite of models for the manufacture of micro-alloyed steels.

To accomplish the project objectives, a multidisciplinary team consisting of a national laboratory, a university, and a steel end user has been assembled. The team will be supported by an international research institute for material characterization and by experts in environmental impact assessment. The section below describes each of the technical tasks to be performed.

Technical Tasks

Task 1: Heat Treating Process

This task will quantify the influence of chemical and microstructural inhomogeneities in the austenite phase on the final heat-treatment response. The microstructure-level models incorporating phase transformation kinetics, polycrystalline plasticity, and recrystallization dynamics will be developed collaboratively by the Oak Ridge National Laboratory (ORNL), Brown University, and Caterpillar. Validation will be accomplished using the unique experimental capabilities and expertise at ORNL for conducting kinetic and metallurgical characterization as well as utilizing Caterpillar's ability to produce heat-treated specimens in precisely specified and controlled conditions. The modeling effort will draw on the significant programs at Brown and Caterpillar that have developed microstructural modeling capabilities.

The coupled mesoscale deformation and recrystallization models developed cooperatively by the three team members will be implemented to study the influence of mill thermomechanical processing variables and mesoscale composition variation on the grain size, grain-size distribution, and austenite grain-boundary character prior to the decomposition of austenite. The coupled deformation and recrystallization models will be used to predict the evolution of austenite grain structure and grain-boundary character distribution during the thermomechanical processing steps involved during secondary fabrication. The output of these simulations will directly feed into an austenite decomposition code that predicts phase

transformation during the heat-treatment operation.

The austenite decomposition code will be a microstructure-level tool, which accounts for alloying element concentration within each grain and grain boundary. For validating the austenite decomposition tool, several experimental techniques will be employed. High-speed quenching dilatometry, high-resolution scanning transmission electron microscopy, and X-ray synchrotron diffraction capabilities at ORNL will be used to quantify the fine (~10 nm to 8 μm) microstructural features that evolve during the various phase transformation sequences in steels. In particular, microanalyses will be performed to characterize any chemical inhomogeneity that might arise as a result of solute partitioning from the solidified microstructure.

Task 2: Machining Processing

A microstructure-level model will be applied to machining simulation of steels to determine their machinability and material state after thermomechanical processing. The model will consist of four main elements integrated into the finite element structure: microstructure simulation, material modeling, material characterization, and material flow and fracture. The microstructure simulation module will assemble individual constituents into a composite material based on microstructural composition, grain size, and grain-size distribution. This information along with residual stress predictions for individual grains will be obtained from Task 1. The material modeling module will account for the response of each constituent to high strains, strain rates, temperature, damage, and effects of loading paths associated with machining. The material characterization part will provide the material modeling module with parameters to define strain rate and temperature-dependent behavior of individual phases. The material flow and fracture module will periodically examine each grain for damage, locate deformed grain boundaries, and generate new boundaries. This module will compute stress, strain, temperature, and damage in each phase based on initial microstructure, material state, tool geometry, and process parameters.

The overall model will be developed collaboratively by Caterpillar and Brown University. Both institutions have strong reputations for machining models that incorporate microstructural elements into the models. The mechanical testing will be performed at Brown University, which has the capability to test samples over a wide range of strain rates in compression, tension, and torsion. Brown University also has the ability to perform jump tests in which the strain rate is changed during the deformation process to ascertain the strain rate sensitivity behavior of each chemistry and microstructure combination.

The microstructural analysis will be performed both at ORNL and at Brown University. At Brown, the primary methods that will be used to examine microstructure will be optical metallography and scanning electron microscopy (SEM). The SEM will be performed on a LEO-1530VP field emission instrument that has a resolution of 1 nm at an incident beam voltage of 20 kV. This instrument is fully equipped with energy dispersive X-ray analysis for chemical composition determination. As needed, the material characterization tasks at ORNL will include SEM, transmission electron microscopy, X-ray and neutron diffraction phase identification and residual stress measurements, and phase transformation kinetic and dilation dilatometry. Available resources will include the Hitachi HD-2000 STEM with SEM, STEM, and Z-contrast imaging capability; the PHI 680 Scanning Auger Microprobe with high sensitivity to light elements; the JEOL 8200 electron Superprobe; and the MMC High Speed Quenching and Deformation Dilatometer. A significant benefit of the majority of these resources is that these instruments can be

operated remotely from outside ORNL so that the collaborating team can interact and interpret results in real-time for these characterization endeavors. Any X-ray (including synchrotron) and neutron diffraction analyses required for this project will leverage the capabilities of the ORNL High Temperature Materials Laboratory Diffraction and Residual Stress Centers. These facilities have unique state-of-the art equipment that enable both room temperature and elevated temperature characterizations to be made up to 2700ºC in vacuum and 1600ºC in air. In addition, ORNL's High Flux Isotope Reactor's Neutron Diffraction Center enables nondestructive depth profiling of macro and micro residual stresses in rather large bulk specimens.

A concerted effort will be made to review and leverage all current developments in this material and process simulation field that is the scope of this project. Microstructure, residual stress, and cutting force measurements obtained by various research groups (e.g., ongoing research at Purdue University by S. Chandrasekar) will be used for model development and validation.

Task 2 as well as Task 1 will be augmented by a parallel project between Caterpillar, Brown, and the Central Research Institute for Materials in St. Petersburg, Russia, in which a detailed examination is being performed on the relationship between composition, microstructure and mechanical properties on steels of highly controlled purity and microstructure.

Task 3: Material Performance and Application

After the materials have been processed and machined, the next concern is to predict their subsequent performance, that is, their strength and resistance to fracture. Thus, the models for material performance need to be developed and validated. These models will explicitly include such microstructural elements as inclusions, precipitates, and grain boundaries and will be based on several finite element methods developed at Brown University.

The first step will be to develop predictive models of damage initiation either by cracking or debonding of second-phase inclusions and precipitates. This modeling will be performed using a cohesive surface framework to model the interface between the inclusion (or precipitate) and the matrix and to model the initiation and growth of cracks within the second phase. Parameter studies will be undertaken to identify measurable and controllable features of the microstructure that are key for damage initiation. The results for damage initiation will be used in a modified Gurson model[1] to predict material performance. Of initial interest will be the prediction of performance in a suite of test specimens that give rise to different plastic strain-stress triaxiality histories so that the predictive capabilities of this modeling can be compared with experimental observations. Three-dimensional calculations of more complex geometries will also be performed to demonstrate the capability of predicting failure in component-like geometries.

At the same time, experiments will be performed that use specimens that have been carefully designed so that their mechanical response can be fully modeled. These specimens will be pulled in tension to various loads and then sectioned so that the microstructure can be observed. Particular attention will be given to identification of the second-phase particles that are present in the material and participate in crack nucleation. This examination will be performed at Brown University using the LEO 1530VP SEM described in the previous task. By performing serial sectioning of the sample and by making maps of the location of particles and determining whether the particles have cracked, debonded, or remained whole and intact, the details of the

[1] A.L. Gurson, "Continuum Theory of Ductile Rupture, Void Nucleation and Growth," *Journal of Engineering Materials Technology*, **99**, (2) (1977).

interactions between the microstructure and mechanics will be determined.

Task 4: Pilot Project

The proposed research will focus on track roller shafts as a pilot component. The track roller shaft represents a component with high production-volume steel at Caterpillar. It serves to transmit the weight of a tractor through the undercarriage (see Figure 1), and can be produced from either conventional steel (heat-treated for strength) or microstructurally improved "micro-alloy" steel. The use of micro-alloy steel has been demonstrated to reduce the cost and environmental impact of the heat-treatment stage, making it currently the preferred material in regions with high energy costs (such as Japan). The use of microstructure-level simulation and sustainability metrics to evaluate and optimize its environmental performance throughout the entire life cycle may lead to further improvements and serve as an example on the effectiveness of integrated methodology.

First, the entire life cycle of a track roller shaft made with a conventional 1500-series steel will be modeled, and environmental resources needed throughout a component life cycle will be assessed. The chemical composition and processing map will be optimized to minimize environmental impact and cost of the component. Then, the modeling process will be repeated for using a micro-alloyed steel, which will be optimized for the same requirements. This study aims to provide optimum chemical compositions and processing road maps for a track roller shaft made with a conventional 1500-series steel and a micro-alloyed steel. In addition, the pilot project will quantify energy and environmental resources required for the entire life cycle of a track roller shaft made with steels and processes mentioned above.

A critical component in this task as well as the others will be the quantification of energy use during production of a part and optimization of the proposed process to minimize energy usage. Caterpillar has already established a project called Bridges to Sustainability, and National Science Foundation (NSF) interns at Brown worked in the summer of 2003 on this project. The tools developed by the NSF-sponsored project will be applied in this project to assess energy usage and savings for the processes used here.

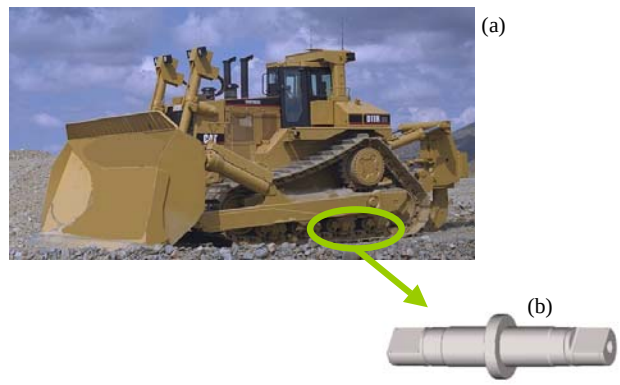

Figure 1. The tractor undercarriage receives the weight of the tractor (a) through a track roller shaft (b).

3. MATERIALS PROCESSING TECHNOLOGY

A. Oxidative Stabilization of PAN Fiber Precursor

Principal Investigator: Felix L. Paulauskas
Oak Ridge National Laboratory
Oak Ridge, TN 37831-8048
(865) 576-3785; fax: (865) 574-8257; e-mail: paulauskasfl@ornl.gov

Project Manager, Composites: C. David Warren
Oak Ridge National Laboratory
P.O. Box 2008, Oak Ridge, TN 37831-6065
(865) 574-9693; fax: (865) 576-4963; e-mail: warrencd@ornl.gov

Technology Development Area Specialist: Sidney Diamond
(202) 586-8032; fax (202) 586-2476; e-mail: sid.diamond@hq.doe.gov
Field Technical Manager: Philip S. Sklad
(865) 574-5069; fax:(865) 576-4963; e-mail: skladps@ornl.gov

Participants

Terry L. White and
Kenneth D. Yarborough, Oak Ridge National Laboratory
Professor Joseph Spruiell, University of Tennessee
Daniel Sherman, Atmospheric Glow Technologies

Contractor: Oak Ridge National Laboratory
Contract No.: DE-AC05-00OR22725

Objectives

- Develop an improved technique for oxidizing carbon fiber precursor with increased line speed, reduced carbon fiber cost, and reduced equipment footprint.
- Verify that fiber properties satisfy automotive and heavy vehicle manufacturers' requirements.
- Conduct a preliminary evaluation of the new oxidation technique's cost impact.

Approach

- Investigate plasma processing in an evacuated reactor, with plasma generated remotely and pumped to the fibers (remote exposure).
- Investigate plasma processing in an atmospheric pressure reactor, with fibers located near the plasma generator (direct exposure).
- Conduct parametric studies to correlate processing parameters and fiber properties.
- Characterize fibers to confirm that they satisfy program requirements.

Accomplishments

- Constructed and evaluated multiple reactor designs for both remote and direct plasma exposure strategies.
- Demonstrated partial oxidation using plasma processing.
- Conducted dielectric measurements to determine the acceptable range of a critical processing variable. The results led to significant changes in the reactor design and processing parameters.

Future Direction

- Utilize an evacuated plasma reactor to conduct studies on reactive chemical species optimization.
- Focus on atmospheric plasma processing as the best route to a robust, rapid oxidation technique. Continue refining the reactor design and processing protocols to achieve complete fiber oxidation.
- Conduct parametric studies and fiber characterization to better understand process effects and the processing window and to quantify fiber properties.
- Conduct rate-effect studies and preliminary cost analysis.

Introduction

The purpose of this project is to investigate and develop a plasma processing technique to rapidly and inexpensively oxidize a polyacrylonitrile (PAN) precursor. Oxidative stabilization is a slow thermal process that typically consumes 70% or more of the processing time in a conventional carbon fiber manufacturing line. A rapid oxidation process could dramatically increase the manufacturing line throughput and appreciably lower the fiber cost. A related project has already demonstrated the potential for greatly increasing line speed in the carbonization and graphitization stages, but the oxidation time must be greatly reduced to fully exploit faster carbonization and graphitization. This project intends to develop a plasma oxidation module that integrates with other advanced fiber processing modules to produce inexpensive carbon fiber with properties suitable for use by the automotive industry. Critical technical criteria include (1) 25 Msi tensile modulus, 250 ksi ultimate strength, and 1.0% ultimate strain in the finished fiber; (2) acceptably uniform properties over the length of the fiber tow; (3) repeatable and controllable processing; (4) and significant unit cost reduction in comparison to conventional processing

Project Deliverable

At the end of this project, complete fiber oxidation will have been demonstrated using a plasma oxidation process. Successful completion of this deliverable is expected to be followed by rate studies and equipment scale-up in a future project.

Technical Approach

Two plasma generation and control techniques are under investigation. The technique called “direct exposure” utilizes nonequilibrium, nonthermal plasma at atmospheric pressure, with the fiber transported through the plasma. The other technique called “remote exposure” uses a more conventional, evacuated (negative pressure) plasma reactor that pumps plasma with the active chemical species from the reactor chamber to another processing chamber in/through which the fibers are transported. Generation and control of chemically reactive species is more readily accomplished in the remote exposure technique. Direct expo-

sure provides better thermal control. Various fiber characterization tools and instruments are used to conduct parametric studies and physical, mechanical, and morphological evaluations of the fibers to optimize the process.

Experimental Results—Remote Exposure

Density measurements and morphological studies were conducted to confirm that the plasma is indeed oxidizing the fiber in remote exposure (evacuated reactor) processing. As oxidation proceeds, the fiber density should increase, with a fully oxidized fiber having specific gravity of ~1.4. Representative density data is tabulated in Table 1, showing that processing is proceeding. In some cases, the density approaches that of fiber exiting the first oxidation furnace in a conventional line. This is remarkable because the plasma oxidation chamber is quite compact, and the experimental work is still in the early feasibility stage.

Table 1. Pycnometer density data

	Pycnometer density, g/cc		Note
Reference values	1.1986		As-received 3K PAN precursor
	1.1485		Unprocessed, after 3.5 h at 0.8 in. Hg vacuum pressure
	1.1428		Unprocessed, after 1.17 h at 0.8 in. Hg vacuum pressure
	~1.25		Exit of 1st conventional oxidation furnace
	~1.4		Fully oxidized precursor, conventionally processed
Sample ID	**Pre-plasma**	**Post-plasma**	
2C	1.1483	1.2267 1.2172	Low pre-plasma density attributed to short preheater that was later lengthened
4C	1.1898	1.2389	
5C	1.1898	1.1996 1.2208 1.2389 1.2398	
6C	1.18 98	1.2821 1.2610	Brown spots on post-plasma fiber
7C	1.18 98	2.2178	
8C	1.18 98	1.2364	
9C		1.2118	
All plasma processing data generated using remote exposure plasma configuration and medium pre-heater temperature profile. Pre-plasma data point is taken after thermal pre-heating and before exposure to plasma.			

X-ray diffraction and dynamic scanning calorimetry (DSC) data were obtained for selected samples that have been partially oxidized by remote exposure to plasma. The DSC data presented were obtained by scanning from 100°C to 350°C at a scanning rate of 5°C per min. This rate was chosen for comparison with data from the literature.

Figure 1(a) compares partially processed plasma precursor to a commercial grade virgin PAN precursor and a fully stabilized sample prepared by the conventional process. This figure illustrates the changes to be

expected in the diffraction patterns during oxidation and those that are occurring with partial plasma oxidation. It can be seen from the X-ray diffraction data in Figure 1(b) that the samples of commercial grade Stage 1-1 through Stage 1-5 and two selected plasma processed samples all exhibit similar diffraction patterns and that they have not changed significantly from the pattern of the PAN precursor. It is therefore difficult to tell how far the Oak Ridge National Laboratory (ORNL) samples have progressed in the oxidation process from diffraction data alone (i.e., X-ray diffraction analysis is not sensitive enough in the first oxidation stage). Oxidation samples were tested in the DSC to further discriminate the oxidation level achieved. The peak temperature decreases and the exothermic heat of reaction decreases as the precursor is oxidized more. ORNL samples were also tested in the DSC and compared to the commercial grade samples. The plasma-processed sample appears to have been affected by the oxidation process to a degree similar to the commercial grade process.

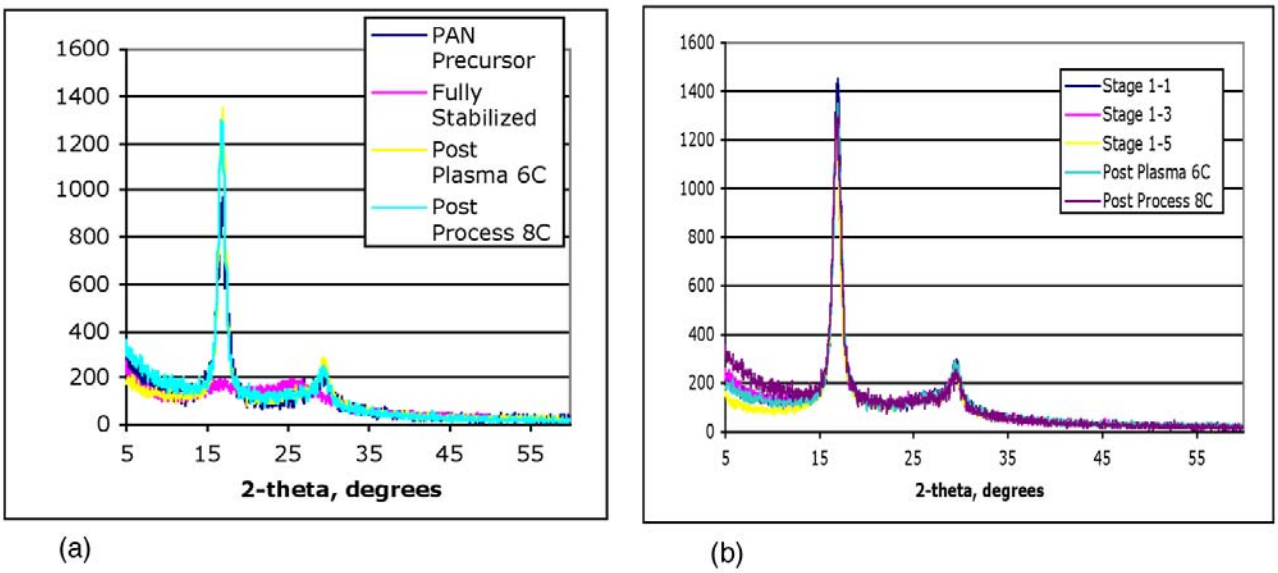

Figure 1. Diffractograms comparing partially plasma-oxidized precursor with virgin precursor and fully stabilized PAN (a). Diffractograms comparing partially plasma-oxidized precursor with partially oxidized precursor taken at various points partway through the first conventional oxidation furnace (b).

Experimental Results—Direct Exposure

Direct exposure in plasma at near atmospheric pressure is expected to provide superior thermal control because the gas flow should convectively heat or cool the fibers. This is deemed particularly important to avoid fiber melting from the exothermic reactions associated with the PAN cross-linking that occurs during stabilization. However, the mean free path of the chemically reactive species is shorter by orders of magnitude than it is in an evacuated environment, and this makes it very difficult to find a combination of process parameters that will oxidize the fibers with acceptable residence time.

The experimental program was focused principally on direct exposure techniques in the last half of FY 2003. Most of the effort was devoted to designing and testing a number of different reactor configurations. Atmospheric pressure plasma processing is itself

a technology in its infancy, and utilizing it to oxidize fiber is necessarily an intensive trial and error effort. A limited degree of oxidation has been achieved— to 1.25 specific gravity starting with material at 1.21 specific gravity. Oxidation levels as well as residence times and uniformity need to be improved.

Because the interaction of atmospheric pressure plasma with carbon fiber is not yet well understood, it has been very difficult to achieve sustained and stable reactor operation. Nevertheless, several experiments in the September 2003 time frame produced promising results. One of the major objectives for the first half of FY 2004 will be to select one or more promising reactor configurations and achieve sustained stable operation, with a corresponding increase in the achieved degree of fiber oxidation.

Figure 2 shows several atmospheric pressure reactor designs that were constructed and tested. Each succeeding reactor design included features that were intended to improve the rate or control the oxidation process in comparison to earlier generations.

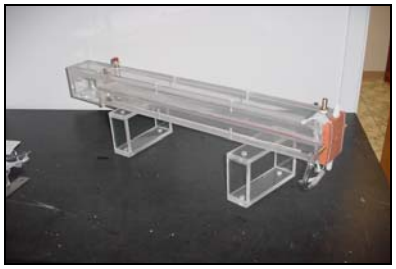

(a). Parallel plate with water electrodes.

(b). Rectangular reactor with water electrodes.

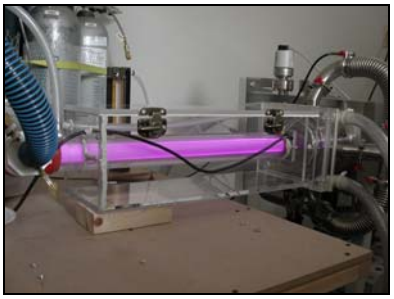

(c). Concentric plates.

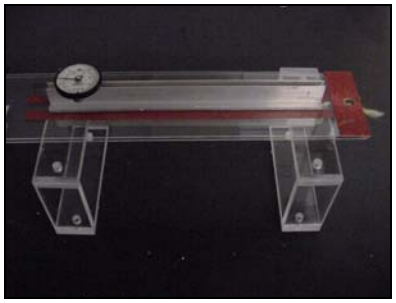

(d). Parallel plates with air heat extracting fins as electrodes.

(e). Surface discharge

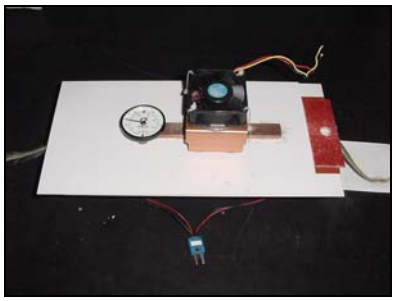

(f). Parallel plates with air heat sinks

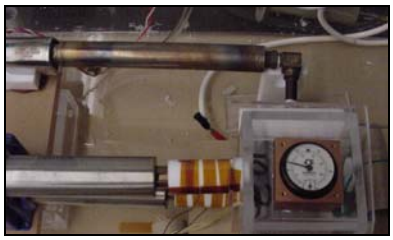

(g), Mini-parallel plates with heat sinks

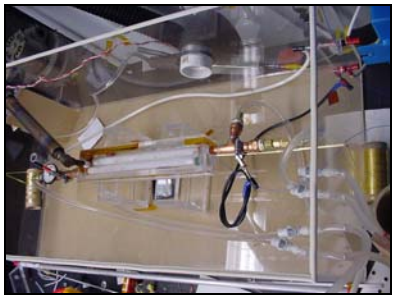

(h). Parallel pipes water cooled

Figure 2. Remote exposure reactors.

Parametric Studies

Techniques and hardware were developed for measuring the fiber dielectric properties over a selected range of oxidation-processing conditions. This is an extension of technology for monitoring the carbonization process by measuring the fiber dielectric properties. Correlation of the dielectric properties with processing conditions is expected to yield insights into the process dynamics. Unoxidized PAN is an insulator, rendering dc conductivity measurements of limited use for monitoring oxidation progress; hence, dielectric monitoring is especially valuable for oxidation. Initial results led to significant changes in the reactor design and processing parameters. This work is continuing, with improvements being made to the dielectric measurement system.

Education

The materials characterization has been conducted in partnership with the University of Tennessee's (UT's) materials science department. Two UT graduate students were engaged to provide characterization support to the project.

Conclusions

The development of plasma-based oxidation technology has progressed at a pace consistent with funding and effort expended. Several generations of hardware have been constructed for experiments in both evacuated reactors and atmospheric pressure reactors. Plasma has been shown to effect partial oxidation of PAN fibers. The researchers expect to achieve complete fiber oxidation in FY 2004.

B. Wrought Magnesium Alloy/Process Development

Principal Investigator: S. R. Agnew
University of Virginia
116 Engineer's Way
PO Box 400745 Charlottesville, VA 22904-4745

Principal Investigator: J. A. Horton
Oak Ridge National Laboratory
P.O. Box 2008, Oak Ridge, TN 37831-6115
(865)74-5575; fax: (865) 574-825; hortonja@ornl.gov

Technology Development Area Specialist: Sidney Diamond
(202) 586-8032; fax: (202) 586-1600; e-mail: sid.diamond@ee.doe.gov
Field Technical Manager: Philip S. Sklad
(865) 574-5069; fax: (865) 576-4963; e-mail: skladps@ornl.gov

---

Contractor: Oak Ridge National Laboratory
Contract No.: DE-AC05-00OR22725

Objectives

- Develop wrought magnesium alloys with better formability than current magnesium alloys.
- Investigate new processing techniques for cost control, texture control, and formability.
- Contribute to basic understanding of deformation, processing, and alloy behavior for this lightweight metal.

Approach

- Explore new processing schemes for magnesium alloy sheets.
- Evaluate the practical formability (deep drawability) of new alloys.
- Determine deformation mechanisms using experimentation and simulation.

Accomplishments

- Demonstrated feasibility of utilizing infrared heating for sheet processing.
- Used equal channel angular extrusion to show the potent effect of crystallographic texture on mechanical behavior.
- Determined that the hardening response, which is critical for secondary forming operations, could be improved by combining low-temperature twinning deformation and annealing or high temperature deformation.
- Demonstrated that initial bending and unbending trials did not change the texture and mechanical behavior as expected from old anecdotal reports.

- Demonstrated that an alloy with a high r-value performed better than the industry standard AZ31through use of the deep drawing tests of our experimental ductile alloys.
- Demonstrated that polycrystal plasticity simulation provides an explanation for changes in r-value and formability with loading orientation and temperature in terms of the fundamental deformation mechanisms of magnesium (i.e., slip of basal and nonbasal dislocations.)

Future Direction

- Conduct a pilot-plant scale test of infrared processing of wrought magnesium sheet fabrication.
- Pursue combinations of annealing and bending of sheet alloys for texture and property control.
- Define further correlations of r-values and refine more new alloys for better formability.
- Develop a warm formability test more relevant to industrial practice (plane strain.)

Introduction

The world market for magnesium has changed substantially in the last couple years. The emergence of China as the leading producer (~50% of the market) of inexpensive magnesium alloys has led to circumstances where magnesium alloy die cast or thixomoulded parts can be less expensive, in some instances, than their aluminum alloy counterparts. There are pros and cons to these events. On the one hand, it may make magnesium a more attractive material choice for a number of applications, such as the chassis of laptop computers. On the other hand there are concerns that the Chinese producers may drive western competitors out of business. Additionally, the reason the prices are so low is that these new producers do not have to abide by western standards of environmental protection and energy conservation. Thus, the end goal of magnesium usage for transportation (energy savings and reduction of emissions) may be lost in a life-cycle analysis which includes production. It is still unclear what the final outcome will be.

In the case of wrought magnesium, the situation is less clear. German steel makers (Thyssen Krupp and Salzgitter) have new magnesium rolling facilities that represent millions of dollars of capital investment. Another leading steel producer from Korea, POSCO, is making plans to enter the magnesium sheet market as well. Here in the United States, the formerly lone magnesium sheet producer in the world, Spectrulite, was in bankruptcy throughout the past year. However, the assets for casting and sheet production were just purchased by Magnesium Elektron (MEL), of the United Kingdom. MEL has been an innovative leader in magnesium technology (particularly gravity-cast alloy development). An example is the WE class of alloys they have developed during the past 20 years, which is eagerly consumed by the Formula One race car industry for engine parts and is considered for some helicopter transmission applications.

Magnesium sheet manufacturers must face a number of technical issues, including

- Rolling magnesium into thin gage sheet currently leads to expensive solutions.
- Obtaining an excellent surface finish has been difficult.
- Corrosion performance of wrought alloys has lagged that of die-cast alloys.
- Sheet formability is limited at room temperature.

Our work during FY 2003 focused on sheet formability issues, and we began

addressing the concerns associated with the cost of sheet products.

It is recognized that two issues limit the sheet formability of magnesium alloys at low temperatures. First, the hexagonal close-packed structure and the apparent lack of easy deformation mechanisms do not accommodate arbitrary strain paths. Second, magnesium alloys develop strong crystallographic texture during wrought processing. We have investigated three possible thermomechanical processing routes to alter the strong crystallographic texture.

- upset forging of conventional extrusions (during FY 2002)
- equal channel angular extrusion (ECAE)
- bending-unbending of conventional sheets.

Texture Control and Hardening Response

ECAE was successful in altering the texture significantly. In fact, the new texture was completely distinct from the conventional extrusion texture; however, it was surprisingly stronger than the conventional extrusion texture (Figure 1). Tensile test results emphasize how potent an effect texture has on the behavior of magnesium (Figure 2). For an alloy that normally only has 15–20% ductility in the extruded condition, we achieved an elongation of >40% along the extrusion axis [see also T. Mukai, M. Yamanoi, H. Watanabe and K. Higashi, *Scripta mater*. **45** (2001) 89 and W. J. Kim, C. W. An, Y. S. Kim and S. I. Hong *Scripta Mater*. **47** (2002) 39]. Furthermore, one of the frequently cited liabilities of magnesium extrusions was also overcome; there is no apparent tension/compression asymmetry. Namely, the flow curves in tension and compression along the extrusion axis look essentially the same. If this process could be altered to produce sheet material, there may be some opportunities to produce sheets with remarkably distinct textures from conventional processes.

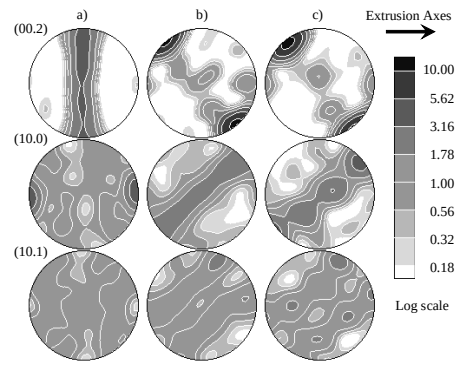

Figure 1. Pole figures (equal area projection) measured using neutron diffraction at Los Alamos National Laboratory show the crystallographic textures in (a) conventionally extruded, (b) ECA processed, and (c) annealed AZ31B. Note stronger texture in the ECA processed materials.

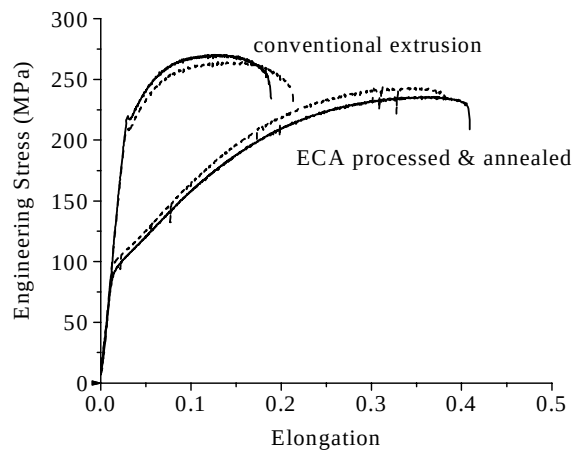

Figure 2. Tensile test results from conventionally extruded and ECA processed and annealed material. The ECA material shows an impressive ductility improvement. The load drops in the flow curve suggest some twinning activity. Curves from two samples of each type demonstrate the reproducibility of the results.

In FY 2002, we explored upset forging of conventional extrusions because the two major deformation mechanisms in magnesium (basal slip and mechanical twinning) would lead to rapid texture

evolution under these conditions. The texture-altered material could then be used to test how the materials mechanical behavior would change. First, the material was compression tested over a range of temperatures, to identify the temperature regime where twinning dominates (since twinning gives rise to a characteristic flow curve in textured magnesium as shown in Figure 3.) Then processing routes involving primarily twinning (at low temperature) and

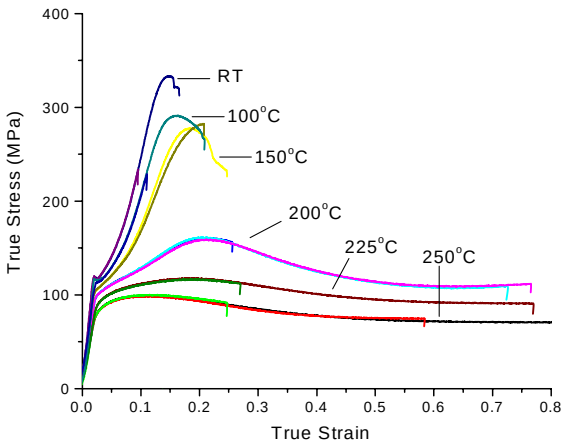

Figure 3. Stress-strain curves from compression tests along the extrusion axis have a shape characteristic of deformation twinning at low temperatures and that of dynamic recrystallization at higher temperatures.

slip (at high temperature) were used to alter the texture. Finally, the material was annealed in order to eliminate the deleterious effect of prior deformation on ductility. The test results suggest that even though the overall ductility was limited to about 30%, it is possible to strongly change the hardening response, which is critical for secondary forming operations (Figure 4). One of the reasons that magnesium alloys fail to exhibit excellent sheet formability is their lack of strain hardening. Altering the texture is, thus, shown to be potent means of altering this trend.

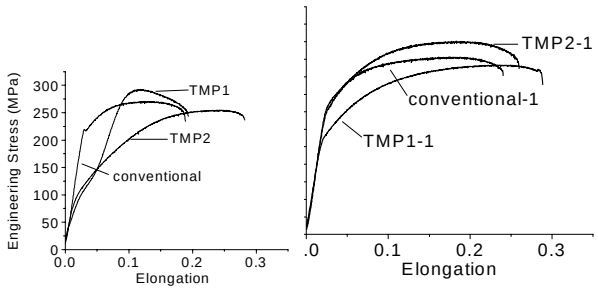

Figure 4. Tensile tests (a) results from conventionally extruded, room temperature upset (TMP1) and high temperature upset (TMP2) and (b) results from the same material after annealing.

Bending-Unbending

During FY 2003, bending-unbending procedure was explored on the basis of some anecdotal reports from some old texts that stated that magnesium's ductility was improved by passing it repeatedly through "sheet levelers," which force the sheet to bend and unbend. The supposed reason for this behavior is very similar to the logic described above for the upsetting of extrusions. The material on the inner side of the bend is forced into compression within the plane of the sheet. This results in extensive twinning of the material on the inner side of the bent sheet. Further, the texture is strongly altered by the presence of twins (Figure 5). Unfortunately, we found that the unbending resulted in "untwinning" as well. Thus, the resulting texture alteration after bending and unbending is not significant. Similarly, the change in the mechanical behavior is not significant (Figure 6). It is suggested that suitable combinations of annealing and bending may result in a benefit to the formability of magnesium sheets, so this will continue to be an area of active research in FY 2004.

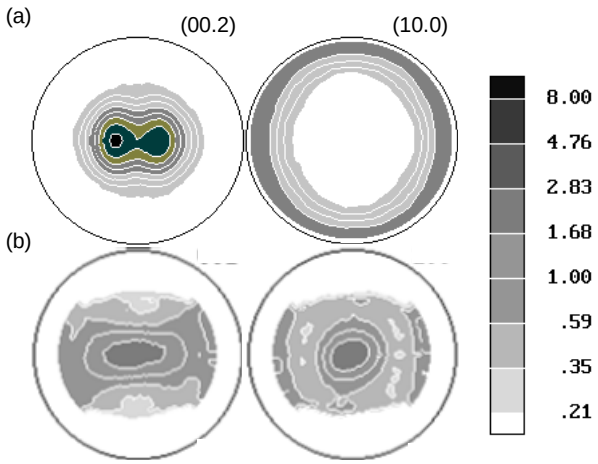

Figure 5. X-ray pole figures show (a) strong initial rolling texture and (b) the texture in a bent sheet that is strongly altered from the initial condition.

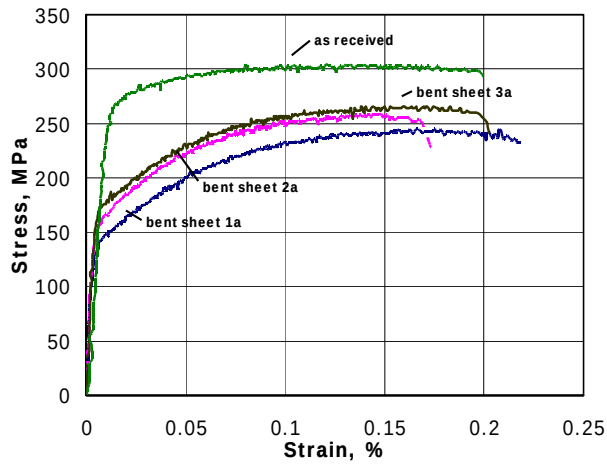

Figure 6. Tensile behavior from sheets processed by bending-unbending where sheet 1a was bent the most severely and sheet 3a the least. The resulting behavior is not dissimilar from a conventional annealed sheet.

Infrared Lamp Sheet Processing

More recently, we have been exploring the possibility of economizing the magnesium alloy sheet fabrication process. The main problem is that magnesium must be rolled at a slightly elevated temperature and that the rolls will quickly extract all of the heat from thin-gage sheets. In current industrial practice, the final "cold" rolling is performed one or two rolling passes at a time with intermediate recovery anneals and reheats. This is very inefficient and drives the cost of inexpensive raw material to a very high price for the final wrought product.

Using rapid radiant heating, it is suggested that magnesium could be efficiently warm rolled. The material could be passed through a radiant furnace between rolling reductions, rather than being passed to an offline conventional furnace. With the furnace immediately before the rolls, the material will receive both a recovery anneal as well as a reheat to allow continued warm rolling. Using a plasma arc lamp with a width of 1 cm and translated at 15 mm/s yielding about 1.5 s of heating resulted in recystallization and a stress strain curve equivalent to a standard furnace anneal for 1 h at 400˚C (see the side views shown in Figure 7). Some surface crystallographic texture improvements were noted. Note that in Figure 7 there is a uniformity of grain size through the 3-mm thickness. Experiments have begun, using a bank of infrared heat lamps with 1 min. warm up and 1 min. at 400˚C, prior to rolling. Figure 8 shows cross section optical micrographs at the top and at the bottom after a fifth warm rolling pass of 15% reduction and subsequent anneal of material with a final thickness of 2 mm. We have also observed that the textures of hot-rolled sheets have been significantly weaker than the material that we have obtained from the commercial vendor (Spectrulite). Incorporating radiant heating into the rolling process will probably result in a softer texture than that produced by conventional processing. This may result in a fringe benefit to the formability of the resulting sheet product.

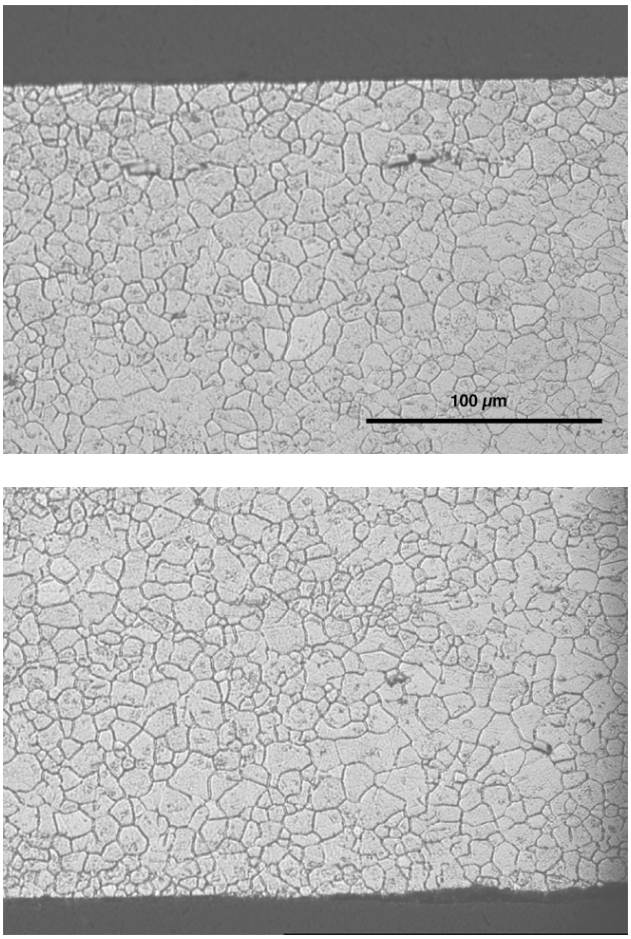

Figure 7. Optical micrographs from top and bottom of 3-mm-thick sheet of AZ31B with the H24 temper after approximately 1.5 s anneal from a plasma arc lamp translating at 15 mm/s at 500 W/cm^2. Recrystallization did occur from this brief anneal and was uniform through the thickness.

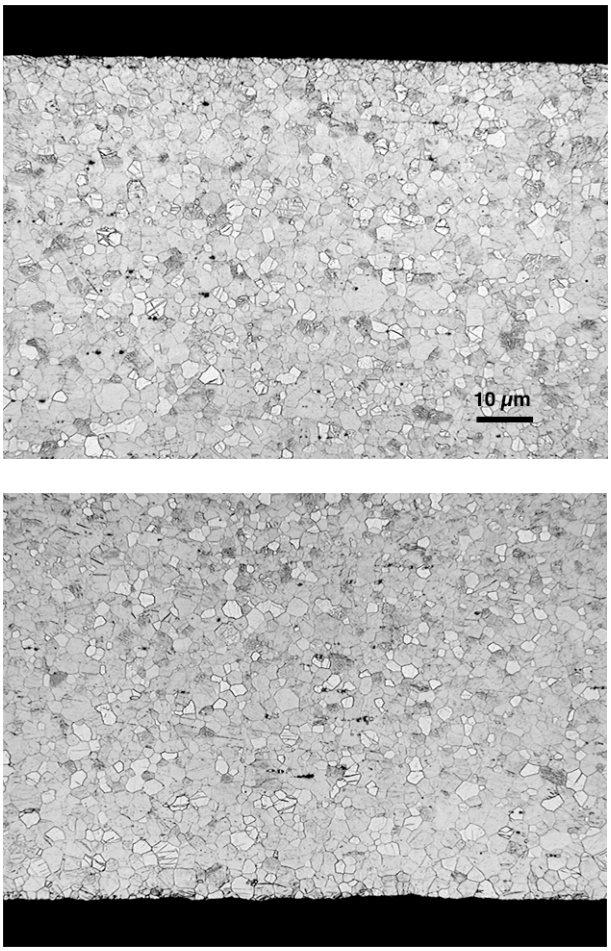

Figure 8. Optical micrographs after infrared lamp anneals from the top and bottom of AZ31B after the fifth anneal and 15% roll with a thickness of 2 mm. The anneals consisted of 1 min to heat up and 1 min. at 400˚C. Again these micrographs show the uniformity of the microstructure through the thickness.

Evaluation of the Practical Formability (Deep Drawability) of New Alloys

During previous years, two alloy systems with exceptional ductility were identified. During FY 2003, we tested the practical formability by first warm rolling thin gage sheets from these alloys and then performing warm deep drawing experiments on these sheets. The Tinius Olsen formability tester with a cylindrical cup drawing die-set having a draw ratio of approximately 1.8 was used as a standard, and tests were performed at a range of punch speeds at temperatures ranging from 100–200°C. Although one of the alloy classes had been reported to be cold rollable in an early publication, and the ductility had been observed to be quite good (Figure 9), we found the deep-drawing performance of WM3, WM4, and WM5 to be quite poor at all the rates and temperatures we explored (Figure 10). In contrast, we found the drawing performance of another alloy class to be superior to the industry standard AZ31 sheet material. Although AZ31B can be successfully deep drawn at

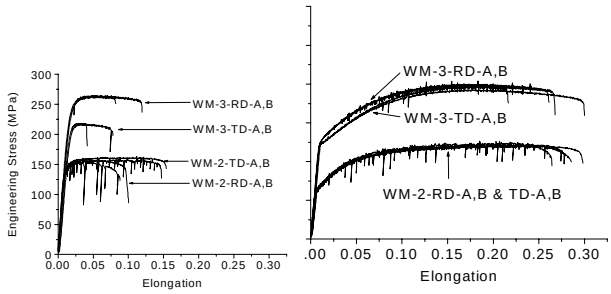

Figure 9. Tensile data from alloys WM2 and WM3 in the (a) as-rolled and (b) annealed conditions are representative of the two alloy classes investigated during our program. Both exhibit excellent ductility and little in-plane anisotropy in the annealed condition. Multiple curves for each sample type are shown.

150°C at low punch speeds (~2.5 mm/min), it is necessary to increase the temperature all the way to 200°C in order to achieve a perfect cup at the highest punch speed of ~250 mm/min. In the case of our experimental alloy WM2, a perfect cup can be drawn at the highest punch speed at only 150°C.

All of these results could be reconciled by examining the r-value of the various alloy sheets. The r-value is a measure of the sheet's anisotropy, specifically its resistance to thinning. A value of 1 means isotropy, and values above one mean a material that strongly resists thinning, while values below one mean a material which preferentially thins. Practical experience, particularly with steels, dictates that high r-values promote drawability. In the present case, it was found that alloys WM4 and WM5 have very low r-values, which is quite uncommon for magnesium sheets, while WM2 has an exceptionally high r-value (even in comparison with commercial AZ31, which has a high r-value, see Figure 11) Thus, the magnesium sheets with high r-values were found to perform the best during deep drawing trials.

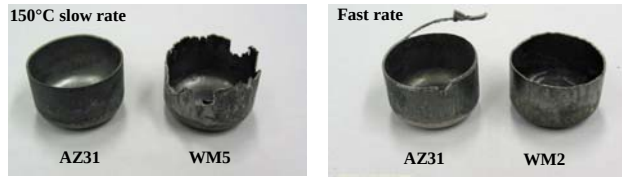

Figure 10. Cup drawing experiments demonstrate the practical formability of magnesium alloys. On the left, it is observed that AZ31 can be deep drawn at 150ºC, while WM5 cannot be drawn successfully at any rate or temperature up to 200ºC. At 150ºC, alloy WM2 may be drawn at the fastest rate; however, AZ31 cannot be drawn at this rate until 200ºC.

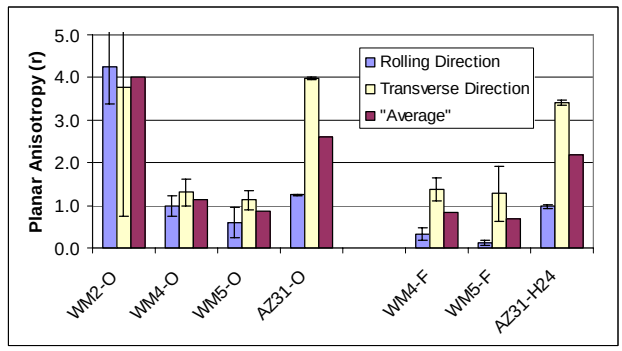

Figure 11. R-value measurements from various alloys, including the industry standard AZ31, in both the fully annealed O temper and the half-hard H24 temper.

During FY 2004, refinement of these alloys is planned to maximize their properties, including strength and ductility, and it is further planned to explore one more system involving dilute additions of zinc and rare earth elements.

Determination of Deformation Mechanisms Using Experimentation and Simulation

Correlating the crystallographic texture and deformation mechanisms with the anisotropy (or r-values) discussed above, led to the determination that magnesium sheets have high in-plane anisotropy (variation of the r-values within the plane of the sheet) at room temperature and that the specific deformation mechanisms and texture of

"cold-rolled" magnesium is responsible for this behavior. Polycrystal plasticity simulation reveals that primarily basal slip occurs during tension along the rolling direction, while prismatic slip is forced during tension along the transverse direction. Recent work using transmission electron microscopy has verified the occurrence of extensive nonbasal slip of <a> dislocations at room temperature.

During the past year, this understanding was extended to the high-temperature regime in an effort to understand why magnesium becomes so formable at even moderate forming temperatures. Again r-value measurement and simulation were used to determine the active deformation mechanisms. The r-values dropped precipitously with increasing temperature (Figure 12). Thus, counter to prior wisdom, the nonbasal (prismatic or pyramidal) slip of <a> type dislocations does not appear to be the main reason magnesium alloys become formable at moderate temperatures. We suggest that nonbasal slip of <c+a> type dislocations is responsible for the observed changes in r-value and formability.

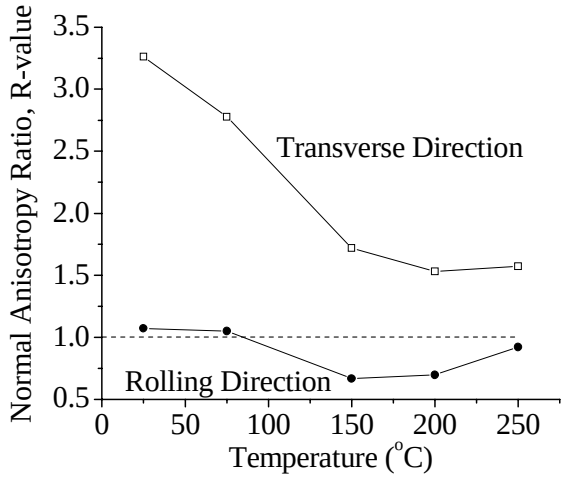

Figure 12. R-value measurements over a range of temperatures shows that the r-value drops strongly in all directions as the temperature is raised.

C. Equal Channel Angular Extrusion

Principal Investigator: R. B. Schwarz
Los Alamos National Laboratory
MST-8, Mail Stop G755, Los Alamos NM 87545
(505)667-8454; email: rxzs@lanl.gov
Co-Investigators: T. D. Shen, J. I. Archuleta

Technology Development Area Specialist: Sidney Diamond
(202) 586-8032; fax: (202) 586-1600; email: sid.diamond@ee.doe.gov
Field Technical Manager: Philip S. Sklad
(865) 574-5069; fax: (865) 576-4963; email: skladps@ornl.gov

Contractor: Los Alamos National Laboratory
Contract No.: W-31-109-Eng-38

Objective

- Conduct research on the theory, synthesis, and properties of soft ferromagnetic alloys having the potential to improve the efficiency of energy conversion devices in the U.S. transportation industry.

Approach

- Use mechanical alloying (MA) (a high-energy ball milling technique) to prepare Fe-rich alloy powders.
- Characterize the powder by X-ray diffraction, scanning differential calorimetry, and magnetometry.
- Consolidate the mechanically alloyed powders by equal-channel angular extrusion and spark-plasma sintering.
- Characterize the compacted alloys by ac and dc magnetic measurements.

Accomplishments

- Used MA to prepare magnetically soft Fe-Cu powders. We established optimal annealing parameters for reducing the residual stress in the Fe-Cu powders, while maintaining the crystallite size below 20 nm, as required for soft ferromagnetic properties. After reducing the residual stresses by annealing, the coercivity is approximately 0.5 Oe, and the saturation magnetization is 1.8 T.
- Studied $Fe_{80}Cu_{20}$ alloys that revealed the potential and limitations of the method.

Future Direction

- Study Fe-Al-Si alloys following the basic lines established in FY 2003.
- Study the consolidation of our mechanically alloyed Fe-Al-Si powders by spark plasma sintering in collaboration with Professor A. K. Mukherjee at the University of California at Davis.

Introduction

The efficiency of electrical distribution grid systems can be increased by decreasing the power losses in step-up and step-down transformers. Because the amount of energy distributed by the grid is very large (3.8×10^{12} Wh for 2000 in the United States alone [1]), even a small increase in efficiency would represent a significant energy savings. Similarly, considerable savings can be achieved by increasing the efficiency of electric motors and other energy conversion devices used in the transportation industry.

Basic requirements for efficient cores in electromagnetic energy-conversion devices are low hysteresis losses and high saturation magnetization. Amorphous (glassy) ferromagnetic alloys are being studied for their potential in providing more efficient cores than those produced from conventional crystalline Fe(Si) alloys. Until recently, amorphous ferromagnetic alloys with coercivities in the tens of mOe [2] were only available as thin, glassy ribbons. These were produced by rapidly quenching a melt layer spread over a rotating copper wheel (melt spinning). To bypass crystallization during the quenching process, the melt must cool at a rate on the order of 10^6 K s^{-1}, which effectively limits the ribbon thickness to 30 to 50 µm. Because the resulting ribbon is so thin, a large number must be stacked to form the massive cores of transformers and motors. Such stacking inevitably leaves air gaps between the ferromagnetic foils, which decreases the packing density of the core. In turn, the low packing density requires longer copper-wire coils, resulting in increased Joule losses in the device. The optimal foil thickness is determined by a minimization of the combined core and Joule losses. An increase in the thickness of the ferromagnetic foils causes an increase in the core losses (due to higher eddy-current losses, which are proportional to the square of the foil thickness) but a decrease in the Joule losses due to a denser core. In conventional power transformers made from crystalline Fe-3 wt % Si laminas (where the laminas can have any thickness), the optimum lamina thickness is about 300 µm. Although we have no equivalent study for amorphous ferromagnetic alloys, because amorphous alloys have higher resistivity than crystalline alloys, the optimal thickness for amorphous laminas is at least 300 µm, which is significantly thicker than that of ribbons formed by melt spinning.

Bulk Ferromagnetic Glasses

In the last decade, researchers have been able to prepare thicker amorphous alloy rods and laminas, which are now termed *bulk* metallic glasses [3-5]. Bulk metallic glasses are multicomponent alloys with particularly high values of the ratio T_g/T_ℓ (between the glass-transition and liquidus temperatures), which enables bypassing crystallization during melt quenching at relatively low cooling rates. For example, a critical cooling rate of only 0.005 K s^{-1} has been measured in $Pd_{43.2}Ni_{8.8}Cu_{28}P_{20}$ alloy [6] and hence glasses of this composition can easily be prepared as 1-in.-diam rods or plates.

The optimal Fe-based compositions currently available for preparing bulk ferromagnetic alloys have critical cooling rates on the order of 10^2 K s^{-1}, making it possible to prepare 4- to 6-mm-thick glassy rods or plates [7,8]. Table 1 summarizes the properties of bulk Fe-based ferromagnetic glasses prepared in our laboratory. Although researchers have proposed various empirical rules for finding optimal compositions suitable for bulk glass production, no generally accepted theory exists for the selection of elements. We used the following reasoning. Because the product has to have a large Fe content, the glasses must belong to the metal-metalloid class of amorphous alloys. Starting with the known ferromagnetic glass $Fe_{80}(P,B)_{20}$ (which can

Table 1. Bulk ferromagnetic glassy rods (1 to 5 mm diam) prepared by flux melting and water quenching

Alloy	X	Density* (g/cm^3)	M_s* (T)	T_C* (°C)
$(Fe_{40}Ni_{40})_{(100-x)/80}(P_{14}B_6)_{x/20}$ (x = 20-22)	20	7.61±0.01	0.87	268
$Fe_{95-x}Mo_5(P_{13}C_7)_{x/20}$ (x = 23 - 25)	24	7.45±0.01	0.96	160
$Fe_{94-x}Mo_4Ga_2(P_{12}B_4C_4)_{x/20}$ (x = 21- 23)	22	7.49±0.01	1.10	219
$(Fe_{67}Cr_4Mo_4Ga_4B_5C_5)_{(100-x)/89}P_x$ (x = 10 - 14.5)	12	7.51±0.01	-	162
$(Fe_{66}Cr_4Mo_4Ga_4P_{12}C_5)_{(100-x)/95}B_x$ (x = 3 - 6.5)	5.5	7.50±0.01	0.83	160
$(Fe_{66}Cr_4Mo_4Ga_4P_{12}B_5)_{(100-x)/95}C_x$ (x = 3 – 8.5)	6.5	7.48±0.01	0.84	153
$Fe_{88-x}Cr_4Mo_4Ga_4(P_{12}B_{5.5}C_5)_{x/22.5}$ (x = 20 - 22.75)	22.5	7.50±0.01	0.83	162
$Fe_{77.5-3x}Cr_xMo_xGa_xP_{12}B_{5.5}C_5$ (x = 2.66 – 4.66)	2.66	7.43±0.01	1.07	213
$Fe_{74}Mo_4P_{13.2}B_{4.4}C_{4.4}$		7.44±0.02	-	198
$Fe_{71}Cr_4Mo_4P_{11}B_5C_5$		7.43±0.02	0.87	126
$Fe_{70}Co_4Mo_4P_{13.2}B_{4.4}C_{4.4}$		7.52±0.01	1.17	233
$Fe_{68}Co_4Mo_4Ga_2P_{13.2}B_{4.4}C_{4.4}$		7.50±0.01	-	241
$Fe_{65}Sb_2Cr_4Mo_4Ga_4P_{11}B_5C_5$		7.44±0.02	0.91	184
$Fe_{62}Co_5Cr_4Mo_4Ga_4P_{11}B_5C_5$		7.43±0.02	0.86	171
$Fe_{50}Co_8Ni_8Cr_4Mo_4Ga_4P_{12}B_5C_5$		7.60±0.02	-	180

* The glass properties in the last three columns are for the composition X given in the second column. M_s is the saturation magnetization and T_C is the Curie temperature.

only be prepared as a 30-µm-thick foil), we partially replaced Fe by elements such as Ni, Mo, Ga, Cr, Co, and Sb, all of which have different molar volumes than Fe, yet a near-zero heat of mixing with Fe. We avoided alloying with elements having a large positive or negative heat of mixing with Fe because such elements would have had a tendency either to phase segregate or to form ordered high-melting-temperature compounds. Melts containing elements of different molar volumes should be better packed and thus have higher viscosity, resulting in a lower critical cooling rate. Furthermore, crystal nucleation should be more difficult in multicomponent melts [9]. We optimized the alloy composition using the empirical criterion of correlating the glass formability with the difference T_x - T_g, where T_x is the crystallization temperature.

Figure 1 shows the dc hysteresis curve for $Fe_{65.5}Cr_4Mo_4Ga_4P_{12}B_{5.5}C_5$ glass. The M_s and T_C values of this glass and others prepared in this study are summarized in Table 1. Notice that M_S ranges from 0.83 to 1.17 T. These M_S values are lower than the M_S values of 2 T found in oriented Fe-3 wt % Si alloys. The Curie temperatures, T_C, of the bulk glasses are

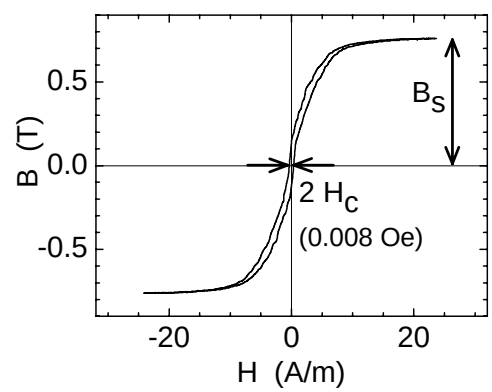

Figure 1. B-H curve measured on an amorphous $Fe_{65.5}Cr_4Mo_4Ga_4P_{12}B_{5.5}C_5$ toroid prepared from a 4-mm-diam glassy rod.

also rather low, ranging from 126 to 268°C. These relatively low M_S and T_C values result from alloying Fe with elements such as Cr and Mo, which is necessary to prepare bulk ferromagnetic glasses but also decreases the moment per Fe atom in the alloy. Because of their low M_S values, the glasses in Table 1 are not applicable to power transformers (which require M_S values of at least 1.5 T). However, these glasses have extremely low coercivity

and are thus potentially useful for sensor applications.

Figure 2 shows the ranges of M_S and H_C obtained for a variety of ferromagnetic alloys. It is apparent from this figure that the

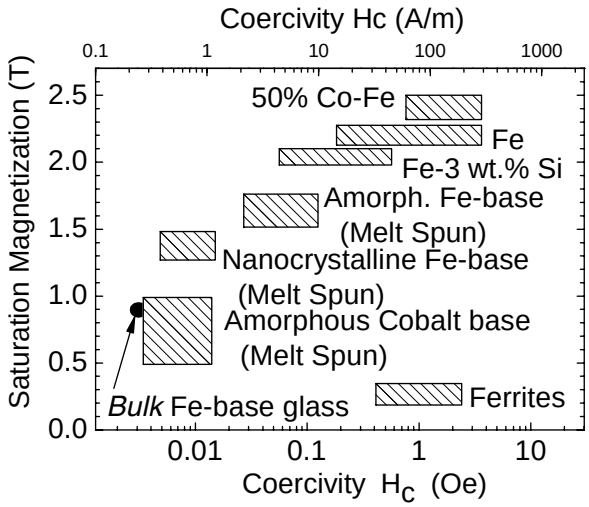

Figure 2. Ranges of saturation magnetization and coercivity in various soft ferromagnetic alloys.

lower H_C values (as required for low hysteresis losses) have been achieved at the expense of decreasing the M_S values. The current challenge is to develop materials having both low H_C and high M_S. So far, this goal has been approached most closely by two-phase materials consisting of nanosized *bcc* Fe particles embedded in an amorphous alloy matrix. Two nanocrystalline alloys, known under the trade names "Nanoperm" [10] and "Finemet" [11], are prepared by the partial crystallization of 30- to 50-µm thick rapidly quenched glassy ribbons. The saturation magnetization of these materials is approximately 1.4 T. Their main drawback is their thinness of gauge, which is not optimal for the construction of power transformers. In the next section we describe another approach to this problem, based on nanocrystalline ferromagnetic powders prepared by mechanical alloying.

Magnetic Properties of Nanocrystalline Ferromagnetic Alloys

The coercivity of crystalline alloys depends strongly on crystal size [12] because the magnetic domain walls interact with the grain boundaries. For decreasing grain size, H_C increases and reaches a maximum for grain sizes of approximately 100 nm. Further decreases in grain size lead to a rapid *decrease* in coercivity, in proportion to the sixth power of the grain size [13]. As the grain size approaches the exchange length, the averaged magneto-crystalline anisotropy of the randomly oriented crystallites offers no resistance to the Bloch walls, and the coercivity approaches the low value that is characteristic of amorphous ferromagnetic alloys. This feature of nanocrystalline ferromagnetic alloys has motivated extensive research of ferromagnetic powders prepared by MA. MA is a simple high-energy ball milling technique that was originally developed to prepare dispersion-strengthened Ni alloy powders [14]. Following MA, the dislocations in the heavily deformed particles are mainly concentrated at walls that delineate cells of lower dislocation density. The crystal size measured by X-ray diffraction corresponds to the size of these cells, which diffract semicoherently.

Table 2 summarizes the magnetic properties in mechanically alloyed powders reported in the literature. As can be seen in the table, none of these powders has a coercivity below 1 Oe, which is usually the value used to classify the material as magnetically soft. The lower half of Table 2 summarizes the magnetic properties of mechanically alloyed Fe-Cu powders. Fe and Cu have negligible solubility, yet, following extensive mechanical alloying, they form extended solid solutions: $Fe_{1-x}Cu_x$ is *fcc* for $0.4 < x < 1.0$, and *bcc* for $0 < x < 0.2$ [15]. Although most of these powders had crystallite sizes below 20 nm, the lowest H_C value reported in these works was 3.8 Oe. This is surprising since the Herzer plot [13]

predicts that for a crystallite size of 20 nm the coercivity should be in the 10^{-2} Oe range. This motivated us to reinvestigate the Fe-Cu system, especially the dependence of coercivity on annealing temperature.

We prepared $Fe_{80}Cu_{20}$ alloy powders by mechanically alloying mixtures of Fe and Cu powders in a SPEX-8000 mill using hardened steel vials. The milling charges were 8 g of powder and 32 g of ¼-in.-diam H-440 steel balls. The weight of the powder recovered after 30 h of MA was within ± 0.1 g of the starting weight, and this indicated that the composition of the alloyed powder was within 1.5% of the starting composition.

Figure 3 shows X-ray diffraction patterns from mechanically alloyed $Fe_{80}Cu_{20}$ powder after annealing at the stated temperatures for

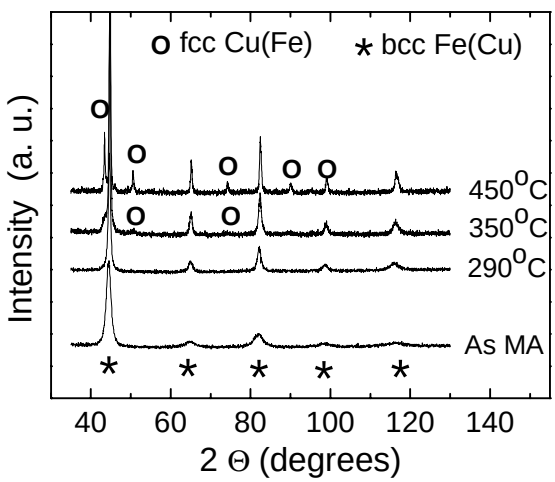

Figure 3. X-ray diffraction patterns of $Fe_{80}Cu_{20}$ powder prepared by mechanical alloying and after annealing for 1 h at various temperatures.

1 h. The as-processed powder is single-phase *bcc* and this metastable structure is preserved up to the annealing temperature of 290ºC. Following anneals at higher temperatures, the alloy separates into Fe-rich *bcc* and Cu-rich *fcc* phases.

The influence of annealing temperature on coercivity, crystallite size, and root mean square (RMS) residual strain is shown in

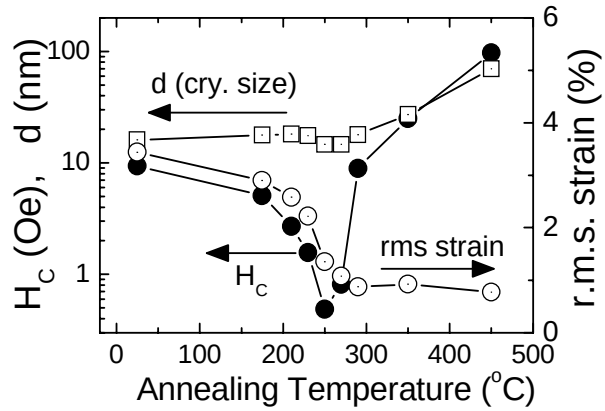

Figure 4. Coercivity, H_C, crystallize size, d, and RMS strain as a function of annealing temperature in mechanically alloyed $Fe_{80}Cu_{20}$ powder.

Figure 4. The crystallite size and the RMS strain were determined from the shapes of the Bragg peaks in Figure 3. Crystallite size is constant at 17 nm up to an annealing temperature of 290ºC. However, for the same annealing temperature range, the RMS residual strain and H_C decrease significantly. The lowest coercivity (0.5 Oe) was obtained after annealing the $Fe_{80}Cu_{20}$ powder for 1 h at 250ºC. Annealing at higher temperatures causes grain growth (as seen in Figure 4) and phase separation (as seen in Figure 3). Both effects increase H_C by providing additional obstacles to the motion of the domain walls. In the range 250 to 290ºC, the crystallite size and the RMS strain remain approximately constant whereas H_C increases rapidly. This suggests that the coercivity increase is due mainly to phase separation, which is only detectable by X-ray diffraction at the higher annealing temperature of 350ºC, when the volume fraction and domain size of the *fcc* phase are large enough to give a discernible X-ray signal. This study demonstrates that obtaining low H_C values in mechanically alloyed powder requires (1) starting from crystallite sizes below approximately 20 nm and (2) a careful annealing treatment that reduces the residual stresses while avoiding phase separation and grain growth. The saturation magnetization of the

Table 2. Coercivity in nanocrystalline alloy powders prepared by mechanical alloying

Material	Treatment	H_C (Oe)	Reference
$Fe_{50}(SiC)_{50}$	MA (various times)	154–320	18
Fe-M (M=Zr,Hf,Co,Si)	MA & anneal	57–6.6	19
$Fe_{100-x}M_x$ (M = Co or Ni, x = 0-100)	MA & anneal	5.1–56	20
$Fe_{100-x}M_x$ (M = Al, Si, Cu, x = 0-50)	MA	3.8–50	21
$Fe_{86}Zr_7B_6Cu_1$	MA + anneal	7.5	22
$Fe_{86}Zr_7B_6Cu_1$	MA & anneal	14–7	23
$Fe_{80}M_{10}C_{10}$ (M = Ta,Hf,W,Mo,Nb,Zr,Ti)	MA & anneal	194–3.8	24
Ni_3Fe	MA & anneal	22–7	25
$Fe_{75}Al_{12.5}Ge_{12.5}$	MA & anneal	37-21	25
Ni_3Fe	MA (various times)	33-73	26
$Fe_{90}W_{10}$	MA (various times)	11–44	27
$Fe_{100-x}Co_x$ (x = 0-80)	MA & anneal.	6.3–17	28
$Fe_{100-x}Si_x$ (x = 0-40)	MA & anneal	74–2.4	29
Fe-(Co,Ni)-Zr-B	MA + anneal	15–44	30
$Fe_{50}Cu_{50}$	as-MA	40	31
$Fe_{50}Cu_{50}$	MA + anneal @ 820 K	300	31
$Fe_{51}Cu_{49}$	as-MA	8	32
$Fe_{51}Cu_{49}$	MA + anneal @ 723 K	640	32
$Fe_{51}Cu_{49}$	MA + anneal @ 923 K	200	32
$Fe_{50}Cu_{50}$	MA (140 h)	110	33
$Fe_{50}Cu_{50}$	MA (440 h)	29	33
$Fe_{50}Cu_{50}$	MA + anneal @ 600 K	29–160	34
$Fe_{50}Cu_{50}$	as-MA	316	35
$Fe_{66}Cu_{34}$	as-MA	289	35
$Fe_{75}Cu_{25}$	as-MA	273	35
$Fe_{90}Cu_{10}$	as-MA	258	35

18. T. D. Shen, K. Y. Wang, M. X. Quan, and J. T. Wang, *J. Mater. Sci. Lett.* **11**, 1576 (1992).
19. N. Kataoka, K. Suzuki, A. Inoue, and T. Masumoto, *J. Mater. Sci.* **26**, 4621 (1991).
20. C. Kuhrt and L. Schultz, *J. Appl. Phys.* **73**, 6588 (1993).
21. C. Kuhrt and L. Schultz, *IEEE Trans. Magn.* **29**, 2667 (1993).
22. R. Schäfer, S. Roth, C. Stiller, J. Eckert, U. Klement, and L. Schultz, *IEEE Trans. Magn.* **32**, 4383 (1996).
23. C. Stiller, J. Eckert, S. Roth, R. Schäfer, U. Klement, and L. Schultz, *Mater. Sci. Forum* **225-227**, 695 (1996).
24. C. Kuhrt, *J. Magn. Magn. Mater.* **157/158**, 235 (1996).
25. H. N. Frase, R. D. Shull, L. B. Hong, T. A. Stephens, Z. Q. Gao, and B. Fultz, *NanoStru. Mater.* **11**, 987 (1999).
25. C. N. Chinnasamy, A. Narayanasamy, K. Chattopadhyay, and N. Ponpandian, *NanoStru. Mater.* **12**, 951 (1999).
26. M. Kis-Varga, D. L. Beke, and L. Daróczi, *Mater. Sci. Forum* **343-346**, 841 (2000).
27. Y. D. Kim, J. Y. Chung, J. Kim, and H. Jeon, *Mater. Sci. Eng. A* **291**, 17 (2000).
28. J. Ding, Y. Li, L. F. Chen, C. R. Deng, Y. Shi, Y. S. Chow, and T. B. Gang, *J. Alloys Comp.* **314**, 262 (2001).

29. Y. J. Liu, I. T. H. Chang, and M. R. Lees, *Scripta Mater.* **44**, 2729 (2001).
30. A. Hernando, P. Crespo, J. M. Barabdiaran, A. García Escorial, and R. Yavari, *J. Magn. Magn. Mater.* **124**, 5 (1993).
31. P. Crespo, A. Hernando, R. Yavari, O. Drbohlav, A. García Escorial, J. M. Barabdiarán, and I. Orúe, *Phys. Rev. B* **48**, 7134 (1993).
32. O. Drbohlav and A. R. Yavari, *J. Magn. Magn. Mater.* **137**, 243 (1994).
33. O. Drbohlav and A. R. Yavari, *Acta Metall. Mater.* **43**, 1799 (1995).
34. B. Majumdar, M. M. Raja, A. Narayanasamy, and K. Chattopadhyay, *J. Alloys Comp.* **248**, 192 (1997).

mechanically alloyed $Fe_{80}Cu_{20}$ powder, measured on a SQUID apparatus at an applied field of 50 kOe, was 1.8 T. M_S remained approximately constant during the annealing treatment.

To prepare laminas of potential use in the manufacture of transformers, the mechanically alloyed $Fe_{80}Cu_{20}$ powder must be consolidated into fully dense laminas. Residual porosity will create pinning centers and thus will increase the coercivity and decrease the permeability of the laminas. Achieving full density is difficult because the mechanically alloyed $Fe_{80}Cu_{20}$ particles have high hardness, in excess of 5 GPa [16], and the consolidation must be done at T < 250ºC. We investigated the consolidation of the mechanically alloyed $Fe_{80}Cu_{20}$ powder by ECAE. This technique consists of pushing a square cross-section ingot through a die having a 90-degree bend. At the bend, the ingot is sheared by 100%. Because the ECAE extrusion preserves the cross section of the product, repeated shearing can be used to accumulate larger strains. In a previous study, we demonstrated that mixtures of Cu and Ag powders consolidated by ECAE were 100% dense [17].

We encapsulated the as-mechanically alloyed $Fe_{80}Cu_{20}$ powder in 0.9 × 0.9 × 4 in.^{3} copper cans. Lids were sealed to the cans by e-beam welding. The encapsulation process was done inside an Ar-filled glovebox (oxygen content below 1 ppm) to avoid exposing the powder to air. Each copper can containing the powder was given a single ECAE pass at room temperature, after which the compacted $Fe_{80}Cu_{20}$ ingot was removed by machining away the Cu can. The relative density of the ECAE-compacted powder was only 72%. This low relative density was attributed to the elevated hardness of the mechanically alloyed $Fe_{80}Cu_{20}$ powder. As a consequence, during ECAE the particles tend to roll past each other rather than deform and cold weld, as is the case when extruding mixtures of low-hardness Cu and Ag powder. A small toroid-shape ferromagnetic core was fabricated from this ECAE ingot, to which we added primary and secondary coils. The miniature transformer was then annealed at 260ºC for 1 h.

Figure 5 shows the dc hysteresis curve measured on the toroidal core made from $Fe_{80}Cu_{20}$ consolidated by ECAE. The hysteresis curve is almost closed, except at low values of the applied field, where the hysteresis curve opens, giving a coercivity of 4 Oe. The area inside the hysteresis curve is 10680 Gauss·Oe. This product corresponds to an energy loss per cycle of 0.125 J/kg. The low permeability of the material, approximately 25 μ_o, is a direct consequence of its low relative density. This material has potential use for the manufacture of magnetic chokes and transformers for flyback converters, especially if the hysteresis losses are further reduced by removing the residual macrostresses developed during the toroid manufacture.

Discussion

Bulk ferromagnetic metallic glasses of the type Fe-*M*-*m*, where *M* is one or more of the transition metals Co, Ni, Ga, Cr, Mo, and *m* is a metalloid such as B, P, or C, exhibit excellent magnetic properties, especially extremely low coercivity. The main

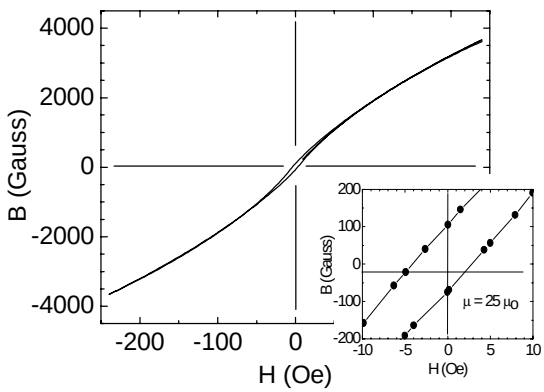

Figure 5. Hysteresis B-H curve for mechanically alloyed $Fe_{80}Cu_{20}$ powder consolidated by equal-channel angular extrusion and annealed for 45 min at 160°C.

limitation of these bulk ferromagnetic glasses is their relatively low saturation magnetization (about half that of oriented polycrystalline Fe-3 wt % Si). Researchers are investigating bulk glasses that contain no Cr or Mo, because these elements lower the Curie temperature [18,19] and thus also lower the saturation magnetization at near room temperature. The extremely low coercivity of the present bulk glasses, coupled with their good mechanical strength (which was not discussed here) makes them attractive for applications such as sensors, magnetic delay lines, and transducers.

Although bulk glasses and crystalline alloys have quite different short-range ordering, amorphous alloys exhibit long-range ferromagnetic ordering. As for crystalline alloys, the magnetic behavior of amorphous alloys depends strongly on residual strain. Obtaining coercivities in the range of 10^{-3} Oe requires removing residual stresses developed during the quenching process. The same is true for nanocrystalline alloys. Nanocrystalline $Fe_{80}Cu_{20}$ powders prepared by MA have low coercivity only after most of the residual stress has been reduced by annealing. The annealing temperature-time window is rather narrow because the *bcc* $Fe_{80}Cu_{20}$ alloy is metastable and thus tends to phase separate. Annealing the powder removes microstresses, those existing within each powder particle. After the powder has been consolidated into laminas or toroids, the product also has macro stresses. It is unlikely that long-range residual stresses can be effectively reduced by annealing within the same temperature window used to reduce the microstresses. Future research in this field should address alloy compositions such as $Fe_{(1-x-y)}Al_xSi_y$, where x and y can be chosen to minimize the magnetostriction.

Acknowledgement

This work was supported by the Office of FreedomCar and Vehicle Technologies of the U.S. Department of Energy.

References

1. U.S. Department of Energy "Annual Energy Review 2001," from www.eia.DOE.gov.

2. R.C. O'Handley, L.I. Mendelsohn, R. Hasegawa, R. Ray, and S. Kavesh, *J. Appl. Phys.* **47**, 4660 (1976).

3. A. Inoue, K. Ohtera, K. Kita, and T. Masumoto, *Jap. J. Appl. Phys.* **27**, L2248 (1988).

4. A. Peker and W. J. Johnson, *Appl. Phys. Lett.* **63**, 2342 (1993).

5. Y. He, J. I. Archuleta, and R. B. Schwarz, *Appl. Phys. Lett.* **69**, 1861 (1996).

6. T. D. Shen and R. B. Schwarz, unpublished results, Los Alamos National laboratory, 2003.

7. A. Inoue and J. S. Gook, *Mater. Trans. JIM* **36**, 1180 (1995).

8. T. D. Shen and R. B. Schwarz, *Appl. Phys. Lett.* **75**, 49 (1999).

9. A. L. Greer, *Nature* **366**, 303 (1993).

10. A. Kojima, H. Horikiri, Y. Kamamura, A. Makino, A. Inoue, and T. Matsumoto, *Mater. Sci. Eng. A* **179/180**, 511 (1994).

11. Y. Yoshizawa, S. Oguma, and K. Yamauchi, *J. Appl. Phys.* **64**, 6044 (1988).

12. R. M. Bozorth, "Ferromagnetism," van Nostrand, New York (1951).

13. G. Herzer, *Scripta Metall. Mater.* **33**, 1741 (1995).
14. J. S. Benjamin, *Sci. Amer.* **234**, 40 (1976).
15. J. Eckert, R. Birringer, J. C. Holzer, C. E. Krill, and W. E. Johnson, *Mat. Res. Soc. Symp. Proc.* **238**, 739 (1992).
16. T. D. Shen and C. C. Koch, *Acta Mater.* **44**, 753 (1996).
17. R. B. Schwarz, J. I. Archuleta, G. Korth, J. Macheret, and T. Lillo, unpublished results, Los Alamos Naional Laboratory (2002).
18. M. Oliver, J. O. Strom-Olsen, and Z. Altounian, *Phys. Rev. B* **35**, 333 (1987).
19. H. J. V. Nielsen, *Solid State Comm.* **30**, 239 (1979).

D. Equal Channel Angular Extrusion Processing of Alloys for Improved Mechanical Properties

Principal Investigator: Thomas M. Lillo
Idaho National Engineering and Environmental Laboratory
MS2218, P.O. Box 1625, Idaho Falls, ID 83415-2218
(208)526-9746; fax: (208)526-4822; e-mail: tml@inel.gov

Technology Development Area Specialist: Sidney Diamond
(202) 586-8032; fax: (202) 586-1600; e-mail: sid.diamond@ee.doe.gov
Field Technical Manager: Philip S. Sklad
(865) 574-5069; fax: (865) 576-4963; e-mail: skladps@ornl.gov

Contractor: Idaho National Engineering and Environmental Laboratory
Contract No.: DE-AC07-99ID13727

Objective

- Investigate equal channel angular extrusion (ECAE) as a deformation processing technique to improve material properties such as strength, formability, fatigue, and corrosion properties.
- Produce advanced, lightweight materials with enhanced formability, higher strength-to-weight ratio, and higher stiffness, ultimately leading to reductions in vehicle weight and thus more fuel-efficient vehicles.

Approach

- Modify the existing ECAE die at Idaho National Engineering and Environmental Laboratory and the furnace design as necessary to allow processing of a magnesium alloy (ZK60A) and an aluminum metal matrix composite (AL6061+B_4C).
- Use ECAE to process materials and a variety of ECAE processing parameters such as processing temperature, number of passes through the die, processing route, and processing speed.
- Characterize the microstructure and mechanical properties of the ECAE-processed material.
- Use microstructure and mechanical property data to model the flow stress of materials processed with ECAE.

Accomplishments

- Modified ECAE die to allow the application of a back stress in the material during ECAE processing.
- Used ECAE to process ZK60A and AL6061+10 wt % B_4C materials under a variety of conditions.
- Characterized microstructure and mechanical properties of ECAE-processed material.
- Characterized mechanical properties of various brasses that had been ECAE processed and annealed in support of flow-stress modeling work.

Future Direction

- Optimize ECAE parameters for ZK60A alloy to obtain maximum superplastic behavior.

- Optimize ECAE parameters for AL6061 + B_4C composites to uniformly distribute the B_4C particulate in the alloy and maximize room temperature ductility.
- Modify ECAE furnace and ECAE process a titanium alloy and titanium alloy composite for increased ductility.
- Continue ECAE processing of materials and their characterization in support of flow-stress modeling.

Introduction

The weight of a structural component is determined by the load it must withstand and the yield strength of the material from which it is made. Materials with a higher strength-to-weight ratio can significantly reduce the weight of structural components in vehicles and provide increased fuel efficiency. In general, the strength of metals and alloys can be increased through reductions in the scale of the microstructure (e.g., grain size, second phase particles). Deformation processing (e.g., rolling, forging) increases strength but also reduces ductility. An annealing heat treatment is often required to bring the material back to a state of reasonable ductility at the expense of a slight reduction in yield strength. Materials subjected to higher levels of deformation strain can be annealed at lower temperatures and possess a finer final grain size and high yield strength. The goal of this project is to use deformation processing to develop high-strength, lightweight materials with reasonable ductility for applications in vehicles. This type of processing will reduce overall vehicle weight and, thereby, improve fuel efficiency.

ECAE is a relatively new deformation processing technique that imparts a great deal of deformation to a work piece without changing the cross-section of the work piece. The work piece enters the ECAE die and is forced into the exit channel (having the same dimensions as the entrance channel) that is at some prescribed angle to the entrance channel, typically 90º (see Figure 1). As the work piece moves from the entrance channel to the exit channel it undergoes a large amount of deformation strain (approaching e = 1, for a 90º intersection of the entrance and exit channels). Because the cross-section remains unchanged, it can be passed through the die repeatedly to accumulate strains greater than e = 20. The thickness of a material would have to be reduced by >99% to achieve a similar strain level by conventional rolling. Furthermore, since the cross-section remains relatively unchanged, the sample can be rotated prior to subsequent passes to obtain different strain paths and potentially different final microstructures and properties (see Figure 2).

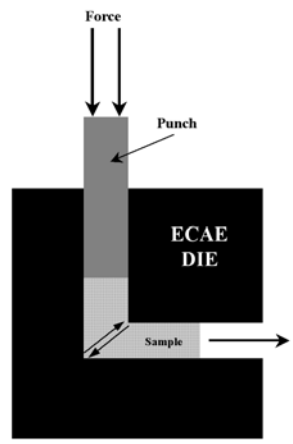

Figure 1. Schematic of ECAE processing.

ECAE processing of simple metals and alloys was investigated during the previous years of this project. The goal of those investigations was to gain an understanding of the ECAE process and the effect of the various ECEA-processing parameters on the

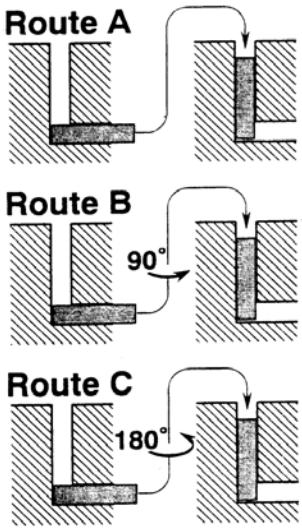

Figure 2. Schematic illustrating sample rotation between subsequent passes through the ECAE die.

resulting microstructure and mechanical properties. The main conclusions revealed by those studies were

- The microstructure is drastically affected during initial passes through the ECAE die and reaches, more or less, a steady state configuration after four passes.
- The route used during multiple-pass ECAE processing produced only small differences in microstructure and mechanical properties.
- ECAE processing could be used to impart high strains (e > 10) to ductile materials.
- Recrystallization of ECAE-processed materials occurred at relatively low temperatures and, typically, the recrystallized grain size was on the order of 1 μm.
- Materials with a low-to-moderate stacking fault energy recrystallized with a very high fraction of twin-related grains (approaching 50%).
- The microstructure of commercially pure metals could not be refined into the nano-crystalline regime by ECAE processing.
- Microstructure developed by the formation of dislocation subcells. The misorientation across the subcell boundaries increased as the number of passes through the ECAE die increased. The development of high-angle grain boundaries required a high number of passes (>10) through the ECAE die.
- Materials of limited ductility tend to fail during ECAE process by either cracking or macroscopic shear banding.
- Finite element modeling (FEM) of the ECAE process shows that significant tensile forces develop on the upper surface of the sample and can cause cracking.
- Application of a back stress on the exiting sample reduces the magnitude of the tensile stresses. If the back stress is large enough, low ductility samples can be ECAE processed without failure.
- Back stress allows the ECAE processing temperature to be lowered, resulting in greater microstructural refinement.

Based on these conclusions, the research during FY 2003 was focused on lightweight alloys with potential vehicle applications. Such alloys typically suffer from low stiffness and formability. The magnesium alloy, ZK60A, was chosen for study with the goal of developing a superplastic material for low-temperature, high strain rate forming. ECAE-processing of this alloy at relatively low temperature (~150ºC) with back stress resulted in a very uniform and fine microstructure with a grain size on the order of 1–2 μm. The superplastic properties were investigated during FY 2003.

The other material studied during FY 2003 was an aluminum alloy metal matrix composite, AL6061+B_4C particulate. Particulate metal matrix composites are made by either consolidation of powders or through additions of particulate to the molten matrix,

which is then solidified. Inhomogeneous distribution of the particulate phase result in poor ductility and an elastic modulus that is less than that predicted by the rule of mixtures. The high-shear strains in ECAE processing should be able to break up agglomerates of particles and redistribute them more evenly throughout the matrix, with a significant improvement in elastic modulus and ductility.

Work in suport of the effort to model the flow stress of metals and alloys also continued during FY 2003. It was realized early on in this project that ECAE could be used to produce very fine grain-size materials—finer than previously obtained by rolling, for instance. This afforded the opportunity to study the relationship between flow stress and grain size at previously unobtainable small values of grain size. The relationship was studied over a wide range of grain sizes (2–200 μm). It was expected that the flow stress would depend on reciprical square root of the grain size, in accordance with theories of grain boundaries as barriers to dislocation movement (i.e., Hall-Petch theory) or as sources for dislocations (theories of Li, Price, and Hirth). However, the flow-stress data for the wider range of grain sizes studied in this work suggested flow stress varied as the reciprocal of grain size and not the reciprocal square root of grain size. A better fit to the data was obtained when the flow stress was plotted against reciprocal of twin grain-boundary spacing suggesting twin grain boundaries were acting as the source of dislocations. The main conclusion of that work is that grain size is only important at the onset of plastic flow and that subsequent strain hardening is independent of grain size; that is, grain boundaries provide an initial source of dislocations but do not participate in strain hardening, only dislocation or dislocation interactions produce strain hardening. A series of brasses, with systematically varying stacking fault energy were ECAE processed, annealed, and evaluated for mechanical properties in support of the modeling work of flow stress.

ECAE Processing of Magnesium Alloys

Two magnesium alloys were used for this study, one was commercial grade ZK60A (Mg-5% Zn – 0.5% Zr) and an experimental magnesium alloy provided by Dr. Daniel Shechtmen, located at the National Institute of Standards and Technology (NIST). (Dr. Shechtmen's alloy is basically ZK60A with additions of 0.5 wt % Ce and 0.5 wt % Y. These additions result in the formation of quasi-crystals that strengthen the alloy.) The goal for the commercial ZK60A was to reduce the grain size to obtain superplastic properties; while the goal for the Shechtmen alloy was to break up and redistribute the quasi-crystalline phase.

Commercial ZK60 samples were ECAE processed using three different sets of parameters:

- 4 passes by the B-route at 260ºC and no applied back stress
- 4 passes by the B-route at 150ºC and 18.3 ksi back stress
- 6 passes by the B-route at 150ºC and 18.3 ksi back stress

The ECAE processing temperature had to be raised to 260ºC on the first sample to avoid failure of the billet during processing without back stress. Figure 3 compares the microstructure as a function of temperature. It is obvious from this figure that ECAE leads to a refinement in microstructure with the refinement being more dramatic at lower processing temperatures. The application of a back stress allowed processing at lower temperatures to obtain greater microstructural refinement.

Table 1 shows the results of elevated temperature tensile tests on the ECAE-processed and as-received ZK60A for two relatively rapid strain rates, 10^{-3}/s and 10^{-2}/s. The as-received material does not show extensive ductility at a strain rate of 10^{-3}/s. ECAE processing increases the ductility

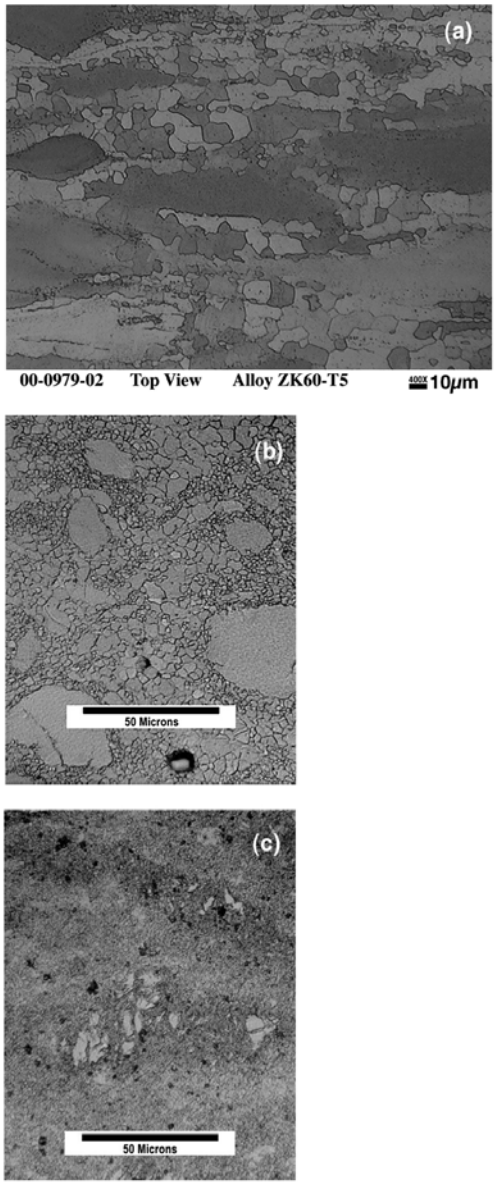

Figure 3. Effect of ECAE processing on the microstructure of commercial ZK60A.

significantly. Increasing the number of passes through the ECAE and lowering ECAE processing temperature results in increased ductility at a strain rate of 10^{-3}/s. This can be directly related to the greater microstructural refinement obtained at lower ECAE processing temperatures, shown in Figure 3. The values for ductility at 200ºC are somewhat lower than found in the literature (422% at 10^{-3}/s by H. Wantanabe, et al.)[1] for ZK60-processed 8B passes at 160ºC. It is assumed that the higher number of passes in that work is responsible for the greater ductility.

Table 1. Tensile properties of ECAE-processed, commercial ZK60A at 200ºC

	As-received	4B, 260ºC, 0 ksi	4B, 150ºC, 18.2 ksi	6B, 150ºC, 18.2 ksi
Strain rate = 1 × 10^{-2}/s				
Yield strength, MPa	N/A	84	70	65
UTS	N/A	95	73	71
Ductility	N/A	87	142	121
Strain rate = 1 × 10^{-3}/s				
Yield strength, MPa	115	77	28	32
UTS	130	78	33	51
Ductility	60	91	60*	223

*Sample failed prematurely at an internal flaw

The results of ECAE processing the modified ZK60A alloy containing quasi-crystals followed those of the commercial ZK60A. However, ECAE processing was modified to account for the increased strength of this alloy. The first two passes were carried out at 250ºC with 9.8 ksi back stress to break up the quasi-crystalline phase on the grain boundary. The ECAE processing temperature was then lowered (200ºC with 11.2 ksi back stress) for the remaining four passes to further refine the microstructure. Figure 4 shows the microstructure (a) before and (b) after ECAE processing. The quasi-crystalline phase is the bright phase in these photomicrographs. ECAE processing of this alloy resulted in the break up and redistribution of the quasi-crystalline grain boundary phase. Quasi-crystalline particles located at the interior of the grains seemed to be unaffected by ECAE processing. Additional reduction of the ECAE temperature is expected to aid in the break up and redistribution of the quasi-crystalline phase.

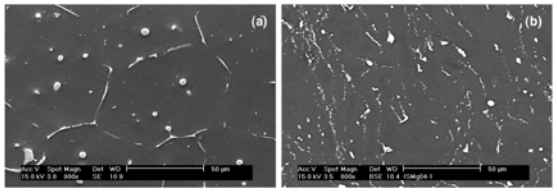

Figure 4. Microstructure of modified ZK60A containing quasi-crystals, as-received (left) and after ECAE processing.

Table 2 shows that the elevated temperature tensile properties of the modified ZK60 alloy exceed those of the commercial ZK60A material (see Table 1 for comparison). The presence of the quasi-crystalline phase increased the strength of the alloy by almost a factor of two. The modified alloy also exhibits greater ductility (~35% greater at 10^{-2}/s and ~14% at 10^{-3}/s). It appears that this alloy has a better potential for high strain rate superplasticity. ECAE processing parameters will be optimized during FY 2004.

Table 2. Tensile properties of ECAE-processed, modified ZK60A (w/quasi-crystals) at 200ºC

ECAE conditions	2B, 250ºC, 9.8 ksi + 4B, 200ºC, 11.2 ksi
Strain rate = 1 × 10^{-2}/s	
Yield strength, MPa	115
UTS, MPa	124
Ductility, %	185
Strain rate = 1 × 10^{-3}/s	
Yield strength, MPa	56
UTS, MPa	72
Ductility, %	260

ECAE Processing of Aluminum Alloy Composites

Prototype metal matrix composites were purchased from Dynamet Technology, Inc. The material consisted of an Al6061 matrix with boron carbide particles (~50 µm in diameter on average) present at a level of either 10 or 20 wt %. Additions of ceramic particles increase the stiffness of the AL6061 matrix, making it more suitable for use in lightweight structural applications. The material was fabricated by powder metallurgy methods and contained agglomerates of boron carbide particles. The B_4C particles appeared to be concentrated around prior aluminum alloy powder particles (see Figure 5a). The interface between adjacent B_4C particles is very weak and acts as a defect during tensile loading, causing premature fracture. The elongation/ductilty of these composites is negligible in the as-received state. ECAE processing (4A passes at 300ºC, no back stress, and 4A passes at 150ºC and 21 ksi back stress) was performed to break up B_4C agglomerates and isolate the particles in the AL6061 matrix.

Figure 5 shows the effect of ECAE processing on the B_4C distribution. Relatively

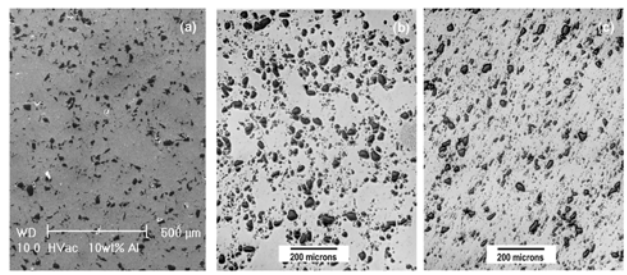

Figure 5. Microstructure of AL6061 + 10 wt % B_4C.

high processing temperatures are required to prevent billet failure (i.e., cracking or shear failure) if a back stress is not imposed on the billet during ECAE processing. The high processing temperature increases the ductility but also reduces the strength of the matrix. The results suggest that the very hard particles are rolling in a soft matrix, somewhat analogous to marbles in bread dough. During deformation, the marbles simply get pushed around in the dough. If the temperature is lowered and a back stress is imposed, the strength of the matrix increases and greater load transfer to the hard particles occurs. The result is better distribution of the particles in the boron carbide agglomerates (see Figure 5, the 4A, 150ºC, 21 ksi sample). It also appears that ECAE processing at low temperature with a back stress has closed residual porosity observed in the as-received material.

Table 3 shows the tensile properties of the ECAE-processed samples. The as-received

Table 3. Tensile properties of ECAE-processed AL6061 and AL6061+10 wt % B_4C

	AL6061-T4 (no B_4C)	
ECAE conditions	4A, 24°C, 0 ksi	4A, 300°C, 0 ksi
Yield strength, MPa	130	116
Ultimate strength, MPa	250	242
Elongation, %	37.5	41.8
Density*, g/cm^3 (%)	N/A	N/A
Elastic modulus, MPa**	N/A	N/A

	AL6061+10 wt % B_4C-T4	
ECAE conditions	4A, 300°C, 0 ksi	4A, 150°C, 21 ksi
Yield strength, MPa	130	146
Ultimate strength, MPa	209	250
Elongation, %	6.0	12
Density*, g/cm^3 (%)	2.61 (97)	2.56 (95)
Elastic modulus, MPa**	75400	78,600

* Theoretical density of AL6061+10 wt % B_4C is 2.69 g/cm^3.
**Elastic modulus for commercial AL6061-T4 is 70250 MPa, and the theoretical modulus for AL6061+ 10 wt % B_4C is ~110,000 MPa.

material broke during machining of tensile bars, suggesting that the as-received material has very poor properties. The tensile bars of the ECAE-processed material were heat treated on the B_4C distribution can be directly assessed. The table suggests that ECAE processing returns the yield and ultimate tensile stresses back to at least the values of commercial AL6061 without particulate additions. The composite still exhibits significantly less ductility than AL6061, but it is significantly more ductile than most metal matrix composites that typically exhibit insignificant ductility. Furthermore, Table 3 shows that higher ECAE processing temperatures are better for eliminating residual porosity, thereby increasing the density, but results in a lower elastic modulus than ECAE processing at lower temperatures. (The elastic modulus was determined by ultrasonic techniques.) However, it should be noted that the elastic modulus still is well below the theoretical elastic modulus of ~110,000 MPa determined with the rule-of-mixtures. Therefore, it appears that an ECAE-processing scheme utilizing initial passes at relatively high temperature followed by passes at lower temperatures may optimize density and elastic modulus.

The results have intrigued Dynamet Technology, Inc., and it is providing more material at cost for FY 2004. If further results on the AL6061+B_4C system support the results presented here, it wishes to explore ECAE processing on titanium alloy metal matrix composites for structural applications.

Modeling Flow Stress

Work in support of flow-stress modeling consisted mainly of tensile testing of materials previously ECAE processed. The effect of twin grain-boundary content on flow-stress behavior was investigated by ECAE processing commercially pure copper at different temperatures by the same route (4 passes by a modified B route with an applied back stress). Tensile specimens were then fabricated and annealed at various temperatures. Table 4 presents the tensile results, ECAE-processing conditions, and the annealing temperatures. Generally, higher ECAE-processing temperatures lower yield strength. The grain size and twin grain-boundary density remain to be characterized before the tensile results can be fully analyzed.

Also the effect of stacking fault energy on flow-stress behavior was studied. During FY 2003 two ECAE-processed brasses with 5 and 10% Zn, respectively, were evaluated for tensile properties. Billets of each composition were subjected to ECAE processing with and

Table 4. Tensile properties of ECAE-processed copper

Sample ID	ECAE conditions	Annealing temperature, °C	Yield strength, MPa	Ultimate strength, MPa	Elongation, %
Cu140 -1	24°C, 4 pass, 5.6 ksi	None	405	431	23
-2	"	300	115	252	63
-3	"	400	54	228	60
-4	"	500	27	224	65
Cu141 -1	125°C, 4 pass, 5.6 ksi	None	378	398	20
-2	"	300	110	247	63
-3	"	400	60	236	60
-4	"	500	30	219	75
Cu142 -1	150°C, 4 pass, 5.6 ksi	None	353	374	23
-2	"	300	97	247	58
-3	"	400	63	230	60
-4	"	500	28	220	73
Cu143 -1	225°C, 4 pass, 5.6 ksi	None	223	291	34
-2	"	300	71	239	65
-3	"	400	54	226	65
-4	"	500	27	224	87

without back stress. ECAE processing corresponded to one of the two following processing schemes:

- 2C passes @ 24°C, anneal 600°C, 1 h, 4A passes @ 24°C, 0 ksi
- 2B passes @ 24°C, anneal 600°C, 1 h, 4B passes @ 24°C, 5.6 ksi

The intermediate annealing treatment was performed to eliminate Zn segregation that developed during casting of the as-received materials. Previously, it was found that heat treatment of ECAE-processed brass at 600°C for 1 h was sufficient to eliminate Zn segregation. Tensile bars were made and tested. However, characterization of the microstructure (grain size and twin grain-boundary fraction) remains before analysis of the data can be completed.

Finally, during FY 2003 a subcontract with Dr. David Field at Washington State University was placed to study the behavior of twin grain boundaries during deformation. As mentioned above, it appears twin grain boundaries act as dislocation sources during deformation. However, this has been a matter of debate for a number of years. Dr. Field was given the task to obtain direct evidence of twin grain boundaries acting as dislocation sources. Dr. Field used orientation imaging microscopy (OIM) to track the misorientation across twin related grain boundaries during deformation of annealed, ECAE-processed copper. Twin grain boundaries acting as dislocation sources will cause the orientation relationship of twin related grains to deviate from the ideal 60° rotation about the <111> direction. Dr. Field did observe the growth and disappearance of some twin related grains. Furthermore he documented a change in misorientation across the twin boundary as deformation proceeded. The results and conclusions of his study are being written up and submitted to a peer-reviewed journal for publication.

Conclusions

The work performed during FY 2003 yielded some promising results and potential uses of ECAE. Generally, it was found that ECAE processing at temperatures as low as possible produced material with the most desirable properties. An applied back stress on the sample during ECAE processing enabled the processing temperature to be reduced. Specifically, ECAE processing was used to refine the microstructure of two magnesium alloys and obtain high ductility (>200%) at moderate temperatures (200°C). Further optimization of the ECAE-processing schedule should allow superplastic forming of these alloys at relatively low temperatures (~200°C) and fairly high strain rates (10^{-2}/s or greater). High strain-rate forming capabilities will allow these lightweight magnesium alloys to be

more economically competitive (high production rate coupled with minimal scrap) with other traditional structural materials such as steel.

ECAE processing was also found to be effective for breaking up grain boundary phases and redistributing second phases. The extent of the effect is governed by the ECAE-processing temperature which controls the strength of the matrix. Hard particles in soft matrix are simply "pushed around" during ECAE processing. Stronger matrices generally afford the break up and redistribution of second phases. Again, lower ECAE processing temperatures are most desirable.

The redistribution of second phases during ECAE was found to be extremely beneficial in an aluminum alloy metal matrix composite (AL6061 + 10 wt % B_4C). ECAE processing at relatively low temperatures (~150ºC) effectively breaks up agglomerates of boron carbide particles in the as-received material. As a consequence, the ductility of the composite was greatly enhanced; that is, <1% in the as-received material to around 12% in the ECAE-processed material. ECAE processing of this composite produced a lightweight material with relatively high stiffness (~78,600 MPa) for an aluminum alloy. Optimization of the ECAE-processing parameters is expected to further increase the mechanical properties of this alloy as well as other lightweight titanium alloy composites.

Overall the main conclusion reached during FY 2003 was that mechanical properties received the most benefit when ECAE processing was carried out at the lowest possible temperature. Low ECAE-processing temperature (without sample failure) could only be achieved through the application of a back stress on the sample during processing. This result has and will allow us to ECAE process a wide variety of material with limited ductility. Materials of limited ductility are commonly found in commercial applications and therefore, ECAE processing of these materials is most relevant.

References

H. Wantanabe, et al., "Low-temperature Superplasticity of a Fine-Grained 2K60 Magnesium Alloy Processed by Equal-Channel-Angular Extrusion," *Scripta Mat.*, **46**, 2002, pp. 851–856.

E. Lightweight High-Strength Steel Alloy Castings for Heavy Vehicle Applications

Principal Investigators: Alan D. Hartman
Albany Research Center
1450 Queen Ave. SW, Albany, OR 97321
(541) 967-5862; fax: (541) 967-5958; e-mail: hartman@alrc.doe.gov

W. L. (Bill) Roberts
PACCAR Technical Center
12479 Farm to Market Road, Mount Vernon, WA 98273
(360) 757-5286; fax: (360) 757-5370; e-mail: broberts@paccar.com

Field Project Manager: Mark T. Smith
Pacific Northwest National Laboratory
902 Battelle Boulevard, Richland, WA 99352
(509) 376-2847; fax: (509) 376-6034; e-mail: mark.smith@pnl.gov

Technology Development Area Specialist: Sidney Diamond
(202) 586-8032; fax: (202) 586-1600; e-mail: sid.diamond@ee.doe.gov
Field Technical Manager: Philip S. Sklad
(865) 574-5069; fax: (865) 576-4963; e-mail: skladps@ornl.gov

---

Contractor: Pacific Northwest National Laboratory
Contract No.: DE-AC06-76RL01830
Contractor: Albany Research Center
Contract No.: 4400000176

Objective

- Develop and demonstrate the unique thin-wall evaporative pattern casting (EPC) technology, also known as lost foam casting, for a selected heavy vehicle chassis or drivetrain component. The project will focus on component design, castability, and performance for the selected vehicle application.

Approach

- Optimize the selected chassis component design.
- Investment-cast the designed component.
- Qualify design by dynamic testing of castings.
- Cast handmade evaporative patterns of component.
- Map the casting chemistry, especially carbon.
- Pursue permanent mold and single-piece evaporative patterns once the casting chemistry is satisfied.
- Cast commercially provided one-piece evaporative patterns.

- Evaluate castings through dynamic testing.
- Transfer thin-wall evaporative steel casting technology.

Accomplishments

- Optimized chassis design using finite element modeling and produced a stereolithographic prototype.
- Cut the stereolithographic prototype in half to facilitate investment molding.
- Produced thin-wall steel investment castings and supplied them to PACCAR.
- Completed dynamic testing resulting in an increase in fatigue life of up to four times over the life of the component currently in commercial use.
- Produced handmade evaporative patterns for proof-of-concept casting trials.
- Made EPCs with four different steel alloys for chemistry mapping.
- Procured a permanent mold for evaporative patterns after chemistry analysis showed that carbon levels could be tolerated with this application and that thin-wall casting is viable.
- Proved that commercially produced one-piece evaporative patterns are beneficial to both the resultant casting carbon chemistry and relative ease of casting with steel.
- Produced steel castings with select thin-wall areas of approximately 0.100 in. thickness by the EPC (lost foam) technology and supplied them to PACCAR for final dynamic testing.

Future Direction

- Evaluate dynamic testing results.
- Transfer the lost foam thin-wall steel casting technology to the commercial sector for this component.
- Evaluate other heavy vehicle components for potential lost foam casting applicability.

Introduction

The Northwest Alliance for Transportation Technologies (NATT) held a forum in late October 1998 with representatives from auto and truck manufacturers, light materials producers, national laboratories, and northwestern universities, among others. The forum provided the opportunity to define research needs and develop contacts for potential cooperative work. Subsequent interactions between the Albany Research Center (ARC) and PACCAR (a heavy-duty Class 8 truck manufacturer) identified areas of research that were appropriate under the NATT program.

Currently, certain aluminum cast components on heavy truck chassis must have thick cross sections in order to meet strength requirements. It would be desirable, not only for dimensional and weight reductions but also from a design standpoint, to replace the thick aluminum castings with thin-walled steel castings. [Although the term “thin-wall” is relative, it is a goal of this project to reduce wall thicknesses in sand-cast steel castings from an industry minimum of about 0.250 inches to 0.080 inches (2 mm)]. Thin-walled steel castings have a potential to increase the strength of a component while maintaining or possibly reducing the weight of an aluminum counterpart.

The EPC process will be used, and the process has demonstrated that thin-section castings can be produced. Pattern draft is minimal, dimensional tolerance and surface finishes approach investment casting quality, and EPC economies are documented, at least in the casting of aluminum.[1–3] The process though, has not been widely used to manufacture steel castings.

In the EPC process, molten metal is poured directly into a polystyrene pattern that is embedded in unbonded sand. The pattern vaporizes, and the metal assumes the pattern's configuration.[4] Each casting requires a new pattern. A partial list of advantages of EPC includes

- elimination of cores
- the option of gluing simple pattern parts together to make a more complex whole
- elimination of sand binders and sand preparation equipment
- reduction of pattern and part draft
- elimination of parting lines
- reduction of post-casting cleaning
- the freedom to orient patterns in molds in a variety of positions to increase options for casting feeding and directional solidification

Although most problems in casting aluminum using the EPC process have been resolved, the techniques for aluminum EPC are not entirely transferable to steel, and additional problems have been encountered. The replacement of a pattern by molten aluminum during pouring is slow, and the pattern and aluminum are in constant contact with one another.[5] When steel is used, however, the pattern tends to evaporate as soon as the hot metal enters the mold.[6] Molds may collapse well before enough metal is available to replace the pattern. Steel castings may be larger than aluminum castings and consequently less rigid. Pattern handling is more difficult, especially if parts have thin walls or rangy sections. Unique casting defects are likely if pattern byproducts are not eliminated before the liquid steel replaces the pattern.

ARC has successfully cast .125-in.-thick, slotted P-900 armor[7] by modifying the EPC process for aluminum casting and adapting it to steel. ARC added three innovations to the EPC process for aluminum to make the adaptation successful:

- Double-walled sand flasks were developed for the application of vacuum to sand molds.
- Continuous narrow-neck feeding systems were used to deliver metal to all casting sections and permit the casting of thin walls.
- Fixtures were designed to prevent pattern damage and to hold critical casting tolerances.

The following steps briefly describe the modified EPC process for steel.

- EPC patterns are constructed by expanding polystyrene beads with pentane (thus eliminating chlorinated fluorocarbons).[8]
- Proper gating and runners are incorporated with the pattern.
- If necessary, to limit distortion, fixtures also are prepared to maintain desired casting contours. The reusable fixtures are easily inserted within a flask along with a pattern. The patterns can be flexed to the fixture contour and attached with string.
- The pattern and fixture are dipped in a slurry of fine silica and binder. Coatings help maintain the integrity of the cavity that results after the pattern evaporates upon pouring and provide a better surface finish.
- The coating is dried, and the pattern is inserted into a vacuum flask. The flask is then filled with unbonded silica sand and vibrated for compaction to make a mold.

The application of vacuum to the mold provides additional flow enhancement to ensure complete pattern filling by effectively increasing the pouring height equivalent to about 1.5 m. The vacuum also collects gases for disposal, adds rigidity to the mold, and prevents cavity collapse. Double-walled molding flasks, the inner walls of which are screened, are used to apply the vacuum. Large-diameter hoses connect the flask with a vacuum system containing a large surge tank. Systems without the surge tank appear to lack sufficient capacity to absorb the surge of gases that are generated when the pattern evaporates. The open top of the flask is sealed with plastic, and the flask is evacuated. A sand pouring basin is placed on the top of the plastic with its opening adjacent to the sprue.

After pouring, the casting is allowed to solidify and cool before removal from the flask. The spent, unbonded sand requires little post-treatment other than cooling before recycling. Casting surfaces are relatively clean, compared with castings made with other processes, because of the absence of sand binders and binder-related defects. The gates can be detached by impact with a hammer. Portions of gating that remain on the casting, although nearly insignificant, can be removed by grinding. The castings can be heat-treated using normal quench and temper cycles.

Casting Component Design

PACCAR identified components for weight reduction or conversion from aluminum. PACCAR performed finite element stress analysis to optimize the distribution of metal without regard to castability, solidification, or any other manufacturing constraints; that is, the component represented an ideal configuration from the perspective of function on a heavy-duty truck.

Therefore, three main questions needed to be researched:

1. Can an optimized component using engineered advantages, such as thin-wall sections, replace existing components at the same or reduced weight while increasing performance?
2. Can the component be cast in steel by the lost foam process and meet specifications?
3. Can a permanent mold be produced incorporating thin- and thick-walled sections to provide a one-piece foam part that can be cast in steel?

To answer question number one, PACCAR provided a stereolithographic prototype created from finite element modeling. This prototype was then used to create an investment mold. Investment steel castings were produced for proof-of-concept testing of the optimized design.

PACCAR expended considerable effort to develop and construct a testing fixture that simulated over-the-road conditions for dynamic fatigue testing of the castings. The castings were tested and proved to last up to four times longer than the current aluminum component. The added benefit was that the steel cast part was equivalent in weight. Therefore, EPC of the component was investigated next.

Evaporative Pattern Casting

The positive outcome of the design allowed us to pursue the question of using EPC. The challenges of lost foam casting with steel included pattern filling in thin-wall sections and carbon pickup being detrimental to performance specifications. Handmade 1.2 lb/ft^3 polystyrene patterns were used for initial testing. The multi-piece patterns were cut, glued at the assembly joints, waxed for casting, and dried.

The pattern was then coated with a ceramic material for protection and surface finish considerations. The dried pattern was next set into a double-walled vacuum flask and buried with loose sand (Figure 1). The

Figure 1. A double wall vacuum flask is being loaded with sand around an embedded foam part for casting.

Figure 2. Molten steel is being poured into a pouring basin feeding a foam pattern within the vacuum flask.

flask was vibrated to compact the sand around the pattern, and the sprue was cut off flush with the top of the flask. A plastic covering was positioned over the sand and sprue top, after which a pouring basin was placed above the sprue before a vacuum was pulled on the flask.

Designed experiments were used to determine the effects, importance, and range of such variables as pouring temperature, vacuum level, sand permeability, sand type and size, and pattern coating. The casting campaign set out to include four different steel alloys cast in triplicate. Casting conditions included a pour temperature of around 3050°F (Figure 2). The patterns were typically cast with 30 in. Hg vacuum, and shakeout occurred 1.5 hours later. Heat treatment included a 45-minute normalized cycle at 1600°F followed by air cooling and then tempering for 45 minutes at 1200°F followed by air cooling.

In general, these observations were made from the handmade foam pattern castings:

- Target melt chemistry was achieved.
- Horizontal pattern filling symmetrically distributed carbon regardless of the alloy.
- Elevated carbon levels were found in the thin sections and in the last areas to fill, with typical carbon increases of approximately 0.45 points.

The success in filling thin sections, along with encouraging carbon pickup levels, showed the feasibility of lost foam casting for this application. Therefore, the decision was made to pursue a permanent mold for the production of one-piece foam patterns.

Permanent Mold

A major challenge presented itself in locating a mold vendor willing to take the risk of producing a mold with very thin wall (~ 0.100 in.) sections in conjunction with thick sections (~0.610 in.). Tempo Plastic Company took the challenge and delivered one-piece foam patterns for casting trials. The one-piece patterns eliminated numerous glue joints that were required in the handmade patterns. However, another variable was added in that the foam pattern density increased to approximately 3.0 lb/ft^3.

The increased foam density did not adversely affect the castability of the pattern or the carbon pickup for steel. In fact, the one-piece foam pattern actually had lower carbon pickup values (approximately a 0.32 point increase) than the handmade patterns. This lower value was attributed to the elimination of the glue and wax joints.

Significant casting results included these:

- Excellent casting surface finish
- Low carbon pickup

- Use of a lower vacuum (12 in. Hg)
- Casting reproducibility

The resulting steel castings were sent to PACCAR for dynamic fatigue testing.

Conclusions

An optimized heavy vehicle component incorporating thin (~0.100 in.) and thick (~0.610 in.) wall sections was designed without regard to castability, solidification, or any other manufacturing constraints. The research has shown that this designed component can be produced out of polystyrene foam and successfully cast using the lost foam casting technique with steel. Dynamic fatigue testing remains to be completed. Results up to this point offer encouragement that the lost foam casting technique can be adapted to steel, making it possible to cast complex structures and thin-wall components.

References

1. P. G. Kohler, "Evaporative Pattern Process: A New Dimension for the Foundry," Modern Casting, August 1981, 36–37.

2. E. Wessman and R. Mrdjenovich, "Update: ECP Goes On Line at Ford's Essex Plant," Modern Casting, March 1985, 30–31.

3. E. F. Longnecker, K. Kanoh, and J. S. Fukuya, "Pioneering Evaporative Foam Iron Casting Production in Japan," AFS Trans., 96, 89–94 (1988).

4. R. Bailey, "Understanding the Evaporative Pattern Casting Process (EPC)," Modern Casting, April 1982, 58–61.

5. S. Shivkumar, L. Wang, and D. Apelian, "The Lost-Foam Casting of Aluminum Alloy Components," Journal of Metals, November 1990, 38–44.

6. Y. A. Stepanov and D. S. Grishin, "Casting Steel in Moulds With Gasifiable Patterns," Russ. Cast. Prod., (Birmingham, Eng.), 1972, 189–192.

7. J. S. Hansen, and P. C. Turner, "Casting P-900 Armorplate by the Expendable Pattern Casting Process," Report of Investigations 9436, U.S. Bureau of Mines, 1992, 1–7.

8. R. H. Immel, "Expandable Polystyrene and Its Processing into Patterns For the Evaporative Casting Process," AFS Trans., 87, 1979, 545–550.

F. Development of an Advanced Squeeze Casting Process for the Production of High-Integrity Truck Components

Principal Investigator: David C. Weiss
Eck Industries, Incorporated
1602 North 8th Street, Manitowoc, WI 54221-0967
(920) 682-4618; fax: (920) 682-9298; e-mail: dweiss@eckindustries.com

Technology Development Area Specialist: Sidney Diamond
(202) 586-8032; fax: (202) 586-1600; e-mail: sid.diamond@ee.doe.gov
Field Technical Manager: Philip S. Sklad
(865) 574-5069; fax: (865) 576-4963; e-mail: skladps@ornl.gov

---

Contractor: Eck Industries, Incorporated
Contract No.: 4000022893

Objective

- Develop the equipment and process technology for an advanced squeeze casting (ASC) process to enable production of high-integrity cast metal components.
  - Integrate the advantages of two casting methods—low-pressure permanent mold and direct squeeze casting—to attain (1) nonturbulent fill of the die, (2) high solidification rates to refine microstructural features, and (3) solidification under pressure to minimize microporosity.
  - Design and build a new kind of casting machine and develop process technologies needed to cast high-integrity truck components from nonferrous alloys.

Approach

- Design and construct a casting machine that integrates a low-pressure metal delivery system suitable for either aluminum or magnesium, reliable gate shut-off technology, and direct application of squeeze pressures up to 103 MPa (15,000 psi). This machine is intended for production.
- Develop a gate shut-off mechanism that will operate reliably in a production environment.
- Select a casting that will be produced in the casting machine built for this project.
- Use fluid-flow and solidification analysis to predict optimum flow conditions for metal entering the mold and differential squeeze requirements.
- Design and build cast tooling.
- Develop process technologies for the low-pressure/squeeze casting of aluminum alloys and evaluate the effect of various process parameters on casting integrity.
- Apply development results to the production of a selected automotive component.

Accomplishments

- Completed preliminary design of the casting machine.
- Designed experiments for development of reliable gate shut-off mechanism.

- Selected a connecting rod for a Bendix truck air compressor as a production part.
- Acquired software for die fill and solidification analysis.
- Completed the preliminary design of cast tooling.

Future Direction

- Complete design of casting machine.
- Complete design of gate shut-off mechanism, and integrate this mechanism with the casting machine control system.
- Fabricate casting machine and install at Eck Industries.
- Complete cast tooling design and fabricate.
- Develop and evaluate ASC process technologies.
- Demonstrate production viability of ASC casting machine and process.

Introduction

Squeeze casting is the solidification of liquid metal under pressure in a closed die. The resultant casting has improved properties and created a more uniform microstructure as compared to those produced by traditional molten metal fabrication techniques. The improved properties are achieved through controlled entry of the metal into the die through large gates. This entry reduces turbulence and high solidification rates, resulting in the refinement of microstructural features.

The method and efficiency of pressure application distinguish the two types of squeeze casting (direct and indirect). Direct squeeze casting is the most efficient (essentially 100%) as it applies pressure directly on the casting. This contrasts with indirect squeeze casting in which pressure is applied using the gating system. The length of the gating system and any partial solidification caused by the gating system prior to complete solidification of the part reduces the pressure applied to the part and results in casting porosity. For the indirect squeeze cast method the dimensions of the die cavity control part dimensions. For the direct squeeze cast method, the part dimensions are controlled by the die cavity dimensions and the finish position of the top die. Thus, the direct squeeze cast method requires precise machine control to attain the desired part dimensions. The hot metal handling technique for transporting the metal from the furnace into the mold or gating system is deficient for both the direct and the indirect squeeze cast methods. The current method introduces additional casting defects such as oxide inclusions that are especially detrimental, causing increased fatigue properties.

Earlier attempts to improve the squeeze casting process by combining the advantages of low-pressure die fill with those of squeeze casting demonstrated the ability to produce high-integrity components; however, continuous production operation of the equipment was not achieved. The machines used were not specifically designed to meet the needs of the process.

Technical Approach

This recently initiated (June 2003) project will (1) design and develop a production-viable ASC machine, (2) develop process technology that will improve the strength and reliability of cast automotive components, and (3) demonstrate the production viability of the equipment and process.

An assessment of the capabilities and limitations of existing cast machine designs demonstrated that

- Low-pressure casting machines typically do not have the structural rigidity to resist the high pressures applied during the squeeze casting process.
- Die-cast and squeeze-cast machines are not designed to accommodate nonturbulent molten metal entry into the die cavity.
- Neither type of equipment is typically set up with the type of hydraulic and electronic controls necessary for the cavity movement envisioned as required for the ASC process.

Therefore, the project team decided to design and build a machine from the "ground up" instead of modifying an existing low-pressure, die-cast or squeeze-cast machine. The project team partnered with Empire Castings, Inc., an experienced producer of low-pressure casting equipment, to design and construct the ASC machine.

Through consultation with Bendix, Inc., an industrial manufacturer of truck components, a casting(s) will be chosen for production in the ASC machine. The selected component will meet the following criteria:

- A level of complexity that can demonstrate the production capability of the ASC machine.
- A requirement for mechanical properties higher than those attainable with commercially available castings.
- An opportunity for the casting selected or one similar to it to move into production with the ASC process.

The casting selected, an air compressor connecting rod, will be modeled for fluid flow and solidification shrinkage. This work will be done in parallel with equipment design. This model should enable us to understand optimum flow conditions for metal entering the mold and differential squeeze requirements, if any, to contend with solidification shrinkage. Modeling of the casting is very important to the success of the program and, potentially, to the details of the machine design. The ASC machine has two mechanisms to feed the casting—low-pressure, nonturbulent fill of the die cavity and high-pressure, direct squeeze to minimize solidification shrinkage. Modeling experiments will explore the interaction of the two feed mechanisms and select process parameters that lead to process optimization. Modeling results will be used to refine the die design and select initial casting process parameters.

After tooling construction and ASC machine delivery, castings will be operated under a range of process conditions anticipated during modeling, using a variety of cast and wrought alloys (Table 1). Analysis of those castings will include radiography, die penetrant inspection, tensile testing, and functional component testing at Bendix. It is anticipated that this part of the program will involve multiple iterations in order to produce the product successfully. Some equipment and tooling modification may be required during this part of the program.

Table 1. Aluminum alloys to be used for casting trials

AA 380	AA 206
AA 356	AA 6061
AA 357	AA 535
AA 319	AA 388

After successful production of development castings, the production viability of the equipment and process will be demonstrated. This will be done by

- Production of a connecting rod with reduced porosity and improved mechanical properties as compared to the current die-cast connecting rod used by Bendix.
- Continuous production of the ASC machine and connecting rod tooling to include at least one 5-h continuous run with the equipment running at least three days in a week.

It is the goal of the project team to implement part production on an ongoing

basis. The production phase of the project will include detailed cost analysis of part production, determination of die-life parameters, and ongoing equipment and tooling development for maximum uptime.

Program Schedule

The scheduled start and end dates for the various program tasks are listed in Table 2.

Table 2. Overall program schedule

	Start date	Completion date
Machine design	June 2003	Nov. 2003
Machine build	Nov. 2003	Mar. 2004
Tooling design	July 2003	Oct. 2003
Tooling build	Nov. 2003	Mar. 2004
Process modeling	Oct. 2003	Dec. 2003
In-gate S.O. development	Nov. 2003	Dec. 2003
Machine install	Mar. 2004	Apr. 2004
Casting development	Apr. 2004	June 2004
Evaluation and testing	May 2004	Oct. 2004
Final report	Apr. 2004	Dec. 2004

Machine Design Status

Initial design (Figure 1) of the 600-ton capacity ASC machine has been completed. Positioning of the top die is accomplished independently of the squeeze-cast cylinder. To maximize machine capability, the melting vessel will be equipped with a crucible furnace. This will facilitate the melting of cast and wrought aluminum and magnesium alloys as well as aluminum and magnesium metal matrix composite alloys.

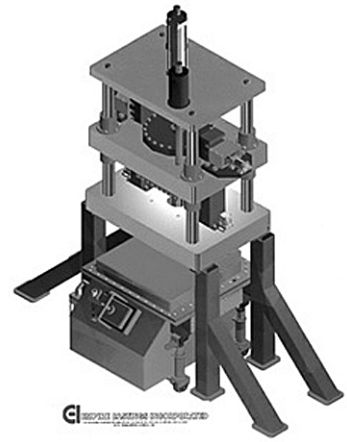

Figure 1. Overall design concept for 600-ton ASC machine.

To match the dimensional capabilities of the die-cast process, a closely controlled volume of liquid metal must be fed into the die cavity. Conventional low-pressure fill technology does not have the capability to accurately meter a fixed amount of liquid metal into the die. Therefore, we will accurately position (± 0.05 mm) the top die to obtain the desired fill volume and use a fill sensor and an independently controlled gate shut-off to control metal volume. Development of a reliable gate shut-off technology is a key part of the experimental program.

Tooling Design Status

The die for the ASC machine consists of a die holder and individual die inserts for the particular part being cast. The die casting tool is shown in Figure 2. The location of the inserts for a test bar blank and an air compressor connecting rod is shown in Figure 3. The size and configuration of the gating will be finalized when the fill and solidification modeling is complete.

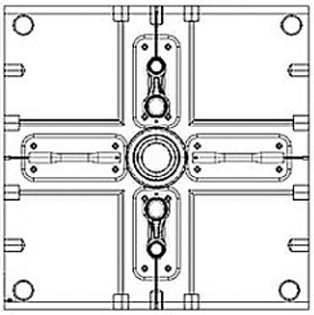

Figure 2. View of cast tooling.

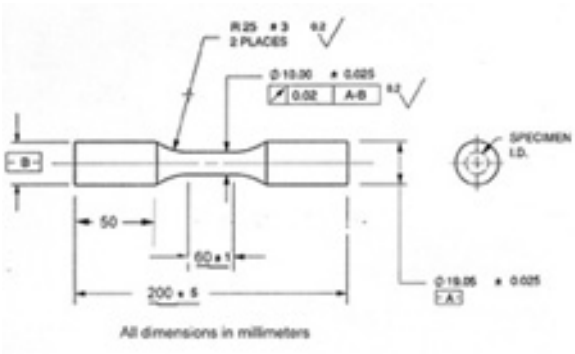

Figure 3. Cast tensile test bar configuration.

Conclusions

Excellent progress has been made on design of a production ASC machine and the cast tooling for development of casting process parameters. All tasks are currently on schedule for completion of the program within the time allotted.

G.Ultra-Large Casting Benchmark Study for Aluminum and Magnesium Alloys: Phase II

Principal Investigator: Thomas N. Meyer, Ph.D.
Consultant
3987 Murry Highlands Circle, Murrysville, PA 15668
724-325-2049; fax: 724-325-9159; e-mail: tnmeng@aol.com

Technology Development Area Specialist: Sidney Diamond
(202) 586-8032; fax: (202) 586-1600; e-mail: sid.diamond@ee.doe.gov
Field Technical Manager: Philip S. Sklad
(865) 574-5069; fax: (865) 576-4963; e-mail: skladps@ornl.gov

---

Contractor: American Foundry Society, Des Plaines, IL 60016
Contract No.: 4000012401

Objective

- Evaluate candidate casting processes for producing magnesium or aluminum alloy lightweight ultra-large thin-wall structural castings for automobiles and light trucks.
- Compare the energy required to produce a minivan inner panel based upon (1) a conventional manufactured assembly of steel stampings and (2) a lighter-weight aluminum casting of the same part.

Approach

- Assess five metal casting processing routes:
  - Multi-port hot chamber injection at pressures compatible with permanent mold systems
  - Single gas plenum driving metal to fill a permanent mold
  - A combination of pressurized gas and vacuum metal filling for producing both magnesium and aluminum permanent mold castings
  - A low-cost semi-solid process to produce aluminum castings
  - A process requiring magnesium chips to produce a cast magnesium component in a semi-solid process
- Determine the energy required to produce an aluminum liftgate inner panel casting for a minivan and the energy required to produce the same component based upon an assembly of steel stampings as is currently practiced
- Recommend steps toward achieving lightweight vehicle structures at costs competitive with those of current structures.

Accomplishments

- Developed a test part configuration for evaluating candidate process capabilities that embodies key casting geometric features typical for ultra-large structural castings: thin/thick/thin

transitions, representative distance between metal entry and knit lines, flow distances, and geometry characteristic of structural components.

- Identified an opportunity to evaluate a large "body on frame" structural part of specific interest to an original equipment manufacturer (OEM) using the Thixomat process (i.e., process 5 under "Approach") and outlined the project tasks, schedule, and conceptual budget.
- Conducted an energy analysis, principally at Oak Ridge National Laboratory (ORNL), that clearly indicates that employing aluminum structural castings saves energy.

Future Direction

- Develop a detailed design of a test part for evaluation of the candidate processes that
  - includes the representative geometry of vehicle structural parts
  - minimizes the cost of tooling
- Fabricate tooling for the test part so that it is compatible with equipment for the different processes of interest (e.g., vacuum die casting, semi-solid aluminum and magnesium processes, and permanent mold processes).
- Using the same test part tool set, evaluate processes in a prioritized order.
- Initiate demonstrations of the semi-solid magnesium process to produce a large body on frame part (i.e., 1.1 m^2) for OEM application through the U.S. Automotive Materials Partnership (USAMP).
- Direct efforts toward development of a reliable molten metal injector system. This will require materials development for key areas of the molten metal pump.

Introduction

The ability to produce aluminum or magnesium ultra-large thin-wall structural castings (ULCs) is key to lightweighting auto and truck structures at costs competitive with those of heavier steel assemblies. Castings offer the potential for both cost and weight reduction compared with sheet components. The definition of a ULC is subject to judgment, but the following specifics are offered to better define ULCs as discussed in this study:

- The part area is greater than 1 m^2 (e.g., typical of a minivan liftgate inner).
- As a result of a combination of weight and stiffness requirements, wall thickness will range between 2 and 3 mm for much of the part area.
- Bosses and attachment areas will be much thicker (e.g., 6 to 8 mm).
- The minimum major dimension is 120 cm.
- The minimum minor dimension is 90 cm.

ULC offer a cost advantage due to reduction in the part count (e.g., 10×) and assembly of stampings to produce the final component. Examples include an auto sidewall aperture structure or a vehicle floorpan frame. This approach also simplifies the supply chain and decreases the time to market. High-strength steels may be used to save weight but only at a cost premium, using established supply chains. As was learned from Ford's conversion of the F-150 radiator support structure from an assembly of steel stampings to a magnesium casting, additional weight can be saved because of system considerations that go beyond simple component substitution. However, sheet components (e.g., steel, aluminum) will be

required for exterior components because castings currently cannot provide the Class A finish required for the vehicle exterior surface.

ULCs offer weight reduction that translates into reduced vehicle fuel consumption and reduced emissions. Such energy and environmental considerations are the primary drivers for lightweighting vehicles. However, a demonstrated advancement in casting technology will benefit other industries that can employ castings. For example, the aircraft industry has been under increasing pressure to reduce manufacturing costs. Heavy ground vehicles such as buses and trucks also will make greater use of lightweight castings.

Many of these opportunities are directed to products that have volumes of less than 50,000 units or even less than 1,000 units per year. Because of high tooling costs for the fabrication and assembly of sheet-formed components, manufacturing costs can be very high at these low volumes. For example, the tooling cost for an inner liftgate panel is $6.5 million. Currently, the heavier steel sheet-formed components are more cost-effective at volumes in the range of 100,000 to 400,000 units. Even for such high volumes, it is anticipated that structural components comprising many individual stampings will not remain cost-competitive versus a single lightweight casting beyond the next 10 to 20 years. Castings will continue to displace assemblies of stamped components.

It is implicit that the newly developed technologies concomitantly at least maintain current safety performance and possibly enhance safety. Structural parts must possess a ductility exceeding 8%, although some specific areas may not require this level of ductility.

Scope

This second-phase casting benchmark study is directed to evaluating processes considered best for producing ULCs of magnesium or aluminum alloys. The first phase, completed in July 2002, identified five casting processes potentially capable of achieving this goal. A cost analysis indicated that these processes are capable of producing ULC components at costs competitive with those of conventional assemblies of steel stampings. Although steel stampings are cost-effective at high production volumes, ULCs are cost competitive from very low volumes to as much as 70,000 units per year. Because of tooling costs, the permanent mold processes provide the lowest-cost ULCs.

Although Phase I identified candidate casting processes for producing ULCs, more information was needed prior to proposing specific demonstration and evaluation projects. Five process routes were assessed:

- Multi-port hot chamber injection at pressures compatible with those of permanent mold systems
- Single gas plenum driving metal to fill a permanent mold
- A combination of pressurized gas and vacuum metal filling (like the Brocast process developed in France)
- A semi-solid process for producing aluminum castings having T5 properties exceeding typical T6 properties
- A semi-solid magnesium process that does not require handling of molten magnesium

A Sixth Alternative

The conventional vacuum die casting process, as practiced at Alcoa, Gibbs, and other foundry operations, was also considered for ULC. Presses and dies may be built with sufficient tonnage (i.e., 10,000 to 20,000 tons). However, the cost of parts, particularly at low volume, may still be an issue because of higher die costs relative to the costs of three low-pressure processes described earlier. For example, vacuum die casting part costs are projected to be 20 to 30% higher than the cost of parts produced by the permanent mold process at volumes

in the range of 15,000 to 30,000 units per year. However, cost reductions for die castings are expected to continue, and vacuum die casting cannot be eliminated as an approach to ULCs.

All of these processes have the potential to produce ULCs at costs competitive with the cost of stamped steel assemblies at various production volumes (i.e., crossover points) established by specific manufacturing considerations. Generally, at still lower volumes, casting becomes the low-cost choice while saving weight.

Permanent Mold Process Alternatives

The first three ULC process alternatives are permanent mold processes.

Multi-port hot chamber injection

Multi-port hot chamber injection at pressures compatible with those of permanent mold systems is an extension of the route pursued by Alcoa from 1996 through 1999. Significant development of the hot chamber injection system is required before the process can realize a low-cost production capability. Unlike in gas pressurization, the metal injection can be controlled precisely. However, significant development of the injector components is required.

Pressurized gas filling

Several factors could limit the size of parts produced with low-pressure gas driven processes (2 and 3). Larger castings require the use of hot runner systems employing heavy mold coatings and tighter temperature control. Such control can be extremely difficult. A second alternative uses multiple feeds, requiring a large pressurized molten metal furnace or a distribution box nearly equivalent in size to the part plan area. A large high-temperature vessel subject to cyclic pressurization can be a real challenge as furnace sizes increase.

The pressurization process that resembles the Brocast process requires similar considerations. During the cycle, pressures can be controlled from 0.05 atm absolute to as high as 15 atm. Using this process in the future for production of full-scale ULCs will require

- manufacture of a metal holding vessel with appropriate fill point locations permanently fabricated in the pressure vessel;
- employing a heated Bosch (i.e., manifold for molten metal) for metal distribution to the mold fill point locations; or
- using multiple smaller metal containers or pressure vessels, provided the spacing between metal entry to the mold is not too close.

Three major challenges are (1) these modifications are significant steps over current capability, (2) tooling technology for such high vacuums does not exist at Brocast, and (3) the intellectual property resides off - shore.

High-Pressure Injection Process Alternatives

The last two processes are more similar to the sixth alternative, die casting (i.e., relatively high-pressure injection). The first is a semi-solid casting process to produce aluminum castings. The properties of castings produced in this process in the as-cast condition (T5 temper) are comparable to castings that are solution-treated and aged (T6 temper). With the elimination of high-temperature heat treatments for ULC parts, dimensional management is significantly eased. In addition, the tooling and caster capital costs are significantly lower than those of vacuum die casting. The maximum casting pressure is 8000 psi, which is 40% below that of some die casting pressures. However, there is uncertainty whether the process can flow metal over distances necessary for ULC parts.

The second process (like the Thixomat process) converts a feedstock of chips (not molten metal) to a semi-solid state and injects them in a process similar to what is used in die casting. Although comparable equipment is not available for aluminum, the process is expected to be compatible with multiple injectors. The commercial application of the Thixomat magnesium casting process has grown rapidly for small thin-wall parts typically found in portable communication, computing, and video equipment. The same process is now aggressively targeting larger automotive parts, and some automotive parts are currently in production. Because it avoids the handling of molten magnesium alloy and provides a high yield, the process is extremely attractive. ULC capability will depend upon major developments under way to perfect hot runners and inductively heat the feed material in the injector barrel.

Current Status

At present, none of the processes is ready to produce ULCs. One might argue that vacuum die casting is the closest to meeting ULC requirements. However, equipment becoming available by April 2004 will enable demonstration of ULC production. Such a demonstration will be based upon a test part design that simulates key features of a ULC without requiring either a large machine or a complex and expensive mold tooling. (Such a test part is described in the final report available through the American Foundry Society.[1]) This can be readily done for all the processes discussed except the multi-port hot chamber injection process.

Tasks, schedule, and conceptual budget were prepared for such a demonstration of each of these processes and vacuum die casting. The cost to demonstrate the ULC capability with the test part is less than $800,000, and the task can be completed in less than 16 months. If a second process is evaluated and the test part tooling is designed to be compatible, the cost of the test part design and the tooling will be substantially lower, and the overall test cost may be less than $450,000. Priorities must be established.

Similarly, tasks, schedule, and conceptual budget to develop a multi-port hot chamber injection system were prepared. The potential for a low-cost product produced by this process is enormous. The pursuit of multi-port hot chamber injection is considerably more expensive ($2.2 million) and will require as much as 2 years for a similar ULC demonstration.

Energy Comparison

A comprehensive energy analysis was conducted to compare structural parts produced in aluminum castings with those produced as a traditional stamped steel assembly. Any such analysis depends upon specific assumptions, but the study clearly indicates that the additional energy for producing the aluminum over steel is saved within the first vehicle lifetime (see Figure 1) and available for subsequent generations without and energy penalty. In a

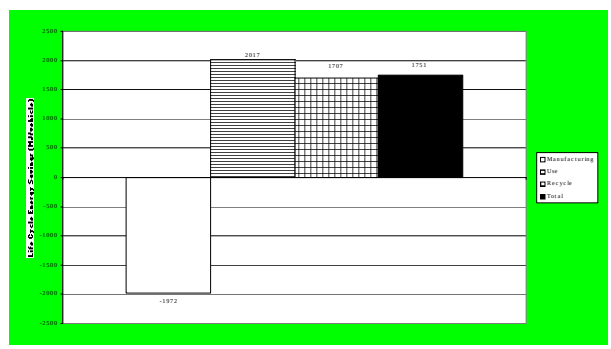

Figure 1: Life cycle energy savings of cast aluminum liftgate vs stamped-steel liftgate.

conservative case of a minivan liftgate inner panel (Figure 2) having a weight savings of 21%, the added energy to produce the aluminum is returned in the first vehicle life. However, more typical weight savings of 30% to 40% provide positive energy benefits within the first few years of vehicle life. This

Figure 2. Casting targeting Daimler-Chrysler liftgate inner.

energy savings, as well as the reduced environmental impact, strengthens both domestic energy independence and manufacturing competitiveness. High-strength-steel stamped components offer another option to save weight, but costs are greater and thus they are not attractive.

Recommendations

- Design a ULC test part and corresponding tooling such that the "test part" represents key features of a structural ULC (e.g., thin/thick/thin transitions, cross section profile, thickness, metal flow to knit-line distance).
- Minimize the cost of tooling.
- Design the tooling to be compatible with equipment for processes of interest (as much as possible).
- Using the test part tooling, begin evaluating ULC capability for each of the processes in order of priority (e.g., probably examining vacuum die casting first).
- Demonstrate production of an OEM body on frame structural component employing the Thixomat semi-solid magnesium process.
- Develop the hot chamber injectors multi-port low-pressure injection system.
- Demonstrate the hot chamber injectors can produce the test part at available commercial facility.

Pressure-driven processes are practiced globally today. Process improvements will naturally continue for high-volume gas-pressurized systems. Issues such as large pressurized furnaces, employment of hot metal manifold systems, and indirect control of metal flow lessen interest in these processes. Thus, gas-pressurized metal permanent mold casting will continue to improve with market forces, without government-shared risk in emerging technologies with new capabilities.

Demands will continue for casting capabilities to become larger and capable of more complex section geometry. This demand is driven by market forces to reduce the cost of manufacturing vehicle structures and regulatory forces for energy efficiency and environmental benefits. Working together, government agencies (e.g., DOE) and OEMS (through organizations like USAMP) will help reduce the technical risks and hasten these benefits to society. Technology conduits (e.g., the American Foundrymen's Society) provide a fertile medium where converging private wants and public needs can be effectively integrated in specific programs to meet these goals.

This is the second phase of a benchmark study to evaluate candidate casting processes for producing magnesium or aluminum alloy lightweight ultra-large thin-wall structural castings (ULC) for autos and light trucks. These parts have projected areas exceeding 1 m^2. Examples include an auto sidewall aperture structure or a vehicle floorpan frame (see Figure 3). ULCs can replace the assembly of ten or more steel stampings. The first phase of the benchmark study, completed in July 2002, identified five casting processes of interest. Castings were determined to be cost-effective beginning at low volumes and continuing to volumes as high as 70,000 units per year. At the highest volumes, the

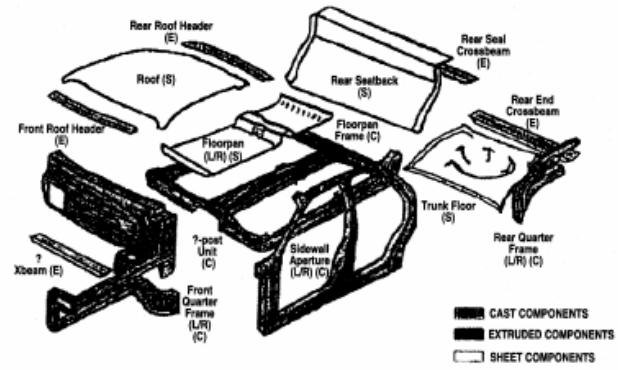

Figure 3. Candidate vehicle cast components.

process of steel stampings continues to be most cost-effective.

Although the lowest costs are projected for a multi-port hot chamber process, technical risks for this technology are judged too great at this time.

Reference

1. T. N. Meyer, *Ultra Large Casting Benchmark Study for Aluminum and Magnesium Alloys: Phase II, AFS Project ORNL-ULC-11, July 2003*.

4. ENABLING TECHNOLOGIES

A. Improved Friction Tests for Engine Materials

Principal Investigator: P. J. Blau
Oak Ridge National Laboratory
P.O. Box 2008, Oak Ridge, TN 37831-6063
(865) 574-5377; fax: (865) 574-6918; e-mail:blaupj@ornl.gov

Technology Development Area Specialist: Sidney Diamond
(202) 586-8032; fax: (202) 586-1600; e-mail: sid.diamond@ee.doe.gov
Field Technical Manager: Philip S. Sklad
(865) 574-5069; fax: (865) 576-4963; e-mail: skladps@ornl.gov

---

Contractor: Oak Ridge National Laboratory
Contract No.: DE-AC05-00OR22725

Objectives

- Develop a realistic, engine-correlated laboratory-scale test method to be used in selecting diesel engine piston ring and liner materials and work with ASTM, through an industry advisory group, to establish it as a standard practice.
- Investigate the effects of oil condition [new versus engine-conditioned (EC) lubricants] on the ability of the new test method to detect small friction and wear behavioral differences in engine materials in a repeatable manner.

Approach

- Review and critique past attempts to develop laboratory tests for piston ring and liner materials.
- Develop a testing protocol for friction and wear in reciprocating, lubricated contacts that simulate key aspects of the diesel engine environment.
- With the assistance of NIST, develop a fluid that simulates the effects of EC oil on the friction and wear response of candidate materials.
- Work with ASTM, through Committee G-2 on Wear and Erosion, to develop and approve a standard practice for conducting laboratory-scale piston ring and liner friction and wear tests.

Accomplishments

- Published a report describing and critiquing past efforts to develop engine-correlated laboratory-scale tests for materials and lubricants proposed for use in both spark-ignition and diesel engines.
- Established an ASTM task group on ring and liner wear within Committee G02.40 on Non-Abrasive Wear. Populated the task group with representatives from diesel engine companies, automotive companies, testing machine manufacturers, oil companies, government laboratories, and universities.

- Developed and published a technique for effectively simulating the surface finish of cast iron cylinder liner bores on simple test coupons.
- Obtained samples of oils run in standardized engine tests. These well-characterized test oils will be used to evaluate the ability of the new test to delineate lubricant condition.
- Prepared a draft standard practice for ASTM subcommittee review.

Future Direction

- Modify the draft ASTM standard practice as needed, based both on advice from the task group and on new laboratory results. Conduct tests in well-characterized engine test oils to evaluate the sensitivity and repeatability of the proposed method.

Introduction

Friction in moving parts robs engines of useful energy and lowers the vehicle's fuel economy. Depending on engine speed, the piston ring and liner system in an internal combustion engine can account for over 50% of the total engine frictional losses. New materials, lubricants, and coatings offer the potential to reduce frictional losses; but the development cost for these materials can be high, especially when full-scale engine tests are involved. Smaller-scale, simulative laboratory tests are an attractive alternative, but they can be useful only if their results correlate well with the materials' performance in real, fired engines.

Truck engine manufacturers and designers need more accurate and cost-effective laboratory screening methods for materials and lubricants. That need was placed high on the industry priority list in the recent DOE/OHVT multi-year plan in friction and wear.

The design of cost-effective laboratory-scale ring and liner simulations is not trivial. Improperly designed simulations can produce misleading results. Materials and lubricants must be induced to react in tests as they would in actual service. Tests should enable the ranking of alternative materials and lubricants in the same order of merit that they perform in service. That requires identifying the major influences on friction and wear behavior and controlling them in the laboratory.

ASTM is an international organization that develops consensus material testing standards. By working through ASTM Committee G-2, Oak Ridge National Laboratory (ORNL) is leveraging its efforts with those of other experienced testing professionals.

In FY 2001, key elements required for effective ring/liner simulation were identified. In FY 2002, the effort was focused on building an industry advisory group and involving ASTM. In FY 2003, friction and wear tests were conducted in new and used engine oils to refine the test methodology and prepare it for the rigorous ASTM standardization process.

Subtleties of Lubricated Testing

Obtaining correlated, repeatable friction and wear test results is much more complex than most people realize. The same combination of materials can produce different friction and wear results when rubbed together using different speeds, pressures, temperatures, motions, and lubricants. Therefore, it was necessary to consider all the possible influences of these factors in developing a laboratory test that effectively ranks materials and lubricants as they would be ranked in more expensive, full-size engine tests. For example, a shaft that always turns in one direction will not necessarily wear at the same rate as a shaft that oscillates back and forth under otherwise similar conditions.

Surface Finish

Friction and lubrication behavior depends on the surface finish, particularly in combustion engine cylinders. The direction and height of the finishing marks affects lubricant flow, fluid retention, and the traction between the surfaces. A special method was developed to prepare cylinder-like grinding patterns on cast iron coupons that can serve as test specimens. The methodology and the data that validated it were published in the 2001 proceedings of the Internal Combustion Engine Division of the American Society of Mechanical Engineers (ASME). Table 1, taken from that publication, shows that reciprocating sliding tests with new and used oil produced similar friction coefficients for a production Caterpillar C-15 diesel engine cylinder surface and for a surface that was simulated using the ORNL finishing technique.

Table 1. Comparison of friction coefficients (μ) for actual versus simulated cylinder liner surfaces[a]

Lubricant	Production liner (μ)	Simulated liner (μ)
None	0.287	0.292
Fresh 15W-40 diesel oil	0.068	0.069
Used (diesel-engine-tested) oil	0.061	0.070

[a]Type 440C stainless steel sphere sliding on test surfaces under 5 N load, 6 mm stroke, and 2 oscillations per second.

Running-in and Alignment

The test-to-test repeatability of friction and wear data depends on reproducing the same geometric fit between test surfaces every time. That requires excellent mechanical alignment, supplemented by an effective running-in procedure. Both aspects were addressed in this work. Dr. John Truhan, Jr., of the University of Tennessee developed a practical method to run-in the surfaces to enable a good initial fit.

In addition, there is a need to be able to calculate the volume of wear that occurs on curved surfaces such as piston rings and liners. Dr. Jun Qu, an Oak Ridge Associated Universities post-doctoral fellow, developed an analytical wear model to enable the more precise calculation of piston ring wear scars that have compound curvatures.

Oil Condition

Previous DOE-sponsored research at Cummins Engine Company indicated that fresh and EC oil can make differences in friction and wear of coatings for engine materials. Therefore, it was important in this work to identify the type of used oil or EC lubricant surrogate that could be used in a standard test for candidate ring and liner materials and surface treatments. Figure 1 shows the effect of applied test load on the wear rates (µm/h) for chrome-plated diesel engine piston rings sliding against cast iron liner materials. The cast iron was prepared to simulate cylinder bores using the finishing method noted earlier. Used diesel engine oil from a commercial engine test, heated to 100°C, was the lubricant. The ratio of liner wear to ring wear is about 5:1, higher than the ratio expected in engines. The reasons for that difference are known and can be accounted for in adjusting the test data to correspond better with engine wear data.

Specimens of five standard engine test oils (used) were obtained from Southwest Research Institute, and fleet-tested oils were obtained from Dr. J. Perez at Pennsylvania State University. Each will be analyzed and subjected to the proposed testing protocol to determine the method's ability to detect differences in the oil condition. Recommendations will then be made as to which oil or formulation should be used in order to obtain repeatable material screening results.

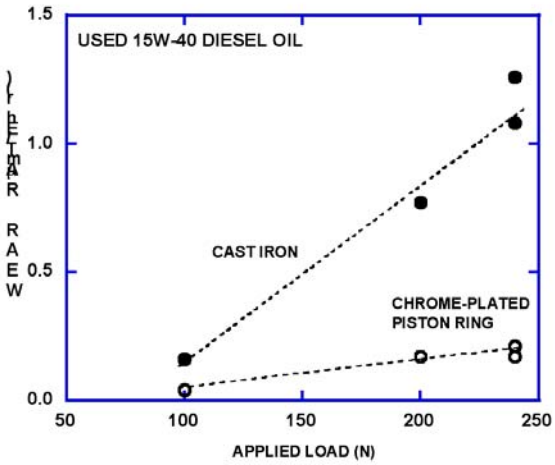

Figure 1. Effects of test load on the wear of piston ring and liner materials in hot used engine oil. Reciprocating tests used an 8-mm stroke length and a frequency of 10 cycles per second.

Development of a Standard

A draft standard has been prepared using the form and style prescribed by ASTM. It has been circulated for comment among the members of the task group on ring and liner wear, established by ASTM Committee G02.40 Subcommittee on Non-Abrasive Wear. A revised draft, based on industry comments, will be submitted for initial balloting at the fall 2003 ASTM committee meeting. It will also be presented for discussion in December 2003 at a joint ASTM D-2 (Lubricants) and G-2 (Wear and Erosion) workshop on new test methods. Undoubtedly, the test method will continue to evolve with input from the broader technical community. Depending on ballot results, it may require several balloting cycles to produce the approved, consensus-based standard.

Conclusions

Considerable progress has been made in developing a standard practice for lubricated diesel engine piston ring and liner materials testing. Past test methods have been reviewed, and new methods have been developed to prepare simulated lining surfaces, analyze complex wear patterns, align test specimens, and run-in the surfaces to improve test repeatability. More work is needed to identify the preferred EC lubricants to enable effective material screening. The ASTM review and consensus standardization process is under way with the preparation of a draft standard practice for ring and liner friction testing.

B. Laser Glazing of Railroad Rails to Reduce Friction

Principal Investigators: George Fenske, Saud Aldajah, Oyelayo Ajayi, Jon Hiller, Charlie Allen, Ron DiMelfi, and Zach Xu
Argonne National Laboratory
9700 S. Cass Ave.
Argonne, Illinois 60439
(630)-252-5190; fax: (630)-252-4798; e-mail: gfenske@anl.gov

Technology Development Area Specialist: Sidney Diamond
(202) 586-8032; fax: (202) 586-1600; e-mail: sid.diamond@ee.doe.gov
Field Technical Manager: Philip S. Sklad
(865) 574-5069; fax: (865) 576-4963; e-mail: skladps@ornl.gov

---

Contractor: Argonne National Laboratory
Contract No.: W-31-109-ENG-38

Objective

- Determine the potential of laser glazing to lower parasitic energy losses between the flange and rail in rail transport.
- Develop a fundamental understanding of the metallurgy associated with the formation of low-friction surface layers during the laser glazing processing, and how these layers reduce friction between rail and wheel.

Approach

- Develop an advanced laser glazing processes to form glazed regions on carbon steels.
- Perform benchtop tests, full-scale rig tests, and field tests of glazed steels and rails to quantify the impact of glazing on parasitic friction losses.
- Characterize glazed and nonglazed steels to elucidate the impact of glazing on the microstructure.

Accomplishments

- Optimized laser processing conditions under which uniform glazed surfaces form on carbon steels.
- Evaluated friction and wear performance of glazed (and unglazed) rail steel by using benchtop and wheel/rail rig tests.
- Characterized the microstructure and hardness of glazed steels.
- Developed a deformation theory for nanocrystalline materials to model friction in glazed steel.

Future Direction

- Perform full-scale rig tests at the Canadian National Research Council (CNRC) facility in Ottawa, Ontario.
- Make go/no-go decision to proceed with development of rail-glazing technology.

- If decision is to proceed, (1) establish contract with Transportation Technology Center, Inc. (TTCI), Pueblo, Colorado, to test glazed rails on a full-scale rail test loop and (2) commercialize rail-glazing technology with Harsco Track Technologies (the railroad track maintenance equipment and service organization of Harsco Corporation).

Introduction

Wheel/rail interactions account for a significant fraction of the energy consumed in rail transport. Past studies have indicated that energy savings could be as high as 24% when friction at the wheel/rail interface is properly managed. The key aspect is control of the friction forces. At the locomotive, high friction between the rail (specifically the top of the rail) and the wheel is desired to ensure adequate traction to keep wheels from slipping and sliding when power is applied. Friction is also required under braking conditions to control the speed of downhill-bound trains or to bring a train to a safe stop. The trailing cars, however, require much lower friction levels under normal train operations. For these cars, a low, controllable friction is desirable because less friction can significantly reduce the energy required to pull a train. Two regions account for most of the frictional losses between the wheel and the rail: the region between the top of the rail and the wheel tread, and the region between the wheel flange and the gage face of the rail. Current wheel/rail lubrication (e.g., application of degradable greases and lubricants) is inconsistently applied and often disengaged by train crews. The research described here focuses on the development of a laser-glazing technique that imparts a durable, low-friction surface to the gage face of the rails to reduce parasitic frictional losses between the flange and rail gage.

Approach

The objective of this research is to develop an advanced laser modification process to form a glaze on the gage face of the rail. Initial results and models predicted the formation of a nanocrystalline surface layer that would impart low-friction properties at the interface. The tasks associated with this project involve

- Process development (laser glazing)
- Friction and wear testing of laser-modified surfaces (glazed and shot-peened)
- Microstructural characterization of laser-modified surfaces
- Development of a model (of surface deformation)

Results

The process development effort primarily focused on laser glazing. Parametric studies were performed to optimize the conditions under which a glazed layer forms on 1080 steel when an Electrox 1.6-kW, pulsed Nd:YAG laser with fiber-optic beam delivery and special beam shaping optics is used in Argonne National Laboratory's (ANL's) Laser Applications Laboratory. Two approaches were developed: one that involved a single pass of the laser over a given area, and one that involved multiple overlapping passes (Figure 1). The Knoop hardness of the martensitic glazed regions was 2–3 times greater than that of the substrate, depending on whether a single-pass (factor of 3 times harder) or multipass (slightly over 2 times harder) process was employed.

A commercial laser-glazing process that utilized high-power diode laser technology was also investigated. In this case, bars of 1080 steel were processed by a commercial vendor (NuVonyx - http://www.nuvonyx.com/) and subsequently tested at ANL (Figure 2a). A third laser modification process (laser shot-peening [LSP]) was also evaluated. Bars of 1080 steel were processed by LSPT (LSP Technologies - http://www.lspt.com/home.asp) to "peen" near-surface

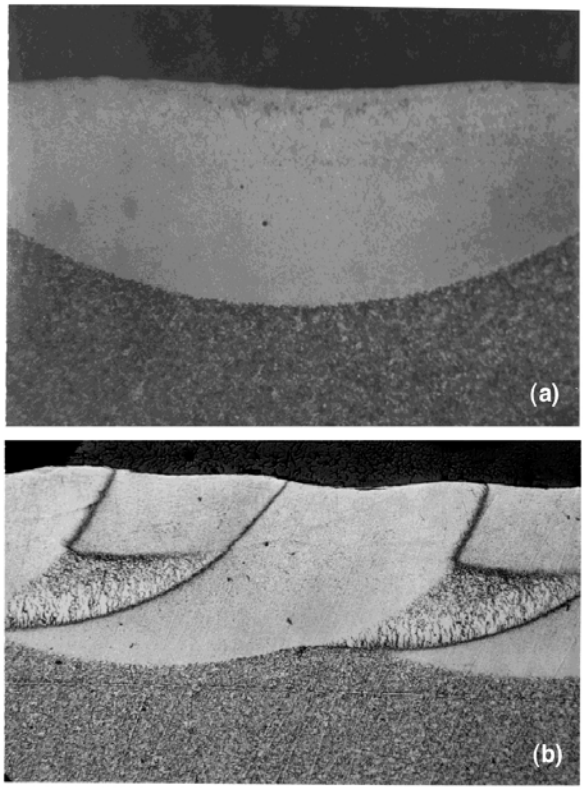

Figure 1. (a) Single-pass laser glazed cross section (b) Multi-pass laser glazed cross section.

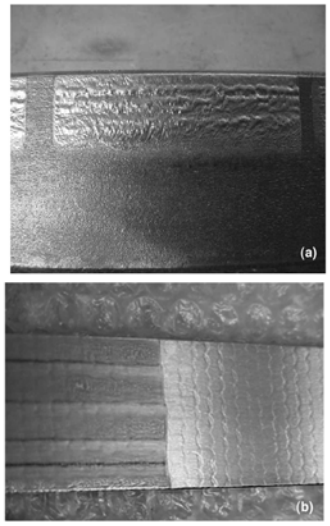

Figure 2. (a) 1080 steel glazed with a high-power diode laser. (b) 1080 steel laser peened (right side) and gazed and peened (left side).

regions (Figure 2b). LSP does not involve melting near-surface regions; rather, it utilizes a laser to shock near-surface regions, thereby introducing high compressive stresses and increased hardness.

Friction and wear tests were performed on laser-treated (primarily ANL's glazed steels) to evaluate the potential of glazing to reduce frictional losses between the wheel flange and gage face of the rail. Initial tests were performed at Falex Corporation by using a low-speed, block-on-ring configuration, and at the AAR test facility in Pueblo, Colorado, by using a full-scale ring/wheel-on-block/rail, operated under controlled slip conditions. Detailed tests were performed at ANL on twin-roller, pin-on-disc (POD), and reciprocating pin-on-flat configurations. Future tests in a full-scale twin-roller configuration are planned at the CNRC facilities in Ottawa, Ontario.

The block-on-ring tests at Falex measured the breakaway (i.e., static friction coefficient) torque/force required to initiate rotation (defined as 0.013 rpm) under various loads (445–4005 N [100–900 lb]) in 100-lb (445-N) increments. (The ring in this case was a Falex standard ring made of S-10 steel with an Rc of 58–63; the block was 1080 rail steel, as received or as-glazed.) Dynamic block-on-ring tests were not performed because earlier tests showed debris accumulation produced unreliable comparisons under dry heavily loaded conditions. The Falex test results showed static friction coefficients of ≈0.35–0.45 for untreated 1080 steel that dropped to values ranging from 0.2 to 0.4 for differing glazing conditions.

The AAR tests were similar to the Falex tests in that they measured the breakaway friction (friction to start rotation) and the friction during maintained rotation. The AAR tests were performed on a segment of

rail that was glazed on the top of the rail; the top of the rail was subjected to pure rolling and, at the end, to rolling/sliding contact (Figure 3). The static friction coefficient of the untreated 1080 rail steel varied from 0.2 to 0.5, depending on the applied load, whereas the friction coefficient of the glazed regions varied from 0.1 to 0.25. Dynamic friction coefficients for the glazed regions varied from 0.2 to 0.35, depending on load, compared with 0.2 to 0.55 for unglazed regions.

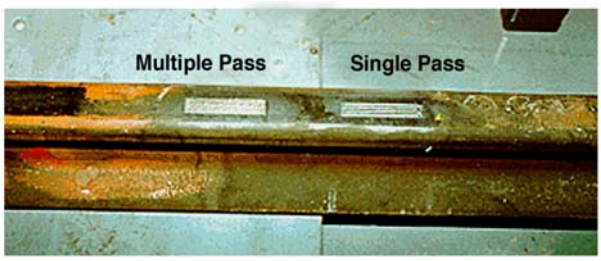

Figure 3. Segment of laser-glazed 1080 rail used in AAR friction tests.

The benchtop tests at ANL were more controlled than the full-scale tests at the AAR facilities. The environment was more repeatable in terms of surface contaminants and more consistent in terms of relative humidity, two factors that significantly affect the frictional response. The POD tests used flats of 1080 steel, glazed and unglazed, that rubbed against stationary balls or pins (52100, 1080 steel, 440C, or alumina). The tests revealed that the composition of the pin/ball had a significant impact of the friction coefficient (Figure 4). The general trend was that the glazing reduced the friction coefficient by 3–35%, depending on the material. The greatest reduction was for the alumina ball sliding against the 1080 steel, suggesting that a strong chemical adhesion mechanism may be active with the metallic counterparts.

A twin-roller test configuration (Figure 5) was also employed to more closely simulate the rolling contact stresses present at wheel-rail interfaces The system shown in Figure 5 was used extensively to simulate the stresses

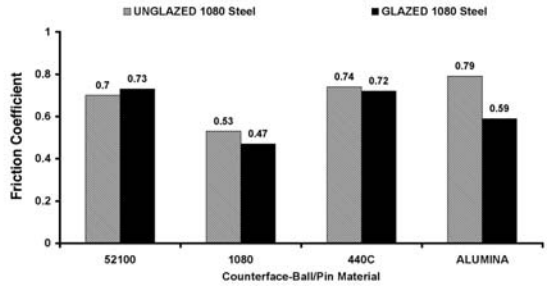

Figure 4. Pin-on-disc friction coefficient data for glazed and unglazed steel sliding against different pin materials.

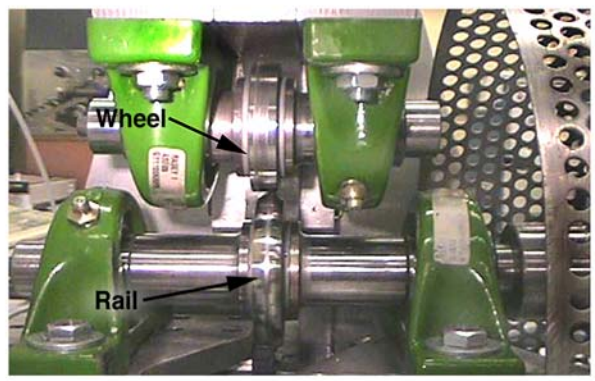

Figure 5. LA-4000 twin-roller test rig used to simulate high contact stresses.

present in 100-ton rail cars. The system is configured to measure the lateral friction forces. Tests were performed with 1045 steel rail and wheel discs that were through hardened (Rc 40) or glazed. The glazing effectively reduced the friction coefficient from roughly 0.4 for the unglazed condition to 0.3 for the glazed rail rotating an unglazed 1045 steel counterpart (Figure 6).

Similar tests were performed on 1045 steel rollers that were treated with a diode laser by a commercial vendor (NuVonyx). The NuVonyx-treated samples also exhibited lower friction than the untreated steel; however, the low-friction behavior did not endure for as long as that of the ANL-treated coupons. The difference in endurance is due in part to the fact that the NuVonyx laser treatment was not as well optimized as the ANL treatment.

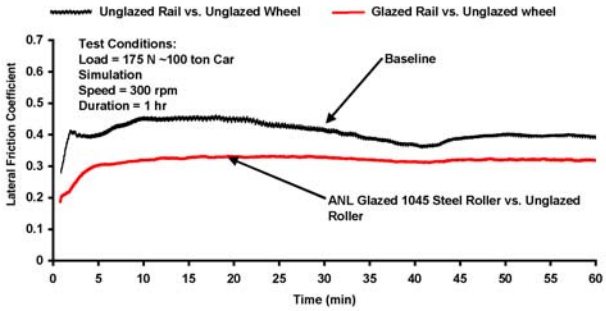

Figure 6. Twin roller friction data on glazed and unglazed 1045 steel.

Tests were also performed to evaluate the durability of the glazed region, in particular to determine whether the glazed region would delaminate from the underlying steel. This is a major concern for railroad applications because delamination could be a precursor to the formation of cracks that lead to rail degradation. Long-term (24–48 h) twin roller tests at a high angle of attack were performed on the twin-roller rig shown in Figure 5. A 24-h test simulates the passage of ≈1100 100-car trains (each loaded at 100 tons). In all cases, the glazed region remained intact and showed no evidence of delamination.

Microstructural characterization of glazed steel coupons was performed to determine whether a "white layer" was produced that could account for the reduced friction. Optical and electron microscopy (both scanning and transmission microscopy [SEM and TEM]) were used to characterize the microstructure. Microhardness was also measured in the glazed regions as a function of depth into the substrate.

Characterization by cross-sectional SEM of as-glazed 1080 steel coupons indicated a martenisitic region (glaze) over the base 1080 steel (pearlitic). High-resolution cross-sectional SEM of multipass laser-glazed 1080 steel that was subjected to rolling-sliding wear at the TTCI confirmed the presence of martensite. The martensite/glazed region consisted of two grain structures: equiaxed and columnar, as shown in Figure 7.

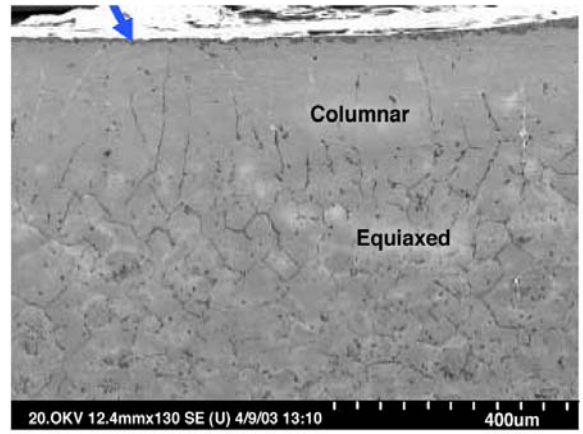

Figure 7. Cross-section SEM of multipass glazed steel subjected to rolling-sliding wear.

The presence of a thin white layer with a different microstructure was not confirmed. A thin layer (2–10 micrometers thick) was observed, but this was attributed to edge rounding that occurred during sample preparation.

The microhardness of several samples was measured. The results were very consistent from sample to sample, even between samples produced by the ANL process and the NuVonyx process. The 1080 substrate hardness was 300–400 Knoop, increasing to ≈1100 Knoop and decreasing to 800–900 Knoop near the surface. Samples that were exposed to multipass laser treatments were softened, the near-surface regions maintained a hardness of 800–900 Knoop; however, in regions further from the surface, the hardness decreased to 500–600 Knoop.

DiMelfi of our group is developing a model for deformation in nanocrystalline metals that is consistent with the observed deformation characteristics of such materials. The model is relevant to this project in that if rapid solidification by laser glazing leads to a nanocrystalline surface layer, that layer will deform in accordance with those observed characteristics. These deformation characteristics support reduced friction and wear. Like metallic glasses, nanocrystalline metals exhibit very high yield strength because plastic flow is not facilitated by

crystal dislocations in such materials. Also, after yielding, flow in nanocrystalline metals is nonhardening, and, therefore, perfectly plastic.

Related to this is the observation that flow is restricted to narrow, shear bands in these materials. This phenomenon leads to plastic instability and limited bulk ductility in tension, but allows considerable plastic flow in compression. In theory, plastic flow is accomplished by sliding along grain boundaries, which, in as-formed nanocrystalline metals, are in a higher energy state than they are in the same metal with a conventional grain size. Physical properties of the boundary—such as atomic arrangement, excess free volume, and other deformation-related properties—are tied to the grain boundary diffusivity. As in many shear-banding situations, flow must initiate at some local stress concentration or weak boundary. The sliding boundary will induce sliding in neighboring boundaries, not so favorably oriented, by imposing an additional local shear stress on them.

In addition, a sliding boundary can experience an increase in excess free volume because flow must occur in a non-conservative way by moving atoms past one another without the aid of dislocations. This excess free volume makes the deformed boundary more susceptible to further flow. Therefore, shear not only propagates across the material from one sliding boundary to another, but it is restricted to a narrow shear band associated with the deformation-weakened boundaries. The result of this mode of deformation can result in not only nonhardening flow (because there are no dislocations), but also strain softening, albeit at a very high flow stress. Hence, energy losses (friction) from plasticity are limited because of the high yield stress, and, if yield does occur, it does so in a nonhardening manner, which mitigates delamination wear.

Conclusions

The technological feasibility of utilizing laser glazing to improve the friction (and wear) performance of steels has been demonstrated. Laser-glazed segments of steel commonly used in railway applications exhibited lower friction in large-scale rolling-sliding and benchtop tests.

Future tasks will address several major barriers that must be overcome before this technology is adopted by the railroad industry as a method to improve fuel economy. These tasks include demonstration tests at the CNRC Ottawa test facilities, and the TTCI test loop in Pueblo, Colorado. The TTCI tests will involve glazing a large segment of rail and placing it in one of the test loops, where it will be exposed to train traffic. Before the TTCI tests, full-scale wheel tests will be performed on glazed rail/wheel sets to confirm that the friction (and durability) improvements observed in prior tests are achievable under full-scale geometries. The CNRC tests are also designed to confirm that the glazed regions will not undergo delamination and potential train derailments at the TTCI test loop.

Publications and Presentations

Saud Aldajah, George R. Fenske, Oyelayo O. Ajayi, and Sudhir Kumar, “Investigation of Top of Rail Lubrication and Laser Glazing for Improved Railroad Energy Efficiency,” presented at 2002 ASME/STLE International Joint Tribology Conference Cancun, Mexico, October 27–30, 2002.

Saud Aldajah, “Tribological Effect of Laser Glazing and Top-of-Rail Lubrication on Wheel-Rail Interaction,” Ph.D. dissertation, Illinois Institute of Technology, Chicago, Illinois, December 2003.

C. Laser Surface Texturing of Seal Faces

George Fenske, Ali Erdemir, Layo Ajayi, Andriy Kovalchenko, Robert Erck
Argonne National Laboratory, Energy Technology Division, Argonne, IL 60439
(630) 252-5190, fax: 630-252-4798, e-mail: gfenske@anl.gov

Technology Development Area Specialist: Sid Diamond
(202) 586-8032, fax: (202) 586-1600; e-mail: sid.diamond@ee.doe.gov
Field Technical Manager: Philip S. Sklad
(865) 574-5069; fax: (865) 576-4963; e-mail: skladps@ornl.gov

---

Contractor: Argonne National Laboratory
Contract No.: W-31-109-ENG-38

Objective

- Evaluate friction and wear performance of laser-textured surfaces.
- Identify candidate components and evaluate performance of laser-textured surfaces for specific applications.
- Optimize laser microdimple size, depth, and density to achieve maximum performance.
- Explore the effects of super-low-friction coatings on performance of dimpled surfaces.

Approach

- Apply laser texturing to water pump face seals of SiC ceramic and evaluate the performance in an instrumented seal tester.
- Conduct oil-lubricated friction and wear tests for laser-textured steel surfaces for both conformal and nonconformal contacts by using both unidirectional and reciprocating sliding.
- Combine near-frictionless carbon (NFC) coatings and other low-friction and wear-resistant coatings with laser surface texturing (LST) for synergistic effects in both ceramic seal and oil-lubricated steel contacts.

Accomplishments

- Characterized size, depth, shape, and density of microdimples on SiC face seals and steel samples by using three-dimensional (3D) microsurface optical profilometry and electron microscopy.
- Determined from seal test results that laser-dimpled surfaces reduced frictional torque by 40 to 60%, depending on face pressure and other test conditions.
- Found that laser-dimpled SiC seal surfaces showed some wear marks, especially after tests under high face pressures.
- Found that, under unidirectional conformal contact sliding, LST reduced the friction coefficient of lubricated steel surfaces substantially, especially under boundary and mixed lubrication regimes.

- Found that LST expanded the range of operating contact parameters for the hydrodynamic lubrication regime to lower speeds and higher loads.

Future Direction

- Characterize the effect of the laser-texturing process on changes to the microstructure and properties in the vicinity of dimples for ceramic (SiC) and steel materials.
- Optimize the dimple parameter for various lubrication regimes and for various seal and engine component applications.
- Combine LST technology with low-friction and superhard coatings for maximum reduction in friction and wear in ceramic face seals and oil-lubricated steel engine components.

Introduction

SurTech Ltd. has developed a laser surface texturing (LST) technology that enhances the overall tribological performance of lubricated sliding and rotating surfaces. This technology involves creation of microdimples (100 µm diam and about 10 µm deep) having a regular pattern applied on a given surface by a pulsating laser beam. Under hydrodynamic lubrication, and in the conformal contact configuration, microdimples on the contact surfaces can lower friction coefficients and may reduce wear. Under oil- or water-lubricated conditions, shallow dimples can serve as reservoirs for oil or water and thus increase the hydrodynamic lubrication efficiency of these surfaces. This low-friction technology has the potential for application in various engine components, such as the interface between the face seal and cylinder liner piston ring.

The main objective of this project is to produce well-controlled dimples on sliding and rotating conformal surfaces and to evaluate their tribological performance under the wide range of conditions typically found in engines and rotating equipment. At this initial phase, the tribological evaluation will focus primarily on rotating face seals and lubricated engine components. The issue of the durability of the dimples and possible optimization of dimple size, depth, and pattern for various lubrication regimes is also being investigated. Furthermore, potential beneficial effects of soft and hard overcoats having superhard and low-friction properties are also being explored.

In FY 2003, efforts at Argonne National Laboratory were devoted to evaluating LST for water pump seals and oil lubrication of steel surfaces. Several SiC face seals and rectangular steel samples were laser-textured with microdimples by Surtech Ltd. Dimpled samples were returned to Argonne for characterization and testing. Some of the seals were tested at Argonne in a mechanical face-seal test machine for wear studies, while a few of the dimpled seals were sent to Western Michigan University for high-precision torque measurements. Argonne has also worked on the application of NFC coatings on a few of the seals to further enhance their friction and wear performance. The textured steel samples were all tested at Argonne.

Results

Seal Tests

In a series of seal tests, Argonne investigated the wear behavior of dimpled SiC seal surfaces. Figure 1 shows a 3D image of a dimpled SiC face seal. As is clear in the figure, the dimples are produced in a geometric array, and they are typically 4 to 5 µm deep and about 100 µm in diameter.

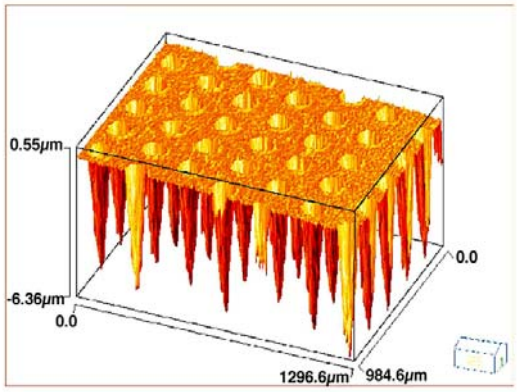

Figure 1. 3D image of laser-dimpled SiC seal face.

After undergoing wear tests on the dimpled surfaces at face pressures of up to 50 psi, the dimples remained mostly intact, but at much higher face pressures, some wear marks were observed, especially at or near the center of the wear tracks (as shown in Figure 2).

Figure 2. Laser-textured surface after wear test at 100-psi face pressure.

The depth of wear groove is about 1 µm. Also, some of the dimples appeared to have been filled with wear debris particles, as evident from Figure 2.

Torque measurements of laser-dimpled seals were performed at Western Michigan University in a highly instrumented seal test machine. These tests involved two control seals of directly sintered silicon carbide with standard production lapped surfaces and two laser-dimpled seals.

During these tests, two repeat tests on control rings showed similar performance, indicating that the test protocol was highly reproducible and reliable. One of the results from these tests is presented in Figure 3. Likewise, the two laser-dimpled rings also performed comparably well. Figure 4 shows the test results from one of those rings. The start-up and changes under pressure during tests often cause some instability in operation, as evidenced by rises in both the torque signal and seal face temperature. This is usually a short term situation and is commonly seen in the operation of all conventional seals. However, the laser dimpled rings had torque values significantly lower than those of the control rings at the same operating pressures, indicating that laser texturing had a positive impact on the performance of SiC seals. A slight reduction in face temperature was also noted for the laser-dimpled seal faces.

After the torque measurements were taken, wear of rotating surfaces was also investigated with a 3D surface profilometer. The results of these studies are summarized in Table 1. As is clear in the data, the wear of laser-dimpled seal faces is slightly higher than that of the control seal. The higher insert wear may have been due to the rougher surface finish of the dimpled seals.

Lubricated Steel Test

Unidirectional sliding tests were conducted on oil-lubricated seals with a commercially available test rig (CSEM) in the standard pin-on-disc contact configuration. The “pin” consisted of a 9.55-mm-diam hardened 52100 steel ball with a nominal hardness of 60 Rc, on which a 4.7-mm-diam flat area was created by grinding. This results in a conformal contact interface with the rotating disc, as shown schematically in Figure 5. The 50-mm-diam, 10-mm-thick disc samples are made of hardened H-13 steel and also have a nominal hardness of 60 Rc. Tests were conducted with disc samples that had ground, polished, and dimpled surfaces. Tests were conducted with normal loads of 2, 5, 10, and 20 N and sliding speeds of 0.015 and 0.75 m/s. All the discs were lubricated

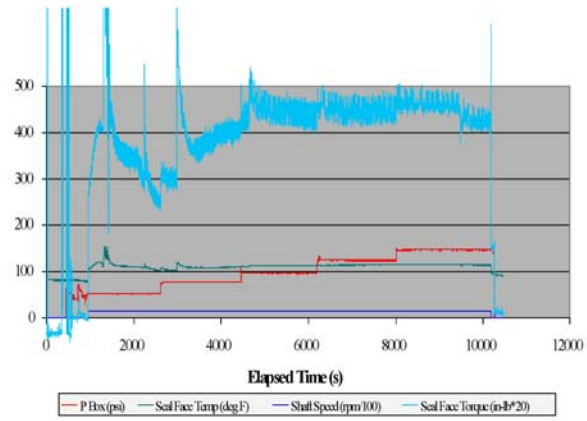

Figure 3. Seal face temperature and torque as a function of time for an untreated (control) seal. The torque signal was multiplied by 20 to show it more effectively on the same axis as chamber pressure and seal face temperature. The tachometer reading was divided by 100, so the operating shaft speed (1800 rpm) shows as 18.

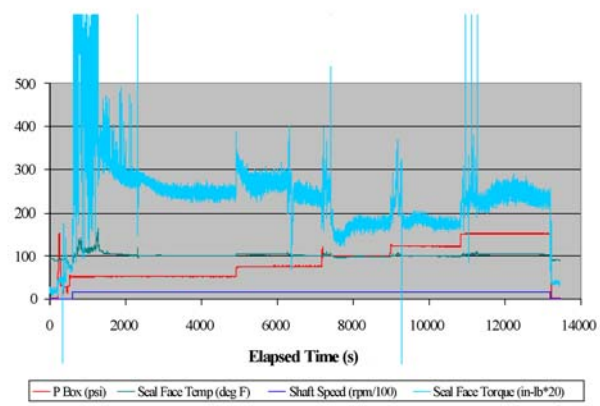

Figure 4. Seal face temperature and torque as a function of time for laser-dimpled seal, verifying significant reduction in torque. The torque signal was multiplied by 20 to show it more effectively on the same axis as chamber pressure and seal face temperature. The tachometer reading was divided by 100, so the operating shaft speed (1800 rpm) shows as 18.

Table 1. Depth of wear in control and laser-dimpled seal faces and counterface inserts

SiC ring	Insert no.	Ring wear, µm	Insert wear, µm	Comments
Control	1	0.55	0.20	Insert shows some roughening across much of the wear track. Band ~1 mm wide at ID shows the most overall wear. Ring shows overall wear of the contact area
Laser dimpled	2	0.71	1.26	Insert appears slightly roughened over entire contact area. Typical wear pattern shows 1-mm band of overall wear at ID. Ring wear pattern is typical; maximum wear at ID of wear track

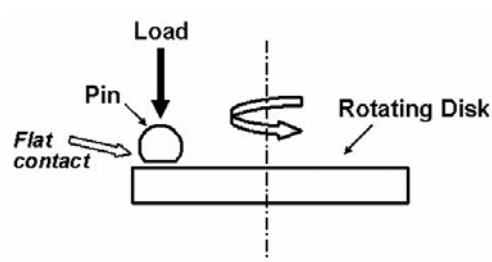

Figure 5. Schematic diagram of lubricated pin-on-disc contact configuration.

with a polyalphaoletin-based commercial engine oil. The test procedure consisted of starting each test at the low speed of 0.015 m/s and a constant load. The sliding speed was increased in 0.05-m/s steps after 3 min at each speed. The test protocol ensured that each test contact started in the boundary lubrication regime but moved into the mixed and finally the hydrodynamic lubrication regime as sliding speed increased.

The variation of friction coefficient with time and hence sliding speed for a typical test is shown in Figure 6. The friction behavior in the test with the ground disc shows the classic Streibeck curve, in which the friction coefficient under the boundary lubrication regime is high, with a typical value of about 0.12. As the sliding speed increases, the oil film thickness also increases. After about 180 s, the ratio between oil film thickness and composite surface roughness [the so-called lambda (λ) ratio] moves the contact into the mixed-lubrication regime, with a concomitant reduction in friction. At much higher speeds, the oil film thickness is high enough to completely separate the sliding surface, and hydrodynamic lubrication is in effect.

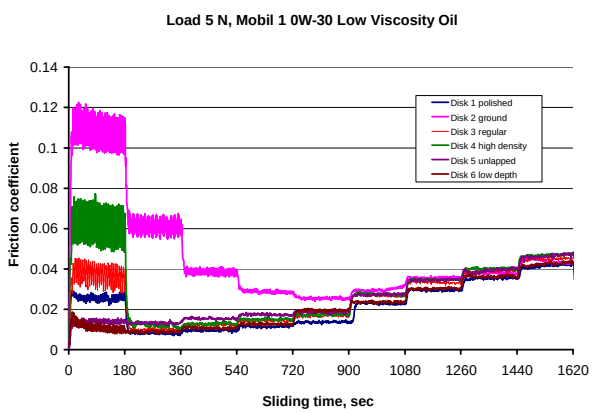

Figure 6. Variation of friction coefficient with time (and velocity) in test with discs having different surface treatments.

The friction behavior for other dimpled and polished discs also shows the same trend, but with much lower magnitudes at the low sliding speeds. This finding suggests that microdimpling either reduces the magnitude of the boundary regime friction coefficient or shifts the operating condition for boundary lubrication to lower speeds. The operating mechanism requires further study.

Discussion

Results obtained so far from seal testing have indicated that laser dimpling of face seals can substantially lower torque, but at the same time it may lead to a slight increase in wear. This is perhaps due to the dimpled surfaces becoming somewhat more vulnerable to micro-fracture and hence wear. The sharp edges of dimples may occasionally cut into the counterface inserts and thus cause higher wear on these surfaces, as shown in Table 1. The exact mechanisms may be much more complicated than speculated here. To overcome these problems, we are currently applying low-friction coatings like NFC on laser textured seal faces. These NFC-coated seals will soon be tested for both torque and wear reduction at Western Michigan University.

Results of the lubricated steel testing for laser-textured surfaces showed that the technology has good potential to reduce friction in components currently operating under the boundary lubrication regime. If the friction reduction is accomplished through the expansion of the hydrodynamic operating regime, it can provide means for engineers to optimize their designs for effective lubrication by incorporating LST on one of the contacting components.

Conclusions

Studies to date have confirmed that laser dimpling has a beneficial effect on the performance of SiC seal faces. Specifically, dimpling substantially reduces torque and thus can increase energy efficiency of electrical motors used in pumps. Laser dimpling causes a slight increase in wear, but we feel that this problem can be reduced or eliminated by applying a low-friction carbon

film, such as NFC, on these surfaces. For oil-lubricated steel surfaces, LST reduced the friction significantly under contact conditions of high-friction-boundary lubrication.

D. Joining of Advanced Materials by Plastic Deformation

Principal Investigator: J. L. Routbort
Argonne National Laboratory
9700 S. Cass Avenue, Argonne, IL 60439-4838
630-252-5065, routbort@anl.gov

Co-investigators: F. Gutierrez-Mora, D. Singh, N. Chen, and K. C. Goretta
Argonne National Laboratory
9700 S. Cass Avenue, Argonne, IL 60439-4838

Technology Development Area Specialist: Sidney Diamond
202-586-8032, fax: (202) 586-1600; sid.diamond@ee.doe.gov
Field Technical Manager: Philip S. Sklad
630-252-506; routbort@anl.gov
(865) 574-5069; fax: (865) 576-4963; e-mail: skladps@ornl.gov

---

Contractor: Argonne National Laboratory
Prime Contract No.: W-31-109-Eng-38

Objective

- Join advanced materials such as ceramics, cermets, intermetallics, and composites by plastic deformation.
- Characterize the interfaces.

Approach

- Apply a modest compressive load to two pieces of similar or dissimilar materials that have had little surface preparation in the temperature region where the materials are known to deform by grain-boundary sliding.
- Examine interfaces by scanning electron microscopy (SEM).
- Measure residual stresses after joining dissimilar materials and compare the measurements with those from finite-element analysis (FEA).
- Measure the strength of the interface by 4-point bend tests.

Accomplishments

- Made strong, pore-free joints with various ceramics, cermets, intermetallics, and composites with and without various interlayers.
- Achieved joint strength equal to that of the monolithic.

Future Direction

- Join intermetallics to ceramics; join biomaterials.
- Use functionally graded materials to distribute and reduce interfacial stress concentrations.

- Measure in-situ grain rotation during deformation or joining using the Advanced Photon Source (APS), pending funding.

Introduction

Joining by plastic deformation has been successfully applied in this program to various advanced ceramics (yttria-stabilized zirconia (YSZ) –alumina composites, mullite, sllicon carbide and titanium carbide whiskers in a zirconia-toughened alumina (ZTA) matrix, metal-matrix composites, and even an electronic ceramic, $La_{0.85}Sr_{0.15}MnO_3$ (1–5). Techniques have been developed to minimize sample preparation procedures and minimize the temperature at which the joining takes place. Among them, a spray application technique[2] and use of nanocrystalline powders or dense interlayers stand out.[2, 6] A patent application is pending. More recently, we have formed pore-free joints in Ni_3Al.

Although it is clear that joining by plastic deformation has few if any serious deficiencies when used to join similar materials, some issues remain to be addressed when dissimilar materials are to be joined. In those cases, when the materials joined have different thermal expansion coefficients at the high temperatures required for plastic deformation, residual stress are generated upon cooling. The thermal residual-stress distribution has been characterized in YSZ–alumina composites by FEA simulation and later compared with experimental observation from Vickers indentation measurements.[1]

During the last quarter of FY 2003, we performed 4-point bend tests on joined pieces of the same and different compositions of YSZ–alumina ceramics. Fracture mechanics principles, in conjunction with fractographic analysis, are used to explain the strengths of joined ceramics in the presence of residual stresses. This report will concentrate on those results.

Experimental Details

Dense YSZ–alumina samples of various compositions (YSZ volume fractions ranging from 20 to 100%) were prepared.[1] The resultant pieces were cylinders ≈1 cm in diameter and 1 cm in height. As-sintered samples without any further surface treatment were compressed together at constant crosshead speed in an Instron Model 1125 equipped with a high-temperature furnace. Experimental conditions were those where plastic flow is known to occur in ZTA, temperatures of 1250–1350°C and strain rates of $\approx 10^{-5}$/s.

As-prepared and as-joined samples were cut into bars of ≈2 × 2 × 15 mm for flexure testing. Four-point bending tests were conducted on samples polished to 1 µm at a constant crosshead speed of 1.3 mm/min using an inner load span of 9.5 mm and an outer load span of 14 mm. Strength was calculated from the maximum load at failure, and at least four specimens were tested per sample type.

FEA was carried out using the commercially available software ANSYS. Stresses in the joined products were simulated by considering a rigid, stress-free interface that is formed at high temperature and during subsequent cooling Residual stresses developed as a result of the different thermal expansion coefficients. The values of the elastic and thermal properties were measured experimentally.[1]

Results and Discussion

Table 1 shows the strengths of monolithic alumina, YSZ, and their composites. Strength for monolithic samples vs. alumina content follows a well-established trend. The strengths varied from 300 MPa for alumina to 1030 MPa for fully sintered YSZ. The strength of ZTA initially

Table 1. Flexure data for monolithic ceramics. Al_2O_3 and ZTA from literature

Material	Strength (MPa)
Al_2O_3	300
ZT80A	560 ± 70
ZT60A	580 ± 80
ZT50A	650 ± 100
ZT20A	1020 ± 150
YSZ	1030

increases and reaches a maximum for 20 vol % alumina and subsequently decreases with further alumina additions. Four-point bending tests were also carried out on ZTA (50 vol % each of zirconium and aluminum, designated ZT50A). Table 2 presents flexure test data for joined samples. Joined and monolithic samples did not exhibit a significant difference in strength. The strength of the joined samples was 620 ±100 MPa, within the experimental value for the monolithic material. whose strength was 650±100 MPa.

Table 2. Flexure data for joined ceramics

Joint	Strength (MPa)	Distance—fracture to interface (μm)
ZT50A/ZT50A	620 ± 100	
ZT60A/ZT40A	530	195
	360	270
	201	540
AT60A/ZT40A	500 ± 50	
ZT60A/ZT0A	440 ± 80	

The fact that the strength of the joined bodies and the monolithic samples was the same (compare ZT50A from Table 1 with ZT50A/ZT50A from Table 2) provides definitive evidence that joining by the plastic flow technique is viable and bodes very well for using the deformation joining technique for real-world applications.

Results were quite different when dissimilar materials were joined. However, as shown in Figure 1, a fracture occurred not at the interface but at some distance away from it, as indicated in Table 1. This is the result of

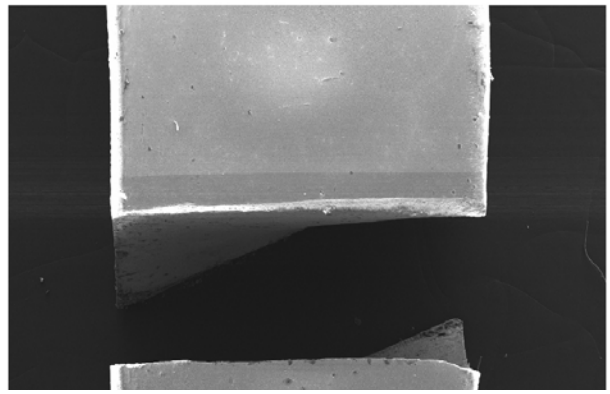

Figure 1. Fracture between ZT40A (upper) and ZT60A (lower). The fracture occurred in the ZT60A piece, not at the interface.

the residual stresses due to the differences in thermal expansion coefficients of the two materials. The distribution of stresses was calculated by FEA[1] and is shown in Figure 2.

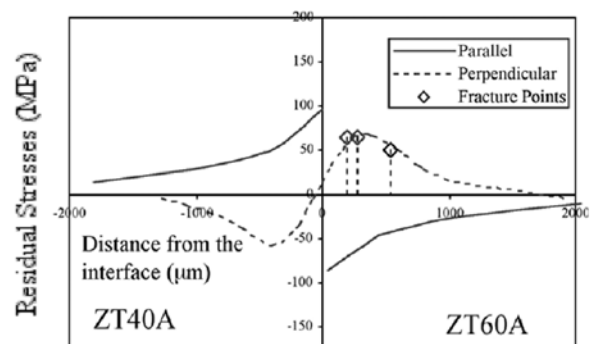

Figure 2. Plot showing the distribution of residual stresses as simulated by FEA for a ZT40A/ZT60A joint. Experimental data correspond to the distance from the interface at which the fracture took place in the flexure test.

A high tensile stress developed in the materials with the lower thermal expansion coefficient. The residual tensile stress resulted in fracture in the weaker material, away from the interface. The decreased strength compared with the value of the monolithic ZT60A can be attributed to the presence of residual stresses. In this regard, the distance from the interface at which fracture occurred is especially revealing.

To study the influence of the stress distribution, a series of joining experiments on the strength of the joined parts was conducted. These experiments consisted of bonding parts with various alumina fractions (ranging from 0 to 40 vol %) to a part of a fixed composition (ZT60A). Measured flexure strengths are shown in Figure 3, along with strength values for the monolithic composites. All samples failed in the ZT60A part, the weaker material, as discussed earlier. Strength was reduced as the difference in composition between the joined parts increased; consequently, the thermal-expansion coefficient and residual stresses increased. However, the reduction in strength was not dramatic. For the experiment involving the largest difference in composition (YSZ joined to ZT60A), flexure strength was decreased by 25% compared with the strength of monolithic ZT60A. These results provide a good indication of the applicability of the plastic joining technique when dissimilar materials with different thermal-expansion coefficients are bonded. It needs to be emphasized again that fracture did not take place at the joint.

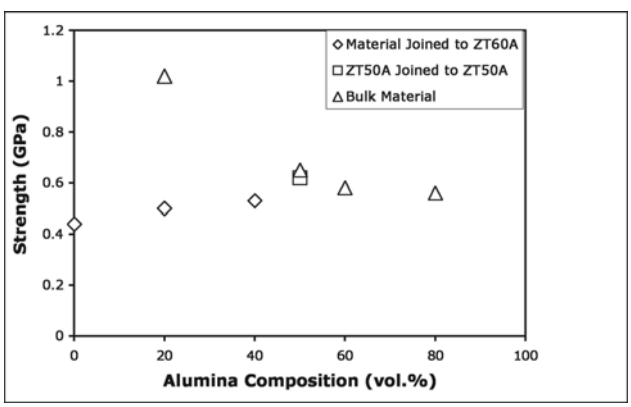

Figure 3. Representation of strength vs. alumina composition for monolithic materials. In the joining experiments, the alumina fraction corresponds to the composition of the materials being joined to ZT60A, while the strength is that of the ZT60A where fracture occurs.

The fracture strength of brittle materials without any surface residual stress can be given by

$$\sigma_f = K_{ic} / Y(a)^{1/2} \qquad (1)$$

where K_{ic} is the fracture toughness, Y is a geometrical factor and is $=2/\pi^{1/2}$ for a sample tested in the four-point-bend mode, and a is the length of the crack. Using the measured physical properties of the monolithic ZT60A and ZT40A, one can calculate that the critical flaws are 37 and 25 µm, respectively. These values are consistent with typical processing flaws.

The influence of residual stresses on the fracture from inherent processing flaws may now be considered. For ceramics with surface residual stresses, the apparent fracture toughness ($K_{Ic}^{app.}$) can be given by the expression

$$K_{Ic}^{app} = K_{Ic}^{o} + K_I^R \qquad (2)$$

where K_{Ic}^0 is the fracture toughness of the stress-free material K_I^R is the stress intensity from the surface residual stress and is given in terms of residual stress (σ_r), half-penny crack length (a), and non-dimensional stress intensity factor (Y) as $K_I^R = \sigma_r Y(a)^{1/2}$

For a four-point-bend test configuration, as used in this work,

$$K_I^R = 2\sigma_r (a/\pi)^{1/2} \qquad (3)$$

Therefore, the apparent fracture toughness is related to the flaw size by

$$K_{Ic}^{app} = K_{Ic}^{o} - 2\sigma_r (a/\pi)^{1/2} \qquad (4)$$

Using a flaw size of 40 µm and the apparent fracture toughness of ZT60A (3.6 MPam $^{1/2}$) as calculated from Eq. (1), the fracture strength is calculated to be 500 MPa, certainly consistent with the measured fracture strength of 530 MPa observed for one of the three samples tested.

The lower strengths of 360 MPa and 201 MPa observed for the two samples were believed to be due to larger flaws. To confirm this assumption, fractography was conducted on the two low-strength samples. SEM, as shown in Figure 4 shows surface damage on the tensile surfaces in two samples. It is likely that this damage was introduced during the sample preparation steps or handling. Typical lengths of this damage range from 70–90 µm. Using a nominal crack length of 80 µm and an apparent toughness of 3.6 $MPam^{1/2}$ for ZT60A, the fracture strength was calculated to be approximately 350 MPa. This value is consistent with that observed for the samples with surface damage (Table 1).

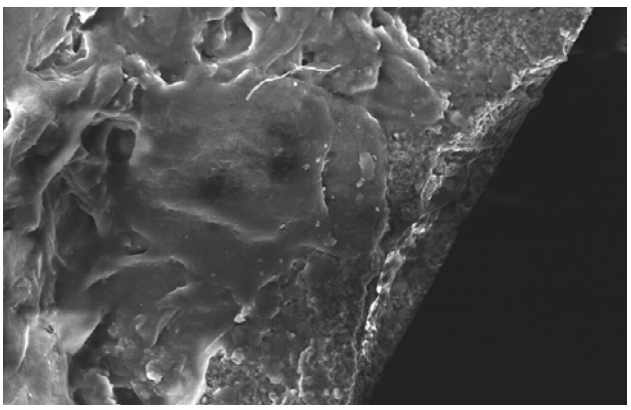

Figure 4. SEM micrograph showing a large flaw on the tensile surface of the ZT60A section from a fractured ZT60A/ZT40A joined sample.

Differences in thermal-expansion coefficients influence not only the mechanical response of the joined part, but also the joining process itself. Figure 2 represents an FEA simulation of the stress distribution along the center of joined pieces of ZTA ceramics. The stresses parallel (shear) and perpendicular (tensile) to the joint interface vary from the center to the edge of the two sections. The stresses parallel to the interface increase in magnitude at locations approaching the interface, whereas the perpendicular stresses decrease near the interface. It is believed that if the magnitude of the shear stresses is high enough and if there is a stress concentration at the interface, spontaneous fracture can occur in the joining process. This is clearly seen in Figure 5, which shows a YSZ-ZT60A sample that fractured spontaneously during joining.

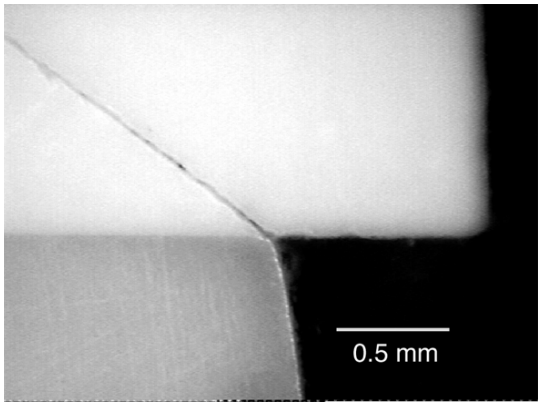

Figure 5. Micrograph of as-joined sample of YSZ/ZT60A. Fracture starts at the free surface and propagates, deviating away from the interface through the weaker material (ZT60A, top).

The fracture originates from the corner that acts as a stress concentrator. At the surface, because of the high shear stresses, the crack is parallel to the interface. As the crack traverses toward the center section, tensile stresses are more dominant and the crack becomes perpendicular to the interface. It is this change in stress intensities from shear to tensile that causes the kinking of the cracks observed for spontaneously cracked joint samples. Moreover, spontaneously cracked samples evince that the interface is strong, resistant, and pore-free, otherwise the sample would have fractured along the line of the joint.

However, the fact that residual stresses can make the joint fail spontaneously imposes a significant restriction upon the materials that can be joined by plastic deformation. The primary objectives are to control stresses, increase the strength of the joint, and, above all, prevent fracture during joining.

An obvious solution was to use an interlayer of an intermediate composition to reduce the residual stresses. However, FEA indicated that the stress reduction was only 30% (Figure 6)

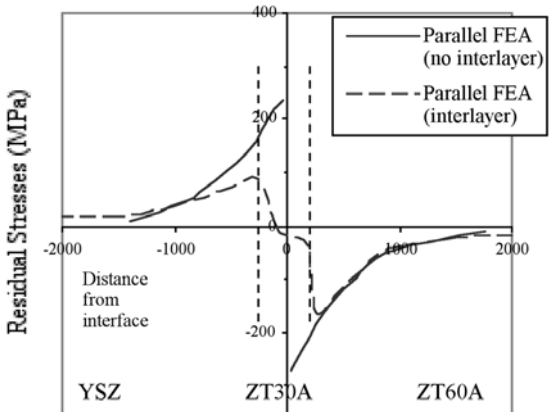

Figure 6. Comparison between residual stress distribution for a direct joint (YSZ/ZT60A) and the same joint using an 0.5 mm-thick interlayer of ZT30A.

ZT60A was jointed to YSZ with ZT30A interlayers of thicknesses of 10, 100, and 1000 µm. All samples exhibited failures similar to those in the direct joining experiment (Figure 7). The failure pattern is consistent with the stress profiles discussed earlier. In future work, we will use functionally graded materials to overcome this problem.

Conclusions

We have shown that we can form pore-free, very strong joints in a wide-variety of important materials by plasticity. We have joined structural and electronic ceramics, metal-matrix composites, Ni_3Al, whisker-reinforced ceramics, and cermets. Previous work has shown that experimental determinations of the residual stress agree with calculated values. Little surface preparation and modest temperatures are required for deformation joining. Those

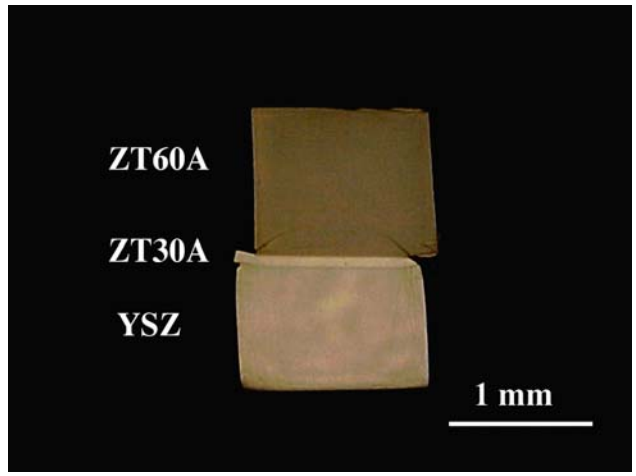

Figure 7. Fracture in a joined sample of YSZ bonded to ZT60A with an interlayer of ZT30A.

factors make the process attractive for commercialization.

It was originally assumed that the materials to be joined were superplastic and that the joining occurred by grain-boundary rotation. Grains would rotate and interpenetrate, resulting in a strong bond. However, many of the materials successfully joined are not superplastic. It is assumed, however, that most of the materials deform by grain-boundary sliding. So we believe that the critical process is the grain rotation that must occur in a grain-boundary sliding process in order to maintain strain continuity and avoid cavitation.

This assumption can be verified by performing in-situ experiments using the APS. Preliminary ex-situ experiments on 2.3-µm grain-sized YSZ have shown that we can identify single grains. Small rotations should allow us to determine the grain orientations. A recent proposal to perform more ex-situ APS experiments received extremely high marks. The ultimate goal would be to measure grain rotation while joining and to compare the rotations with those predicted from deformation theories.

References

1. F. Gutiérrez-Mora, K. C. Goretta, S. Majumdar, J. L. Routbort, M. Grimdisch,

and A. Domínguez-Rodríguez, "Influence of Internal Stresses in Superplastic Joining of Zirconia Toughened Alumina," *Acta Materialia*, 50, 3475–3486 (2002).

2. K. C. Goretta, F. Gutiérrez-Mora, J. J. Picciolo, and J. L. Routbort, "Joining Alumina/Zirconia Ceramics," *Mat. Sci. and Eng.*, A341, 158–162 (2003).

3. F. Gutierrez-Mora, K. C. Goretta, J. L. Routbort, and A. Dominguez-Rodriguez, "Joining of Ceramics by Superplastic Flow," in *Advances in Ceramic Matrix Composites VII*, *Ceramic Transaction # 128*, edited by N. P. Bansal, J. P. Singh and H. T. Lin, p. 251, The American Ceramic Society, Westerville, Ohio, 2002.

4. N. Chen, F. Gutierrez-Mora, R. E. Koritala, K. C. Goretta, J. L. Routbort, and J. Pan, "Joining Particulate and Whisker Ceramic Composites by Plastic Flow," *Comp. Struct.,* 57, 135–139 (2002).

5. F. Gutierrez-Mora and J. L. Routbort, "Electrical Characterization of a Joined Electroceramics $La_{0.85}Sr_{0.15}MnO_3$," *J. Am. Ceram. Soc.*, 85(9), 2370–2372 (2002).

6. F. Gutiérrez-Mora, A. Domínguez-Rodríguez, J. L. Routbort, R. Chaim and F. Guiberteau, "Joining of Yttria-Tetragonal Stabilized Zirconia Polycrystals using Nanocrystals, " *Scripta Mat.*, 41, 455–460 (1999).

E. Friction Stir Joining and Processing of Advanced Materials, Including Metal Matrix Composites

Principal Investigator: Glenn J. Grant
Pacific Northwest National Laboratory
P.O. Box 999, 902 Battelle Blvd.
Richland, WA 99352
(509) 375-6890; fax: (509) 375-44; email:glenn.grant@pnl.gov

Project Manager: Moe Khaleel
Pacific Northwest National Laboratory
P.O. Box 999, 902 Battelle Blvd.
Richland, WA 99352
(509) 375-2438; fax: (509) 375-6605; moe.khaleel@pnl.gov

Technology Development Area Specialist: Sidney Diamond
(202) 586-8032; fax: (202) 586-1600; email: sid.diamond@ee.doe.gov
Field Technical Manager: Philip S. Sklad
(865) 574-5069; fax: (865) 576-4963; email: skladps@ornl.gov

Contractor: Pacific Northwest National Laboratory
Contract No.: DE-AC06-76RL01830

Objective

- Investigate and develop friction stir joining (FSJ) and friction stir processing (FSP) as viable industrial joining and processing techniques for advance materials including aluminum metal matrix composites (MMCs), titanium, and high-strength steel. This project includes three main task areas:
  - develop an appropriate tooling that will survive the abrasive and/or high-temperature environment found when friction stir joining or processing aluminum MMCs, steels, and titanium
  - investigate the FSP process to modify the surface of materials for advantageous near-surface mechanical and thermal properties
  - develop numerical models to help in the application of the process to new materials.

Approach

- Develop characterization and test methods to distinguish between different tool material/base material pairs.
- Develop a performance database of different bulk tool materials for FSJ/P of aluminum MMCs.
- Develop tool coatings as an alternative technique to prevent tool wear in a wide range of conditions.
- Experimentally determine the feasibility of making near-surface graded composites by FSP in aluminum, titanium, and steel to create functionally graded materials with enhanced surface properties.

- Develop numerical models that can describe the thermomechanical conditions and material flow during FSJ/P.

Accomplishments

- Developed test methods to distinguish between different tool material/base material pairs using instrumented plunge tests.
- Developed numerical models using modified computational fluid dynamics codes that describe material flow around tools as a form of Couette-Taylor Flow.
- Created near-surface regions in aluminum and steel that are enriched in ceramic particulate by physically stirring powders into the surface, utilizing a spinning friction stir tool.

Future Directions

- Further develop tool materials for steel and titanium FSJ/P.
- Develop process parameters and conditions necessary for surface modifications of steel and titanium.
- Develop friction stir surface processing for thermal barrier applications.
- Develop the process of reaction surface processing to create, by solid-state chemical reactions, new phases at the surface.

Introduction

Friction Stir Joining

Developing and manufacturing energy-efficient vehicles requires a multidisciplinary approach. One of the key strategies for making vehicles energy-efficient is to manufacture them from lighter materials. Structural and functional requirements, however, lead to a situation where no single lightweight material is appropriate for all applications. A modern, weight-optimized vehicle structure is a hybrid of many materials. A critical problem that has emerged in the development of these hybrid structures is that for many material combinations, traditional joining technologies (like fusion welding or mechanical fastening) are not appropriate. For some highly specialized materials, like aluminum MMCs, titanium, and high-strength steels, a better joining technology can have significant impact on whether these materials have a role in future vehicle structures.

In the past ten years a new joining technology, FSJ, has emerged that has the potential to join many lightweight materials. This process, invented by TWI, Ltd., is a solid-state process that employs severe plastic deformation to create joints between a wide variety of different materials. A typical FSJ butt joint is depicted in Figure 1. The weld is created by clamping the materials to be joined and plunging a spinning tool into the surface. The spinning tool is then translated down the joint line, leaving behind a weld zone characterized by a fine-grained, dynamically recrystallized microstructure. Typically, the tool is spun at 400 to 2000 rpm and translated down the joint line at a rate of 4 to 300 in./min depending on tool design, base material, and thickness. As the tool rotates and translates, complex flow patterns develop in the base material that create an intimate mixing of materials from both sides of the weld. Heat input during plastic deformation generally creates a temperature in the weld between 0.6 and 0.8° of the absolute

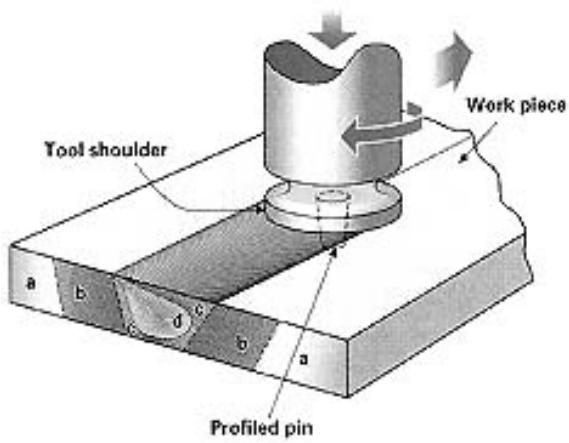

Figure 1. Friction stir joining and processing is accomplished by plunging a spinning tool into a material and translating the tool across the surface to form either a joint or a surface-processed region.

melting temperature, so no liquid phase is generated.

FSJ is capable of producing aluminum and magnesium alloy welds as good or better than fusion welds in terms of joint efficiency, mechanical properties, and environmental robustness. A significant advantage of the process for application to hybrid structures is that (because no melting occurs during the process) a large variety of dissimilar material joints are possible, including dissimilar aluminum and magnesium joints that are not possible with conventional fusion welding.

In the past five years, FSJ has been shown to be a commercially important, energy-efficient, and environmentally friendly process for joining aluminum. However, many opportunities exist for other higher-strength, lightweight materials to be considered if good joining technologies existed for these materials as well. The objective of this project is to investigate how FSJ can be applied to advanced materials, including Al-MMCs, titanium, and steels. Moving the FSJ process from "soft" materials like aluminum and magnesium into advanced, higher-strength alloys has proven to be challenging because of the mechanical and thermal demands on the tool materials. In steels, for instance, the tools must survive forge loads in excess of 10,000 lb and tool temperatures of 1100°C. A primary challenge is to develop pin tool designs and materials that can survive the high temperature and/or abrasive wear conditions under which the tool must operate.

Friction Stir Processing

Recently, a new research direction has emerged as an outgrowth of FSJ that recognizes that the same solid-state deformation process can be used to modify the surface of a monolithic material for enhanced properties. This new research direction is called friction stir processing (FSP).

Several applications of FSP have been investigated during the course of this project, including surface modification to improve wear resistance, create bulk superplastic properties, and improve the near-surface defect and porosity distribution in Al-MMC castings. Work during FY 2003 concentrated on the first application—creating a wear-resistant surface using FSP.

This work was designed to test the feasibility of using FSP to stir in ceramic particulate from the surface into a base material to produce a near-surface MMC. Work during previous years demonstrated that it is possible to create a discontinuously reinforced zone of 20-micron SiC or Al_2O_3 particles in a 6061 aluminum base alloy (Figure 2). Microscopy has shown that the stirred region is developed as deep as the pin probe (2 to 3 mm in our tests); it is defect free and forms a graded metallurgical bond with the underlying surface. No interface is developed between the composite zone and the base material. This process has the potential to produce a customizable surface. The surface zone has the potential to be orders of magnitude thicker than with conventional coating technologies, which has the added benefit of producing a graded structure that does

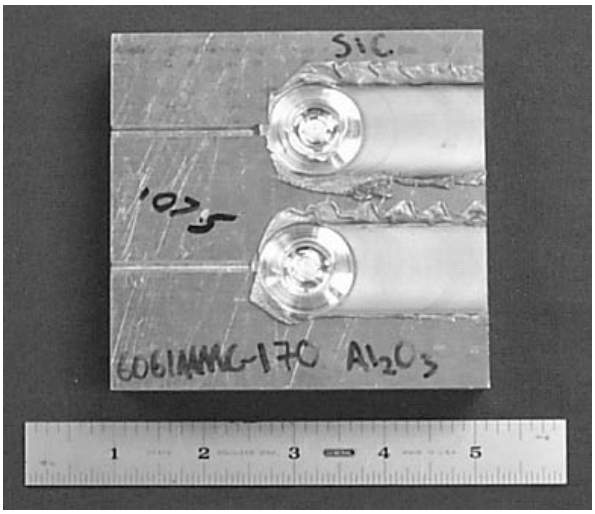

Figure 2. Friction stir processed 6061 plate with ceramic particulate incorporated into the surface by FSP

not have a sharp interface with the underlying substrate, thereby avoiding many of the problems seen in conventional coatings (CTE mismatch, etc.).

While lightweight, wear-resistant materials could benefit from this compositing technique, perhaps the greater application could be in ferrous or hard alloy systems. Hard particle reinforcement of the surface of steels, titanium, or brasses may have numerous industrial applications in reciprocating assemblies, engines, or other situations where both bulk strength and surface wear resistance is needed. Titanium or lightweight, high-strength steels with surface wear resistance may have numerous applications in both lightweight structures and lightweight vehicle power systems. Testing the feasibility of hard particle incorporation into titanium and steels is just beginning and will be a subject for next year's work.

Approach

The basic objective of this project is to investigate and develop FSJ and FSP as viable industrial techniques for advanced, lightweight materials. The approach is to (1) to develop new tool materials and designs that will allow us to make successful joints in Al-MMCs, titanium, and steel and (2) to explore the potential to modify the surface of conventional aluminum and magnesium alloys as well as advanced materials with the goal of improving wear, corrosion, or mechanical properties. This program is divided into three main tasks. The first task focuses on experimental testing of pin tool materials to identify critical factors for tool materials and design. The second task explores surface modification of metals by stirring ceramic powders into the surface to create functionally graded materials for wear and thermal management applications. The final task area supplements the first two and uses numerical modeling to gain understanding of material flow and microstructural development during FSJ/P to aid the design of appropriate FSJ tools.

Tool Materials Testing

Work during FY 2003 emphasized testing of appropriate tool materials for use in joining and processing aluminum-based MMCs. FSJ pin tool materials for joining and processing standard aluminum and magnesium alloys are hot-working tool steels (or Ni-alloy MP159 for harder 7xxx alloys). These tool materials show virtually no wear during FSJ/P of standard alloys. Al-MMCs, however, will cause significant tool wear after only a few inches of weld.

In an effort to characterize this wear and standardize it on a test method that could be used to compare many tool material–base material combinations, an instrumented plunge test system was implemented (Figure 3). These tests were designed to provide insight into the interaction between different tool materials and different types of Al-MMC base materials. Tool materials were plunged at a fixed load into the surface of 0.75-in.-thick MMC plates.

During the test, plunge rate, torque, and temperature were measured. Different tool materials showed significantly different

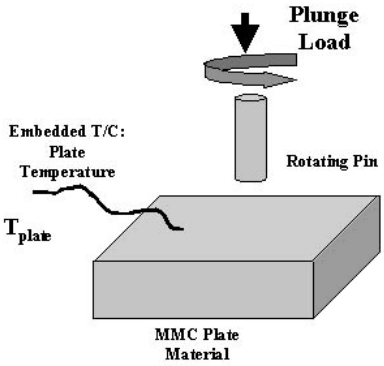

Figure 3. Schematic of instrumented plunge testing (top). Plunge pin in H13 tool holder (bottom). Test pins are fabricated from different materials and plunged into several different base materials to develop a test matrix.

plunge rates and spindle torques, as was expected from the heat flow characteristics of the tools. Three tool materials serve to bracket most of the plunge conditions encountered during testing—H13 tool steel, tungsten carbide, and silicon nitride (Figure 4). All other tool materials fall within a performance envelope defined by these three. For different combinations of tool and base materials, each of these had different plunge rates, heat generation, and base-metal deformation characteristics. Wear characteristics were also different, with H13 performing very poorly as expected (Figure 5), while the cemented carbides performed well. One of the best performers from a low tool wear perspective

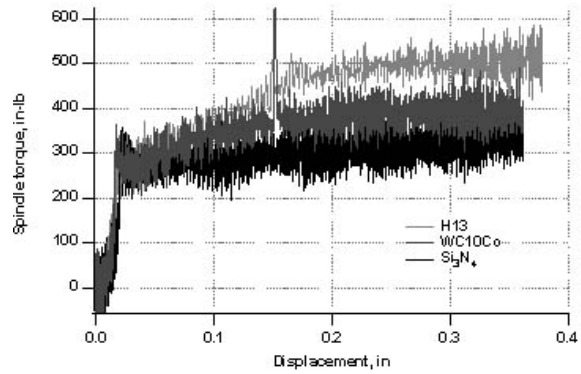

Figure 4. Graph of spindle torque vs. plunge displacement at a constant load. H13, tungsten carbide, and silicon nitride show different behavior in plunge testing.

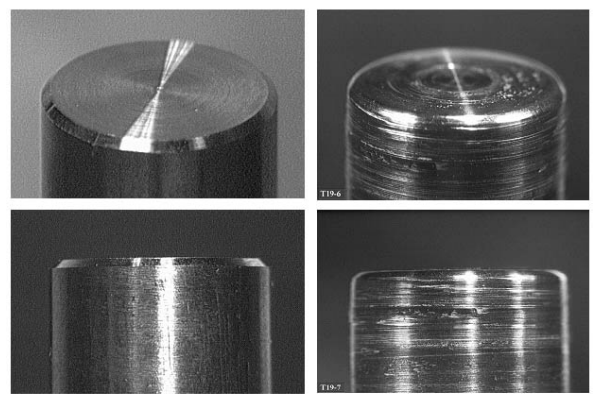

Figure 5. Wear performance of H13 in an instrumented plunge testing. The image on the right shows wear after 60 s of plunge testing.

was a powder metallurgy ferrous MMC product composed of 35% rounded TiC particles in a matrix of impact- resistant tool steel.

Tool Coatings Development

Of all the tool materials tested during FY 2003, the best successes in terms of low tool wear were tungsten carbide with 10% cobalt and a TiC-reinforced, impact-resistant tool steel called Ferrotic. But even with these excellent materials, some wear still exists that can negatively impact tool survival in a volume joining application and negatively impact the joint integrity because of joint

impurities. Therefore, the project has pursued the idea of tool coatings to prevent wear. Results from this year's work indicated that it is possible to protect the tool with an adhered layer of base metal promoted by tool coatings. Many candidate coatings were tested, but chrome carbide was the most successful in sticking aluminum base material to the face of a rod of H13 tool steel plunged into an MMC base plate (Figure 6). Surface wear on the tool was reduced under the adhered material.

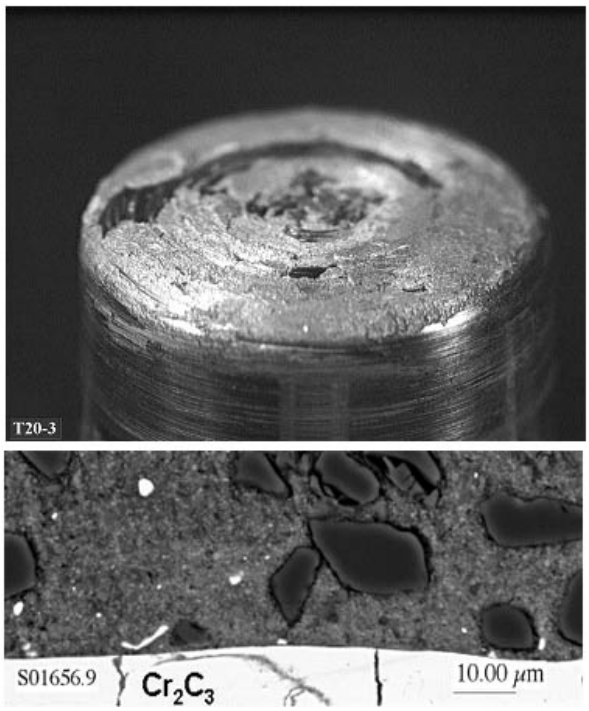

Figure 6. Chrome carbide coatings were successful in developing adhered metal zones on plunge pin tools (upper figure). Intimate, void-free contact exists between the Cr_2C_3 layer and the matrix aluminum (lower figure).

The study of coatings will continue in FY 2004 with the important goal of moving the idea into high-temperature materials. Coatings will be applied by electrospark deposition at Pacific Northwest National Laboratory (PNNL) and by laser deposition at the South Dakota School of Mines and Technology (SDSMT).

Another important discovery from the tool wear studies was that the bulk of the wear occurs during the initial tool plunge into the MMC base material. This is due in part to the higher flow stress of the initially cold material. To mitigate this, the project is now investigating the use of an induction preheater in front of the friction stir tool to preheat the base material. Work at SDSMT has also shown that using a preheater can increase welding speeds as well, which is an important consideration for the economics of volume applications.

Friction Stir Surface Processing

In FY 2003, the project was successful in creating functionally graded, near-surface MMC regions by friction stir surface processing. Two regions of particle enrichment were noticed—a near-surface region within 200 microns of the surface and a deeper region around the weld nugget. The surface region can contain as much as 50 area % ceramic particulate. The deeper region has a lower particulate area fraction, but in cross-section, it can show good distribution (Figures 7 and 8). These regions were created using a friction stir tool to physically stir surface-placed SiC powders into bulk 6061 T651 plate. Several tool

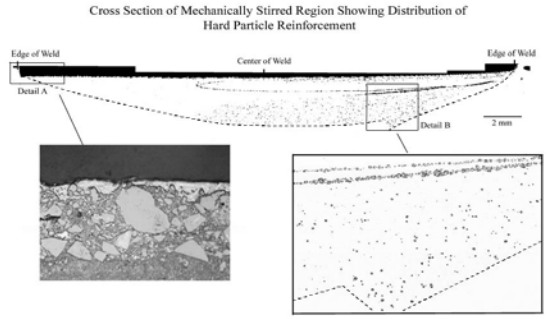

Figure 7. Silicon carbide distribution in 6061 T651 plate using a three-pin tool (PNNL internally funded work in FY 1999). Note the wide region of well-distributed particulate to a depth of 3 mm below the surface.

Figure 8. Silicon carbide distribution in 6061 T651 plate using a step spiral tool. High particle concentration occurs near the top surface, on the advancing side edge, and on the more homogeneous distribution in the nugget region.

designs were explored (Figure 9) in addition to many ceramic powder particle distributions and surface placement methods.

The work is ongoing to establish appropriate conditions for good particle distribution. One persistent feature noted from experimental work is that the particles tend to be distributed in regular bands. Figure 10 shows the distribution of particulate 0.025 in. below the surface (plan view). Figure 11 shows a cross-section micrograph of one of these bands showing the increase in microhardness within the band caused by fine ceramic particulate reinforcement. Microhardness values in the particle-enriched areas are over twice that in the bulk material and are periodic because of the banded distribution (Figure 12).

Experimental work at SDSMT has also revealed the possibility of creating in situ surface composites. When the precursor powders include both SiC and aluminum powder, the surface-processed regions contain an abundance of a fine-grained Al-Fe-Si intermetallic. This reaction is occurring well below the temperatures normally needed, which suggests the possibility that the severe plastic deformation that occurs in FSP may be providing energy for some solid-state reactions that were not previously anticipated. Thermodynamic calculations on numerous potential solid-state reactions

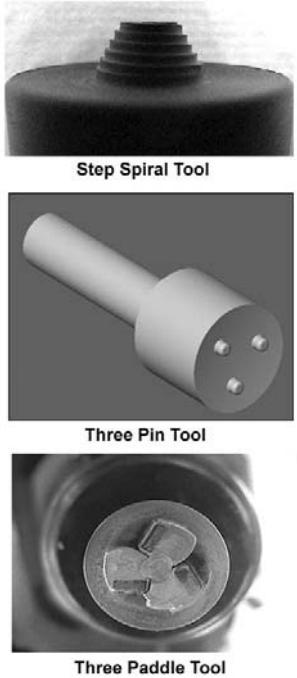

Figure 9. Different tool designs produce different particle distributions and flow characteristics

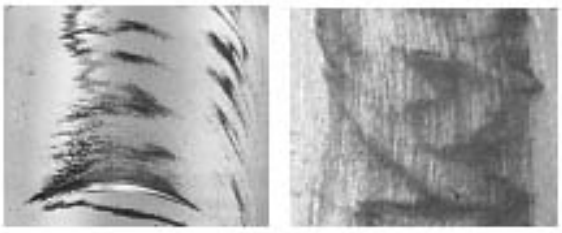

Figure 10. Plan view section cut 0.025 in. below the surface of the weld, showing banded distribution of SiC particulate when using a step spiral tool.

indicate that energies available during FSJ/P may be high enough to initiate the formation of some compounds, like TiB_2, from elemental constituents, especially considering all the new surface being generated by the severe plastic deformation under the pin tool. Project activities next year will include pursuing this work in aluminum, as well as in steels and titanium where in situ composites may have even greater application than in the aluminum system.

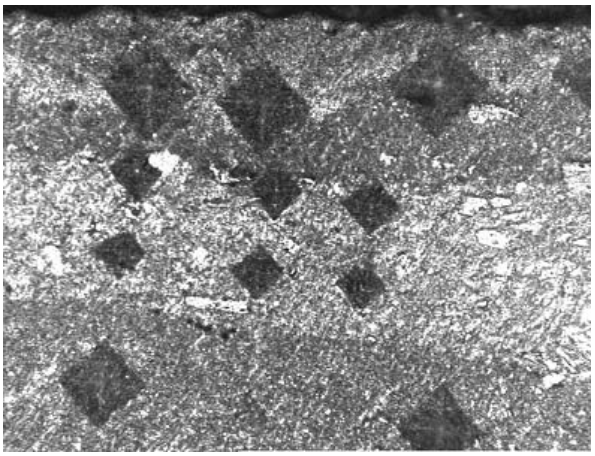

Figure 11. Microhardness across SiC particle-rich band.

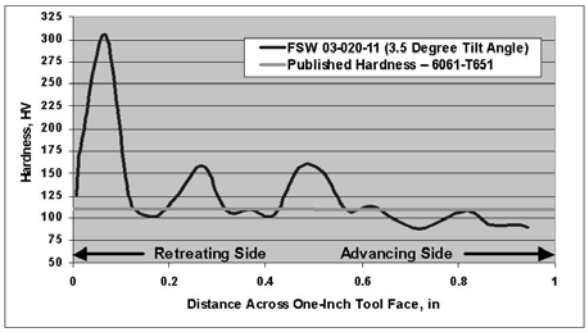

Figure 12. Microhardness values taken perpendicular to weld travel direction, showing periodic hardness distribution caused by the banded structure.

With these successes, researchers are now stirring powders into higher-temperature base materials. At present, we are stirring TiB_2 into 1018 steel and anticipate moving to titanium 6-4 by early 2004. FSP of ferrous or titanium materials is a technology in its infancy. Very little is known about processing conditions needed to incorporate powders or even about the feasibility of the process in some metallurgical systems. Also, use of this process to create ceramic particulate-reinforced surface zones in steel or titanium requires high-temperature FSP tools. Although some interim solutions exist for the high-temperature tool wear issue (this project uses high-density tungsten, 25% rhenium, and/or polycrystalline cubic boron nitride tools), tool survivability is an area that needs to make progress before the process can be fully implemented into the domestic industry.

Conclusions

FSJ/P technologies will enable the application of many lightweight materials in the next generation of transportation systems. Many advanced materials, such as Al-MMCs and certain high-strength steels, are in need of lightweight, cost-effective joining technologies before their widespread use is considered. Solid-state FSJ/P avoids many of the problems with fusion joining and represents a revolutionary change in joining technology. Problems still exist, however, mostly related to the survivability of tool materials during joining. A companion program at Oak Ridge National Laboratory is making significant advances in the development of bulk, high-temperature tungsten-based tool materials, and research at PNNL is focusing on coating strategies in an ongoing effort to address the tool-wear issues. The results of this work will allow designers to anticipate structures that are a hybrid of many different materials joined together into lightweight assemblies. These results will help achieve the goal of producing lighter and more fuel-efficient vehicles.

F. Friction Stir Processing of Advanced Materials

Principal Investigator: Zhili Feng
Oak Ridge National Laboratory
1 Bethel Valley Road, Oak Ridge, Tennessee 37831
(865) 576-3797, fax: (865) 574-4928, e-mail: fengz@ornl.gov

Technology Development Area Specialist: Sidney Diamond
(202) 586-8032; fax: (202) 586-1600; e-mail: sid.diamond@ee.doe.gov
Field Technical Manager: Philip S. Sklad
(865) 574-5069; fax: (865) 576-4963; e-mail: skladps@ornl.gov

---

Contractor: Oak Ridge National Laboratory
Contract No.: DE-AC05-00OR22725

Objectives

- Establish a method for specification of friction stir tool materials based on the relationships between workpiece and tool material properties.
- Characterize the mechanical properties and microstructures of joints created by friction stir processing (FSP).
- Investigate the feasibility of using FSP to modify the surfaces and surface properties of materials.

Approach

- For tool materials, conduct experimental evaluations of commercially available and experimentally formulated tool materials under FSP conditions.
- For particular workpiece materials, select the tool material based primarily on high-temperature strength, wear resistance, and chemical compatibility.
- Evaluate mechanical properties and their correlation with microstructures produced by FSP.

Accomplishments

- Purchased and installed a purpose-built FSP machine at Oak Ridge National Laboratory (ORNL).
- Made a major breakthrough in tool materials for FSP of high-temperature alloys such as steels and titanium alloys.
- Completed testing to study the interaction of tool materials with Al-based, metal-matrix composites.
- Used FSP to improve the surface strength and fatigue properties of high-strength Al alloy castings.

Future Direction

- Conduct additional plunge testing to better establish reference behaviors.
- Refine the method used to analyze friction coefficients and conduct additional testing to measure this important parameter for tool material–work material interactions.

- Produce specimens to measure the influence of FSP on the fatigue behavior of the A319 and A356 castings.
- Use transmission electron microscopy to characterize the microstructure improvements to the cast surfaces.
- Conduct x-ray diffraction experiments to evaluate the residual stress distributions in FSP surfaces.
- Obtain cast magnesium specimens and use them to begin evaluation of FSP on their microstructures and mechanical properties.
- Conduct preliminary evaluation of friction stir welding aluminum to 6061+20 wt % Al_2O_3 composite.
- Access the ability of FSP to produce rapidly solidified surface microstructures.

Introduction

Friction stir welding (FSW) is a relatively new (invented in 1991) solid state joining method that is now well established for the production of very high-quality welds of aluminum alloys of all types. The process is accomplished using a rotating, non-consumable tool that is translated along the length of a joint as illustrated schematically in Figure 1. The FSW process relies only on the energy of the rotating welding head to produce the weld. If the materials at the joint are in intimate contact, then a solid state bond can be formed. No supplemental power input is required by the process, and no melting of bulk materials occurs. Instead, the joint is produced by deformation processes. In principle, FSW can be used to join many types of similar and dissimilar material combinations, provided that tooling can be found that operates in the hot working temperature range of the workpieces. It may also be used to modify the surfaces of materials rather than to produce joints. Consequently, FSW is a subset of a more general set of materials processing operations referred to as friction stir processing (FSP).

Because melting is avoided, FSP also has potential for operating on many materials that are difficult or impossible to weld or process by more conventional methods, including alloys that are susceptible to solidification cracking, metal-matrix composites (MMCs), and oxide-dispersion-strengthened (ODS) alloys. For example, a benefit of FSP compared with conventional welding processes is that in aluminum-based alloys it is possible to make welds where the strength of the fusion zone is identical to that of the base metal alloy. For many fusion-welded Al alloys, the fusion zones are typically weaker than the base metal, so FSP offers a significant performance advantage. Additionally, because the energy input used for FSP is relatively low (no melting occurs), the heat-affected zones and residual stresses associated with the welds are relatively small. Minimizing the weld heat-affected

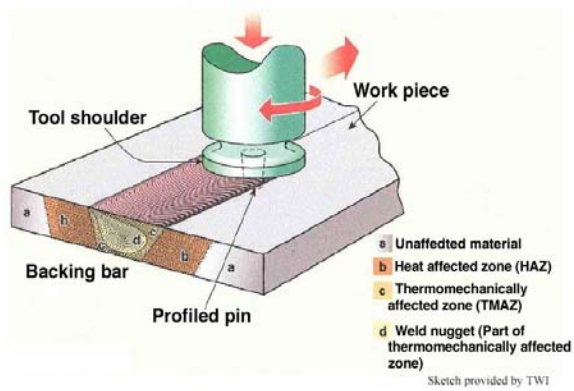

Figure 1. Schematic representation of friction stir welding.

zones reduces concerns about property gradients across the weld joints. Lower residual stresses mean that distortion associated with FSP is not as large a concern as with conventional welding. FSP is revolutionizing the welding of Al alloys by producing cost-effective welds with higher quality and lower distortion than is possible using fusion welding techniques.

The potential that FSP has for application to a wide range of materials is offset by the technical challenges of tool materials development. To illustrate this point, consider FSP of Al alloys. In this case, tool steels are typically used for the FSP rotating tools and the Al is frictionally heated to its hot working temperature range of 300–500°C. In that temperature range, tool steels are considerably stronger than the Al, partly because their melting temperatures are much higher (pure Al melts at 660°C; pure Fe melts at 1536°C). By analogy, an appropriate tool material to use for FSP of steel would require a melting temperature of about 2500°C or higher to have reasonable durability. No such materials are widely available. In addition to melting temperature issues, good FSP tool materials are also likely to require relatively high strength, toughness, and thermal shock resistance. Wear resistance will also be important especially for FSP of MMCs and ODS alloys. For example, the steels used for FSP tooling on Al MMCs typically deteriorate at relatively high rates. This limits tool life and the length of a continuous weld. Also, wear debris from the FSP tooling is incorporated into the microstructures where it may become an undesirable inclusion. Chemical reactivity between tool and workpiece materials will also be a major concern for long tool life. Presently, the relationships that define acceptable tool material properties are not well established, and this is the primary barrier for application of FSP for a wider range of materials than Al alloys, including MMCs, ODS alloys, and alloys with higher temperature capabilities than Al.

In this project, the materials used for welding will include Al alloys, magnesium alloys, Al-MMCs, ODS alloys, steels, titanium, and other advanced materials such as metallic glasses. A variety of dissimilar joints will be considered. Developments from the weld tasks will be extended to evaluate FSP to modify surface properties through friction cladding. Surface modification may include (1) modifying the intrinsic surface of a material by frictional heating, (2) adding another material such as metallic glass on a metal surface, or (3) modifying a surface that was initially treated by a separate process such as treating a thermal sprayed surface by frictional heating.

Acquisition of FSP Machine

The HSWR Materials Program helped support the acquisition of the state-of-the-art friction stir research machine shown in Figure 2.

Figure 2. Friction stir processing machine recently acquired from MTS Corp.

The capabilities of the FSP machine include

- Simultaneous force- or displacement-controlled operation of three independent axes
- Adjustable, adaptable pin tool for on-the-fly mode switching between fixed, adjustable, and self-reacting welding mode

- Computer controlled operations and key process parameter monitoring
- Capability to make nonlinear, variable thickness, and double curvature weld
- Welding speed up to 35 mm/s; weld thickness from 1 to 40 mm

The FSP machine was installed and operators trained, and the machine is now available for use.

Tool Material Development

Alloy design activities have led to the development of two new alloys that represent significant advancements beyond existing capabilities for welding high-strength alloys such as steels and titanium alloys. Initial testing has confirmed the performance potential of the new alloys. Further development and refinement of the alloys is continuing. However, this information is considered business sensitive at present and cannot be reported in any detail.

Evaluation of Materials for use on Al-MMCs

A simple plunge test was used to evaluate some of the interactions between 6061 + 20 wt % Al_2O_3 plates and flat-faced, cylindrical pin tools of H13 steel, WC bonded with 10 wt % Co, and gas pressure sintered Si_3N_4. The 12.5-mm-diam pin tools were rotated at 800 rpm under a normal force of 13,344 N and then driven into the plates to a depth of approximately 10 mm. Each test consisted of two segments—a constant-displacement-control plunge to a depth of 1.5 mm followed by a constant-force-control plunge from 1.5 mm to about 10 mm.

The forces supported by the pin tools in the constant displacement segments varied with pin tool material, as shown in Figure 3.

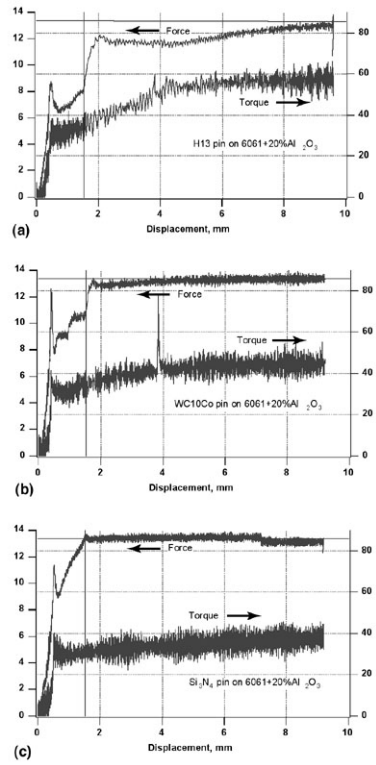

Figure 3. Variations of normal force and spindle torques during plunge tests.

Vertical lines are placed at 1.5 mm to distinguish between the segments of the seating plunges and the test plunges. In all three cases, the constant-displacement-rate seating segments show initial spikes in normal load as the rotating pin tools were driven into the plates. The normal forces increased throughout this period, but those measured at the end of the seating segments varied with the tool material. These normal forces were 8,362 N for the H13 tool, 10,991 N for the WC10Co tool, and 13,246 N for the Si_3N_4 tool. During the test segments, the normal forces rapidly approached the requested setpoint of 13,334 N that is indicated by horizontal lines in Figure 3. For the H13 pin tool, the measured force never actually attained the setpoint value. In contrast, the 13,344 N force was supported during the test by both the WC10Co and the Si_3N_4 tools. The measured spindle torques showed initial

rapid increases followed by slight gradual increases as the tests were run to completion. The pin rotational speed of 800 rpm was maintained during each test. The normal force and spindle torque measurements were combined to calculate an effective friction coefficient, μ_{eff}, for each data set as shown in Figure 4. The data are referred to as effective friction coefficients because the measurement techniques and geometry do not lend themselves to an analysis that would yield a friction coefficient according to a classical treatment. However, the normal force and the tool rotation speed of the plunge test do approximate those of actual FSW. The flat face of the cylindrical pin tools also approximates the shape of FSW tools without the complication of a pin or other intricate details of tool shape. Having test conditions that closely match application conditions is desirable when measuring friction properties. Consequently, the effective friction coefficients given in Figure 4 may then be considered representative of the actual friction conditions for those material couples during FSW. The effective friction coefficient values are also in the range of friction coefficients found for dry contact between other metal-metal couples, but somewhat higher than those between martensitic stainless steel (like H13) and similar Al-MMC. The increases of effective friction coefficient during the plunges were at least partially due to frictional drag between the pin shafts and plunge hole surfaces. This was evidenced by visible scuffing on the pin tool shaft surfaces after testing.

Further analysis indicated that the effective friction coefficients play an important role in the heating that occurs during FSP. The rate of heating during FSP will be proportional to the effective friction coefficient. From a practical point of view, high heating rates are desirable because they will contribute to maximizing the speed of the process.

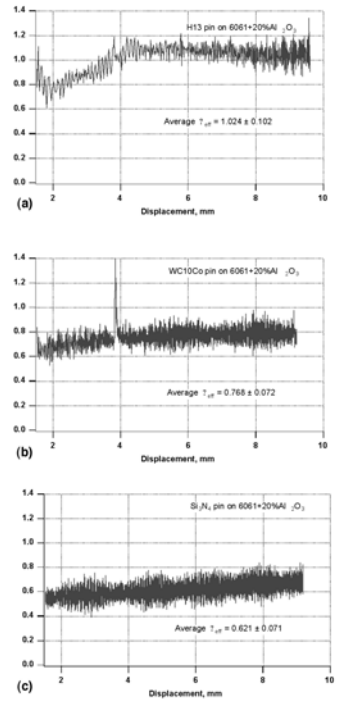

Figure 4. Variations of effective friction coefficients during force-controlled test segments.

FSP Surface Modification of Al Castings

Experiments were conducted in collaboration with staff of Ford Research and Advanced Engineering to evaluate the effects of applying FSP to the surfaces of Al alloy castings. Two types of cast alloys were used A319 (Al-6Si-3.5Cu wt %, nominal) and A356 (Al-7Si-0.3Mg wt %, nominal). Both of the alloys are generally produced as either sand or permanent mold castings that are widely used in engine, driveline, and suspension components in a wide variety of automobiles and light trucks. Most of these applications involve dynamic loading, and the interest in FSP is as a means of improving durability and reliability. Ingots for the as-cast experiments were supplied by Ford. The plates that were machined from the ingots had dimensions of 16 × 50 × 200 mm. The tools used for FSP were made from H13 tool steel. Several tools were evaluated for

the work, but the one used for the bulk of the FSP work had a 13-mm-diam shoulder with a pin having a diameter of 5.2 mm and a length of 3.4 mm. The pin shoulder was slightly concave with a smooth surface. The pin had a hemispherical nose and was smooth over its entire surface. The process parameters used with this pin were 1000 rpm with a translation speed of 1.7 mm/s. These initial experiments were conducted on a milling machine that was not instrumented or set up especially for FSP. However, FSP trials indicated that conditions of constant position of the tool relative to the plate surface produced better results than when a constant load was applied to the tool. Experiments were conducted to set the tool position using appearance and flash formation as acceptance criteria. After a relative position was established, it was used for all remaining experiments.

After processing conditions were established, single-pass FSP/W "beads" were produced for metallographic examination using views from both the weld surfaces and the cross sections. The effect of the FSP on the microstructure of A319 is shown in Figure 5. FSP produced a distinct boundary between the stirred zone and the base metal of the casting. Compared with the cast base metal (to the right in Figure 5), a relatively uniform distribution of small, somewhat regularly shaped particles was produced by the FSP. In addition, shrinkage porosity was closed in the stir zone. The results of applying FSP to the A356 were basically identical.

Hardness testing showed that the base metal hardness was preserved in the stir zones for both casting alloys. These data also showed that hardness was more uniform in the stir zones with soft spots associated with either porosity or large Al dendrites being largely eliminated.

To get a more detailed assessment of the effects of FSP on the casting properties,

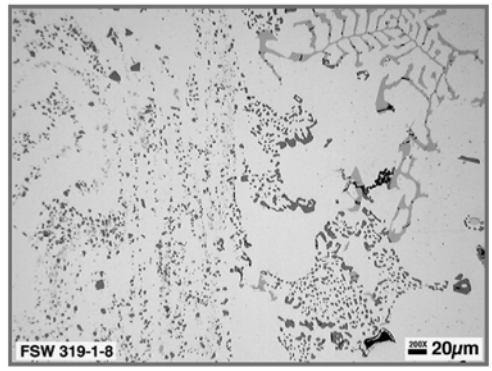

Figure 5. Optical micrograph taken on the surface of an FSP bead on A319 Al casting. The boundary between base metal and stir zone is approximately in the center of the micrograph with the base metal on the right and the stir zone on the left.

additional cast bars were produced using a series of overlapping FSP beads. A total of six overlapping beads were used on the machined bars to produce stirred volumes of approximately 3 × 25 × 150 mm as shown in Figure 6. Subsize tensile specimens were then cut from both the stir zones and the base metal. The specimens from the stir zones had gage lengths that were entirely within the stir zone. The gage dimensions were 2 × 12.5 mm. Figure 7 shows a surface with overlapped beads and the size and orientation of the tensile specimens relative to the cast bars.
The tensile tests were done at room temperature using a nominal strain rate of 0.001/s. Three specimens were tested for each condition, and the results are shown in Figure 8 for A319 and in Figure 9 for A 356. In both cases, the stir zones had considerably more ductility than the corresponding as-cast base metal. Further testing and data analysis will be required to draw firm conclusions about the data. However, the initial indication is that FSP is likely to produce significant surface or local improvement of the mechanical properties of Al castings. These findings

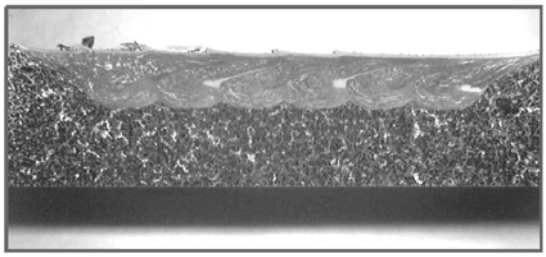

Figure 6. Photograph showing cross section view of overlapping FSP bead on a bar of A356.

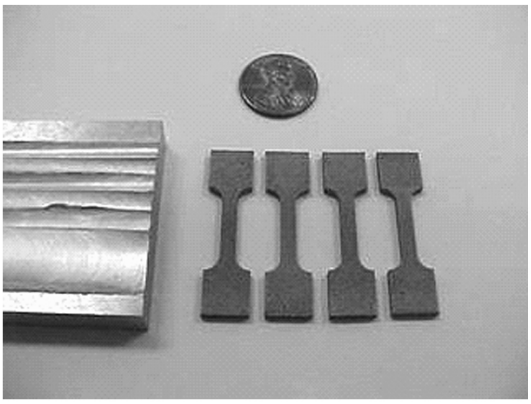

Figure 7. Tensile specimens used to measure properties of FSP stir zones on Al castings.

have the potential to support wider use of Al castings in vehicles, and they could directly impact weight reduction.

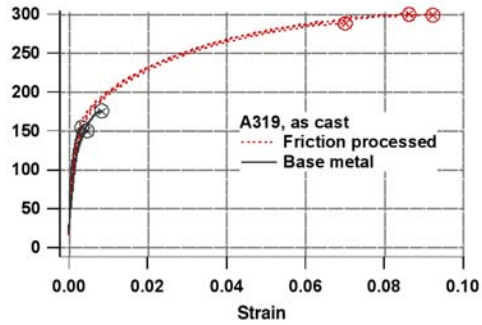

Figure 8. Stress-strain plot from room temperature tensile tests of A319 base metal and FSP stir zone.

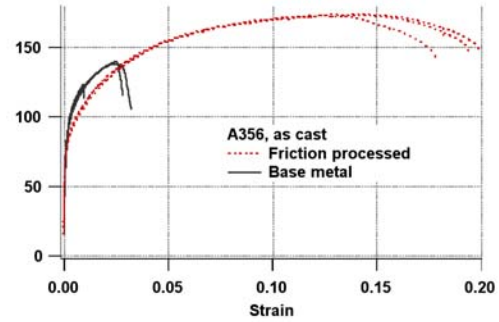

Figure 9. Stress-strain plot from room temperature tensile tests of A356 base metal and FSP stir zone.

G. Basic Studies of Ultrasonic Welding for Advanced Transportation Systems

Principal Investigator: Zhili Feng
Oak Ridge National Laboratory
1 Bethel Valley Road, Oak Ridge, Tennessee 37831
(865) 576-3797, (865) 574-4928, e-mail: fengz@ornl.gov

Technology Development Area Specialist: Sidney Diamond
(202) 586-8032; fax: (202) 586-1600; e-mail: sid.diamond@ee.doe.gov
Field Technical Manager: Philip S. Sklad
(865) 574-5069; fax: (865) 576-4963; e-mail: skladps@ornl.gov

---

Contractor: Oak Ridge National Laboratory
Contract No.: DE-AC05-00OR22725

Objective

- Develop a fundamental understanding of the ultrasonic welding (UW) process.
- Establish process conditions to optimize joint properties of aluminum (Al) alloys for auto body applications.
- Explore opportunities for joining dissimilar materials.
- Explore the feasibility of ultrasonic processing in other novel and unique situations in materials processing such as making powders more dense, producing functionally graded components, modifying surface properties, and producing dissimilar material joints.

Approach

- Perform UW experiments to develop correlations of process parameters with joint properties.
- Characterize details of joint microstructures.
- Model the fundamental interactions of ultrasonic waves with solids.

Accomplishments

- Purchased and installed the UW system.
- Demonstrated the breadth of potential applications of the UW process, namely, the feasibility of metallurgical bonding of steel, Al, and magnesium (Mg) alloys to themselves and bonding of dissimilar joints between steels and Al alloys.
- Observed certain unique phenomena at the bonding interfaces under different process conditions,
- Initiated development of theoretical models to determine the vibration amplitude distribution in simple plate configuration.

Future Direction

- Continue the welding process development for dissimilar materials, including joining amorphous metals.
- Study the structure-property relationship of joints.

- Conduct experiments to determine the importance of vibration normal to the bond interface in the bonding process.
- Model the acoustic energy distribution in the weld joint.
- Study the residual stress distribution in the bonding region.
- Assess the ability of ultrasonic processing to enhance the densification of powder metal compacts.
- Explore the feasibility of ultrasonic bonding of nanoparticles.

Introduction

In response to a highly competitive global market, environmental concerns, and the government fuel conservation and safety mandates, the U.S. automotive industry is aggressively pursuing high-performance and energy-efficient vehicles that involve increased use of lightweight and high-strength materials (such as Al alloys, composites, Mg alloys, and advanced high-strength steels). The use of these new materials presents significant technical challenges to the existing body-assembly joining processes such as electrical resistance spot welding (RSW). A number of issues exist in applying RSW to Al sheet metals and coated steels, including unacceptable electrode life, weld quality, and performance. Furthermore, because of metallurgical incompatibility, fusion welding of dissimilar metals (Al to steel, for example) is generally very difficult, if not impossible.

As material joining is one of the major manufacturing processes used to assemble auto-body structures, the auto industry is actively considering a number of alternative welding technologies that would enable the increased use of lightweight and high-performance materials. Many of the alternative processes involve innovative solid-state joining in which metallurgical bonding between the same or dissimilar materials can be created without melting. One of the solid-state-based joining processes is UW.

UW relies on mechanical vibrations at frequencies higher than the upper limit of normal human hearing (about 18 kH). Figure **1** shows the basic process setup for making spot welds in metals. An electromechanical converter (such as a piezoelectric transducer) converts high-frequency electric current to mechanical vibrations. The mechanical vibration is then modulated and amplified by the booster/horn before it is applied to the workpiece through the sonotrode. A moderate clamping force is applied to ensure the mechanical vibration is transferred to the sheet-to-sheet interface (the faying surface) where the weld is created. Typically, the mechanical vibration is at 20–40 kHz with an amplitude range of 5 to 50 μm. The power delivered to the workpiece is in the range of several hundred to several thousand watts, although more powerful UW power sources are being developed. Another important aspect that must be considered in auto-body assembly is the production rate. The welding time of UW is relative short, usually in the range of a less than a second to several seconds. This is in principle comparable to the production rate of electric RSW currently used in assembly lines.

As far as the basic bonding process is concerned, UW is a variation of friction welding. As shown in Figure 2, the combination of clamp pressure and mechanical vibration produces several important effects in the formation of the metallurgical bond at the workpiece interface. The lateral mechanical vibration of the sonotrode causes a small amount of relative motion between the workpieces at

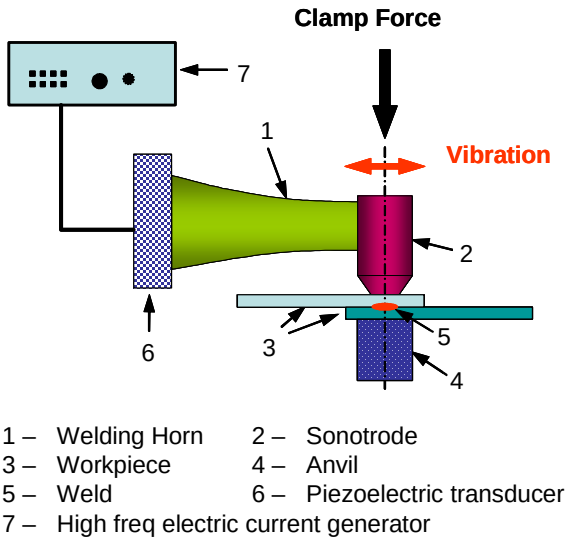

Figure 1. Schematic setup of ultrasonic welding process.

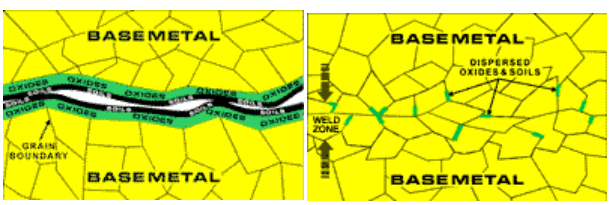

Figure 2. Schematic representation of bond interface before (left) and after (right) ultrasonic welding.

the interface. The frictional action at the interface due to the relative motion and the pressure breaks the surface oxides and other contaminants. As a result, clean metal surfaces are brought into contact under pressure. Frictional heating also occurs at the bond interface. The heating promotes both localized deformation and diffusion in the region where the pressure is applied. Similar to other friction welding processes, when this process is optimized, metallurgical bonds can be obtained without melting at the bonding interface. The self-cleaning nature of UW and its ability to form metallurgical bonds without melting are both important advantages of the process. Another characteristic of UW that could be exploited is its apparent ability to soften metals as a result of the interactions of ultrasonic waves with microstructural features. This phenomenon is known as acoustic softening.

UW creates a joint without bulk melting. Thus, the ultrasonic weld is inherently immune to welding defects associated with the solidification process in fusion welding. These include the solidification cracking and porosity due to absorption of gaseous impurities (N, H, O) by the liquid metal that are common in electrical RSW of Al alloys. Also, unlike the copper-based electrode used in electrical RSW, the sonotrode in UW can be made of high-strength materials that are inert to chemical attaching from the material to be welded. It is expected that the life of the sonotrode would not be a critical factor limiting the production rate and the quality of the welds. Therefore, UW offers several significant advantages over current methods of joining Al alloys. Indeed, industry test data indicate that compared with resistance spot welded Al, ultrasonic joints have higher and more predictable strength and weld quality. The UW process is considered to be one of the primary candidates for spot welding of Al body structures.

At present, studies by the auto industry have been primarily on nonheat treatable 5××× series Al alloys, focusing on application issues. This program investigates UW of heat-treatable and other lightweight materials, including the joining of dissimilar materials such as steel to Al and Al to Mg.

Welding

Welding trials were conducted on a Sonobond UW system, acquired specifically for this program. The machine operated at 20 kHz and had a maximum rated power output of 2500 W. The welding system, shown in Figure 3, consists of a power supply and the welder. The power supply generates 20 kHz of electric current, which is fed to the piezoelectric transducer in the welder. The mechanical ultrasonic vibration is transferred to the workpiece through the horizontal mounted horn and the vertical

Figure 3. The Sonobond ultrasonic welder used in this program.

sonotrode. The clamping pressure was applied pneumatically by compressed air.

All welds were made using a 1 × 4-in. coupon as shown in Figure 4. This is a standard coupon dimension commonly used by the auto industry for weldability testing of resistance spot welds.

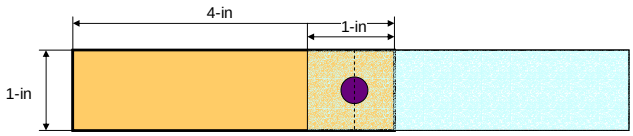

Figure 4. Coupon dimension used in welding trials.

The feasibility of UW of various combinations of materials (Al alloys, steels, Mg alloys) commonly used in the automotive industry was investigated first. Most materials tested had a nominal thickness of 1 mm. It was found that the UW process was relatively robust. The following material combinations were successfully bonded together in this program (see Figure 5):

- Al1100 to Al1100
- Al3003 to Al3003
- Al2024 to Al2024
- Al6061 to Al6061
- Al6111 to Al6111
- Al6061 to Al2024

Figure 5. Ultrasonic welds made of various material combinations. From top to bottom: Al2024 to Al6111, Al6111 to Al6111, Al2024 to Al2024, Al1100 to Al1100, DQSK steel to Al2024, DQSK steel to DQSK steel, and Mg AZ31 to Mg AZ31.

- Al6111 to Al2024
- DQSK steel to DQSK steel
- DQSK steel to Al2024
- Mg alloy AZ31 to Mg alloy AZ31

It should be noted that, although metallurgical bonding of these material combinations was feasible, the mechanical properties of some of the material

combinations need to be improved through welding process development and optimization that are planned in FY 2004.

In an effort to investigate the interface phenomena during UW, a series of dissimilar welds between Al2024-T3 and Al6061-T4 were made under various energy and clamping force conditions. These two Al alloys have very different etching response rates to Keller's reagent. This allowed for selective etching to reveal the interface region of the weld. This approach circumvented the difficulties in studying the bonding interface made of the same material.

The baseline conditions for a good-quality weld were at 750 J and 70 psi. A process range test revealed that, under the current testing setup, no metallurgical bonding was produced when the energy level was below 500 J. When the energy input exceeded 1000 J, severe sticking of the workpiece to either the sonotrode or the anvil was experienced. Thus, the following process parameter ranges were selected for the bonding interface study:

- Power: 2400 W
- Energy range: 500 to 1000 J in 50 J increments
- Pressure: 50 to 90 psi in 10 psi increments

It should be noted that the impedance of the system could vary significantly during welding. Thus, the actual welding power level is not a constant but varies accordingly during the process. The actual welding power variations during welding were not measured in this phase of the program.

Microstructure Characterization

Both optical microscopy (OM) and scanning electron microscopy (SEM) were employed to characterize the microstructure changes in the vicinity of ultrasonic welds. The initial portion of this study concentrated on ultrasonic welds between dissimilar Al alloys (Al2024 and Al6061). The difference in etching rates of the two alloys in Keller's reagent was used to distinguish the two alloys, especially at the weld interface (see Figure 6). In a similar fashion, the difference in average atomic numbers between the alloys permitted backscattered electron (BSE) imaging to reveal the distribution of the different alloy regions as well as precipitate phases (Figure 7).

The macrostructure of two 2024/6061 ultrasonic welds is compared in Figure 6. The two welds were produced at the same power setting (2400 W) but at different ultrasonic energy levels (750 and 950 J). In all the microstructure photos in this section, the Al2024 was the upper sheet and was in direct contact with the vibrating sonotrode, which applied both the ultrasonic energy and the bonding pressure. The Al6061 was the lower sheet and was supported by the stationary anvil. From Figure 6(a), the weld interface appears as a good metallurgical bond over a diameter slightly wider than the impression left by the sonotrode (indicated by the roughening of the upper surface of the Al2024 sheet by the knurled surface of the sonotrode). A significant bowing of the weld interface occurs into the Al6061 sheet near the center of the weld relative to the unjoined surfaces. As the lower surface of the Al6061 sheet is essentially flat, it appears that mass transport of the Al6061 has occurred. A similar bowing of the weld interface into the Al6061 plate occurred for the higher-power weld (Figure 6b), though the effect is less obvious as a result of the slight bending of the entire welded piece that might result from the welded piece sticking to the anvil at this high energy level and subsequent straining of the specimen during removal. A slight waviness of the weld interface occurs at the higher ultrasonic power level.

Both OM and SEM examination of the edges of the ultrasonic weld at higher magnification revealed structures that indicated extensive material deformation at the interface. The surface appeared to

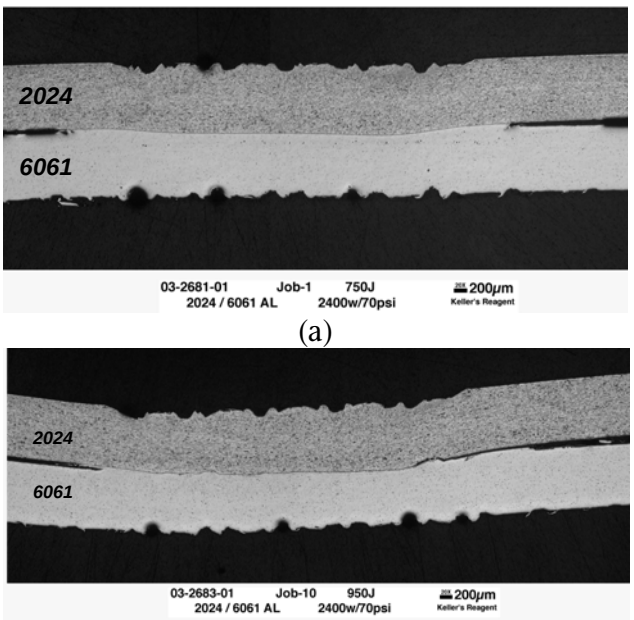

(a)

(b)

Figure 6. Optical micrographs of Al2024 and Al6061 ultrasonic welds made at 2400 W and 70 psi: (a) 750 J and (b) 950 J.

undergo extensive folding/extrusion due to the friction action at the interface. This effect was more pronounced at higher bonding pressure (90 psi in Figure 7). The OM (Figure 7a) of the etched weld reveals flow lines in the deformed material, and BSE images of the same area in the SEM (Figure 7) Images show that the extruded material is all the darker-imaging Al6061. In addition to the deformation, most of the weld edges exhibit cracklike features, which are always into the Al6061 side of the interface, never into the Al2024. The causes for the formation of this type of feature are not clear at the moment, and further studies are planned to understand this phenomenon. The undeformed base Al6061 material exhibits fine (5–50 μm) original grain structure, as shown in Figure 7b. However, the grain structure of the deformed material at the interface is not apparent even at higher magnification or BSE contrast level. It is presumed that the high residual stress and dislocation density in the extruded material significantly reduce the BSE channeling contrast responsible for the grain structure

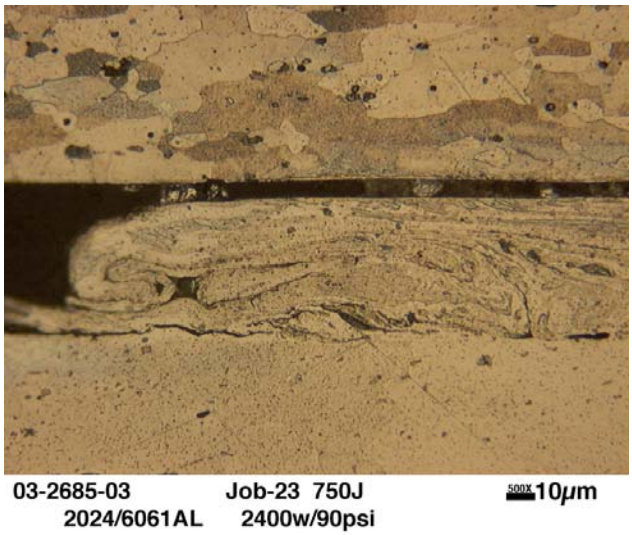

(a)

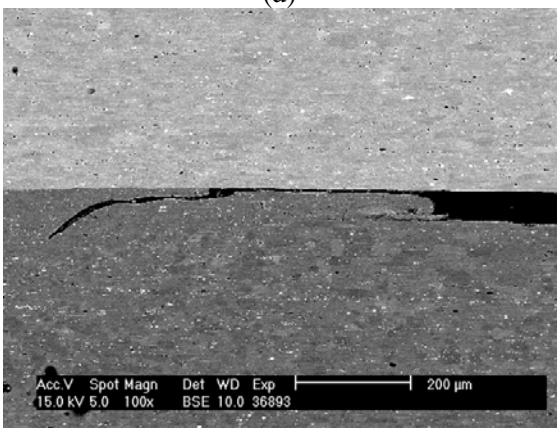

(b)

Figure 7. (a) Optical micrograph and (b) SEM micrographs of Al2024/Al6061 ultrasonic welds made at 2400 W ultrasonic energy, 750J power, and 90 psi. The Al2024 material is the upper sheet.

contrast in the relatively undeformed Al6061 base matrix.

The BSE images reveal other microstructural features of the ultrasonic welds at higher magnification, including the weld interface structure and the precipitate structure. The increased tendency for waviness of the weld interface with increased ultrasonic energy input is shown in Figure 8. At 750 J power, the interface is generally flat to within 1–2 μm (Figure 8a), whereas waviness of ~10–20 μm is observed

at 950 J (Figure 8b). The difference in the BSE image contrast of the two alloys permitted the extent of intermixing during UW to be estimated (Figure 9a). At some regions of the weld interface, the BSE contrast changes between those two levels over distances of ~300 nm. This is an upper estimate for the zone of intermixing at the interface because the spatial resolution of BSE images is determined by both the incident probe (nominally <10 nm) and the lateral extent of the excited volume for BSE emission at 5 kV (~250 nm). Therefore, the observed resolution of the BSE image at the weld interface is dominated by the excited volume and does not represent the actual width of the transition zone.

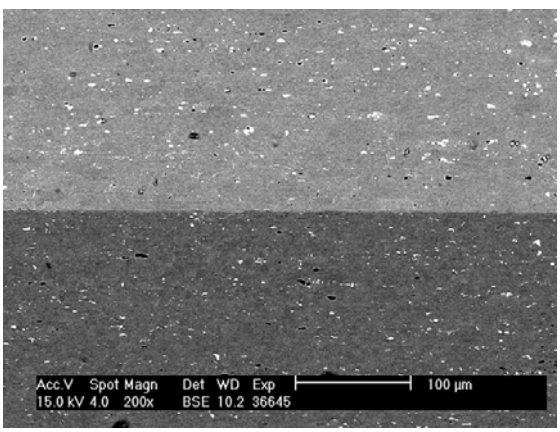

(a)

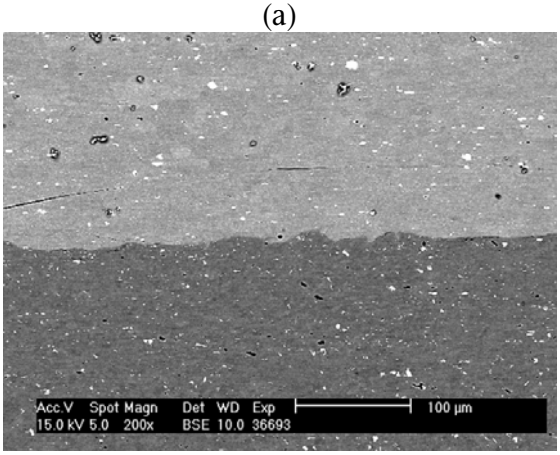

(b)

Figure 8. BSE images of 2024Al/6061Al ultrasonic welds made at 2400 W, 70 psi and either (a) 750 or 950 J power. The 2024Al material is the upper sheet.

The precipitate microstructure of both alloys is revealed in Figure 9b.

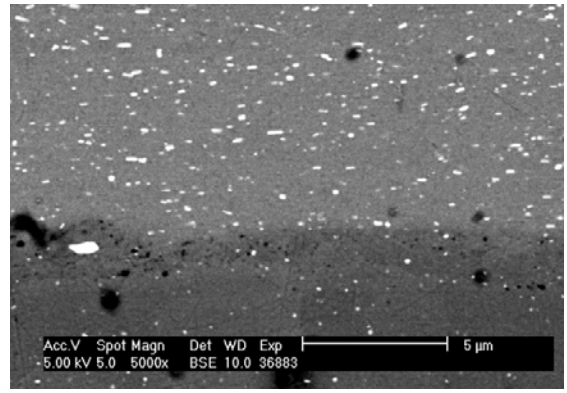

(a)

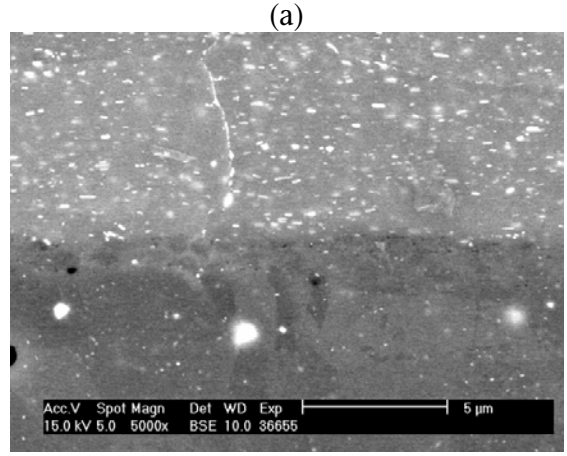

(b)

Figure 9. BSE images of Al2024/Al6061 ultrasonic welds (2400 W, 750 J and 70 psi). Al2024 is the upper sheet. The bright line in (b) is presumed to be dislocation decorated by Cu-enriched precipitates.

The coarse precipitates in the Al6061 are enriched in Fe and Si with lower enrichment of Cr and Mn relative to the matrix, whereas the precipitates in the Al2024 are Cu-enriched. The bright line in the Al2024 matrix is taken as evidence of heterogeneous nucleation of Cu-enriched precipitates on a dislocation. No evidence exists of a gradient in either size or number density of the Cu-enriched precipitates as a function of distance from the weld interface. In addition, the observed precipitate microstructure near the weld interface is

comparable to that observed in the unbonded Al2024 sheet more than 5 mm outside of the weld. This observation indicates that the local heating near the weld interface from the localized absorption of ultrasonic energy does not exceed the solvus temperature for the Cu-enriched precipitates. If this phase is the equilibrium θ phase, the maximum temperature must be <490°C and therefore below both the melting temperature of Al and the eutectic temperature of the alloy. If the precipitate phase were one of the metastable phases, the maximum temperature would be lower, as the solvus of these precipitates is lower than that of the equilibrium phase. For these reasons, the mechanism of UW does not involve melting, even localized melting at the interface.

In some of the BSE images near the weld interface, there are indications of a narrow zone at the interface that exhibit slightly different contrast (e.g., 1–2 µm in thickness in Figure 10a). As this dimension is significantly smaller than the average grain sizes of either alloy near the weld interface (~10 µm for the Al6061 and ~30 µm for the Al2024), electron backscatter diffraction (EBSD) and orientation imaging microscopy in the SEM were used to further characterize the microstructure near the weld interface. Image quality maps reflect the clarity of the EBSD pattern at each point in the map and reveal the local microstructure (Figure 10a). The coarser grain structure of the Al2024 is evident, and a narrow, dark band is present at the weld interface. This lower image quality probably indicates localized strain in that region. Smaller grains are present in the Al2024 adjacent to the dark interface zone. These grains may indicate recrystallization of a layer of deformed material. Inverse pole figure maps reflect the local crystallographic orientation of a specified direction (e.g., surface normal) at each point in the map (Figure 10b). The shades of the local orientation reveals that the dark layer at the

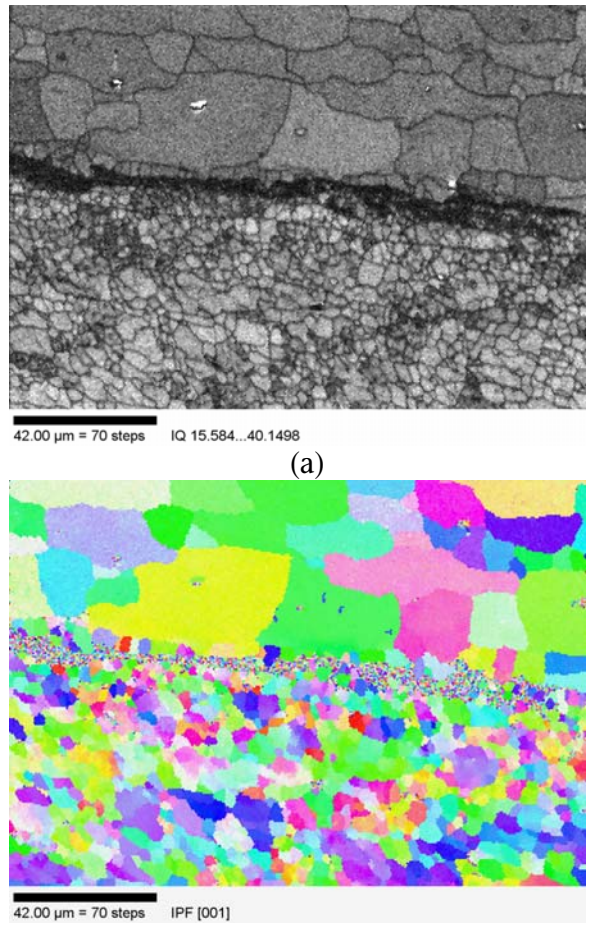

Figure 10. Orientation imaging maps for Al2024/Al6061 ultrasonic weld made at 2400 W ultrasonic energy, 750 J power and 90 psi. Shade/color coding in (b) gives the crystallographic orientation of the local surface as normal. The Al2024 is the upper sheet.

interface does not exhibit a grain structure at the resolution of this inverse pole figure map (~1 µm). In related work with Ford Research and Advanced Engineering under a recent MPLUS project, we were able to demonstrate that both recovered and recrystallized regions were at the weld interfaces of ultrasonically welded 6111Al. That work required inverse pole figure maps at spatial resolutions of 0.2 µm. In order to acquire such maps for the current materials, the development of an improved specimen-

preparation technique for these dissimilar alloy welds will be required.

Process Modeling

In order to determine the displacement amplitude distribution generated in a plate during UW, two different numerical techniques were used to solve the wave equation for a plate. The first technique was a decomposition of the problem by setting up dual grids for the in-plane x- and y-displacements. These quantities satisfy two coupled second-order partial differential equations derived from elastic plate theory. By treating the problem in this manner, we can solve the resulting homogeneous matrix equations by singular-value decomposition methods, which is much faster than comparable finite-element and finite-difference methods. Boundary conditions on the plate (i.e., clamped edges, where the displacements are zero, or free edges, where the stresses are zero) can be varied to suit the application simply by changing the appropriate elements of the decomposition matrix; thus this approach is well-suited to modification that will permit driving the plate with an external source, as occurs during UW.

The second technique is a new PDE solver that converts the problem into a simple boundary element problem. This approach solves the wave equation analytically for any set of boundary points, thus allowing much higher precision of the solution without requiring more computer memory and time.

Computer codes were developed, implementing both techniques to find the eigen values (resonance frequencies) and eigen vectors (displacements) for a rectangular plate. The first example tested was to solve for the in-plane (extensional) resonant modes for a square plate one unit on a side, having clamped edges. Our programs found a series of such resonances, the first occurring for a normalized frequency of 0.578. Assuming Al for the plate material and a size of one meter square, this corresponds to a frequency of about 3.1 kHz; thus for the plate sizes of interest to this program, the driving point of the ultrasonic transducer will probably be quite critical. This value would scale inversely with the plate dimension. The program also determines the plate displacements for each mode, which can then be plotted. Examination of the first few modes yielded displacement patterns typical of elastic resonant modes and provided confidence that the code is working correctly.

Knowing the resonant frequency and modes is important for the study of UW. First, from our results it is evident that small plates should behave differently from large plates at the same frequency. This point has not been considered before in the study. Second, the type of resonance oscillation will impact the distribution of acoustic energy, thus influencing the efficiency of the welding process. More detailed study is needed for understanding the dependence of the energy distribution on the size and the shape of the plates.

Conclusions

A number of major accomplishments and significant progress have been made in FY 2003. The program progressed well along the proposed milestones. Feasibility has been demonstrated for UW of steel and Al and Mg alloys to themselves, and for welding dissimilar joints between steels and Al alloys. The interface study using dissimilar welds between Al2024 and Al6061 revealed a number of important phenomena at the interface under different process conditions. The development of theoretical models allows for interrogation of the geometry effects on the distribution of acoustic energy that would have significant implications in the application of the UW process.

Acknowledgements

Dr. Michael Santella, Dr. Edward A. Kenik, Dr. Xiaoguang Zhang, and Dr. William Simpson of Oak Ridge National Laboratory were part of the program team. Their contributions to the program are acknowledged.

H. Attachment Techniques for Heavy Truck Composite Chassis Members

Principal Investigator: Lynn B. Klett
Oak Ridge National Laboratory
P.O. Box 2009, Oak Ridge, TN 37831-8048
(865) 241-8112; fax: (865) 574-8257; e-mail: klettlb@ornl.gov

Principal Investigator: Darrell R. Herling
Pacific Northwest National Laboratory
P.O. Box 999, Richland, WA 99352-0999
(509) 375-6905; fax: (509) 375-4448; e-mail darrell.herling@pnl.gov

Technology Development Area Specialist: Sidney Diamond
(202) 586-8032; fax: (202) 586-1600; e-mail: sid.diamond@ee.doe.gov
Field Technical Manager: Philip S. Sklad
(865) 574-5069; fax: (865) 576-4963; e-mail: skladps@ornl.gov

---

Contractor: Oak Ridge National Laboratory, Pacific Northwest National Laboratory
Contract No.: DE-AC05-00OR22725, DE-AC06-76RL01830

Objectives

- Overcome the technical issues associated with joining composite materials in heavy vehicles by developing technically robust and economically attractive joining techniques.
- Develop and validate one or more joint designs for a composite structural member attached to a metal member that satisfy the truck chassis structural requirements both economically and reliably.
- Solicit input from truck original equipment manufacturers (OEMs) and suppliers on the technical hurdles and needs for joining structural composite members in heavy vehicles, and use this information to guide the joint design and development activities.
- Publish information on the design, modeling, and testing methodologies that are developed to support the incorporation of composite materials into other chassis components.

Approach

- Collaborate with Delphi and the National Composites Center (NCC) and their OEM partners to identify and address technical needs related to the manufacturing, joining, and implementation of a composite chassis component.
- Design attachment components and configurations in close coordination with the composite structural component development.
- Use modeling techniques to predict the performance of various joint designs, taking into account damage mechanisms and fatigue/life requirements.

- Characterize various composite materials and mechanical joint configurations through mechanical testing, considering variables such as hole size, spacing, location, hole fabrication method, bolt preload, inserts, combined loading, vibration, fatigue, and durability.
- Validate joint design for the composite structural member through track testing.

Accomplishments

- Participated in the Value Added Value Engineering workshop with Delphi and its industrial partners to identify design concepts and technical barriers.
- Conducted a literature survey on attachment technologies for composites with a focus on solutions for hybrid joints, including the effects of three-dimensional (3D) reinforcement, bolted joints, and fatigue testing.
- Reviewed the modeling and testing capabilities at Oak Ridge National Laboratory (ORNL), Pacific Northwest National Laboratory (PNNL), and Delphi in order to most effectively distribute tasks in testing, design, and analysis while avoiding duplication of efforts.
- Acquired equipment to upgrade a 220-kip testing machine (actuator, grip supply, etc.) to allow for structural component and joint testing.
- Established a test matrix for coupon testing for baseline steel-steel joints, as well as for the steel-composite system of interest.
- Selected commercially available, component-independent material and identified appropriate mechanical tests to investigate levels of damage resulting from various hole fabrication methods and bolt preload levels as well as ways to mitigate the negative effects of the damage.

Future Direction

- Conduct static and fatigue tests of composite specimens with holes fabricated by various methods such as drilling, water jet cutting, drilling undersized components, and reaming. Investigate design modifications, such as inserts, molded-in holes, and 3D reinforcement to minimize the damage in the composite and improve the fatigue life of the joint.
- Evaluate steel-steel joints through lap shear and cross-tension testing to establish fatigue performance of the existing configuration, which will be used to design and optimize the composite-steel joint.
- Utilize finite element modeling with input from the composite and joint tests to optimize and predict the performance of the composite-steel joint.
- Continue discussions with various OEMs to gain an understanding of the successes and failures associated with previous research efforts to incorporate composite materials into chassis structures.

Introduction

Currently, polymer matrix composites are used for several nonstructural components for heavy vehicles, including hoods and roof fairings. In these cases, relatively inexpensive materials, such as sheet molding compound (SMC) with short, randomly oriented reinforcing fibers, are used to reduce weight, improve aerodynamics, and reduce part count. Potential exists for additional weight reduction in the chassis, which accounts for approximately 12% of the weight of a raised-roof sleeper, by replacing heavy steel structural members (Figure 1) with fiber-reinforced composites. Likely, these structural components will be made with more expensive composites reinforced with

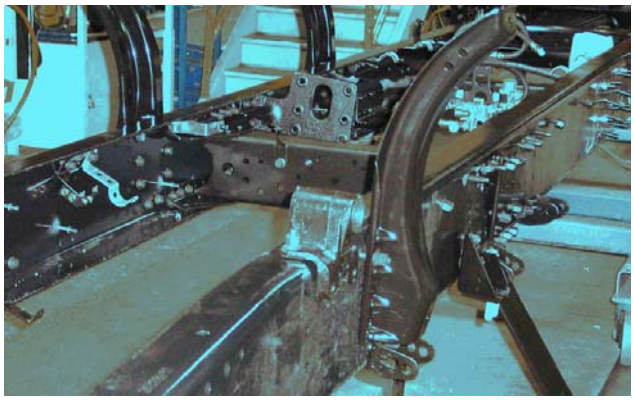

Figure 1. Representative chassis assembly for a Class 8 truck showing a variety of steel members bolted together.

oriented long fibers. The financial incentives for weight reduction in heavy vehicles, which will offset some increase in materials cost, include improved fuel efficiency, increased payload, and reduced truck traffic volume.

In May 2003, ORNL and PNNL began collaboration on a four-year research effort focused on developing technically robust and economically attractive joining techniques to overcome the technical issues associated with joining lightweight materials in heavy vehicles. This work is being performed concurrently with an industry program, led by Delphi, to develop and commercialize composite chassis components, which will require resolution of the joining challenges. The initial focus of research is development and validation of one or more joint designs for a composite structural member attached to a metal member that satisfy the truck chassis structural requirements both economically and reliably. Broadening the effort to include other structural joints, including composite-to-composite joints, is anticipated. Durability track testing of the first prototype composite component and joint is planned for the last half of 2005.

Major Technical Issues

Economics is one of the main hurdles for developing successful composite structural members and joining technologies for a heavy vehicle chassis. Attachment solutions have been developed and are fairly well understood for aerospace applications, but both the composite and joint materials are high performance and expensive. For the heavy vehicle industry, only a modest cost premium can be justified based on weight savings. Therefore, the joint design must have an acceptable cost, which includes costs for raw material, fabrication, tooling, assembly, repair, and replacement costs. Additionally, the chassis structural components will have a life expectancy of a million miles, which is many times that of automotive components.

Mechanical fasteners, such as bolts, have several advantages for structural joints, including ease of assembly and disassembly and the existence of well established design guidelines. However, these guidelines were developed primarily for metals and are not directly applicable to polymer matrix composites.

A major concern for composite materials is stress risers due to the presence of holes through the composite thickness. Holes can have a detrimental effect on strength, stiffness, and reliability by disrupting the fiber load path. If the composite and joint are not designed properly, damage and failure can occur as a result of creep or fatigue. Introduction of the holes through drilling, stamping, or piercing can also cause differing amounts of damage in the composite, which may result in delamination and crack initiation sites. This damage can also expose the fibers to the harsh environment of the roadway and lead to degradation of the composite member. Although some preliminary research has been done, the issue of holes in thick composites is not well understood.

Adhesive bonding is attractive for use with composite materials because of the continuous connection the bond line creates. This bond line distributes loads over a large area, thereby reducing stresses at the holes. The proper use of adhesives can also improve

fatigue resistance by damping vibrations while allowing for reduced joint weight. However, several drawbacks are present with the use of adhesives: difficult disassembly without destroying the substrate, potential degradation due to environmental factors, difficulty in inspection to ensure adequate bonding, and difficulty with surface treatment requirements. Additionally, the joint must be properly designed so that the adhesive is loaded primarily in shear, tension and/or compression, while avoiding peeling and cleaving forces.

With proper design, continuous-fiber reinforced, as well as short-fiber reinforced, composite materials can be highly fatigue resistant, even under high load. This includes both carbon and glass-reinforced composites. Additionally, 2D and 3D composite structures can be reasonably damage tolerant because of their ability to distribute stresses around damage zones. Typically, in a cross-ply laminate or a braided or woven fabric composite under fatigue loading, a slow accumulation of damage occurs which eventually leads to failure. Also, in flexural fatigue, the stress state is complex and not easy to model with an S/N curve. A significant technical hurdle is the inability to efficiently model damage accumulation and fatigue resistance of such 2D and 3D composite structures and predict performance with classical laminate theory.

Both selection of the composite material and the composite fabrication method can have a great impact on the tolerance of the material to holes and fatigue. The variety of choices of fiber and matrix materials, fiber reinforcement configurations, and processing methods leads to the high degree to which these composite materials can be tailored for specific applications; however, it also contributes to the difficulty in designing for structural applications. There is neither a comprehensive database of material properties nor a complete understanding of material behavior under different loading conditions with different stress risers. The material and processing variables also make composite materials difficult to model numerically.

ORNL researchers have extensive experience in adhesive bonding technology for and durability testing of automotive composites, and they are currently investigating the performance and durability prediction of hybrid joints (riveted and adhesively bonded) for attachment of automotive composites to metals. Where appropriate, the design and testing methodologies and lessons learned from these research efforts will be applied to this project.

Damage Caused by Hole Fabrication and Bolt Preloading

The initial joint design will likely include mechanical fasteners requiring holes in the composite member. In order to gain an understanding of the effect of hole-drilling method on the performance of the composite materials, a testing matrix has been developed for a commercially available pultruded fiberglass composite. These tests will be component independent, and the results will serve as a baseline for further testing of composites with 3D reinforcement and with design modifications to improve the performance at the holes such as the use of large washers to distribute the load, inserts, adhesive bonding, etc. The pultruded fiberglass composite was selected for these baseline tests because of the good availability of material and relatively low cost. It is anticipated that the results of the tests will translate to long fiber-reinforced materials manufactured using other fabrication methods.

The test coupons will have a thickness of 3.2 mm (1/8 in.) with a hole size of 12.7 mm (1/2 in.). Open hole tension and fatigue tests will be conducted on coupons with holes fabricated by different methods that may include water jet cutting, drilling undersized and reaming to final dimension, diamond hole saw machining, and traditional drilling. PNNL has nondestructive evaluation

capabilities for quantifying the damage in materials associated with processes such as hole drilling, and will examine the test specimens prior to and after the test to compare the levels of damage associated with each hole fabrication method and the mechanical loading. A preferred hole fabrication method will be chosen, with input from the industrial team, based on the test results and consideration of the costs and complexity of the fabrication method. The selected hole fabrication method will be used for the remainder of the coupon and component tests.

In order to determine the effects of the level of bolt preloading on the mechanical properties of the composite materials, bearing tensile and fatigue tests will be conducted on the pultruded fiberglass composites. Two levels of preload will be used for torqued bolts, and one level of preload using huck bolts. It is anticipated that the huck bolts will yield a more consistent preload level. Typically, preload levels for torqued bolts have a higher degree of scatter. The next step will be to include design modifications, such as inserts, post-hole treatement (i.e., resin wicking), molded-in holes, and 3D reinforcement of the composite, in an attempt to minimize the damage in the composite (see Figure 2) and improve the fatigue performance of the resulting composite-metal joint.

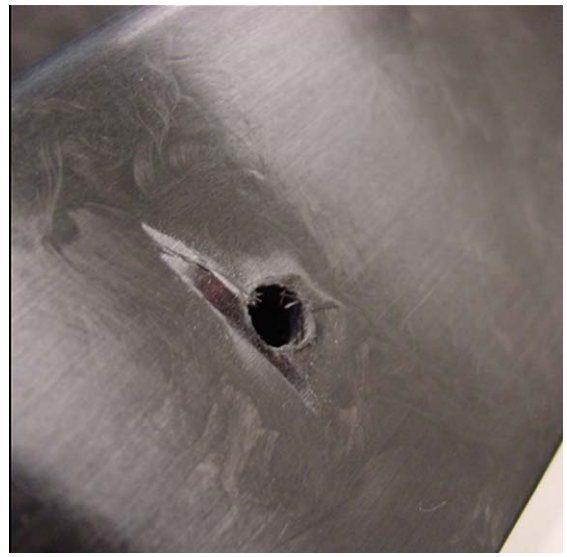

Figure 2. Damage in backside of composite from standard metal drill bit in drill press with thin steel backing plate.

Mode I and II Joint Testing

In previous work at PNNL, different joining technologies for dissimilar metal assemblies were developed and evaluated. One of the project goals was to develop a complementary experimental and numerical approach that would result in a more thorough understanding of the effects of different joining methods on vehicle structural integrity and long-term performance. This previous work provides knowledge regarding the joining of dissimilar materials and performance characterization of these joints.

To be consistent with existing performance testing methods of steel joints, the experimental work in this investigation will consist of lap-shear and cross-tension specimen designs (Figures 3 and 4) for one-directional loading conditions. Uni-directional tension tests are performed to characterize the joint strength of the bolted joints.

Tension-tension cyclic fatigue tests with a stress ratio of 0.1 are performed to characterize the fatigue behavior of the joints. The same fixtures and assemblies used in the static tests are used in the fatigue tests. The cyclic fatigue tests are conducted in load control with constant amplitude until failure or a run-out criterion of 5,000,000 cycles is reached. Failure is defined as total separation or fracture of the specimen into two parts. Specimens are tested at varying load levels to evenly distribute the failures between 10,000 cycles and run-out. A minimum of 10 fatigue tests will be performed for each coupon configuration. Tests are conducted at room temperature with a test frequency of approximately 20 Hz and with a sine

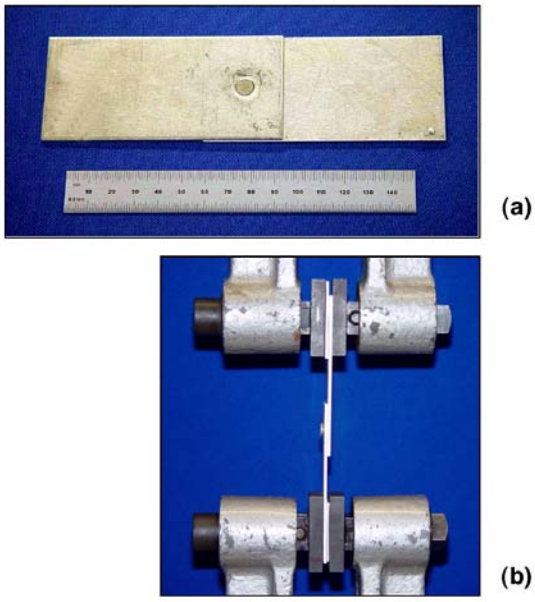

Figure 3. Fixture for static and fatigue testing: (a) lap shear specimen, (b) lap shear assembly.

waveform. The fatigue tests results are plotted in the form of *S-N* curves.

A combined experimental/analytical approach will be used for the hybrid joint development. First, the experimental methods described above will establish the fatigue behavior targets for the current steel-steel joint configurations based on the existing design. The baseline testing results will then be converted to a single fatigue master curve for the joining method using equivalent stress intensity factor vs. life or structural stress vs. life approach. This master curve will be used in the subsequent design and evaluation of hybrid composite-steel joints.

After the composite component design is identified, composite-steel joint coupons will be fabricated for hybrid joint master curve generation. Force components from the system finite element analysis will then be used to predict the expected life of the joint subjected to the specified global loading

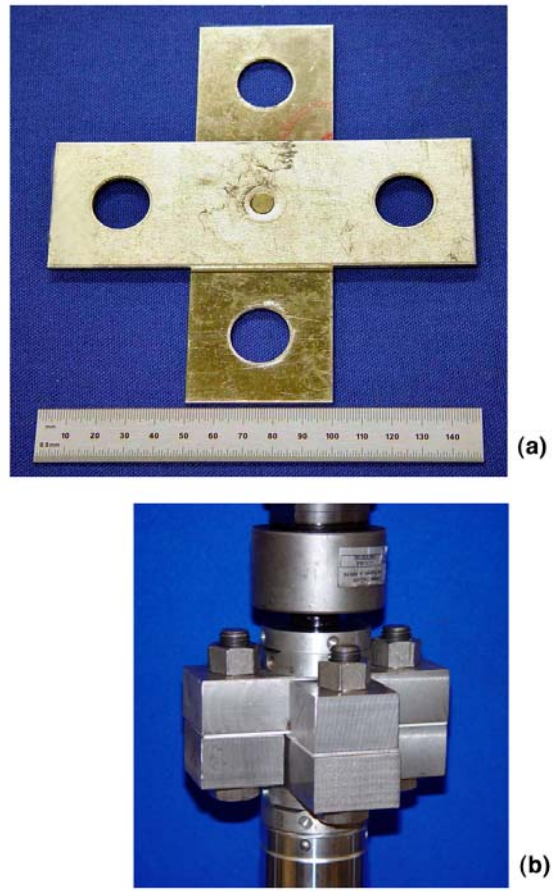

Figure 4. Static and fatigue testing (a) cross tension specimen and (b) cross tension assembly fixture.

conditions. Several iterations of this process are envisioned to improve the fatigue life of the joints so that the final joint design meets the desired cycle value or percentage of the baseline steel joint value.

Modeling Tools

The composite member that will be prototyped initially is a replacement for an existing metal component and bolted joint, which has been characterized for loads and stress distributions. The finite element method (FEM) will be used for the design of the structural member and the joint, taking into account the geometry, fastening methods, and hole size and spacing. Existing

commercial solvers can be applied in this initial stage of design. Three such codes that are currently used by the project partners include NASTRAN (one of the first available codes and considered to be the industry standard), ABAQUS, and Genesis. The goal will be to design a joint that effectively spreads the load over a large area.

In addition to these well established codes, Genoa, a package developed specifically for composite material analyses, may be used. This software uses an iterative process to solve finite element problems on the structural part level and on the microscopic fiber-matrix level. Genoa offers unique damage and fatigue life prediction capabilities for composite materials. Although the code has been released to the public only recently, it has an impressive record in the aerospace industry. If Genoa is adopted for this project, it will be the first use of this code for non-aerospace application.

In addition to these tools, software previously developed for automotive composite projects at ORNL or PNNL might be used in later stages of the project for detailed analysis of microscopic damage in the composite part. For modeling fiber loading and damage in composite material system at the macroscopic scale, a continuum mechanics approach can be adopted. In this usually phenomenological approach, the actual damage and deformation mechanisms are ignored and just their effect on the overall response is accounted for through one or more variables, called damage parameters. Another option is to use a micromechanical approach to model the development of microcracks in the matrix, fibers, and fiber-matrix interface.

PNNL has developed a method of linking these two approaches to more accurately predict composite performance for complex situations such as damage propagation in hybrid polymer composites. As necessary, this modeling methodology will be applied to the composite joint design, especially as it relates to predicting changes in load distribution around bolt holes due to composite damage (mechanical or environmental) and hole production methods.

Modeling Approach

A submodeling technique is planned for the design of the composite structural component and joint. First, a system model will be evaluated and divided into subsystems, which will be analyzed in greater detail. If necessary, the model can be further subdivided. Specifically, the system model will consist of the entire truck chassis. The relevant subsystem, in terms of joining, is the single joint assembly of the composite and steel members. If needed, the joint at a single fastener can be modeled as a subsystem of the joint assembly. This approach allows separation of the structural member design task from the joining task, and the modeling effort can be accelerated by processing smaller models.

As a first step, the structural member design team will use existing system models from the industrial partners as well as newly developed models to design a replacement of the existing steel component with an equivalent composite counterpart. The goal will be to match the stiffness and strength of the steel part without significantly changing the footprint of the existing joint. The bolts in the joint will be modeled initially as rigid links, yielding approximate loads in the bolts. The bolt loads combined with information about stress and strain fields will be useful in the joint design. The initial composite design will most likely be unacceptable to meet the cost and weight reduction goals. However, it will provide a baseline for subsequent design iterations in this project.

As a result of the hole-fabrication and bolt preload testing, the relationship between damage in the composite material and fatigue life will be established. The finite element analysis results from the system model will indicate the clamping forces

expected in the joint. Acceptable levels for the clamping force and the corresponding damage in the composite material will guide redesign efforts.

5. LIGHTWEIGHT VEHICLE STRUCTURES

A. Lightweight Stainless Steel Bus Frame: Phase III

Principal Investigator: J. Bruce Emmons
Autokinetics Inc.
1711 West Hamlin Road, Rochester Hills, MI 48309
(248) 852-4450; fax: (248) 852-7182; e-mail: jbemmons@autokinetics.com

Technology Development Area Specialist: Sidney Diamond
(202) 586-8032; fax: (202) 586-1600; e-mail: sid.diamond@ee.doe.gov
Field Technical Manager: Phillip S. Sklad
(865) 574-5069; fax: (865) 576-4963; e-mail: skladps@ornl.gov

---

Contractor: Autokinetics Inc.
Contract No.: 4000010114

Objectives

- Investigate and demonstrate the mass saving potential of ultra-high-strength stainless steel as applied to the structure and chassis of a full-size urban transit bus.
- Finalize design and analysis and build a full-scale prototype of the body structure and chassis.
- Investigate all of the fundamental feasibility issues related to the structure and chassis
  1. Fabricate and test large lightweight stainless steel sandwich panels
  2. Fabricate roll-formed, high-strength stainless steel sections
  3. Test feasibility of lightweight stainless steel cantilever seats
  4. Design and fabricate lightweight stainless steel independent suspension
  5. Integrate the traction motors into the suspension design

Approach

- Execute the basic body structure, including the floor and roof sandwich panels, pillar assemblies, longitudinal rails, and suspension subframes.
- Choose prototyping techniques that emulate the intended production process as closely as possible to aid in developing robust but cost-effective manufacturing techniques essential to meeting the objectives of the project.
- As computer-based design and analysis details of the bus develop, conduct hands-on physical experimentation in parallel to support the concepts and methods.

Accomplishments

- Finished the floor panel—(completed but made obsolete by enhanced design).
- Delivered the roof and floor panels—(completed but made obsolete by enhanced design).
- Fabricated subframe and wheel house components.
- Completed tooling and fixtures for the pillars and subframes.

- Completed the subframe subassemblies.
- Completed the pillar subassemblies.
- Produced a hybrid power train compatibility report.
- Produced an investigation and selection report dealing with suspension components.
- Produced an investigation and selection report dealing with traction motors.
- Developed design enhancements for suspension subframes.
- Developed design enhancements and process plan for sandwich panels.
- Fabricated a sample panel and tested it to extreme load.
- Designed and fabricated fixture and equipment for sandwich panel welding.
- Fabricated and tested all sandwich panel segments.
- Developed design for front and rear crash-energy absorbers.
- Performed analysis and testing of stainless steel, energy-absorbing tubes.
- Developed design of specialized resistance welder for joining sandwich panel segments.

Future Direction

- Complete the design and building of a segment welder for joining panel edges.
- Assemble the primary structure of the bus.
- Complete the fabrication and installation of suspension components

---

Introduction

Advanced technology transit bus concepts have made significant advancements in terms of light weight and fuel economy. However, these gains have come at the expense of higher manufacturing costs. In spite of attempts to use life-cycle costs to justify their purchase, initial cost remains a major obstacle to the introduction of fuel-efficient buses.

Autokinetics was approached by the Office of Heavy Vehicle Technologies (OHVT) of DOE to attempt to solve this problem. Specifically, the OHVT asked Autokinetics to develop concepts for a lightweight urban transit bus based on the use of high-strength stainless steel. In the passenger car field, Autokinetics had developed structural and manufacturing techniques for the cost-effective use of stainless steel in spaceframes and suspensions. The OHVT wanted to determine whether this approach could be applied to transit buses as well.

The program was structured in three phases:

- Phase I – Initial Concept Development
- Phase II – Concept Verification and Initial Design
- Phase III – Final Design and Prototyping of Body and Chassis

Phase I and Phase II have been successfully completed. Phase III will result in a full-size body structure and suspension that will be tested statically and dynamically. The development of an optimized hybrid powertrain and other vehicle systems will be addressed in a separate project.

This project was unusual in that no formal mass or cost targets were given. The object was to save as much mass and cost as possible.

Pillar Subassemblies

In this reporting period, the previously roll-formed pillars were spot-welded to the attachment brackets that will connect to the edges of the floor and roof panels at final assembly. The fixturing of this pillar subassembly provides the dimensional control that will set a consistent distance between floor and roof panels in the finished vehicle. The complete set of pillar sub-assemblies for the bus is shown in Figure 1.

Figure 1. Pillar subassemblies.

Floor and Roof Sandwich Panels

Perhaps the single most important technical development in the entire bus program is the ongoing effort to successfully fabricate stainless steel sandwich panels for the floor and roof. These panels are simple in concept and potentially inexpensive to manufacture, but our experience has shown that attention to detail and proper execution are essential for success.

The decision to use corrugated cores as opposed to honeycomb cores was made early in the program. The small loss of structural efficiency is more than offset by the substantial cost savings. Corrugated cores can readily be roll-formed in large quantities, and can be attached to the face sheets by welding rather than bonding or brazing. A literature search revealed that at least two types of welding had been used to make this type of sandwich panel. Resistance welding techniques were developed first, followed by laser welding. A supplier experienced in making both types of panel was contacted. It was jointly decided to make the panels for the bus using laser welding.

Laser Welded Panels

The fabrication of laser-welded sandwich panels was begun in FY 2002. The completion of a full set of 4 × 8 ft panel segments has been reported on previously. The final butt-welding of the floor- and roof-panel assemblies was delayed. This was the result of the poor fit-up between the individual panel segments, making laser butt-welding of the as-fabricated panel segments impossible. After initial unsuccessful attempts to TIG-weld the joints resulted in excessive distortion, the supplier attempted to weld the panels together using a hybrid laser/MIG welding technique. This also resulted in excessive distortion. In an effort to salvage the existing hardware, the panel segments were sent to an outside supplier to have all the mating edges laser trimmed to produce an accurate enough fit to allow the laser butt-welding. This solution required a deviation from Autokinetics' design intent. After trimming, one-half of the face sheet butt-welds were in an unsupported location. To overcome this, T-shaped backup bars were added to provide the support required to clamp and weld the seams between subsections. This stopgap measure added approximately 300 pounds to the weight of the finished panels.

To implement the welding procedure, the supplier completed the design, fabrication, and installation of a specialized fixture for clamping and supporting the floor and roof panels because the edges of the individual panel segments are laser butt-welded together. This fixture was used in conjunction with the panel transporter (supplied by Autokinetics and described

below) to perform the final assembly welding of the floor and roof panels.

The degree of difficulty and potential for damage associated with handling and transporting the very large corrugated panels seemed to justify the construction of a special panel transporter. The primary objectives were to protect the edges of the panels and provide enough support to prevent the panels from buckling. This could be accomplished by clamping a channel-like structure along the edges of the panels. Additionally, such a device may be useful to hold and align the panels during final assembly, as it provided a continuous full-length straight edge. A design was developed to assist final panel assembly as well as ensure the integrity of the panels during transport. The design consisted of standard 6-in. steel channel around the periphery of the panels. The large surfaces (top and bottom of the transporter) were spanned by plywood.

The procedure was to stand the transporter on edge and incrementally feed the panels in through the removable ends as the subsections were welded together. Once complete, the finished panel was secured in place by tightening the wedge-like clamping blocks between it and the inside of the channel section. The transporter was designed to be compatible with the Autokinetics lifting rig so the entire unit could be lifted by crane from a single point. Additionally, a hand maneuverability method was developed to move the transporter through tight quarters. This consists of a specially designed "trailer" axle and dolly.

A set of laser-welded floor and roof panels was delivered by the supplier to Autokinetics in February 2003, more than 8 months behind schedule. The finished panels consisted of 17 segments that had been butt-welded together to form a one-piece roof and a three-piece floor (designed to be joined to the suspension subframes to complete the floor assembly). Initial inspection of the panels revealed that many of the laser welds were unattached. This raised a concern about the integrity of the remaining welds. A sample section was sent to Oak Ridge National Laboratory (ORNL) for inspection with a new non-destructive, infrared imaging technique. The images showed minimal attachment in most of the welds examined. At this point, destructive testing was considered appropriate, and it was found that most of the welds could be popped apart quite easily with a screwdriver, showing a dramatic lack of penetration. The reason for the poor weld integrity has not been explained by the supplier, but it is likely the result of incorrect weld parameters, or inconsistent clamping, because earlier samples had shown the material to be quite weldable. With no viable plan to repair the defective welds or inspect the quality of the remaining welds, the panels were deemed not usable and therefore had to be rejected.

Resistance Welded Panels

Based on the lessons learned, Autokinetics began investigating the resistance welding alternative. It was felt that this approach may be better suited than laser welding for low-volume series production, which is characteristic of bus manufacturing. In addition, parts holding, fixturing, and process/quality control were all identified as areas in need of improvement. This was considered of significant added value to the project and received the approval of DOE project management. AK Steel, a partner in the project, generously offered to contribute additional custom-rolled stainless steel and brake-formed corrugated cores for the fabrication of the new panels. To investigate the potential quality and strength of resistance-welded panels, a sample roof panel measuring 2 × 8 ft was made and tested by Autokinetics. As is seen in Figure 2, the flatness and quality of this panel is far superior to that of the laser-welded roof panel on which it is resting. A static load test rig was designed and constructed to apply a uniformly distributed bending load to the

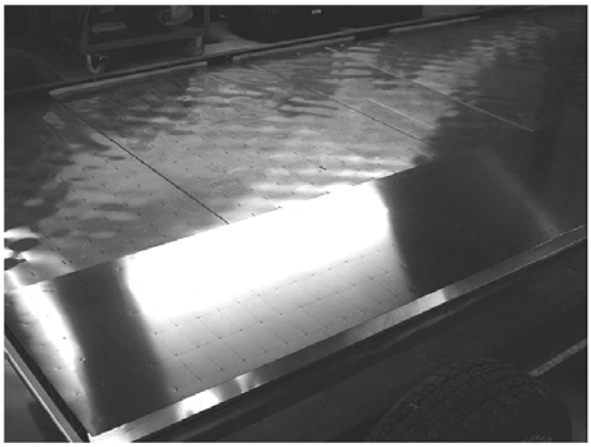

Figure 2. Sample resistance welded roof panel on top of laser welded roof.

Figure 3. Panel static proof load test rig.

face of the panel. The load is applied by four hydraulic cylinders through a set of distribution beams. The hydraulic pressure is measured to calculate load. This arrangement is shown in Figure 3. The sample panel easily supported the load required by the Altoona Bus Research and Testing Center with no permanent deformation. The applied load was progressively increased to more than five times the Altoona required load. The permanent deformation was only on the order of 1/32 in. No weld failures occurred at any point in the testing. The magnitude of this safety margin indicates that the sandwich panels may be over-designed, and future additional weight savings may be possible.

The floor and roof panels were redesigned with a different edge configuration to facilitate the joining of the segments using resistance welding. Initial tests indicate the resulting joints will be robust, with little or no distortion. A process plan was developed for the series production of sandwich panels. A key element of this plan is a concept for a pair of automated spot-welding fixtures capable of maintaining flatness and alignment of the elements of the sandwich as they are being welded. These fixtures would use multiple electrodes and transformers to perform a full row of spot-welds simultaneously. With this plan as a guide, a prototype nonautomated welding fixture was designed, which simulates the production process fairly closely. The prototype panel welding fixture is shown in Figure 4. A standard single-point welding gun was modified by extending and reinforcing the arms so that the center of a 4 × 8 ft panel could be reached. Locating features on the fixture and on the welding tips aided the rapid and accurate placement of each weld. After this simple manual fixture was set up, a full set of floor and roof segment panels was completed in about 2 weeks. The flatness, alignment, and lack of distortion in this set of panels were far superior to those of the earlier laser-welded panels. This will greatly facilitate the final assembly of the bus structure.

To ensure weld integrity, the static loading fixture, which was used for the sample panel, was employed to apply a proof load to every floor- and roof-panel segment. The applied loads were equivalent to three times the Altoona requirement for the floor and four times the Altoona requirement for the roof. No weld failures or permanent deformations were observed. This simple and quick nondestructive quality control test is a practical enough procedure to be used in production.

Figure 4. Prototype panel welding fixture.

Suspension Subframes

The suspension subframes also were extensively redesigned to improve the structural efficiency, simplify the fabrication, and make the floor-panel fabrication easier. Instead of welding each subframe to the bottom of the floor panel, the new subframe design replaces a section of the floor panel. This has the benefit of breaking the floor panel into three more manageable subassemblies, and it eliminates the trimming operation around the wheelhouses. It also has the functional benefits of increasing the ground clearance and improving underbody aerodynamics. This effort was not a specific deliverable of the project, but was considered important for the success of the program. The design for the prototype that was built is shown in Figure 5.

All of the stainless steel components for the front and rear subframes and wheelhouses were laser cut and brake formed

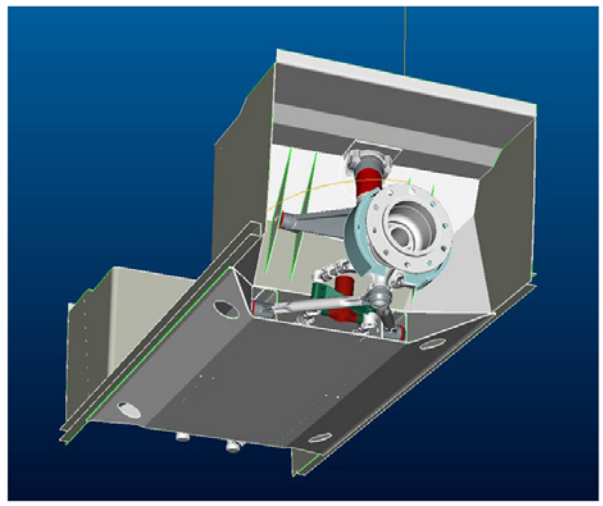

Figure 5. Suspension subframe design.

by 3-Dimensional Services in only 10 days. The quality and workmanship were outstanding. During this time, Autokinetics completed the rather minimal fixturing for the subframes. The subframes were designed to be somewhat self-fixturing using precision, laser-cut gage holes. The subframe and wheelhouse components were delivered to Autokinetics where they were welded together using a combination of spot welding and TIG welding.

Suspension / Driveline

An important aspect of the design strategy for this bus is to develop a versatile platform that can accommodate a wide variety of advanced propulsion systems. To support this strategy, Autokinetics completed an investigation into the compatibility of the new bus design with various potential combinations of advanced propulsion components. Viable packaging solutions were found for all of the configurations studied. These included small diesel engine/generators, microturbine generators, and fuel cells.

The traction motors and controllers were ordered from PreMag. This involved considerable interaction with PreMag to specify a suitable mounting interface and to accommodate the somewhat enlarged

cooling provisions. As of the date of this report, the motors and controllers have not been received and are seriously behind schedule. PreMag claims to have had difficulty with the molding of the stators. If PreMag is unable to deliver in a reasonable amount of time, an alternate motor supplier will be used.

The initial bearings selected during suspension concept development were reviewed by Timken, who found them to be undersized. A new bearing was selected and the rear suspension successfully repackaged around it. The front suspension has not yet been updated, but no serious difficulties are anticipated.

Crash Energy Management System

Autokinetics has independently developed a unique crash energy management system for passenger vehicles based on the inversion of stainless steel tubes. This concept was adapted for use on this bus project. As can be seen in Figure 6, the front bumper of the bus is supported by a

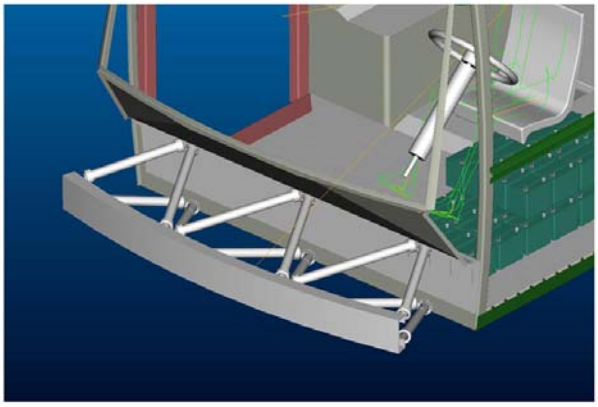

Figure 6. Crash energy management structure.

set of 12 round tubes in a triangulated arrangement. Each tube is attached at both ends by a bendable "plastic" hinge (not shown in the illustration), which limits the amount of bending moment that is applied to the tube. On impact, the tube is driven onto a forming device that turns the tube inside-out, thus absorbing large amounts of energy.

The energy-absorbing tubes have been tested by Autokinetics, AK Steel Research, and General Motors Research. A force vs. displacement curve indicates that the E/A tube very closely approaches an ideal constant force device. Drop-tower testing performed at GM Research indicates that very little strain rate effect is associated with this material. It is hoped that future testing at the High Strain Rate Facility at ORNL will more accurately quantify this finding.

Non-linear finite element analysis of the tube inversion process has been performed by Autokinetics using ALGOR software. The mesh size has been considerably refined compared to earlier analysis, and it shows fairly good correlation with test data. The analysis tool will continue to be used to investigate changes in material properties, wall thickness, tube diameter, and inverter radius.

Design of Specialized Segment Welder

Preliminary welding tests indicate that the panel segments can be successfully joined together using resistance welding. It is expected that this method will result in far less distortion than MIG, TIG, or laser welding. It will also be faster and more consistent.

A specialized spot-weld gun will be required to reach at least halfway across the floor and roof. This welder, along with its support stand, has been designed and is being built. Completion is expected by mid-November. This equipment is not a specific deliverable of the project but is being built at Autokinetics' expense. After the welder is operational, the final assembly of the bus body structure will begin. An illustration of the framing assembly sequence is shown in Figure 7.

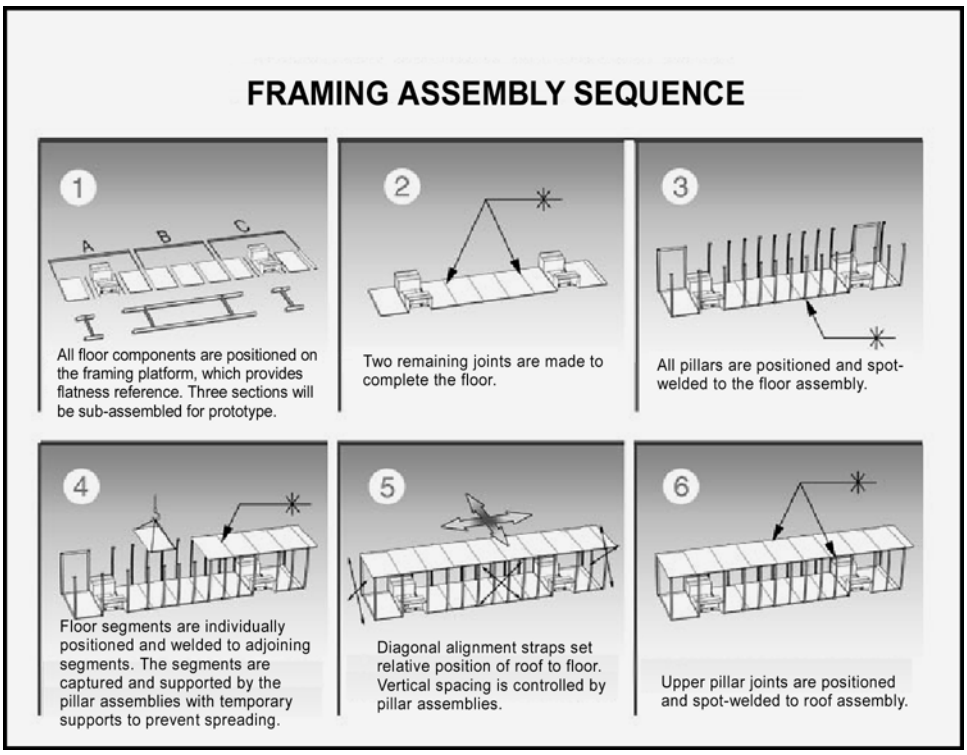

Figure 7. Framing assembly sequence.

Dissemination and Commercialization

11/5/02—JBE presentation to WestStart/Calstart—Technical Assessment Committee. Response was very favorable, and WestStart support was recommended.

11/5/02—Meeting with GET to discuss commercialization in Japan. Ray Geddes and Koichi Okuda attended. (Ray Geddes has since passed away. The status of the GET effort is currently unknown).

11/7/02—JBE attended WestStart Advanced Transportation Industry Conference in Los Angeles.

2/19/03 thru 2/21/03—JBE attended "Clean Heavy Duty Vehicles for the 21st Century" Conference sponsored by WestStart in Tempe, Arizona.

10/01/02, and 1/09/03—Meetings and continuing communication with John Friedl, entrepreneur, who is developing a business plan to manufacture commercial delivery vans using Autokinetics' structure technology.

Conclusions

Over the course of the past year, Autokinetics has become increasingly confident that high-strength stainless steel has the potential to achieve mass reductions of bus structures on the order of 60%. It also appears that this can be achieved in a practical and cost-effective manufacturing system, using existing processing technology. The ability to form, cut, weld, and cast stainless steel into strong, lightweight structures has now been well demonstrated. Almost all of the major body structure components have now been fabricated, so little if any schedule slippage is expected in the mass prediction for the body structure.

B. Large Castings for Advanced Cab Structures

Principal Investigators: Mark T. Smith
Pacific Northwest National Laboratory
PO Box 999 Richland, Washington 99352
(509) 375-4478; fax: (509) 375-4448; e-mail: mark.smith@pnl.gov

Tony Petree
Freightliner, LLC
4747 N. Channel Ave. Portland, Oregon 97217-3849
(503) 745-8687; fax: (503) 745-69800; e-mail: tonypetree@freightliner.com

Technology Development Area Specialist: Sidney Diamond
(202) 586-8032; fax: (202) 586-1600; e-mail: sid.diamond@ee.doe.gov
Field Technical Manager: Philip S. Sklad
(865) 574-5069; fax: (865) 576-4963; e-mail: skladps@ornl.gov

---

Contractor: Pacific Northwest National Laboratory
Contract No.: DE-AC06-76RL01830

Objective

- Develop the design for a prototype cast structural component for use in an advanced heavy truck cab design.
- Evaluate cast structure performance and durability under simulated vehicle service conditions.

Approach

- Contract with the Alcoa Automotive products group to assist in the detailed design and manufacturing assessment tasks associated with the effort.
- Collaborate with Freightliner to conduct in-kind design development and manufacturing process studies to determine the economic and technical feasibility of the large casting process for cab structural components.

Accomplishments

- Completed the design of a large one-piece cast cab component that will replace the fabricated multipiece cab component.
- Conducted finite element modeling analyses, which showed that the redesigned cast component meets simulated durability and crashworthiness requirements.
- Completed evaluating the use of self-piercing rivets for joining cast-to-wrought aluminum materials under static and dynamic loading conditions.
- Completed the final report for the project, detailing the design features and overall performance.
- Held a final project review at Freightliner to review the design and cost models.

- Determined that if a large casting capability becomes available, large cast components can be cost and performance competitive with more conventional fabricated assemblies in Class 8 heavy truck applications.

Introduction

Current manufacturing methods used for lightweight aluminum truck cabs typically involve the assembly of numerous simple detail parts and assemblies using rivets and mechanical fasteners. Although cost-effective and durable, this materials and manufacturing approach often limits part shape and complexity; it dictates the use of constant sheet or extrusion wall thickness, and it requires labor-intensive assembly. Developments in casting technologies for large casting size and reduced wall thickness offer the opportunity to design and manufacture complex, highly shaped components using relatively inexpensive tooling and casting process technology. The purpose of this project was to explore the potential of using large aluminum castings in selected truck cab structural component applications.

Project Approach

The project involved the selection of a large, complex cab component that was suitable for redesign into a large casting. Design development and structural analysis of the component led to a final large casting design. Under contract to Pacific Northwest National Laboratory (PNNL), Alcoa Automotive Engineering was tasked with development of the large casting design. Alcoa, PNNL, and Freightliner staff met several times to select a design for a component that was suitable for the ultra-large casting process being developed in parallel by Alcoa. PNNL investigated the issue of joining wrought to cast aluminum materials using self-piercing rivets, and the component design was engineered so that self-piercing rivets could penetrate through the casting and into the wrought material. Following component selection, Alcoa developed a design for an optimized large casting that incorporated variable wall thickness, cast features for pass-through and mounting brackets, and the incorporation of multiple fabricated parts into a single casting envelope. All casting design features were selected to be compatible with the Alcoa ultra-large casting process.

After development of the digital component design, Freightliner staff conducted static and dynamic structural and crash analyses of the component using existing cab models. These analyses resulted in several design modifications prior to finalizing the design. As part of the final design report, Alcoa completed a cost model for the casting for the component at two different production volumes. In both cases, the cast component was found to be competitive with the existing fabricated parts, assuming that the large casting equipment had sufficient casting work (other components) to keep the facility fully utilized.

As a result of Alcoa's decision not to complete commercialization development of the ultra-large casting process, the PNNL/Freightliner team determined that there was not sufficient reason to continue with the proposed prototype stage of the project. The project is now considered complete.

Conclusions

The project studying large casting for cab structures was completed with the development and analysis of a large cast component design. The final design resulted in a 27% reduction in weight and a 70% reduction in part count. Under typical production assumptions, it appears that a large casting is cost competitive with the baseline fabricated component.

C. New-Generation Frame for Pickup/Sport Utility Vehicle Application

Principal Investigator: Curt A. Lavender
Pacific Northwest National Laboratory
P.O. Box 999, M/S K2-03, Richland, WA 99352
Tel: (509) 372-6770; Fax: (509) 375-4448; e-mail: curt.lavender@pnl.gov

Kurt M. Knop
DaimlerChrysler Corporation
14250 Plymouth Road
Detroit, MI 48227
Tel: (313) 659-6076; Fax: (313) 635-5221; e-mail: kmk4@daimlerchrysler.com

Technology Development Area Specialist: Sidney Diamond
(202) 586-8032; fax: (202) 586-1600; e-mail: sid.diamond@ee.doe.gov
Field Technical Manager: Philip S. Sklad
(865) 574-5069; fax: (865) 576-4963; e-mail: skladps@ornl.gov

---

Contractor: Pacific Northwest National Laboratory
Contract No. DE-AC06-76RLO 1830

Objective

- Evaluate the design of an optimized hybrid materials frame that represents a new generation of pickup/sport utility vehicle (PU/SUV) frame applications and vehicle architecture.

Approach

- Apply high-risk manufacturing and design methods to the PU/SUV frame to reduce mass while meeting cost goals consistent with a high-production vehicle.

Accomplishments

- Completed vehicle testing by DaimlerChrysler at the DCX Proving Grounds using a PU/SUV platform equipped with the hybrid frame.
- Proved through accelerated testing that (1) the hybrid frame design had sufficient strength and durability to meet the vehicle performance requirements, and (2) the frame was probably somewhat overbuilt and heavier than required, even with a substantial weight reduction.
- Established performance, packaging, and weight targets for the second iteration of the new-generation frame "the next-generation frame" (NGF).
- Created a design for the NGF that projects a greater weight reduction and a decrease in the number of parts compared with the current steel baseline frame.
- Created a computer-aided engineering (CAE) model of the NGF to evaluate impact; noise, vibration, and harshness (NVH); and durability of the NGF.
- Made CAE and design iterations for attachments based on the early findings of the durability analysis.

Future Direction

- Complete the CAE/design iterations. Data generated from the CAE model results and the characteristics of the high-risk manufacturing methods chosen for the NGF will be used to establish a test plan.
- Validate the CAE analysis by DCX using a dynamic sled test of the front section of the frame.
- Evaluate challenging attachment sections of the frame by laboratory testing at Pacific Northwest National Laboratory (PNNL) and Oak Ridge National Laboratory (ORNL).

Introduction

Increased consumer demand for PUs/SUVs has resulted in increased fleet fuel consumption. The trend toward consumer demand for PUs/SUVs has been predicted to increase. By 2005 the fuel demand for this class of vehicle will exceed that for passenger automobiles.[1, 2] The objective of this project is to explore manufacturing methods and materials to reduce the mass of the SUV/PU frame, thereby reducing fuel consumption for this class of vehicle.

During the second quarter of FY 2003, DaimlerChrysler completed vehicle testing at the DCX Proving Grounds using an SUV/PU platform equipped with a hybrid frame. Results of the accelerated testing have proved that (1) the hybrid frame design had sufficient strength and durability to meet the vehicle performance requirements, and (2) the frame was probably somewhat overbuilt and heavier than required even with a substantial weight savings from the current baseline steel frame.

The next phase of the project will evaluate the use of a lighter frame, the NGF. The NGF uses a CAE approach and higher-risk manufacturing technologies. The projected weight for the NGF, shown in Figure 1, is lighter than the previously tested new-generation frame and requires 35% fewer components.

Approach

The successful accelerated testing of the next-generation hybrid frame indicates that further road testing as an evaluation tool will not be required, and the CAE design will be validated by dynamic "sled" tests of full-size front-ends and high-strain-rate mechanical testing of critical components at ORNL. Strain rates used for the dynamic tests will be determined by the CAE impact simulation, and results will be compared with results from the sled tests.

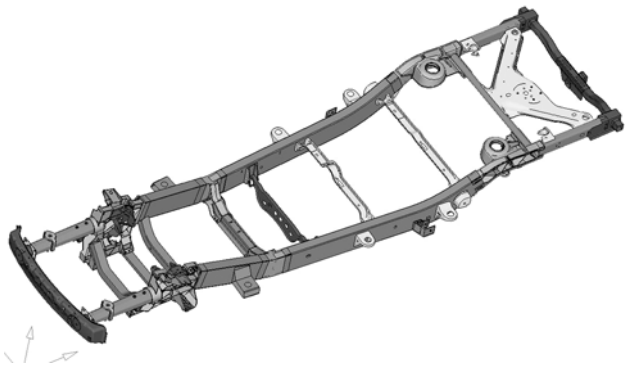

Figure 1. Next-generation frame design.

Progress

Preliminary CAE results indicate that there are no major structural design faults in the NGF and that minor adjustments to attachment points will be required to lower the predicted stress in all areas of the frame to desired levels. Differences were observed in the NVH response of the NGF and of the baseline steel frame. The complete NVH analysis is performed using an entire vehicle model to predict driver and passenger comfort level. Initial review of the NVH data indicates that the response can be tuned to match the baseline frame by re-design of attachment brackets, which would have minor effects on the frame design.

Future Direction

The CAE/design iterations shall be completed. Data generated from the CAE model results and the characteristics of the high-risk manufacturing methods chosen for the NGF will be used to establish a test plan. The CAE analysis will be validated by DCX using a dynamic sled test of the front section of the frame. Challenging attachment sections of the frame will be evaluated by laboratory testing at PNNL and ORNL.

References

1. *EIA Annual Energy Outlook 2002*, DOE/EIA-0383 (2000), Energy Information Administration, December 2001.
2. *Transportation Energy Data Book*: *Edition 21*, ORNL-6970, Oak Ridge National Laboratory, September 2001.

6. APPLICATION OF INNOVATIVE MATERIALS

A. Advanced Materials for Friction Brakes

Principal Investigator: P. J. Blau
Oak Ridge National Laboratory
P.O. Box 2008, Oak Ridge, TN 37831-6063
(865) 574-5377; fax: (865) 574-6918; e-mail:blaupj@ornl.gov

Technology Development Area Specialist: Sidney Diamond
(202) 586-8032; fax: (202) 586-1600; e-mail: sid.diamond@ee.doe.gov
Field Technical Manager: Philip S. Sklad
(865) 574-5069; fax: (865) 576-4963; e-mail: skladps@ornl.gov

---

Contractor: Oak Ridge National Laboratory
Contract No.: DE-AC05-00OR22725

Objectives

- Identify, test, and analyze the friction and wear characteristics of advanced materials and surface treatments that enable weight reduction in truck brake components while equaling or bettering their performance. Materials of interest include intermetallic alloys, ceramic composites, titanium (Ti) alloys, and novel surface treatments.

Approach

- Develop and build a subscale brake material testing apparatus that will enable friction studies of advanced materials at speeds and pressures similar to those experienced by full-sized brakes.
- Investigate the nature of changes to the surfaces of materials that occur as a result of frictional contact under high-energy-input conditions. Relate these to material properties.
- Develop an improved understanding of the role of friction films in vehicle braking and apply that knowledge to the exploration of promising new truck brake materials.
- Examine the characteristics of brake material wear particles and their role in total vehicle emissions.

Accomplishments

- Designed and built a subscale brake testing apparatus instrumented to record applied force, friction force, surface temperature, and vibration.
- Selected and tested a variety of materials with the potential to serve as lightweight brake components.
- Investigated the effects of wet and dry braking conditions on frictional behavior.
- Used infrared imaging to study frictional heating of both cast iron and ceramic brake materials.
- Evaluated the friction and wear compatibility of metals, polymers, and ceramics with Ti alloys.

- Evaluated the effects of surface roughness on the friction of commercially-coated Ti alloys.
- Characterized wear particles that are generated in tests of candidate brake materials.

Future Direction

- Evaluate currently-available commercial coatings and explore new coating technologies for use on Ti alloys for use as lightweight brake rotor materials.
- Identify appropriate materials that are frictionally compatible with Ti or coated Ti alloys.

Introduction

New, more aerodynamic designs for energy-efficient heavy trucks can improve their fuel economy. Advanced tires with lower rolling resistance can also improve energy efficiency. However, as these measures decrease the effective drag on trucks, the demands on their braking systems must increase. Braking system technology involves design, instrumentation and control, and materials aspects. This project specifically addresses the latter. Brake materials must exhibit a balance of properties, including frictional stability over a wide temperature range, good thermal transport, dimensional stability, corrosion resistance to road de-icers, and wear resistance. From a practical standpoint, they must also be cost-competitive. Opportunities exist to employ advanced materials to create lighter-weight braking systems that will enable new technologies to raise the fuel efficiency of a vehicle without compromising its safety and reliability.

This project is aimed at evaluating advanced structural materials and surface treatments that show potential as truck brake friction materials. Testing such new materials is made more cost-effective by using small specimens to screen the most promising candidates. To this end, a subscale brake tester (SSBT) was designed and built. It was instrumented to measure normal force, friction force, surface temperature, and vibrations during braking. An attachable water spray system enables study of the effects of wet and dry braking. The SSBT has been a workhorse in recent studies involving a variety of both traditional and nontraditional brake materials. Test results are supplemented by optical microscopy, electron microscopy, and transmission electron microscopy to study friction-induced film formation.

Candidate Materials

Studies of the structure, composition, and physical properties of candidate materials eliminated low-melting-point, brittle, corrosion-prone, and environmentally unacceptable materials. A list of evaluated materials, with brief comments about them, is presented in Table 1. Typical SSBT specimens of these materials are shown in Figure 1. Dark annular rings on these 5-in.-diameter disc specimens show the thin films that are produced by sliding contact. Films like these also develop on the opposing brake lining materials.[1]

Of the materials in Table 1, it was decided to focus on Ti alloys for several reasons: new, cost-effective methods for processing Ti are being developed; resistance to corrosion by road de-icing compounds is very good; and the high-temperature strength of Ti alloys is better than that of aluminum matrix composites. In addition, one manufacturer of Ti alloy discs for racing vehicles (Red Devil Brakes, Mt. Pleasant, PA) has developed a promising coating process for Ti and provided several brake pad compositions for evaluation.

Since tribology data for Ti are relatively rare, preliminary friction and wear tests were

Table 1. Issues associated with certain candidate materials for lightweight truck brakes

Material	Issues
Traditional gray cast iron and commercial brake pads	Served as a reference with which to compare data for other materials
Aluminum matrix-based composite materials containing silicon carbide hard particles	Lightweight, but low melting point creates concerns for use in heavy trucks with hot brakes; attacked by road de-icers
Intermetallic alloy based on Fe_3Al	Modest weight saving; not commercially available at low cost; wears by cutting chip formation (metallic flakes)
Ceramic composite of carbon and silicon carbide	Expensive; good frictional performance at high temperatures; fibrous wear particles produced; machining and handling present some problems
Titanium alloys	Lightweight and stiff; very good high-temperature strength and corrosion resistance to salts; considerable data from aerospace R&D; poor wear characteristics and low thermal conductivity

Figure 1. Candidate brake disc materials after friction testing on the SSBT: commercially-coated Ti (upper left), experimental ceramic composite (upper right), uncoated Ti alloy (bottom).

performed on two Ti alloys provided by TIMET Corporation (Ti-6Al-4V and Ti-6Al-2Sn-4Zr-2Mo). The first is a workhorse aerospace alloy, and the second was designed for higher-temperature applications. A fixed sphere (pin) sliding on a rotating, flat disk was used as the test geometry for initial screening. Table 2 summarizes the results of these experiments on the Ti-6Al-4V alloy. Similar data were obtained with the other alloy. In examining the data, it should be noted that most braking systems operate within friction coefficients of between about 0.35 and 0.55.

Table 2. Average sliding friction coefficient (μ) of pins of various materials sliding on Ti-6Al-4V alloy disks.

Pin material	μ at 0.3 m/s	μ at 1.0 m/s
440C stainless steel	0.50	0.35
Alumina ceramic	0.47	0.36
Silicon nitride ceramic	0.49	0.44
PTFE (Teflon™)	0.28	0.29

[a] Load 10 N, sphere diameter 9.53 mm, air, room temperature.

While friction data for all materials but the PTFE seemed reasonable for brakes, wear data from these tests, reported elsewhere, were unacceptably high. Thus surface treatment or coating will be needed to make Ti a viable brake material. Larger-scale pad-on-disc tests were performed on the SSBR to compare bare Ti-6Al-4V alloy with commercially coated Ti-6Al-4V alloy cut from the same billet.

Subscale Pad-on-Disc Tests of Titanium

The SSBT was used to conduct higher-speed sliding friction tests on both coated and uncoated Ti discs. Coated discs were thermally sprayed with a proprietary ceramic particulate composite in a metallic binder (Red Devil Brakes). A semi-metallic, racing-grade pad material from the same

commercial source was used. The effects of applied pressure, speed, and surface finish were investigated. As shown in Figure 2, friction of the as-coated Ti was higher and somewhat more variable, but it was more in the range for typical vehicle brakes. Optimization of the surface finish and more rigorous "burnishing" can produce a stable friction layer that reduces such frictional fluctuations. The coated brakes ran slightly hotter, but their wear was so small as to be unmeasurable in the current experiments. Additional research on Ti-based materials, exploring alternative coatings, is planned for FY 2004. Attention will be paid to the role of friction-induced surface films and the selection of a suitable pad material.

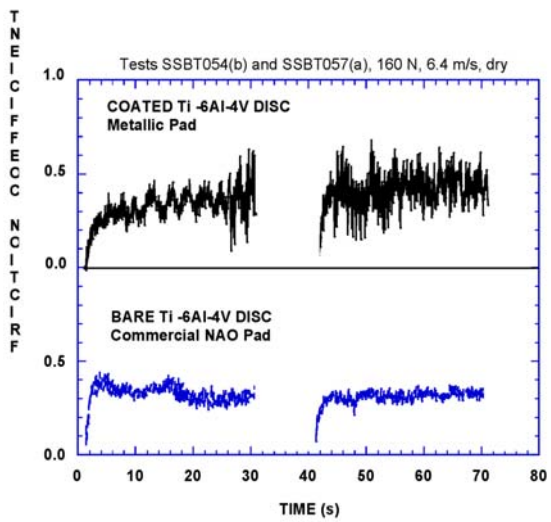

Figure 2. Friction traces for tests on bare and coated titanium for two pad applications at a sliding speed that equates to about 30 mph on a full-sized truck.

Conclusions

Studies have been conducted of a variety of candidate lightweight truck brake materials. Of these, Ti alloys offer a number of attractive characteristics, but their low thermal conductivity and wear behavior must be enhanced. The use of surface coatings or treatments is expected to enable the materials to perform quite well as brakes. Further work in FY 2004 is planned to better understand the friction and wear behavior of Ti alloys and to evaluate several alternative coating methods.

References

1. P. J. Blau. "Microstructure and Detachment Mechanism of Friction Layers on the Surface of Brake Shoes," *J. of Matls. Engr. and Performance*, *12*(1), 56–60, 2003.

B. Advanced Composite Structural Cab Components

Principal Investigator: Ashok B. Shah
Delphi Corporation, Saginaw Steering Systems,
3900 Holland Road, Saginaw, MI 48601
(989) 757- 4988; fax: (989) 757-4295; e-mail: ashok.shah@delphi.com

Technology Development Area Specialist: Sidney Diamond
Phone: (202) 586-8032; fax: (202) 586-1600; e-mail: sid.diamond@ee.doe.gov
Field Technical Manager: Philip S. Sklad
Phone : (865) 574-5069; fax: (865) 576-4963; e-mail: skladps@ornl.gov

---

Contractor: Delphi Corporation
Contract No.: 4000009401

Objective

Develop an advanced composite cab structural component for a Class 8 tractor:

- Develop the design, materials, and manufacturing process for utilizing continuous-oriented, fiber-reinforced composites for affordable commercialization within 3 years of beginning the project.
- Reduce the existing mass by at least 30% from 22.8 kg to 15.96 kg.
- Meet or exceed the performance of existing materials.

Approach

- Organize a value analysis/value engineering (VAVE) workshop to generate different options for design and manufacturing.
- Develop finite element (FE) analysis for predictive engineering and develop design options.
- Perform a cure-cycle study, make necessary panels, and study Class A surfaces.
- Conduct design failure modes effects and analysis (DFMEA).
- Construct prototype parts and verify proposed design using a design validation (DV) test.
- Release final design, construct production tools, and validate the production phase.
- Begin production.

Accomplishments

- Held VAVE workshop, generating options for design and manufacturing.
- Developed FE analysis models, using proposed materials to predict part performance.
- Performed cure-cycle study, made composite panels, conducted Class A activities
  - Conducted DFMEA.
  - Constructed tools for prototype constructions.
  - Made prototype parts.

Future Direction

- Complete DV test.
- Refine FE models using new information from DV test.
- Develop final design and process.
- Release final design, construct production tools, and validate the production phase.
- Begin production.

Introduction

Weight can be reduced and fuel efficiency increased in trucks and tractors, without compromising structural integrity or utility, by incorporating innovative designs that strategically utilize modern lightweight materials.

The Advanced Composite Structural Cab project aims to reduce the mass of a Class 8 tractor cab structure while maintaining its performance by using oriented fiber technology that is typically used in the aerospace industry. The selected structure is a chopped-glass, reinforced-vinyl ester approximately 3 mm thick with nonoriented 55% chopped-glass mat preform and local steel backing. The trim panel is 27% glass-filled sheet molding compound (SMC) in a polyester matrix.

Value Analysis/Value Engineering

The team conducted a VAVE workshop with the original equipment manufacturers (OEMs) in September 2000. Baseline design options and ideas were generated at this workshop. These ideas were used to start the three-part design. When the team chose to consider a two-part design, a few more mini-VAVE workshops were conducted. Technical experts generated lists of new ideas and technologies at these workshops; some of those concepts were used to define design options.

Finite Element (FE) Analysis Models and Design Options

The OEMs provided IGES files and drawings for the current production part, along with various fasteners used in the part. Based on performance requirements and the FE results, key load case performance criteria such as sag and twist were identified. Twelve load cases were considered for the design.

Initially, a three-part design was considered. Several design options were created and optimized for weight and performance using this model. However, the design did not meet the weight and cost targets. A two-part design option was presented to the project team during the February 13, 2003, quarterly meeting. The project team agreed to pursue a two-part design.

Several options for two-part design were created; Table 1 shows the weight target comparison. The project team decided to use the TA3-5 option to start prototype activities even though it did not quite provide a 30% weight reduction.

The design team is still working on more options, including options to reduce the flange area to 3.0 mm, use foam for reinforcement shapes, and create metal reinforcements that will help reduce cost and weight.

Cure-Cycle Study

In order to determine the proper tooling and cure cycle, a potential resin supplier conducted a cure-cycle study. The goal is to make a resin recipe that will meet a 22-min full-cure cycle at 120°F. The 120°F cure cycle

Table 1. Design matrix

Design option	TA-1-2	TA-3-1	TA3-1-rev1	TA-3-2	TA3-3	TA3-5
Total Weight Kgs	19.71	16.46	17.09	17.36	16.82	17.03
Weight Savings	9%	24%	21%	20%	23%	25%
Performance	Comparable to baseline	Improved performance	Improved performance	Improved performance	Improved performance	Improved performance
Trim Panel mass Adhesive	Thinner 0.294kg Plexus	Existing SMC 0.7kg Plexus	Existing SMC 0.7kg Plexus	Existing SMC 0.7kg Plexus	Existing SMC 0.7kg Plexus	Existing SMC 0.7kg Plexus
Fabric	Quad	Tri#	Tri #	Tri #	Tri **	Tri **
Flange area thickness	6.00 mm *	6.00 mm	6.00 mm	6.00 mm	6.00 mm	6.00 mm
Foam Core density	Single pc 4lb/ft3	Multi pc 4lb/ft3	Multi pc 4lb/ft3	Multi pc 4lb/ft3	Multi pc 4lb/ft3	Multi pc 4lb/ft3
Hinge Reinforcement	Existing - 1 pc 3.18 mm	*HR3-1* design in 5 pcs	*HR3-1* design in 5 pcs	*HR3-1* design in 5 pcs	*HR3-1* design in 5 pcs	*HR3-1* design in 5 pcs
Ribs	*Unribbed*	*0.81-1.55 mm*	*1.5mm*	*1.23-1.66 mm*	*0.50- 2.43 mm*	*0.70- 2.17mm*
Attachment points with Fasteners	Existing	Existing	Existing	Existing	Existing	4 pcs Existing 2pcs thin, Latch area extened
Risk	Low	Low	Low	Low	Low	Low

6.00mm * =3.0.mm composite material plus 3.00 mm of resin only to make it 6.00 mm
= Specialty fabric- special order required
** = Off-the shelf fabric

will present less degradation of the composite tool yet meet the intended production volume. Cure-cycle curves will be prepared at room temperature, 120ºF, and 140ºF. The expected completion of this study is December 2003.

Composite Panels

The manufacturing constraint of making oriented 1.5-mm thin panels was addressed by making panels with a 30% fiber volume. The significance of this is that the fiber volume used is closer to that of traditional molding practices using nonoriented fiber, yet it allows panel thickness reduction from the traditional 3.0 mm to 1.5 mm. Three sets of panels using the resin and process intended for production were made, and their physical properties are being evaluated.

Class A Surface Activities

The development of a Class A surface for structural components using three-dimensional woven fabric was conducted. Three trials were conducted using the resin transfer mold (RTM) process with three different sources and three different types of tools (aluminum, composite, and multiple insert tooling). Each of the three used a low-profile polyester resin system known for its Class A quality. Each achieved the best surface quality so far using a similar laminate lay-up and an in-mold coating. The initial studies showed that a greatly improved structure using the same amount of material can be achieved.

The Class A activities were suspended because more time and resources are needed. A current production part or equivalent will be utilized for this project.

Design and Process Failure Modes Effects and Analysis

A system-based DFMEA was initiated at the Delphi facility. The team conducted another DFMEA with OEM engineers. The process is being continued with the ranking of all items. A follow-up DFMEA will be conducted with the OEM engineers after the DV tests are completed. Potential suppliers will be responsible for performing process failure modes effects and analysis.

Prototype Activities

Two composite tools using the TA3-5 design concept were made in Delphi's Salt Lake City labs in June 2003. The first tool was made for composite parts, and a second tool was made for foam.

As no computer-assisted design data were available at that time, the tools were made from the current production part using splash. Unfortunately, that technique could not accommodate the shrinkage factor for the foam tool. Another difficulty was that the tool was made using composite material as opposed to the normal practice of using aluminum tools, because of time and cost factors. An external heating element was required to make good-quality parts. However, the tool design did not permit us to add the plumbing needed. External heating blankets were utilized to overcome this difficulty. First, the foam supplier made some foam sets without hardware to set up the process parameter. Then more sets of

foam sets were delivered with hardware molded in.

Starting July 14, 2003, the team started making prototype parts. The first part was infused in 1.5 min. The part was about 2.0 kg heavier than design because of the foam's inconsistency. The second part was not filled completely. After the unsuccessful third trial, the team members met at the supplier's location on July 30, 2003, to resolved this problem, and they decided to use a low-pressure vacuum infusion method. Prototype No. 5 was made using foam without any hardware. It was completely filled and looked good overall. Most of the regions had composite thickness as intended. However, there were some areas where composite panels were thicker than intended. This was the result of foam being under-sized. The foam intended for production will be made using metal tools, and that should solve this problem.

The team decided to drill holes in the composite tools to locate all metal attachments. During the first week of August 2003, the composite tool was sent for a coordinate measurement machine (CMM) check. Based on the CMM reading, holes were drilled, and the tool was prepared to make prototype parts with hardware.

Prototype part 6 leaked in one area and was not filled completely. Prototype 7 did not fill in one small place. Prototype 8 filled to almost 95% and looked good. The team decided to send this part for a CMM check. The CMM check on the part revealed that three areas were slightly off because the tool was warped. A fixture was made to correct this problem. Prototypes 9 and 10 did not fill as desired, especially in one particular area on the top of the part. The team believes that this problem can be corrected by adding a flexible seal in the area where the part does not fill. The team also decided to bond metal strips on the backside of the tool to provide uniform pressure.

Plans for Fiscal Year 2004

The team will complete the DV tests, complete the final design, and start working on production tools. The production tools are expected to be completed around March 2004. Production validation tests are expected to be completed by June 2004. Start of production in a limited quantity is expected by July 2004. By the end of September 2004, full-scale production is scheduled.

C. Advanced Composite Structural Chassis Components

Principal Investigator: David E. Witucki, PE
Delphi Corporation – Saginaw Steering Systems Division
3900 Holland Ave., Saginaw, MI, 48601
(989) 757-4984; fax: (989) 757-4295; e-mail: david.witucki@delphi.com

Technology Development Area Specialist: Sidney Diamond
(202) 586-8032; fax: (202) 586-1600; e-mail: sid.diamond@ee.doe.gov
Field Technical Manager: Philip S. Sklad
(865) 574-5069; fax: (865) 576-4963; e-mail: skladps@ornl.gov

---

Contractor: Delphi Corporation
Contract No.: 4000009401

Objectives

- Develop an economical, long-fiber-reinforced manufacturing procedure utilizing continuous and/or oriented chopped fibers for structural chassis components for Class 7 and 8 trucks.
- Reduce mass of these components by 60%.
- Commercialize and produce these components, reducing vehicle mass by about 50 kg/vehicle and significantly increasing North American carbon fiber demand annually, within 5 years of beginning the project.

Approach

- Conduct value analysis/value engineering workshop(s) to conduct function analysis and brainstorm solutions using composites for each component function.
- Develop finite element analysis (FEA) models at both the component and system level. Conduct structural optimization (topology and shape/sizing) on components for "material efficient" designs.
- Build and test prototypes.
- Secure production orders for the components developed within the scope of the project.

Accomplishments

- Received customer production part approval of two different models of lateral links. Completed first order of more than 1000 lateral links. Submitted samples and obtained initial order from second commercial vehicle customer. Composite lateral links are 66% lighter than current steel, resulting in almost 5 kg/system mass savings.
- Completed design of proof-of-concept composite-reinforced, thin-wall steel tube main support.

- Completed fabrication and assembly of all metal components of main support. Completed molding of first composite-reinforced support.
  - Tier 1 partner used composites research and design concepts to develop and commercialize an aluminum z-beam, which resulted in over 27 kg mass savings per system. Combined with the mass savings of the lateral link, this project will have realized 32 kg of the 50 kg target for system mass reduction by the end of FY 2003.

Future Direction

- Complete building and testing the proof-of-concept reinforced main support. This product has the potential for over 20 kg additional mass savings.
- Complete the cost model for reinforced main supports.
- Select the appropriate support for commercialization.
- Investigate lower cost lateral link designs and processes.

Introduction

In response to a request for proposals from Oak Ridge National Laboratory (ORNL) in February 2001, a submission from Delphi Corporation led to the award of a subcontract for the development of advanced composite structural chassis components with the objectives listed above.

Sponsored by the DOE, the subcontract is scheduled to run for three years with an estimated cost of $2.5M. This project is a 50/50 cost share between ORNL and industry. In this project, Delphi Corporation, the world's largest automotive Tier 1 supplier, partnered with an industry-leading Tier 1 supplier to the truck and trailer industry and focused on three components in a chassis/suspension system: lateral links, main supports and z-beams.

Lateral Link Status

A key project milestone (limited-volume commercialization) for the lateral link was realized at the beginning of FY 2003 with the acceptance by Delphi of the first 1000-piece order from its Tier 1 partner. Two different models of the link (different lengths for different applications) have been approved through the production part approval process (PPAP), and several hundred are in use in the field.

Glass and standard modulus carbon-fiber-reinforced prepreg are the materials utilized in the manufacture of the links. The bulk of the material is carbon-fiber reinforced to obtain the buckling stiffness required. Tubes are mandrel roll-wrapped, cured, and threaded. Metal inserts are then bonded at each end. The glass prepreg is employed for the threading operation and protective outer layer.

Current composite links offer a 67% mass reduction and outperform the mainstream steel in buckling load capacity and three-point bending, and they also have a significantly higher natural frequency. Examples of both link assemblies are shown in Figure 1.

Although the lateral link can be deemed a success both technically and commercially, costs are still somewhat prohibitive for applications other than lower-volume niche markets. In 2003, efforts were made to develop lower-cost designs and processes to broaden the market potential and increase the impact on fleet fuel efficiency. Two options that were built as prototypes were hybrids (thin-walled steel overwrapped with composite) and pultrusion. Cost models for the hybrid design were not favorable, and costs for pultruded designs are still being analyzed. Pultruded samples are currently in

Figure 1. Typical steel (top) and composite lateral link assemblies.

design validation testing, with results expected by December 2003.

Because the properties of the composite tube are significantly superior to those of the steel, a lower-cost roll-wrapped option is also being considered. In this option, the number of carbon fiber unidirectional layers will be reduced, and the glass fabric on the inner diameter will be placed only at the ends instead of along the entire length. It is anticipated that this will yield up to a 20% cost reduction.

Delphi has requested that additional project funds be transferred from the project to the ORNL materials laboratory for continued durability and buckling testing of these lower-cost alternative designs.

Main Support Status

A significant amount of design effort was spent on the main support during FY 2003. The main thrust of this design was toward carbon-fiber reinforcement of a relatively thin-walled steel tube. Although the design of the tube reinforcement remained stable throughout the year, much difficulty was encountered in obtaining a solution for the interface between the tube and the mounting hardware and brackets.

The initial all-composite interface design was not cost-effective. When all steel hardware was used in the design, mass targets were not met. As a compromise, a hybrid interface was designed in which thin steel brackets were welded to the tube (see Figure 2). These brackets were then reinforced with composites with the rest of the tube.

The current prototype design yields a mass savings of approximately 30% or 23 kg per system.

Six steel framework subassemblies (Figure 3) were fabricated during August and September 2003. The first composite-reinforced assembly was run during the first week of October and is shown in Figure 4 prior to any finishing work.

These prototypes are fabricated by placing dry fabrics with specific fiber orientations around the tube and brackets. The entire support is then bagged and infused with epoxy resin. For production, mold tooling would be used for application of the reinforcement material.

Testing of the reinforced main supports is scheduled for November at Delphi's Tier 1 partner. Several load cases are included in this testing, including vertical beaming, braking, and side load.

Z-Beam Status

At the beginning of FY 2003, Delphi's Tier 1 partner announced its intention to commercialize an aluminum version of the

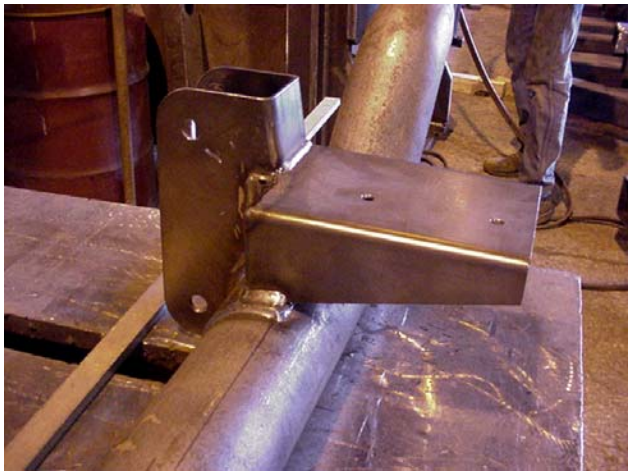

Figure 2. Steel interface-bracket assembly on subplate welded to tube.

Figure 3. Prototype steel framework ready for composite fabrication.

Figure 4. First composite-reinforced main support just out of cure oven, prior to any finishing work.

z-beam based on FEA topology optimization completed for a composite design. The cast aluminum solution reduced the mass by approximately 7 kg and was at cost parity with or below the current cost of welded steel designs. Because four z-beams are used in each system, total system mass was reduced by 28 kg.

Based on the success of the aluminum, work was suspended on composites for the first half of FY 2003. Composites were considered again for a heavy-duty application in the April thru June timeframe, but cost models were not favorable, and work was suspended again.

Plan for Fiscal Year 2004

Completion of the building and testing of the proof-of-concept prototype that used a reinforced main support will occur in FY 2004. Commercialization of this component in the chosen application is questionable because Delphi's Tier 1 partner has expressed interest in a multipiece design for its next generation of products. Unfortunately, these designs are not currently "composite-friendly." During the first quarter, alternative applications will be investigated and pursued. Delphi has already begun negotiations with a second, larger Tier 1 partner.

A minor amount of resources will be dedicated to validate lower-cost lateral links through building and testing the prototype. As higher volumes are required, funds will be required for production tooling of inserts and threading of the tube.

Because of changes in the project scope mentioned earlier, a request for contract modification will be submitted by Delphi in early November to update the budget, scope, cost-sharing schedule, milestones, deliverables, and commercialization plan. Delphi recommends that funding not used because of underspending on this project be made available for other projects.

D. Carbon Fiber Sheet Molding Compound for Class 8 Vehicle Hoods

Principal Investigator: Nicholas A. Rini
Volvo Trucks North America, Inc
P.O. Box 26115; Greensboro, NC 27402-6115
(366) 393-2771; fax: (336)-393-2773; e-mail: nicholas.rini@consultant.volvo.com

Cliff Eberle, Project Manager
(865) 574-0302; fax: (865)574-8257; e-mail: eberlecc@ornl.gov

Technology Development Area Specialist: Sidney Diamond
(202) 586-8032; fax: (202) 586-1600; e-mail: sid.diamond@ee.doe.gov
Field Technical Manager: Philip S. Sklad
(865) 574-5069; fax: (865) 576-4963; e-mail: skladps@ornl.gov

---

Contractor: Volvo Trucks North America
Contract No.: 4000010928

Objective

- Develop carbon-fiber-reinforced sheet molding compound (SMC) and processing techniques that will enable serial production of Class 8 truck hoods with structural integrity, Class A surface quality, significantly reduced mass, and competitive cost compared with existing glass fiber SMC molded components.

Approach

- Accumulate material property data to establish reliable design properties that can be utilized for engineering design analysis.
- Perform finite element analysis of a carbon fiber SMC-based, Class 8 hood design.
- Evaluate consistency and repeatability of carbon fiber SMC material properties, processing techniques, and surface quality.
- Evaluate mass savings and costs.
- Confirm predicted results by constructing prototype hoods and performing accelerated endurance tests.

Accomplishments

- Completed preliminary short beam shear tests to screen carbon fiber materials most likely to provide the desired mechanical properties.
- Completed preliminary spiral flow trials to compare molding-related parameters of materials.

- Completed preliminary evaluation of surface quality based on carbon fiber SMC molded in existing glass fiber SMC component molds.
- Initiated review of hood surface and structural component assembly and bond interfaces.

Future Direction

- Continue evaluation of carbon fiber SMC materials.
- Pursue process developments to enhance exterior panel Class A surface quality.
- Continue evaluation of assembly processes relating to adhesive materials, bond gaps, and processing.
- Follow up Class 8 truck hood costs and weights based on carbon fiber SMC material and process developments.

Introduction

The mass of light automotive and commercial heavy-duty vehicles can be reduced utilizing modern, lightweight, high-performance composite materials. The reduction in vehicle mass translates into an increase in fuel efficiency. Currently, polymeric carbon fiber composites are used in low-volume, high-performance applications such as spacecraft, aircraft, and race cars. Carbon-fiber-reinforced composites can reduce vehicle body mass by 40 to 60%. However, market conditions and technical barriers inhibit their use in high-volume automotive applications.

Class 7 and 8 trucks offer a lower production volume, lower technical barriers, and adequate financial incentives that justify a modest price premium for competent lightweight materials. The aim of this project is to accelerate the commercial implementation of high-performance, lower-cost carbon fiber SMC body components for Class 7 and 8 trucks. As utilization of carbon fiber SMC develops and the technology matures, it is foreseeable that carbon fiber SMC will migrate into the high-volume automotive market.

This project was initiated by performing a comparative finite element analysis of a hood configuration made of glass fiber SMC material that had been validated through modeling, accelerated endurance tests, and field tests. Based on expected carbon fiber physical and mechanical properties, hood structural and surface component material thicknesses were reduced through several iterations to determine the effect on hood system stress states and displacements. Modal analyses were performed to determine mode shapes, and complete vehicle models were used to obtain dynamic responses in the frequency domain. Fatigue life comparisons were made based on the complete vehicle model transient analyses.

Based on the initial investigation, it was concluded that a competent hood could be produced with a 40 to 60% reduction in hood mass if a carbon fiber SMC material could be produced that would consistently provide the physical and mechanical properties targeted.

Carbon Fiber SMC Material Search and Comparative Testing

A search was initiated to find suppliers of polymers and carbon fibers combined in a useable SMC. Materials from Zoltec, SGL, Toray, Grafil, and others were evaluated. Early on, two significant obstacles became evident: completely wetting the carbon fiber and defilamentizing the fiber bundles. Work with suppliers is ongoing to optimize chemistry and processes to consistently provide carbon fiber SMC material with the targeted material properties. Short-beam

shear tests using ASTM D2344/D 2344M were used to screen material samples with various combinations of resins and additives. More than 150 samples were evaluated. Materials that performed well in the short-beam shear screening were used to make plaques to measure material properties. Good progress has been made in obtaining the targeted mechanical properties, as shown in Table 1.

Table.1. Percentage of target values achieved

Property	Tensile strength	Tensile modulus	Flexural strength	Flexural modulus
Percentage achieved	93%	91%	96%	96%
Coefficient of variation	0.05	0.09	0.09	0/07

Class A Surface Quality Development

The carbon fiber SMC material, which exhibited mechanical properties closest to the targets, was utilized in preliminary molding trials to assess the status of surface quality. Existing automotive exterior panel molds were used, and processing parameters were set similar to those for the glass fiber SMC component. The assessment of the surface quality of the initial parts appeared promising. However, a substantial effort will be required in process engineering and process optimization to achieve Class A surface quality.

Assembly Process Evaluation

Evaluations of various proposals for bond gaps, adhesives, and assembly processes were begun. At this time, no definitive direction has been reached. Work in this area will proceed concurrently with the carbon fiber SMC material and process developments.

Cost and Weight Evaluation

Initial concept work has concluded that a 40 to 60% weight reduction is within range, as plaques in the required reduced material thicknesses have been molded. Early cost estimates of the carbon fiber SMC material are encouraging. However, a great deal of work remains to ensure that material, processing, assembly, and finishing costs are competitive with complete glass fiber SMC components.

Conclusions

Good progress has been made in finding promising materials and beginning process development. The early work is very encouraging, as target material properties are being approached. Process development has begun, and assembly process investigations are ongoing. The potential cost and weight reductions appear realistic and within reach.

E. Advanced Composite Support Structures

Principal Investigator: James Grutta
Delphi, Inc.
Saginaw Steering Systems
3900 Holland Road, MDC-2
Saginaw, MI 48601-9494
(801)-568-0161; fax (801)-565-8091; jamesg@macqc.com

ORNL Project Manager: Cliff Eberle
(865) 574-0302; fax: (865) 574-8257; e-mail: eberlecc@ornl.gov

Technology Development Area Specialist: Sidney Diamond
(202) 586-8032; fax: (202) 586-1600; e-mail: sid.diamond@ee.doe.gov
Field Technical Manager: Philip S. Sklad
(865) 574-5069; fax: (865) 576-4963; e-mail: skladps@ornl.gov

---

Contractor: Delphi, Inc.
Contract No.: 4000021806

Objective

- Lead the rapid implementation of lightweight composite materials in Class 7/Class 8 vehicles via the development of advanced composite support structures, including chassis lateral braces and primary beams.

Approach

- Research four topic areas: joining, modeling, designing and processing. Coordinate the joining task with the project "Attachment Techniques for Heavy Truck Composite Chassis Members" to leverage resources.
- Study and test various joint designs and mechanisms, including mechanical fastening and adhesives. For mechanical fastening, assess parameters such as pre-drilled versus post-drilled holes, as well as hole geometry, spacing, bolt tension, and inserts.
- For the modeling task, study predictive numerical techniques to aid in joint and overall part design. Use several computer-aided engineering vendors to determine which would best complement the fiber architecture, fatigue, and damage analyses, which are needed to accurately predict joint and part response in this application. Use commercial finite element analysis (FEA) software to optimize the part geometry, including thickness variation, fiber orientation, fiber architecture, hole location, peek performance, and the minimization of mass and cost.
- Conduct the design using the results of the joining and modeling sections to determine a process to fabricate prototype parts for testing.

Accomplishments

- Successfully completed the value analysis value engineering (VAVE) workshop to determine the main attributes/requirements and their weighting of the lateral brace.

- Conducted an in-depth literature survey on attachment technologies for composites, with a focus on solutions for hybrid joints, effects of 3-dimensional (3D) reinforcement, bolted joints, and fatigue testing.
- Established a test matrix for coupon testing for baseline steel-steel joints, as well as the steel-composite system of interest.
- Selected commercially available, component-independent material and identified appropriate mechanical tests to investigate levels of damage resulting from various hole fabrication methods and bolt preload levels, as well as ways to mitigate the negative effects of the damage.
- Set up a vacuum infusion lab at Delphi Research Labs (DRL) to fabricate the initial test panels.
- Identified several software vendors as compatible with structural composite elements and interviewed them regarding their capabilities.
- Chose one commercial FEA software package to perform the structural analysis and design optimization and another to handle damage simulation and fatigue modeling.

Future Direction

- Continue FEA design and optimization, plaque testing, and fiber architecture determination in FY 2004.
- Conduct a requirements and concepts gate review to finalize the part geometry. Begin manufacturing the prototypes in 2005. In the second quarter of 2005, choose unique applications for both original equipment manufacturers (OEMs), followed by VAVE workshops and FEA and design optimization.
- In the last quarter of 2005, conduct the design and development gate review and initiate production part building.
- Optimize the final design, which will be submitted to track testing during the last quarter of 2006.
- By 2007, finalize the manufacturing process, supply product prints, and validate the product. PPAP will occur in the first quarter of 2007.
- Follow a similar approach for the primary beams project, beginning in the third quarter of 2005.

Introduction

The purpose of this project is to lead the rapid implementation of lightweight composite materials in Class 7/Class 8 vehicles via the development of advanced composite support structures, including chassis lateral braces and primary beams. Mass reductions are targeted for 50%. The benefits of mass reduction in commercial vehicle applications are well known. They include increased fuel economy and larger payload, which translates into fewer total trips and therefore fewer vehicles on the road. This leads to less traffic, which aids highway safety and decreases emissions. Support structures offer an opportunity for significant weight savings. However, this area of the vehicle also represents a large hurdle in terms of composite applications and market acceptance.

Composite lessons learned from previous industry primary beam studies and the technological achievements gained during the lateral brace study, when applied to the primary beam study, should result in a potential mass reduction exceeding 100 kg for a typical Class 8 tractor.

Our team is resolved to develop fiber-reinforced-composite technologies for these structural applications while determining the extent of their *durability*. In this respect, 3D fiber architecture will be examined. Composites with fibers in the Z direction have shown improved

ability to hold the in-plane fiber architecture together under high fatigue and creep. They also resist interlaminar crack propagation, which may lead to delamination. Attachment technology will be developed, including but not limited to preformed holes in the fabric before consolidation, metal plate inserts, and post-forming (e.g. drilling) operations. This joining technology will require development, but we expect it to be applicable for both lateral brace and primary beam composite attachments.

This work is being coordinated with "Attachment Techniques for Heavy Truck Composite Chassis Members," led by Oak Ridge and Pacific Northwest National Laboratories, to help resolve the joining challenges of this program.

VAVE Workshop Results

The VAVE workshop and its pre-event were successful in providing the necessary roadmap for this program. First, a current production lateral brace was chosen for the first phase of this program. Prints and design specifications were also provided. It is for a bulk hauler (heavy-duty) application.

The major attributes of this program were determined and weighted. Attribute weighting assumes that the minimum requirement has been satisfied for all attributes; hence it determines where additional effort should be focused after minimum requirements are satisfied. Cost factors emerged as the major attributes of concern—the top three attributes were cost related. The purchased cost premium, the actual cost penalty for mass savings, is the most important attribute.

Cost of assembly was the second-most-important attribute. The OEMs pointed out that a process that is very disruptive to their assembly lines would be difficult to integrate and would be expensive if new equipment and training had to be implemented.

Warranty (after-sale cost) was the third-ranking issue. An issue important to the immediate financial costs of warranties is that a new composite member cannot be returned from the field more often than its steel counterpart. Otherwise, the image of structural composite materials incorporated into a heavy-duty truck chassis could be tarnished for a long time to come.

Process robustness was found to be the fourth most important attribute. This actually represents the scrap rate of the product before it is sent to the assembly line.

Modeling

Modeling includes FEA, optimization, and prediction of damage, fatigue, and failure. Many software vendors were interviewed and evaluated for participation in this project. Our main criteria were

- Composite design-analysis tools to aid in finite element modeling of composites, such as the prediction of fiber angle orientation from a 2D fabric in a general 3D mold configuration (draping). Such tools exist and are composite-specific.
- Process simulation for composites.
- Modeling of composites with 3D fiber architecture.
- Modeling of joining of composite parts to other composite or metallic parts, such as in bolted connections or adhesive bonding.
- Nonlinear material modeling of composites, specifically for stiffness degradation and material failure.
- Durability assessment for composite structures.

A composite capability matrix of the major commercial FEA packages was developed. The comparison was limited to the codes available at Delphi. We believe that there will be a need to use more than one FEA code for the design analysis in this project, since it is unlikely to that one code can do it all or will be familiar to everyone. One commercial FEA software package was chosen to perform the structural analysis and design optimization, and another was chosen to handle damage simulation and fatigue modeling.

Joining and Material Characterization

Initial test specimens were fabricated using an E-glass/vinyl ester system. A 3D woven 72-oz fabric was chosen. For these tests, we used material with equal amounts of 0º and 90º glass fiber and a 1.7% by weight through-thickness z-fiber) reinforcement.

The first four plaques created used a glass plate as a bed and a vacuum bag as the opposite surface. The samples fabricated had noticeable dimples on the vacuum bag side surface. These dimples were created where the z-reinforcement stitching went through the material. The glass-side surface was smooth. The dimples could create sites for crack nucleation, which would not be present in a two-sided resin transfer mold. In order to create samples with a more uniform surface, a tempered glass plate was used as a top plate and then the vacuum bag material was placed over the glass. The plaques created using the glass plate had smooth surfaces and were thought to be much more representative of an eventual production part.

Tensile testing has been performed using 0º, 90º, and 45º samples. The 0º direction is in the direction of the fabric as it comes off the roll; 90º is across the roll. The samples were tested according to ISO 527-4 (1mm/min). Presently, E_{12} is calculated based on an assumed Poisson ratio obtained for a similar E-glass/vinyl ester system from another project. The Poisson ratio will be measured pending repair of the appropriate equipment.

A neat resin plaque was created and cut into six "dog bone" specimens 75 mm long with a gage section of 5.1 × 3.0 mm. They were tested at a rate of 1mm/min. Five of the six samples yielded usable data.

These test results will be used as inputs for the FEA software. DRL began initial damage simulation/fatigue software training the week of November 17. The first model to be analyzed using the damage simulation/fatigue package will be a tensile bar. The software has a library of material characteristics that will enable a "first pass" analysis of a component. We will compare this initial analysis with the actual data. This comparison will give us a confidence level when using the damage simulation/fatigue software to evaluate a material system for which we do not have samples readily available for testing. The data will also enable tuning of the software to our composite system.

Conclusions

This project has been successful in identifying an application and receiving appropriate input from its members to correctly determine areas of focus for its study. Additionally, the format for determining which software to use for process and performance modeling (including fatigue and fracture) will prove to be valuable as the program continues. Coupling the efforts of this program with the project "Attachment Techniques for Heavy Truck Composite Chassis Members" has already shown to be invaluable in efficiently gaining progress on our goals. We are close to our timeline and anticipate continued success as we dive deeper into fabricating and testing parts and applying our modeling techniques.

F. Hybrid Composite Materials for Weight-Critical Structures

Principal Investigator: Mark T. Smith
Pacific Northwest National Laboratory
P.O. Box 999 Richland, Washington 99352
(509) 375-4478; fax: (509) 375-4448; e-mail: mark.smith@pnl.gov

Principal Investigator: Bill Roberts
PACCAR Technical Center
12479 Farm to Market Road, Mount Vernon, Washington 98273
(360) 757-5286; fax: (360) 757-5370; e-mail: broberts@paccar.com

Technology Development Area Specialist: Sidney Diamond
(202) 586-8032; fax: (202) 586-1600; e-mail: sid.diamond@ee.doe.gov
Field Technical Manager: Philip S. Sklad
(865) 574-5069; fax: (865) 576-4963; e-mail: skladps@ornl.gov

---

Contractor: Pacific Northwest National Laboratory
Contract No.: DE-AC06-76RLO1830

Objective

- Develop and demonstrate (1) the application of hybrid composites and composite/metal hybrids to heavy-duty vehicles and (2) the ability of these material choices to be integrated into moderate-volume production.
  - Develop and demonstrate the potential for major weight savings (>50% on a component basis) in critical structures applicable to truck cabs and support components.
  - Demonstrate via proof-of-principle experimentation the basis for use of hybrid metal-composite systems to reduce weight.

Approach

- Investigate the potential of new materials and manufacturing technologies to effect major weight reductions for heavy-duty vehicles.
- Assist in demonstrating the applicability of composites and composite/metal hybrids to operational vehicles with little or no cost impact.
- Provide the experience base to develop the design and analysis tools, as well as the scientific understanding of the factors affecting molding and materials performance.
- Provide the materials suppliers with a market that can stimulate demand, leading to an increase in their production capacity. This will help reduce materials costs by creating higher volumes.

Accomplishments

- Completed the modeling of a door system for an existing PACCAR truck model and calibrated it against previous PACCAR models and experimental load/deflection data by Pacific Northwest National Laboratory (PNNL) staff.
- Ran a series of modified models simulating the addition of local carbon fiber stiffening strips. Developed an optimized reinforcement that provides a reduction in deflection of greater than 50%.
- Received the first sets of hybrid glass/carbon fiber preforms for liquid molding from the National Composites Center (Kettering, Ohio).
- Completed evaluation of test methods for the various hybrid materials.
- Provided several production doors from PACCAR to PNNL for application of the stiffening system. Prior to delivery of the doors, PACCAR performed baseline deflection tests that are currently being repeated with the carbon fiber stiffening strips applied.
- Began fabrication of prototype components for the hybrid door design by several vendors. The PACCAR/PNNL team recently completed the formal design review and design release meeting.

Future Direction

- Complete components for the hybrid door prototype demonstration during December 2003 and early January 2004.
- Complete the design of the door assembly fixtures and tools by PACCAR in preparation for prototype assembly.
- Complete assembly of three prototype hybrid doors by PACCAR and conduct truck cab structural testing.
- In conjunction with Mercia, update manufacturing cost models and review cost results for the hybrid door designs with PACCAR.
- Compile a final report at the conclusion of the prototype demonstration phase.

Introduction

Current materials and manufacturing technologies used for heavy vehicle door systems are often dictated by the high cost of tooling and the relatively low production volumes for Class 8 trucks. Automotive-style stamped door designs, whether of steel or aluminum, require multistage stamping dies that are generally cost-prohibitive at lower production volumes (<50,000 units per year). Alternate materials, such as glass-reinforced sheet molding compound (SMC), require less expensive tooling and can provide Class A finish; but the relatively poor specific properties of SMC tend to compromise design and result in a heavier door system. For many production truck cabs, a simple aluminum extrusion frame is used with a flat aluminum sheet riveted to the frame. Although this approach does not require expensive tooling, the use of constant cross-section extrusions in the frame is less than optimum; and it requires more assembly labor than other approaches. PACCAR, a world leader in Class 8 truck design and manufacturing, teamed with PNNL to explore alternate “hybrid” door system designs that minimize tooling cost and per-part door cost, while providing a lightweight, structurally stiff, automotive-styled door.

Project Approach

The initial approach to development of the hybrid door system was to perform a structural analysis of an existing PACCAR door design and determine what the design and performance goals should be for new-generation door systems. PACCAR provided a number of weight, cost, and performance parameters that it considered important for future door designs. PNNL was tasked to survey existing and emerging materials and manufacturing approaches that could be applied to a new door design. Following completion of this survey and analysis of existing door designs, PNNL, with design assistance from Mercia, Ltd., developed a series of five door design concepts that included combinations of large die castings, extrusions, carbon- and glass-reinforced composites, and conventional SMC and stamped aluminum exterior panels. Following a concept review meeting with PACCAR, an optimized hybrid door design concept was selected. The door concept was then defined using computer-aided design tools and analyzed with finite element models to validate performance, weight, and cost. After determining that the prototype design met or exceeded all performance and projected cost targets, PNNL and PACCAR selected methods to produce prototype components for the full-scale assembly and testing phase of the project. The finite element model of the prototype door system is shown in Figure 1.

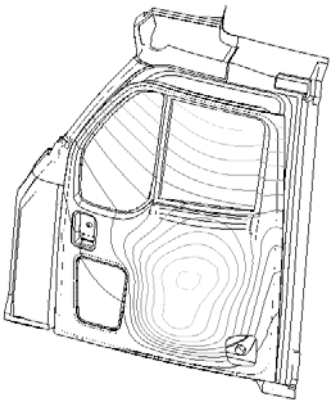

Figure 1. Finite element model of prototype door system under simulated loading conditions.

Conclusions

A door system has been designed and analyzed by the PNNL/PACCAR team. Development of three prototype doors for cab testing is currently under way. The hybrid door design provides attractive weight and cost savings compared with automotive-style stamped door designs, and it provides significantly reduced part count and assembly cost. Development of prototype door assemblies is currently under way. When complete, it will be subjected to a full range of cab durability testing by PACCAR.

G. Application of Carbon Fiber for Large Structural Components

Principal Investigator: Mark T. Smith
Pacific Northwest National Laboratory
P.O. Box 999, MSIN: K2-44, Richland, WA 99352
(509)375-4478; fax: (509)375-2186; e-mail: Mark.Smith@pnl.gov

Technology Development Area Specialist: Sidney Diamond
(202) 586-8032; fax: (202) 586-1600; e-mail: sid.diamond@ee.doe.gov
Field Technical Manager: Philip S. Sklad
(865) 574-5069; fax: (865) 576-4963; e-mail: skladps@ornl.gov

---

Contractor: Pacific Northwest National Laboratory
Contract No.: DE-AC06-76RLO1830

Objective

- Develop selective reinforcement technology that can be applied to large cab components to improve specific stiffness and strength while reducing overall component weight.

Approach

- Determine how well the low-cost carbon fibers can be hybridized with glass fibers to provide substantial weight and cost reductions in large cab components.
- Develop a system for preforming carbon and glass fibers together that will allow components to take maximum advantage of the capabilities of selective reinforcement alignment and property contribution.
- Develop models for the analysis of hybrid chopped-fiber preforms and composites that allow the thermal and structural properties to be developed and compared with experimental analysis.
- Perform structural testing to define the limits of applicability of the carbon/glass hybrid reinforcement materials to the large structures and develop guidelines for applications that may be used by original equipment manufacturers (OEMs).
- Design and develop critical subsection components of large structures to use in correlation with the predictive models, and validate the structural application criteria. Determine the capability to fabricate the materials in full-scale components, and determine the performance of these full-scale components in real application scenarios.

Accomplishments

- Developed short-fiber composite models for predicting properties of hybrid composite structures.
- Completed experimental testing of hybrid composite panels for model correlations.
- Developed a method to measure fiber angles for determining the level of anisotropy in chopped-fiber composites.
- Completed a set of designs of experiments on a new resin system for use with the hybrid composites.

- Completed initial runs on a large test tool with short-fiber composite preforms.
- Developed a large-scale subcomponent tool specifically to mimic design attributes applicable to several structural and appearance components.
- Performed initial runs on a large test tool with short-fiber composite preforms at a tier-one supplier.
- Developed hybrid fiber preforms for a test tool and demonstrated initial successful molding with hybrid fiber and resin system.
- Prepared samples for testing from large structural components.

Future Direction

- Scale up to test production parts.
- Continue testing new hybrid resin system.
- Develop modified tooling to be compatible with processing rates and materials selection for large hybrid structures.
- Analyze and experimentally verify techniques developed for improving appearance on components to demonstrate applicability to hybrid system.
- Verify tooling on bench and component scale parts.

Introduction

Selective reinforcements with higher-stiffness fibers have the potential to reduce both costs and weight simultaneously even at today's market costs. Their introduction is hindered by a lack of understanding of the fibers in existing processes, as well as the need to develop robust methods of preforming glass and carbon fiber materials together. In addition, the capability to meet Class A surface finish specifications is required, which requires potential development of bonding agents as well as the ability to model thermal and structural performance of the materials in a hybrid system. The recent development of composite systems combining carbon fiber reinforcement with low-cost automotive and marine resin systems provides the opportunity for selective reinforcement of a broad range of structural composite components.

The purpose of this project is to develop the design and materials processing technology to facilitate the application of low-cost hybrid glass fiber and carbon fiber reinforcements on large composite components, resulting in reduced weight and improved structural performance. The project will also seek to advance low-cost carbon fiber materials developed by industry by advancing the introduction of low-cost resin systems that are compatible with current heavy vehicle structural composites.

Predictive Modeling

Summary of the Modeling Approach

A computational tool called the Eshelby-Mori-Tanaka approach (EMTA) has been developed to predict the elastic and thermal properties (thermal conductivity, thermal expansion coefficients) as well as the elastic-plastic responses for short-fiber composites.[1] The EMTA model makes use of the Eshelby equivalent inclusion method in which fiber characteristics (including shape) are accounted for through the so-called Eshelby tensor while the constituents' properties, volume fractions, and fiber interactions are taken into account through the homogenization procedure. EMTA can handle two types of fibers mixed and embedded together in a resin matrix (hybrid

composites). Planar orientation is assumed and obeys the fiber orientation distribution density of the form: $\rho(\theta) = \lambda e^{-\lambda\theta}$, where θ is the orientation angle measured with respect to the major fiber alignment axis (or fiber orientation distribution axis), and λ denotes a parameter governing the randomness. When θ is very small ($\lambda \rightarrow 0$), the fibers are randomly oriented; they are aligned for large values of λ. Between these two limiting cases, a given value of λ designates a fiber orientation distribution, which can be rather random or rather semi-oriented. EMTA can be used as a standalone code to predict the basic homogenized composite properties. It has also been introduced into ABAQUS by means of the user subroutine UMAT of this code for structural analyses.

Unsymmetrical Hybrid Composite Laminates

Unsymmetrical hybrid composites made of different composite layers, which are not symmetrical through the thickness, are of particular concern because of the mismatch of coefficients of thermal expansion (CTE) between the layers, which can lead to unacceptable structural deformations. On the other hand, adjusting the CTE by means of trial-and-error approaches is time consuming and expensive. Therefore, numerical methods to predict the CTE of the composite layers and the governing microstructural parameters (fiber volume fraction, aspect ratio, orientation distribution, etc.) are very helpful in assisting the design of unsymmetrical hybrid composite laminates.

The following discussion illustrates the procedure based on the EMTA for adjusting the CTEs for a hybrid laminate made of carbon/vinyl ester and glass/vinyl ester (hydrex 100) layers. First, an initial molded hybrid panel without adjustment of fiber volume fractions or orientations was analyzed. The panel dimensions are 610 mm × 610 mm × 3.302 mm. The EMTA thermoelastic model implemented in ABAQUS was used to determine the warpage of this panel due to its cooling from the curing temperature (65.55ºC) to the room temperature (24ºC). The comparison of the predicted and experimental deformed configurations serves to validate the modeling results. The mismatch of CTE is then remedied by adjusting the fiber orientation distribution and volume fractions. The CTEs of the constituent materials are given in Table 1. The CTEs of the glass and carbon tows filled with vinyl ester were predicted using the EMT model (provided in Table 1).

Table 1. Thermal expansion coefficients of the constituent materials and the fiber tows filled with hydrex 100.

	α_1 (×E6/°C)	α_2 (×E-6/°C)	α_3 (×E-6/°C)
Carbon[a]	-0.7	10	10
E-glass[a]	5.4	5.4	5.4
Vinyl ester[b]	70	70	70
Carbon/vinyl ester[c]	-0.011935	38	38
Glass/vinyl ester[c]	7.7081	36.525	36.525

a Source: *Handbook of Composites*.[2]
b Based on the values of thermoset polyester given in *Handbook of Composites*.[2]
c EMTA prediction.

The parameter λ, which characterizes the fiber orientation distribution, is about 0 for the glass layer and 1.1 for the carbon layer. Hence, glass fiber orientations are more random than those of the carbon fibers. Figure 1 shows the predicted deflection (displacement u_3) resulting mainly from the mismatch of the in-plane CTEs (α_1, α_2) between the carbon and glass layers. The predicted deformed shape agrees well with the experimental one shown in Figure 2.

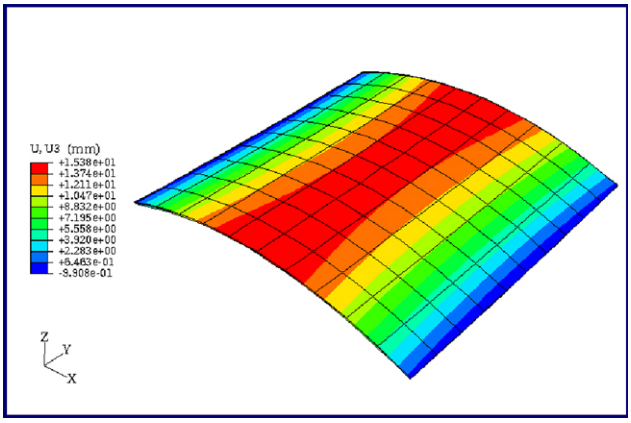

Figure 1. Prediction of the deformed shape and out-of-plane deflections for the analyzed hybrid panel after molding.

Figure 2. Warpage of the hybrid panel after molding.

Predicted and experimental deformed configurations are presented in Figure 3 in terms of the spatial coordinates *X*, *Y*, and *Z*. In both configurations, the *Z* coordinates were determined on the top surface of the hybrid panel. The predicted values correlate well with the experimental results.

To reduce the mismatch of CTE, the first remedy is to realize the same orientation distribution for the carbon and glass fiber tows. If the carbon tows' orientations are as completely random as those of the glass tows for $\lambda \to 0$, such orientations will lead to the

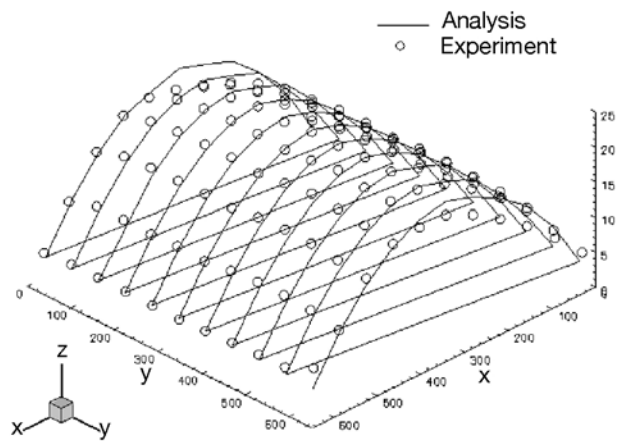

Figure 3. Experimental and predicted deformed coordinates for the analyzed hybrid panel after molding.

predicted variations of the in-plane CTE as a function of the fiber tow volume fraction shown in Figure 4. For a given glass tow volume fraction, these curves provide the corresponding carbon tow volume fraction, which must be realized so that the mismatch of CTEs is zero. In this example, the glass tow volume fraction is fixed at 0.5155 while the carbon tow volume fraction is initially 0.6771. These values were obtained knowing the volumes and the fiber volume fractions of the glass layer and of the carbon layer as well as the fiber volume fractions of the tows. In order to realize the same in-plane CTE for glass and carbon layers, the carbon tow volume fraction must be adjusted at 0.42, which gives rise to the carbon volume fraction of 0.27 in the carbon layer. Finally, Figure 5 shows the simulation results for the adjusted case. The deflection is practically reduced to zero as the result of the suitable adjustments of fiber orientations and the carbon tow volume fraction in the carbon layer.

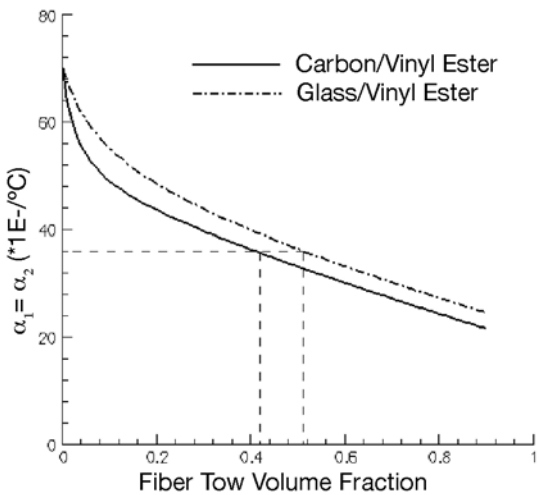

Figure 4. Variations of the in-plane CTEs of the carbon and glass layers with the fiber tow volume fraction.

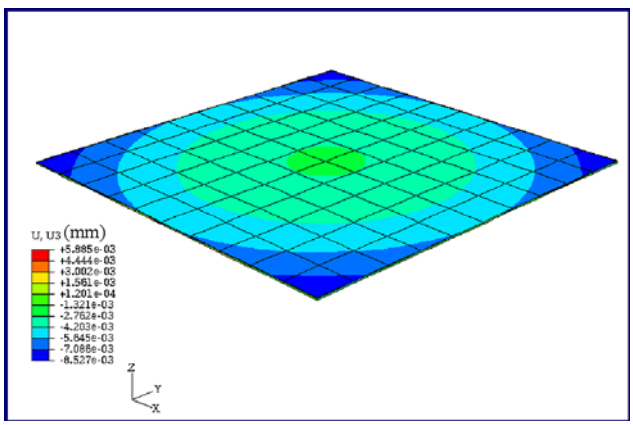

Figure 5. Prediction of the deformed shape and out-of-plane deflection for the analyzed hybrid panel after adjustments of fiber orientation distribution and fiber volume fraction for the carbon layer.

Experimental Testing

As previously mentioned, test panels were fabricated from preforms created by the National Composites Center (NCC). Figure 6 shows a typical carbon/glass hybrid panel. The panels had varied two target levels of volume fraction of glass and/or carbon. The hybrid panels also had three levels of carbon fiber in addition to the glass. Carbon volume levels were 3%, 9%, 15%, and 45%; the

Figure 6. Typical carbon/glass hybrid panel.

balance were random glass, with the exception of the 45%. These were made in two nominal thicknesses of 2.5 mm and 4.0 mm. There were also fiber-directed preforms of carbon fiber for comparing how well the properties could be controlled for a specific orientation. The panels were then resin transfer molded (RTM) with a standard polyester RTM resin from Reichhold Corp.

The panels were then laid out for specimen orientation and cutouts. The specimens were oriented with one referenced edge of the panel, and specimens were then removed with one set being parallel (0%) and the other being perpendicular (90%) to the referenced edge.

Tensile and flexural specimen geometry followed the ASTM D638 Type I Tensile and ASTM D790 Four-Point Bending Standards, respectively. Specimen profile measurements were taken and recorded, including width and thickness for each specimen. The specimens were also asymmetric in the panel through thickness.

The tensile specimens were bonded glass-to-glass with the carbon layers on the outer surfaces, then cut to the specification geometry. The double bonding was used to avoid bending moments during testing. Double extensometers were then used to measure the axial elongation and the width strain during axial loading. From this double extensometer measurement, a three-dimensional strain response can be

calculated. These data are then used to develop the elastic stiffness matrix and constitutive equations for model development. The flexural specimens were tested both with the carbon side up in compression and down in tensile for four-point bending. This allowed the modeler to be able to compare how well the prediction correlated with experimental data.

Fiber orientation measurements were made for determining the randomness factor for the EMTA model. Figure 7 shows a 3% carbon fiber preform that was used to determine the random pattern of the chopped material applied to the preform.

Figure 7. Composite hybrid preform with 3% carbon fiber chop.

The preform digital image was then used in a software package from which fiber orientation was measured relative to the bottom edge. The orientation was from 0 to 180º. Figure 8 shows the output data from the Figure 7 panel. The data show very good randomness with no defining pattern. NCC also provided some fiber-directed preforms for evaluation. The panels were to have 0 and 90% directed fibers. Figure 9 shows the fiber-directed panel from which data was collected. These measurements proved to be more challenging, with the dark background and little contrast. The lighting was extremely important for enhancing the fiber tows on the surface.

Figure 10 shows the histogram data of the Figure 9 measurements. A pattern is developed by the preferential orientation of

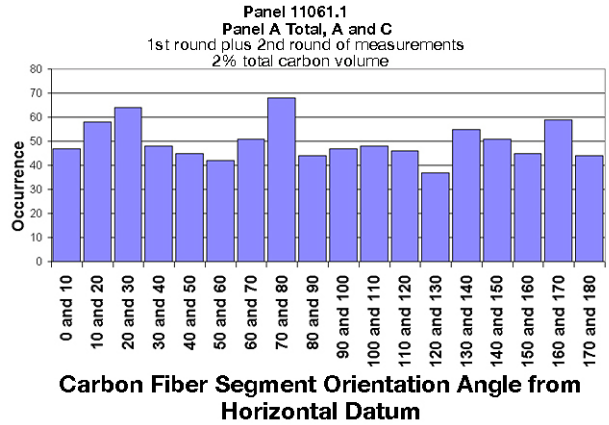

Figure 8. Histogram of fiber orientation.

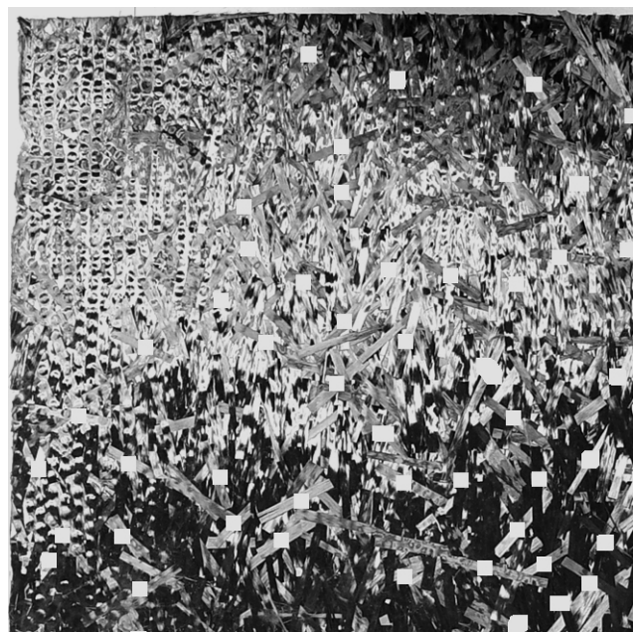

Figure 9. Fiber-directed panel.

the chopped fiber pattern program from the chopper gun. The histogram shows a bimodal distribution of fibers at approximately +45 and 60%.

Model and Experimental Correlation

A representative region of the specimens was used and discretized in three-dimensional finite elements for the simulation of the tensile stress/strain

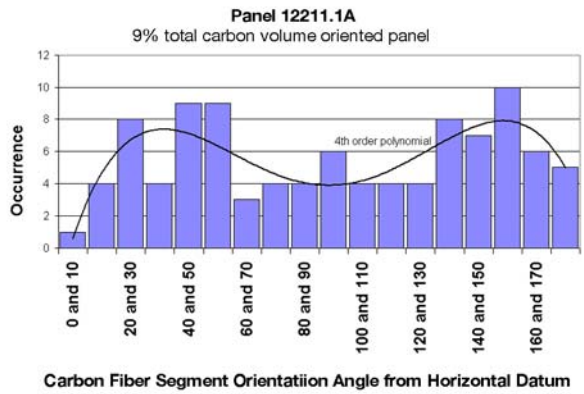

Figure 10. Histogram showing bimodal distribution of carbon fiber.

responses. This region is 13 mm wide (actual specimen width)and 26 mm long. The average thicknesses of the glass and carbon specimens are 4.7 and 5.5 mm, respectively. The major fiber alignment axis is parallel to the loading direction. Figures 11 and 12 present the simulated tensile stress/strain responses compared with the experimental results for the glass/vinyl ester and carbon/vinyl ester specimens tested until failure. The simulated curves were obtained using the elastic EMTA model (dashed line) and the incremental elastic-plastic EMTA model (solid line) implemented in ABAQUS. The glass/vinyl ester specimens could undergo higher deformations than the carbon/vinyl ester ones. In the former case (Figure 11), after a linear behavior at small strains, the responses become nonlinear at higher applied stresses; in the latter case, the nonlinearity of the responses is negligible. The nonlinearity results mainly from two different material origins. The first origin is damage by matrix cracking, fiber/matrix decohesion, and fiber pullout and breakage at the final stage. The second cause results from the plastic deformations of the matrix material. In this report, damage was not modeled, and only the plasticity of the polymer matrix was accounted for.

Figures 11 and 12 show good correlations of the predicted results with the experimental values except around the final

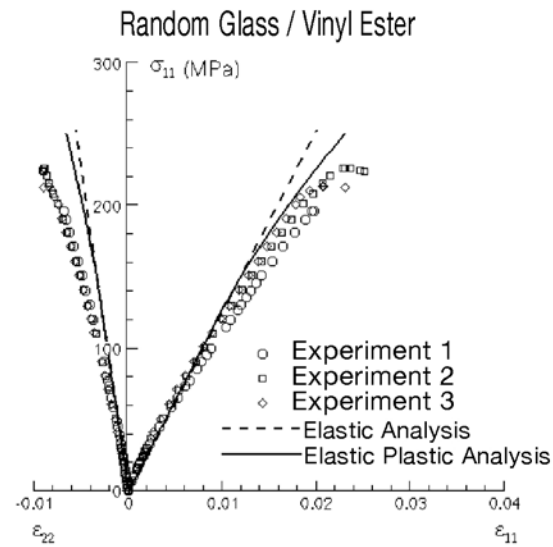

Figure 11. Tensile stress/strain responses of the random glass/vinyl ester specimens.

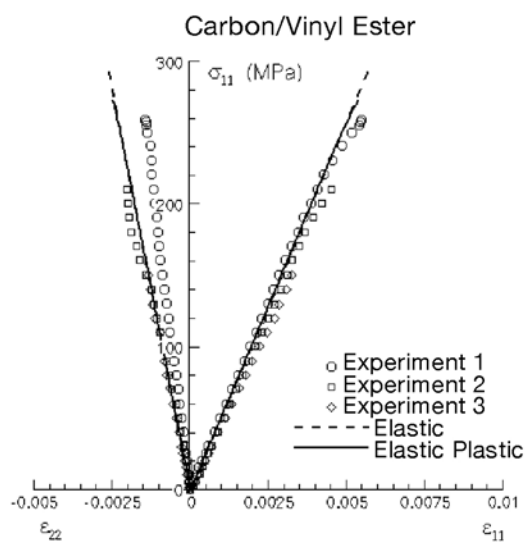

Figure 12. Tensile stress/strain responses of the random carbon/vinyl ester specimens.

loading stage, where excessive accumulations of damage led to failure of the specimens.

Flexural tests (based on the ASTM D790 standards) were conducted for glass/vinyl ester, carbon/vinyl ester, and carbon/glass/vinyl ester specimens. The latter are made of two layers—one carbon/vinyl ester and one glass/vinyl ester layer. In all specimens, the major fiber alignment axis is parallel to the width

direction. Figures 13 and 14 show the predicted load/deflection curves compared with the experimental values also presented on the same figures for the glass/vinyl ester and carbon/vinyl ester specimens. In all cases, the vertical deflection was determined at the center of the bottom surface of the specimen. Good correlations with the experimental results were obtained with the use of the elastic-plastic EMTA model. It is noted that excessive damage leading to final failure caused the load to drop at the end of the loading. Prior to final rupture, the elastic-plastic solutions predict the load/displacement responses very well. An elastic-plastic analysis using the large displacement (geometric nonlinearity)option in ABAQUS was also carried out in order to determine the effect of large displacements, which

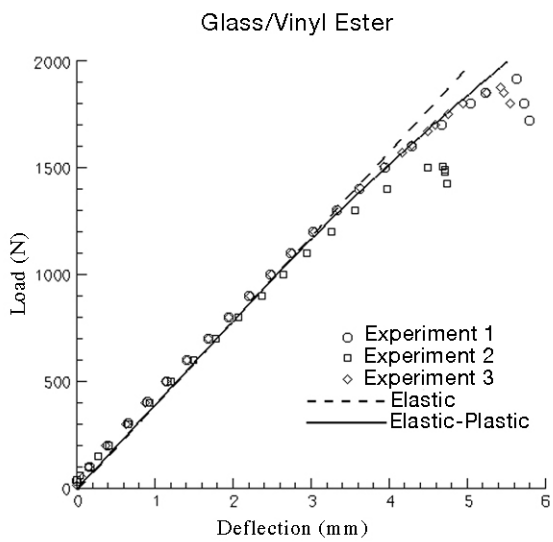

Figure 13. Flexural load/deflection responses of the random glass/vinyl ester specimens subjected to four-point bending.

occur around the end of the loading, on the overall responses. The corresponding solution for the carbon/vinyl ester specimen is denoted as "NLG Elastic-Plastic" and is presented in Figure 14. Compared with the elastic-plastic solution of the same problem,

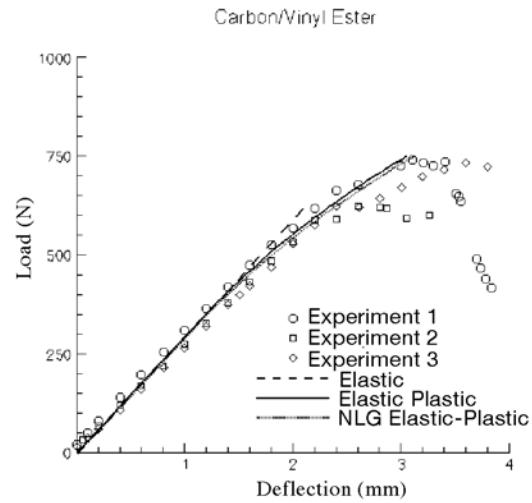

Figure 14. Flexural load/deflection responses of the random carbon/vinyl ester specimens subjected to four-point bending.

it is noted that the geometric nonlinearity is negligible. This is because the maximum deflection is of the same order of magnitude as the specimen thickness. Therefore, it is not necessary to carry out elastic-plastic analyses accounting for geometric nonlinearity for these specimens.

The predicted and experimental load/displacement responses for the four-point bending carbon/glass/vinyl ester specimens are presented in Figure 15. The test configuration was such that the carbon/vinyl ester layer is the upper layer. Figure 15 shows a noticeable scatter in the experimental results, especially at high loading levels leading to failure. The predicted elastic-plastic curve deviates from the elastic one when the deflection has attained 1.4 mm. It is also noted that early occurrence of damage has led to failure of these specimens at relative low load levels as observed in the carbon/vinyl ester specimens (Figure 14).

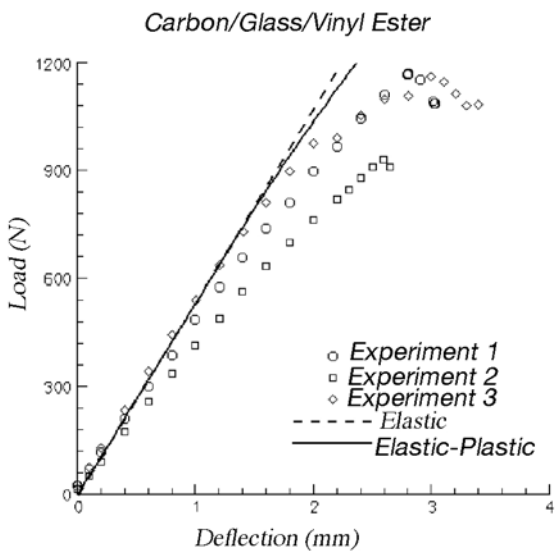

Figure 15. Flexural load/deflection responses of the random carbon/vinyl ester specimens subjected to four-point bending.

Hybrid Resin Evaluation

A Minitab design of experiments was run using a full factorial design with two levels and three factors. The interests in the experiments were to help determine which components gave the most control over the gel time. The factors of interest were temperature, cobalt content, and catalyst. The output measurements were gel time, peak exotherm time, and peak temperature.

The experiments were run on a Haake Rheocord 90 mixer using Brabender medium-shear mixing blades. The new hybrid resin from Reichhold was used. The catalyst, cobalt promoter, and temperature were controlled for the experiments.

The data were collected based on time, temperature of the resin, and the torque value during the mix. The gel time was taken as the first inflection of the torque curve. This is based on the torque value beginning to climb during resin gelling. The resin temperature also begins to increase relative to the same point as the gel time. The peak exotherm time is taken at the peak temperature that the mixture reaches before cooling down.

Figure 16 shows a Paretto chart that illustrates the standardized effects from the experiments. The Minitab output compares the different factors and combinations of effects. The Paretto chart clearly indicates that temperature has the most effect on gel time, followed by the cobalt content. The combined effect of cobalt and temperature also is a key contributor to the gel time.

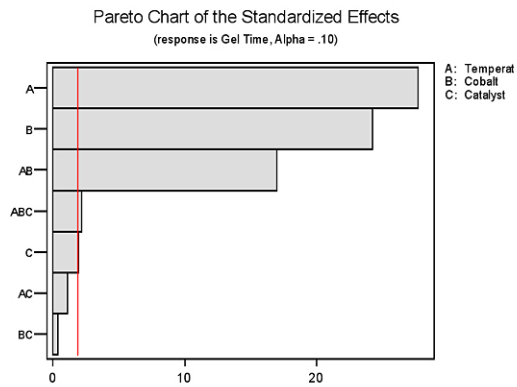

Figure 16. Paretto chart for gel time.

The catalyst showed very little effect on the gel time, and the trend was for the lower catalyst content to trend higher in peak exotherm temperature. However, the difference in peak temperatures is not statistically valid and is not being considered a concern.

Preform Evaluation

Several different preform styles have been considered and evaluated for the program to date, including commercial and development variations to achieve the goals for fiber hybridization. Using the DOE/Automotive Composites Consortium P4 preforming cell at the National Composites Center, hybrid flat preforms were made in a continuous process by modifying equipment to meet requirements. This was a distinctly different approach to the previous efforts where separate preforms of carbon and glass were made and later bonded together by NCC. Issues were seen in the distribution of binder in this approach, especially given the

preferred flat tow form of carbon fiber being used. Molding of these panels indicated a lack of binder and/or lack of fully developed strength for interlayer adhesion, especially in the glass fiber layer. Preforms were later developed for a multisided test tool, as well as for the large test mold used for full-scale evaluation trials. These confirmed the lack of development of binder strength at the interface, because the all-carbon preforms molded extremely well, and the glass preforms showed issues with fiber washout and lack of preform integrity.

A preform fabrication cell was developed to allow rapid changes to the preform structure and subsequent molding trials. This allows evaluation of specific approaches to be made more efficiently and cost-effectively. Hybrid preforms were developed that have given complete mold filling and wetout capability and provided samples for mechanical property testing. Work is continuing to make this process repeatable and predictable.

Preforming development continues on two fronts. Small tests are preformed for both the flat glass mold and multifaceted test tools for determining permeability and resin/preform interactions, and large preforms are made for evaluation of scale-up factors and the ability to meet design feature performance for subcomponent test tooling.

Large Evaluation Tool

In order to evaluate the capability of the process and materials to meet the demands of industry, a proof test component tool was developed. This tool has all the features anticipated in designs, and it was used to evaluate the hybrid process for achieving performance given the requirements of these features. It is not expected that all features may be molded and perform as expected. The goal of the development is to determine the limitations of the hybrid fiber system and, provide designers and OEMs with guidelines for which lightweight materials will be applicable, and to provide information on methods to design and manufacture these fibers.

Project personnel initially ran the evaluation tool over a week-long period at a tier one supplier. Figure 17 illustrates the size of the test tool for evaluating complex preforms and mold filling. It was immediately apparent that this was not a desirable development process because the systems for preforming, resin transfer molding, and resin optimization had to be developed independently and then brought in to the test. Limited capability to modify preforms and resin systems was achievable, given that the on-site capabilities were not necessarily geared toward development programs.

Results from the trials showed problems with the binder capability of the preforms, and the interaction of the resin system softened the binder over time. (This was not observed to this extent in smaller-scale test tools because the resin had much lower contact times with the preforms before the smaller tools were completely filled and the flow stopped.) All-carbon fiber preforms were much more successful than glass fiber preforms, and several test sections were useful for fabrication of coupons, etc. Indications from the test were that resin temperature and tool temperature control were critical for this system. This led to the work on the resin development experiments. Mold temperature was seen to be a significant issue, which has led to new approaches to tool design and build that are being evaluated.

A new cell was set up for R&D purposes with preforming modifications and resin modification possible in a more appropriate environment. Also, several options for molding were built in that were not possible in their existing production environment but could easily be implemented once proven. Running this cell, several successful test panel runs were made late in the year that used hybrid preforms and met the requirements of the overall process. These

Figure 17. Mold cell for test tool setup for large-part molding.

have provided samples to be tested early in the next phase. Development of parameters has been much more controllable; and several advanced options for preforming, molding, and materials are being investigated.

Based on initial results, the potential to meet industry requirements is very promising for the process. Researchers expect to achieve this capability on a scale that will provide confidence to adopt this lightweight materials technology. Figure 18 illustrates a successful hybrid carbon/glass composite from the test tool in Figure 17.

Figure 18. A successful carbon/glass hybrid composite part from the large test tool.

Conclusions

- In conclusion, a wealth of information has been gained from the tier one molding trials and the design of experiments on resin systems. The molding trials show that preform loft and strength need more fine-tuning. Carbon fiber preforms operation was especially promising; however, the initial glass fiber performance was disappointing, especially compared with lab trials. The tooling needs to have better temperature and resin flow control. Resin heaters for the two components will help in

viscosity and the addition of fillers in the future. Molding parameters will have to be addressed in a much more rigorous manner than this industry has been accustomed to, and statistical process control will become more of a norm to achieve consistent results. Samples of large-scale, as-molded hybrid fiber components are now available for testing and optimization. These have shown a significant increase in capability to the industry regarding potential component weight reduction.

- The design of experiments confirms that gelling was an issue for tier one suppliers and that researchers should be able to adjust the fill points based on the fill time-to-gel. The design of experiments indicates (1) the importance of temperature control on the tooling and cobalt content in the resin for completion of the fill and (2) the need to optimize cycle time to increase throughput for production cycles.

- A computational tool using the EMTA has been developed for the thermo-elastic and elastic-plastic analyses of short-fiber polymer composites. The tool was created by implementing the EMTA-based constitutive models into ABAQUS. The simulations of the tensile and flexural tests conducted on glass/vinyl ester, carbon/vinyl ester, and carbon/glass/vinyl ester specimens have provided good predictions of the composite responses, which were in agreement with the experimental results.

- The computational tool can be used to determine the basic properties needed for the design of short-fiber polymer composites, such as effective thermal and elastic properties, and tensile and flexural moduli of the composite laminate. Moreover, the ability to account for plastic deformations using the incremental elastic-plastic EMT model enables the composite behavior to be modeled at high loading levels, leading to deformations that exceed the elastic limit. The model inputs are fiber (or fiber tow) and matrix properties, fiber (or fiber tow) volume fractions, aspect ratios, and the orientation parameter (λ). This computational tool offers the flexibility to adjust these parameters so that the resulting homogenized properties and responses satisfy the design criteria in terms of desired properties and deformation limits. The tool can therefore be used to assist in the design and manufacturing of short-fiber composite structures.

- The design of experiments confirms that gelling was an issue for tier one suppliers and that suppliers should be able to adjust the fill points based on the fill time to gel. The design of experiments indicates the importance of (1) temperature control on tooling (2) cobalt content in the resin for completion of the fill and (3) cycle time optimization for increased throughput for production cycles.

References

1. B.N. Nguyen, K.L. Simmons, G.J. Grant, M.T. Smith,"A Computational Tool for Analysis and Design of Short-Fiber Polymer Composites." Prepared for submission to *Composites Science and Technology* (2003).

2. ASM International, *Engineered Materials Handbook: Composites,* ASM International, Metals Park, Ohio (1987).

H. High-Conductivity Carbon Foam for Thermal Management in Heavy Vehicles

Principal Investigators: B.L. Armstrong
Oak Ridge National Laboratory
P.O. Box 2008, Oak Ridge, TN 37831-6063
(865) 241-5862; fax: (865) 574-6918; e-mail: armstrongbl@ornl.gov

Oak Ridge National Laboratory
P.O. Box 2008, Oak Ridge, TN 37831-6250
(865) 241-4554; fax: (865) 576-6183; e-mail: mcmillanad@ornl.gov

Technology Development Area Specialist: Sidney Diamond
(202) 586-8032; fax: (202) 586-1600; e-mail: sid.diamond@ee.doe.gov
Field Technical Manager: Philip S. Sklad
(865) 574-5069; fax: (865) 576-4963; e-mail: skladps@ornl.gov

---

Contractor: Oak Ridge National Laboratory
Contract No.: DE-AC05-00OR22725

Objective

- Develop an understanding of the heat rejection demands of heavy vehicles and develop designs that utilize the superior performance of high-thermal-conductivity carbon foams.
- Coordinate efforts with a heavy vehicle manufacturer, an engine manufacturer, and a heat exchanger manufacturer in order to target the designs toward their understanding of the new vehicles' heat loads.

Approach

- Study fundamental mechanisms of heat transfer using carbon foam.
- Develop a testing method to evaluate foams and designs using the foams.
- Work with industrial partners to develop a complete understanding of heavy-vehicle-related issues.

Accomplishments

- Published a report summarizing the durability of graphite foam under simulated typical operating conditions.
- Constructed a cost model to determine the largest cost factors in the manufacture of graphite foam
- Developed a heat transfer model. Researchers determined that pressure drop across the foam is proportional to the flow length of the foam. In addition, permeability of the foam plays a role in the thermal performance.

Future Direction

- Continue collaboration with the Georgia Tech Research Institute (GTRI) on sub-scale and possibly full-scale airfoil heat exchangers.
- Evaluate potential on-vehicle tests to be performed at partner's facilities

---

Introduction

A novel technique for creating pitch-based carbon foam was developed at Oak Ridge National Laboratory (ORNL)[1, 2] before 1997. This technique uses mesophase pitch as a starting material but does not require the costly blowing or stabilization steps seen with typical carbon foams.[3]

The ORNL foam is an open-cell structure with highly aligned graphitic ligaments; studies have shown the typical interlayer spacing (d002) to be 0.3356 nm, very near that of perfect graphite (0.3354 nm). As a result of its near-perfect structure, thermal conductivities along the ligament are calculated to be approximately 1700 W/m•K, with bulk conductivities 180 W/m•K. Furthermore, the material exhibits low densities (0.25–0.6 g/cm^3) such that the specific thermal conductivity is approximately four to five times greater than that of copper. The very high surface area (20,000 m^2/m^3) combined with the high thermal conductivity suggests that graphite foam has significant potential for application as a thermal management material.

One issue of importance with regard to the performance of the ORNL foam is durability in typical operations. It is hoped that by understanding how the foam behaves in environments approximating actual operating parameters, researchers will learn how to modify the foam as necessary to meet application-specific needs. To this end, several durability studies have been undertaken, the constraints directed by either the research team or by industrial partners. The studies include thermal cycling, compression testing, corrosion, erosion, vibration, and salt spray (fog). This study was completed with joint funding from OATT and HSWR.

Results

Thermal cycling

Determining the effect of thermal cycling on the properties of graphite foam is important for the advancement of certain applications in the automotive industry. Graphite foam has a very low compressive modulus (0.08–0.114 GPa) compared with other materials commonly used in thermal cycling applications, such as aluminum (70 GPa). This low modulus value is expected to make graphite foam highly shock-resistant. Thermal cycling testing was carried out in two stages. The first stage was material durability testing, intended to determine whether the graphite foam itself could survive thermal cycling. The second stage, interface testing, was intended to study the effect of thermal cycling on the interface between the flat tubes and the foam on a subscale heat exchanger.

In the material durability test, foam blocks, press-fit with tubes, were tested for heat loss at the following intervals: 0, 3670, 6833, 16150, 26150, 36150, and 46150 cycles. The testing was accomplished by installing a foam block into a heat exchanger rig in which hot water was passed through the tubes and cooling air was blown over the foam block. The heat loss, or heat removal, was measured and plotted as shown in Figure 1. The figure shows a plot from the copper tube set, which is representative of the other three-tube material sets. A slight decrease in properties was found in the earliest cycles; then a plateau was exhibited and no further statistical changes were seen.

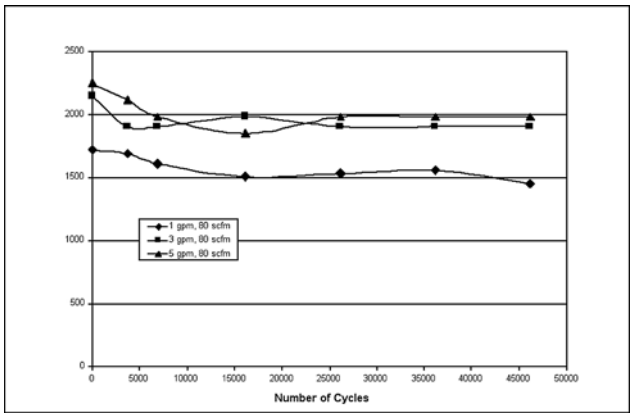

Figure 1. Water heat loss vs cycles.

This reveals that no significant degradation of the foam occurs foam as a result of thermal cycling.

In the sub-scale heat exchanger test, the bonding interface was visually inspected after every 4 h of testing. Visual inspection showed no apparent degradation of the interface. Even though visual inspection does not give a quantitative measurement of the status of the interface, this is an initial attempt to study this effect. Future efforts will focus on developing the means to quantify this property as a function of heat transfer.

Compression testing

Compression testing normally is conducted using a cylinder of a given ratio of length (*L*) to diameter (*D*). This ratio is typically between 1 and 3 (an L/D ratio of up to 10 may be used when very accurate measurements of the modulus are required). With larger ratios, the material being tested may buckle, giving rise to instability. With smaller ratios, end effects are more prevalent, resulting in barreling. Because brittle materials do not experience a significant amount of plastic deformation, a smaller ratio is used for these materials (typically 1.5 or 2). A ratio of 1 was chosen for the graphite foam, as it exhibits brittle failure and, furthermore, no deformation is observed; it appears that the foam fails locally in the ligaments, nearly a layer at a time. The tests were performed on 1-in. cubed samples of graphite foam to provide Young's modulus, compression strength, and strain to failure. These measurements are important in those applications in which it is necessary for the foam to exhibit some degree of structural integrity, for example, heavy-vehicle radiators.

After more than 42,000 thermal cycles (the same cycles used as in the thermal cycling tests), the graphite foam exhibited no statistical change in compressive stress (Figure 2) or compressive modulus (Figure 3). These results indicate that no structural changes or damage took place as a result of thermal cycling.

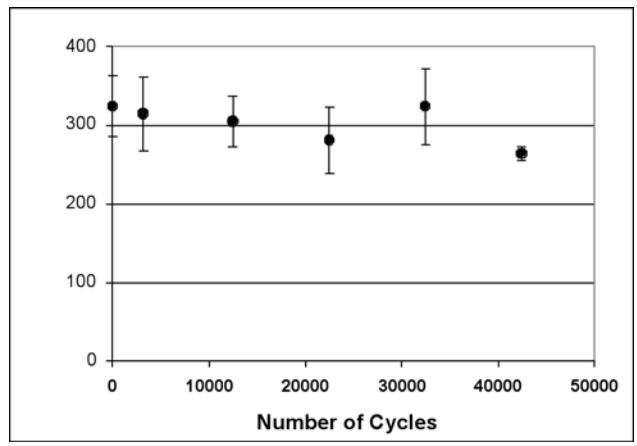

Figure 2. Graphite foam thermal cycling compression test results: maximum compression stress.

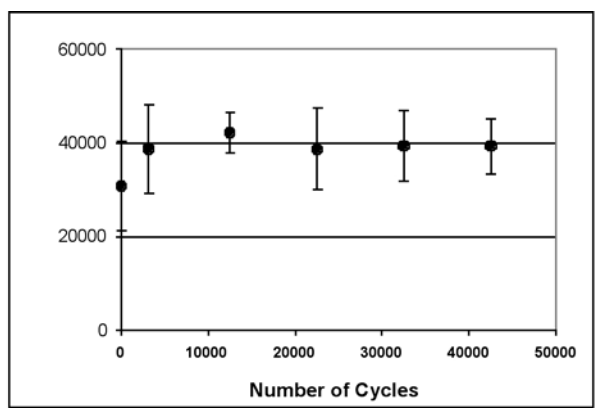

Figure 3. Graphite foam thermal cycling compression test results: compression modulus.

Graphite foam does not appear to be affected mechanically by thermal cycling. No effective decrease in properties was measured. Work is ongoing to verify that ASTM C 695 is indeed applicable to graphite foams; ruggedness testing was completed in summer 2003. Round-robin tests will begin in 2004.

Corrosion in propylene glycol/water mixtures

The use of graphite foam for power electronic applications has been proposed to dissipate heat in a variety of applications, including heat sinks, heat spreaders, and cooling inverters. In certain applications (e.g., a closed-loop heat sink that requires the use of a refrigerant), corrosion of the graphite foam in the presence of the evaporant or coolant becomes a concern—especially as it affects materials properties such as thermal conductivity, phase stability, and the reliability of a braze or weld. The reliability of the bond between the foam and a metallic substrate becomes increasingly important in an application such as a cooling inverter, in which no mechanical options are available for bonding the foam to the substrate. To address these issues, a corrosion study was completed.

A modified SAE J1211 standard test was used to expose samples of foam for 1000 h each at room temperature, 60°C, and 100°C in a 50% propylene glycol/50% water mixture (Zerex™). The samples consisted of untreated foam, nickel-coated foam, and nickel/polyvinylpryllidone (PVP)-coated foam. These samples were bonded to aluminum, copper, brass, and stainless steel plates using 50/50 (tin/lead) solder. In addition, unbonded samples of untreated foam, nickel-coated foam and nickel/PVP-coated foam were exposed at the same conditions to provide a base material control. After 1000 h of exposure at each of the three temperatures, each sample joint was examined visually and with scanning electron microscopy (SEM). Thermal conductivity was also measured.

A summary of the effects of temperature, foam treatment (coated or uncoated), and substrate on thermal conductivity after exposure in Zerex is shown in Figure 4. These results serve only as trend indicators for the

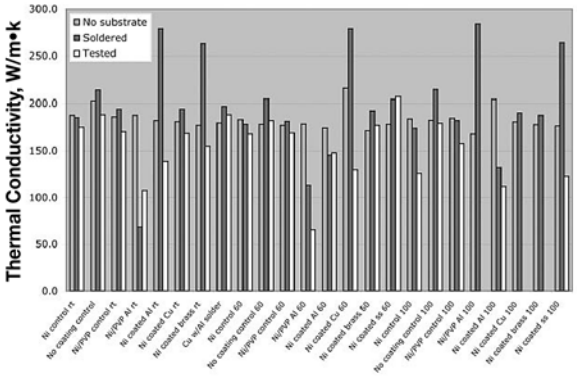

Figure 4. Effects of corrosion on thermal conductivity after 1000 h in Zerex solution at room temperature, 60°C, and 100°C.

feasibility of using this technique, as only one sample was tested for each condition. If the margin of experimental variation is calculated in the three control samples, the minimum variation seen even before testing is approximately 5%. Thus only variations above 5% were considered. The greatest effect upon thermal conductivity and viability of the solder was seen at the highest temperature condition, 100°C. Only one of the eight samples tested at 100°C showed no effect of temperature on thermal conductivity, and that sample was the uncoated control. Three of the eight samples tested at 100°C failed. Two of these samples—the nickel/PVP-coated foam soldered to an aluminum substrate and the nickel coated-foam sample bonded on to a brass substrate—failed at the solder or joint, i.e., the sample and substrate were found completely separated in the solution after exposure. The nickel-coated foam sample bonded to copper did not fail during testing (i.e., it was not separated upon removal after

testing), but it separated upon being mounted into the fixture for measuring thermal conductivity.

It is evident even from this brief study that the foam structure itself is unaffected by exposure to Zerex at temperatures of up 100°C and times of 1000 h. However, thermal conductivity and the mechanical integrity of the solder attaching the substrate and foam will be a factor in the foam's ability to survive and the stability of its thermal conductivity values. This study is being reproduced using multiple samples for each condition to determine whether the observed trend at 100°C or any other trends are real. One sample, the uncoated foam sample, did survive the exposure to Zerex at 100°C with no effect on thermal conductivity. For some heat sink/power electronic applications in which only a mechanical bond is used, the result is very encouraging and shows that graphite foam is indeed a valid material for use. In addition, the variability of the thermal conductivity and survivability of nickel-coated foam samples at 100°C appears to depend upon the substrate/solder combinations. To address this effect, current work is examining different solders and substrate combinations that will also be included in future corrosion studies.

Erosion

The erosion tests performed on the graphite foam samples were designed to measure the mass loss and mass-loss rate at a given impinging air velocity. These tests will reveal the graphite foam material loss based on preparation procedures (e.g., coatings and other surface treatments).

Graphite foam specimens were machined from a billet of commercial graphite foam processed under documented conditions. Each erosion specimen was machined into a 1-in. cube with a 0.25-in. hole machined through in the center of the specimen. Each specimen was weighed to get the baseline weight prior to testing and then mounted in a fixture. The outlet air nozzle was mounted approximately 3 in. from the specimen, centered on the 0.25-in. hole. Air was blown onto the graphite foam specimen at an approximate velocity of 1600 ft/min face velocity for 5 min.

After 5 min, each graphite foam specimen was removed and weighed in order to get the post-test weight. The mass loss was reported by subtracting the post-test weight from the pre-test weight, and the mass-loss rate was reported by dividing this value by 5 min. The mass loss rate of the raw graphite foam was calculated to be 0.0049 g/min at a continuous velocity ,while the loss rate for the nickel-coated foam was calculated to be 0.0013 g/min at a continuous velocity.

The mass-loss rate exceeded acceptable limits set by industrial partners. While the nickel coating significantly decreased the mass-loss rate, the overall rate was still found to be unacceptable for any application in which the foam would be subjected to impinging airflow.

The test setup described has been modified significantly to accommodate higher velocities, including the use of an adjustable jig and various coatings (e.g., raw, copper-coated, nickel-coated, and silver-coated foam). Two samples of each coating were used, one with straight holes and one with rounded holes as stress concentrators. In future testing, each sample will be exposed to impinging air flow for 5 min, weighed precisely, exposed for 5 min more, weighed again, and so forth until either the sample catastrophically fails or a plateau is reached.

Vibration

Vibration testing of graphite foam mounted to a metallic substrate was conducted to provide information on the degradation within the graphite foam, as well as any debonding that may occur at the interface between the graphite foam and the metallic substrate. The response of the graphite foam specimens was dependent on

the vibration test parameters. An industrial partner supplied the test parameters.

Graphite foam specimens evaluated by the vibration test were mounted to aluminum, copper, brass, and stainless steel sheet metal substrates to provide a structurally sound base for mounting the specimens to the vibration table. The specimens used for this test measured 0.625 in.^{3} The different substrates were used to determine how the varying mechanical properties of the metals, mainly their damping characteristics, affected the response of the graphite foam to the given vibration test conditions.

The thermal conductivity of each specimen was measured, prior to the vibration testing, so that a direct comparison could be made following the testing, which would reveal degradation within the graphite foam and in the interface between the graphite foam and the metallic substrate. Eighteen specimens were evaluated in the test. None of the specimens showed any visual degradation or debonded from the metallic substrate. The thermal conductivity measured following the vibration test showed there had been no change compared with the thermal conductivity measured prior to testing. The lack of variation in the thermal conductivity, except experimental error, led to the conclusion that no structural degradation had occurred to the graphite foam ligaments that impart the high thermal conductivity of the graphite foam.

Salt spray (fog)

Graphite foam samples were tested by exposure to a salt fog to indicate the material's relative corrosion resistance under controlled test conditions. An independent laboratory, Environ Laboratories, LLC, located in Minneapolis, Minnesota, conducted the tests.

The full report from Environ Labs was prepared to ASTM standards and was received in July 2003.

ORNL measured changes in mass and thermal conductivity. These results serve only as indicators of feasibility or trend, as the instrumentation used during the thermal diffusivity measurements (from which the conductivity is calculated) was been called into question during this test period. The variability in the baseline conductivity data does not agree with prior data on this commercial foam; further, the variability is not as great in the tested data. Examination of the instrumentation is currently under way; further tests using joined samples are on hold until this issue is resolved.

GTRI Collaboration

Georgia Tech Research Institute has a patented aerodynamic heat exchanger (AHE), a high-lift airfoil section that incorporates a conventional radiator to provide heat transfer and cooling to an automobile (passenger or heavy vehicle). If flow is allowed through the airfoil, it can seriously degrade the aerodynamics of the system. Thus a study, jointly funded by OATT and OHVT, was undertaken to determine the effectiveness of ORNL's graphite foam in this novel airfoil design; the foam has excellent heat transfer characteristics while engineering designs may allow tailoring of the porosity.

Three AHEs were tested under the same conditions, a conventional radiator manufactured by Visteon (like the one installed in the GT MotorSports Formula SAE race car), a solid graphite foam core, and a corrugated graphite foam core. Each core had cooling tubing passing through internal channels (Figure 5), and for all configurations, the airfoil was mounted on a strain-gage balance below the floor to measure forces and moments. Data were taken first to determine the aerodynamic characteristics of each core by monitoring the slot blowing pressure at a constant angle of attack as well as the tunnel pressure. Then the thermal performance was measured

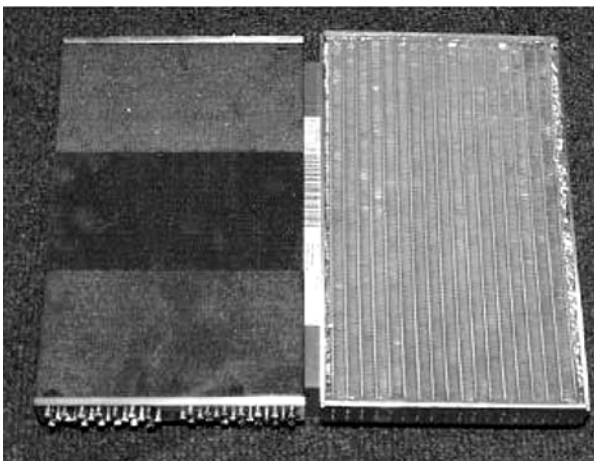

Figure 5. Solid graphite foam and corrugated foam radiator cores.

by having a constant coolant flow rate for variable pressure; further, the tunnel speed was also varied.

The heat transferred from the coolant can be expressed as

$$Q = \dot{m}_c C_p (T_{c_{IN}} - T_{c_{OUT}})$$

Measurements were made for each configuration at several freestream velocities, coolant flow rates, and blowing rates. Figure 5 shows the comparison of the graphite foam cores with the conventional Visteon core. Interestingly, the solid graphite foam core performed as well as the conventional core but with significantly less drag (Figure 6). Thus the dense graphite foam core has been shown to be an effective heat transfer medium that does not significantly affect the aerodynamic performance of the AHE.

Conclusions

The results from these studies are encouraging and indicate that the graphite foam performs well in most environments. Some issues have arisen with the choice of solder and/or substrate in certain environments, and tests are ongoing to further optimize these systems.

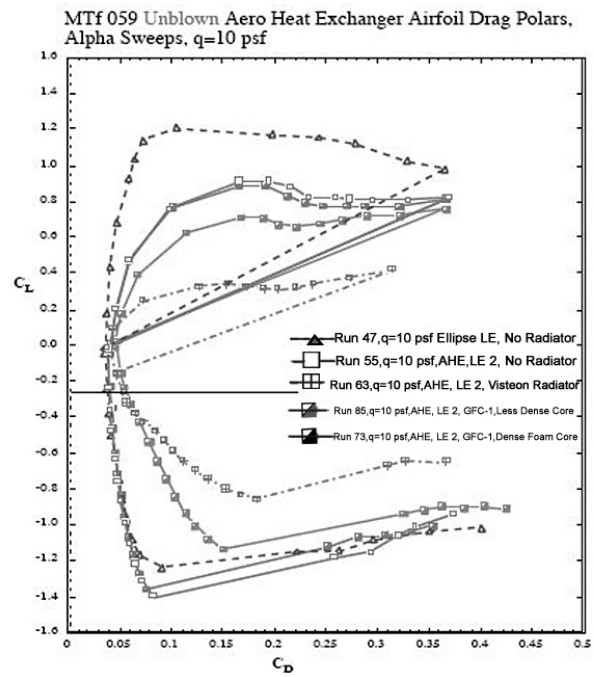

Figure 6. Unblown airfoil lift/drag polars as a function of angle of attack with and without radiators installed.

References

1. Klett, J. "High Thermal Conductivity, Mesophase Pitch-Derived Carbon Foam," in *Proceedings of the 1998 43rd International SAMPE Symposium and Exhibition, Part 1 (of 2)*, Anaheim, California, 1998.

2. Klett, J., "High Thermal Conductivity, Mesophase Pitch-Derived Graphitic Foams," *Journal of Composites in Manufacturing*, **15** (4), pp. 1–7 (1999).

3. Kearns, K. "Graphitic Carbon Foam Processing.," in *21st Annual Conference on Composites, Materials, and Structures*, Cocoa Beach, Florida, 1997.

I. Lightweight Functional Composite Materials

Principal Investigator: Timothy D. Burchell
Oak Ridge National Laboratory
P.O. Box 2008, Oak Ridge, TN 37831-6088
(865)576-8595; fax: (865)576-8424; e-mail: burchelltd@ornl.gov
with Alex Gabbard, Joe Strizak, and Jane Howe, ORNL

Technology Development Area Specialist: Sidney Diamond
(202)586-8032; fax:(202)586-1600; e-mail: sid.diamond@ee.doe.gov
Field Technical Manager: Philip S. Sklad
(865)574-5069; fax:(865)576-4963; e-mail: skladps@ornl.gov

Contractor: Oak Ridge National Laboratory
Contract No.: DE-AC05-00OR22725

Objective

- Demonstrate adsorbed natural gas (ANG) storage densities at levels comparable to compressed natural gas storage but at significantly lower pressure and at comparable cost.

Approach

- Conduct research in six task areas:
  1. Process development and physical property characterization
  2. Materials characterization
  3. Modeling and simulation
  4. Prototype tank design construction and testing
  5. Vehicle testing
  6. Economic analysis

Accomplishments

- Made progress in analysis of selected samples from the ANG test system toward better understanding its performance. Developed a storage monolith capable of storing >180 V/V methane at 900 psi (September 2002).
- Characterized carbon materials using high-resolution transmission electron microscopy (TEM), scanning electron microscopy (SEM), small-angle neutron scattering (SANS), and inelastic neutron scattering (INS). Alternate carbon fibers and fiber precursors have been evaluated (March 2002).
- Initiated computer simulation work using a reverse Monte Carlo (RMC) approach.
- Performed a series of 12 experiments on samples machined from carbon monoliths selected from the Big Tank, along with additional tests using a modified experimental procedure.
- Completed the test and evaluation of the demonstration fuel tank (September 2002)

- Prepared a report on characterization of microporous adsorbent carbon-fiber-based monoliths made from alternate fibers (September 2002).
- Completed the design of an in-vehicle demonstration natural gas fuel tank (March 2002).

Future Directions

- Initiate vehicle testing in FY 2004.
- Initiate economic analysis in FY 2004.
- Determine why the storage monoliths used in the demonstration tanks did not perform at the expected level.

Process Development and Physical Property Characterization

Progress has been made in analyzing selected samples from the ANG test system toward better understanding its performance. Three monoliths were selected from the assembly, one from an end of the assembly, another from about one-fourth of the way through the assembly, and one from the center. Each monolith was sectioned and machined, providing test specimens for the Oak Ridge National Laboratory (ORNL) methane adsorption test apparatus (MATA), shown in Figure 1. Data were accumulated on the first specimen, indicating a best case V/V (liters of gas per liter of tank volume) of 96-97 rather than the 140-150 V/V range projected for the system. Results indicated uniform density of material from the inner regions outward to the edges, resolving questions about possible variations in density such that only portions of the monolith volume were active in methane adsorption. Because each monolith was made using the same formula and with the same process, and each was activated similarly (although with some variations in final activation), differences in density of material producing inactive adsorption zones could account for lower-than-expected performance. Densitometry results confirmed uniformity of monolith density.

A new carbon fiber material with different properties was acquired. The material previously used contained fibers of solid cross section. SEM and TEM examination revealed that only a thin, outer layer of fiber was activated; the remainder of the fiber, about 80% or more of cross section, was not activated and therefore inactive in adsorption (Figure 2). The new fiber material included hollow fibers. Although they were of poor uniformity and a mixture of components compared with the refined material used in monolith formulation and tested in the ANG test system, use of the hollow fibers introduces the potential of increased surface area for activation. Development and testing of specimens with the new material is currently under way. A second type of new, high-quality carbon fiber material has been ordered; preactivated fibers are projected to increase the monolith surface area, thus increasing total adsorption.

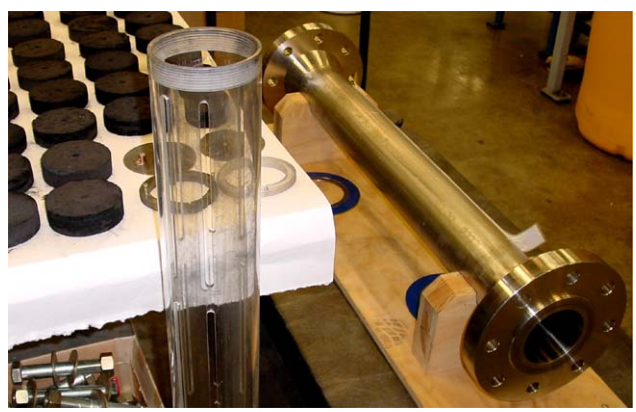

Figure 1. The major parts of the MATA are the test specimens, the stainless steel cell, and the Plexiglas liner. The dimension of each test specimen (the "puck") is *Φ4.45 in. × 1.21 in.*

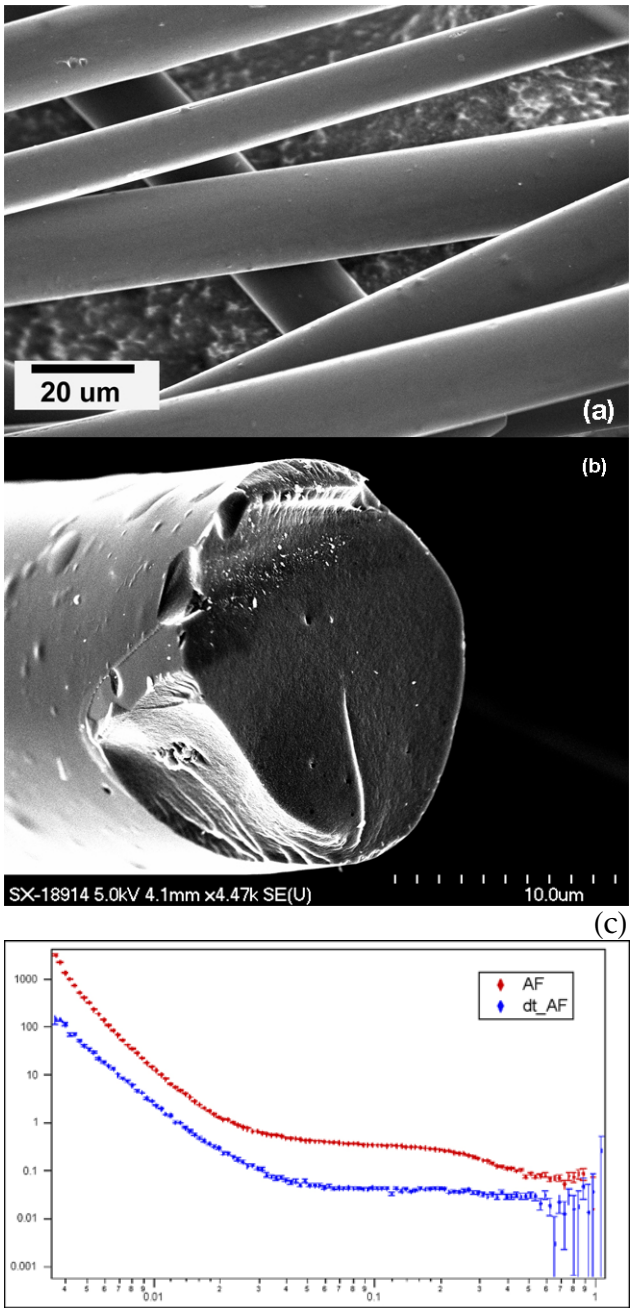

Figure 2. SEM images of the pre-activated Carboflex® fiber are shown in (a) and (b) SANS data shown in (c) of the Carboflex®. Deuterated sample is labeled "dt "

Materials Characterization

Characterization of carbon materials has been carried out using high-resolution TEM, SEM, SANS, and INS. The SANS study was undertaken at the Intense Pulsed Neutron Source at Argonne National Laboratory in early March 2003. The INS experiments were performed at High-Flux Isotope Reactor (HFIR) at ORNL

Experiments on Gas Storage Carbon

Carbon monoliths SMS48, SMM19, and Carboflex®, an activated pitch-derived carbon fiber, are the materials of interest. The contrast matching agent was deuterated toluene (chemical formula: C_6D_5-CD_3). The objective of the contrast matching SANS was to evaluate the open and closed microporosity of the gas storage carbon materials.

Figure 2 contains two SEM images of the activated Carboflex fibers. Images of SMS44 are included in Figure 3 because its microstructure is very similar to that of SMM19 and SMS48. The microstructure of Carboflex is drastically different from that of the carbon monoliths. Figures 2 and 3 also contain the SANS data for Carboflex, and SMS48 plotted in log-log scale. Again, the structural difference is revealed in the SANS scattering curves. As expected, each deuterated sample has much lower scattering intensity at the high-q region, suggesting that the pores have been filled with toluene. Results of the SANS data analysis are summarized in the following discussion. The average micropore size of the Carboflex is 1.5 nm, slightly larger than the two monoliths at 1.3 nm. The microporosity (for all the pores of less than 2 nm) is 9% and 10% for the SMM19 and SMS48, respectively. The microporosity of the Carboflex is 6%. The deuterated samples have very low closed porosity (<0.2%). Considering the margin of error, it is concluded that these materials have no closed micropores. In addition, because toluene penetrates into the micropores, all three deuterated samples show an increase of average pore size to 2.9 nm. Estimated error is about 15% for all the reported data.

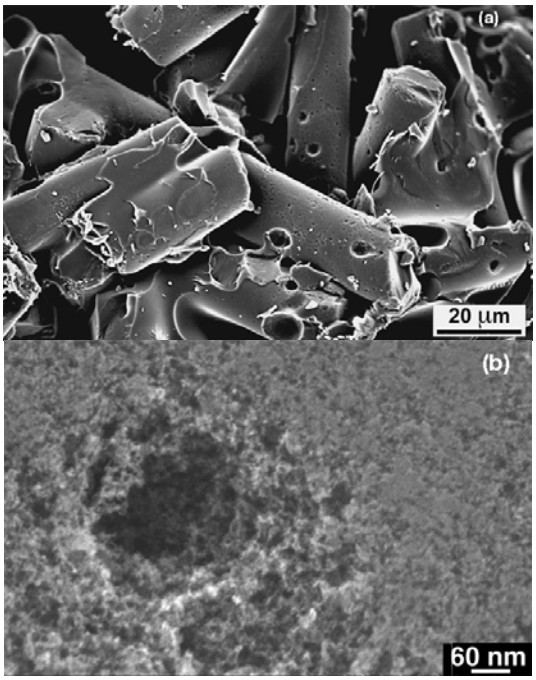

(c)

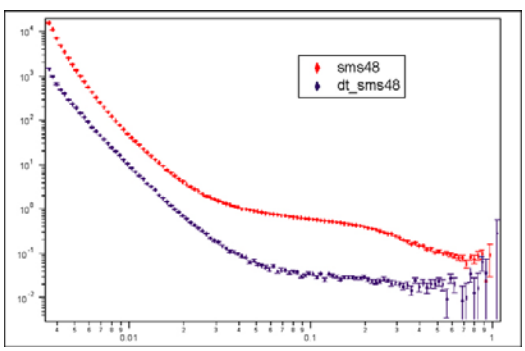

Figure 3. SEM images of the monolith SMS44 are shown in (a) and (b). Its structure is very similar to that of SMM19 and SMS48. SANS data for the carbon monolith SMS44 are shown in(c).monolith SMS44 are shown in(c).

Monolith in Methane

INS of the gas storage carbon monolith (NGS003) was carried out on the triple-axis spectrometer, HB1 at HFIR in October 2002. It was a proof-of-principle experiment that demonstrated that INS experiments can be performed on storage material. The study showed that no preferred adsorption sites exist on the carbon surface. A more detailed study on a modified setup will be undertaken in FY 2004.

Modeling and Simulation

Computer simulation work has been initiated using a reverse Monte Carlo (RMC) approach. It is imperative to conduct the calculation on a structure model that resembles the true features of the carbon material. Based upon this project's high-resolution TEM work, such a model is constructed with sufficiently large size and is filled with spheroidal interconnecting micropores. The initial calculation indicates that the pair distribution function (PDF) of the model matches reasonably well with the experimental data found in the literature. Figure 4 contains a sketch of the models and their radial distribution functions.

Prototype Tank Design Construction and Testing

Part 1

A series of 12 experiments were performed on samples machined from carbon monoliths selected from the Big Tank (Figure 5), along with additional tests using a modified experimental procedure (see discussion in Part 2). The methodology for performing each test used the existing guideline, MET-CIMT-SOG-124.

Adsorption performance indicates repeatability with an average of 3.58 g (+0.185g; -0.143 g) at 500 psi for an average of 8.77 wt %, and 4.413 g (+0.595 g; -0.138 g) at 900 psi for an average 9.78 wt %. Increasing fill pressure to 900 psi, +80%, increases stored methane by just 23%, which was accounted for mostly as adiabatic compression rather than adsorption. Accounting for methane retained in the carbon, deliverable methane averaged 88.07 V/V at 500 psi and 117.36 V/V at 900 psi. Retained methane averaged about 15% for all tests at 500 psi and about 20% for the 900 psi tests, indicating that subsequent deliverable

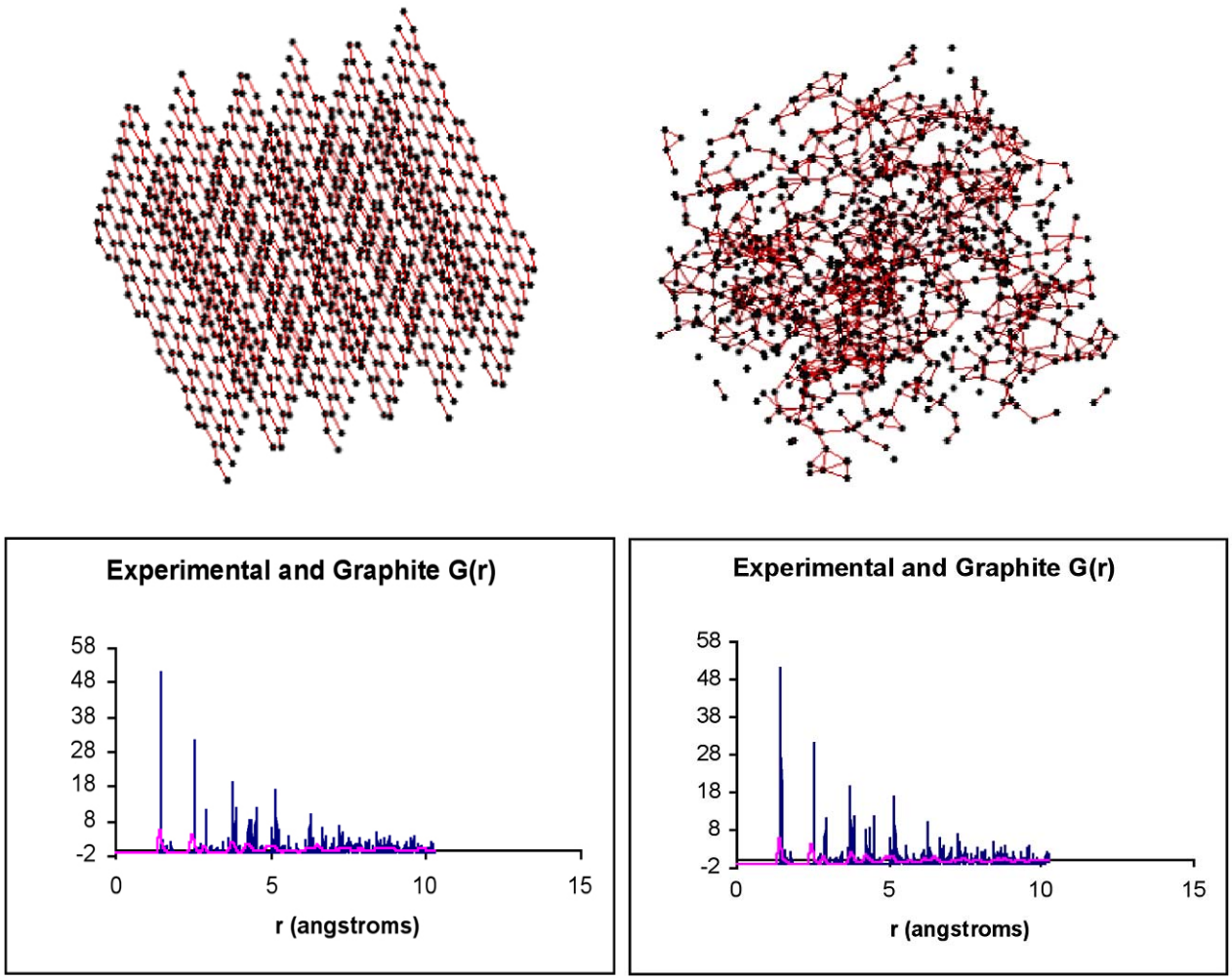

Figure 4. Graphite or disordered carbon is the initial starting structure for RMC simulation (experimental curves are the lighter, smaller peaks in the chart): (a) the graphite structure and its radial distribution function (RDF)and (b) disordered carbon and its RDF. The experimental peaks broadened and shifted relative to graphite.

charges of methane under ambient conditions, without prior vacuum extraction of residual gas in the carbon, is reduced proportionately. The potential of second and subsequent charges is expected to deliver about 75 V/V at 500 psi and 94 V/V at 900 psi.

When methane is introduced to the specimen, adsorption is rapid, as indicated by temperature peaking within 2–3 min. Rapid adsorption of methane is also supported by no additional methane take-up during specimen exposure to elevated pressures over times up to 1.5 h. Rapid saturation of specimens indicates that increasing specimen density may produce improved storage capacity. If adsorption is linear with density, increasing the density by 30%, from the tested average of 0.61 g/cc to a proposed density of 0.8 g/cc, will likely increase adsorbed methane at 500 psi to the range of 900 psi performance, ~4.65 g or ~10 wt %, from the same BET material and the same burn-off, while having little affect on adsorption time. Such a linear relationship suggests that 0.95 g/cc may deliver 135 V/V at 500 psi and 181 V/V at 900 psi; the later achieves the currently targeted DOE milestone. With the new pre-activated fibers received recently, along with the prospects of

additional activation after specimens are made, higher-performance monoliths may result. A second set of monoliths constructed of hollow fibers, or fibers with increased external surface area, is likely to add to performance.

The research team recommends performing a similar series of experiments using the new materials and the established monolith fabrication method used for making the Big Tank material. In addition, the research team recommends that a second set of specimens be made from sample material with some hollow fibers, or fibers of increased external surface area. These fibers may further enhance performance.

Part 2

A series of pressure tests were conducted on one specimen with the density of 0.645 g/cc to examine the effects of exposing "clean" specimens (heated and evacuated as prescribed by the guideline) to pressurized methane in charges of 0–100, 0–200, 0–300 psi, etc., to reveal the characteristics of heat of adsorption and incremental adsorption. This experiment indicates that the performance is predictable from isotherm plots for this material, and that beyond about 200 psi, additional loading as adsorbed methane is slight. The 0–200 psi produces the greatest heating effects and accounts for 73% of contained methane at 500 psi. Isotherm plots show rather linear adsorption after rapid initial loading, indicating that available sites for adsorption are largely filled when they are initially exposed to methane. Retained methane of ~19% (in the 500 psi case) indicates that with discharge, many adsorption sites retain methane such that second and subsequent chargings yield proportionately reduced deliverable methane. Results from this method, 89.6 V/V at 500 psi, agree with deliverable methane data from the previous tests, M_D = 88.07 V/V, within 2%.

As noted in the above recommendation, the second method also indicates that increasing density may produce greater adsorption and greater deliverable yield. If adsorption is linear with density, increasing specimen density to 0.95 g/cc translates to the deliverable volume at 500 psi of M_D = 132 V/V. If activation is also linear, increasing activation from 1300 m^2/g to about 1500 m^2/g may yield stored volumes of 152 V/V, further supporting the recommendation to fabricate and test new monoliths made from newly acquired material. To achieve the DOE milestone of 180 V/V with specimens of 0.95 m^2/g, assuming linear relationships, activation to about 1775 m^2/g is required.

The research team recommends that monoliths be made from new material and activation be attempted at near 1800 m^2/g. Then testing should be repeated as outlined.

Publications

Tim Burchell, Jane Howe, Alex Gabbard, and Mike Rogers, "Adsorbent Carbon Fiber Composites for the Storage of Natural Gas," SAMPE 2003. (Third place winner and winner of the award Best Paper of SAMPE 2003.)

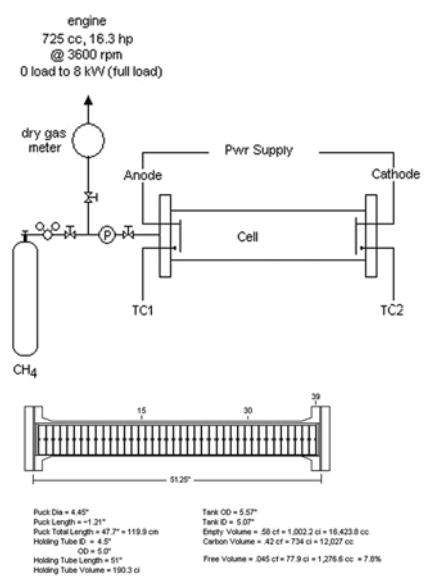

Figure 5. (a) Schematics of the ORNL MATA and (b) the dimension of the gas cell, the Big Tank.

7. MAINTENANCE, REPAIR, RECYCLE

A. Effects of Highway Ice-Clearing Treatments on Corrosion of Heavy Vehicle Materials and Components

Principal Investigator: Elizabeth V. Stephens
Pacific Northwest National Laboratory
P.O. Box 999, Richland, WA 99352-0999
(509) 375-6836; fax: (509) 375-4448; e-mail: elizabeth.stephens@pnl.gov

Principal Investigator: Dane F. Wilson
Oak Ridge National Laboratory
P.O. Box 2009, Oak Ridge, TN 37831-8048
(865) 576-4810; fax: (509) 375-6605; e-mail: wilsondf@ornl.gov

Technology Development Area Specialist: Sidney Diamond
(202) 586-8032; fax: (202) 586-1600; e-mail: sid.diamond@ee.doe.gov
Field Technical Manager: Philip S. Sklad
(865) 574-5069; fax: (865) 576-4963; e-mail: skladps@ornl.gov

---

Contractor:Pacific Northwest National Laboratory, Oak Ridge National Laboratory
Contract No.: DE-AC06-76RL01830, DE-AC05-00OR22725

Objective

- Evaluate the corrosion that may be associated with the various ice-clearing chemical systems that are in use by the various states and regions for snow and ice control.
- Develop a more fundamental understanding of the interaction of these chemicals with representative heavy vehicle materials and structures.
- Develop a unified modeling procedure to represent "rust jacking" (displacement of brake friction materials) caused by stresses induced by corrosion products at the interface of the brake shoe and the friction liner.

Approach

- Evaluate heavy truck corrosion damage to identify materials, components, and safety-related systems affected by anti-icing/deicing treatments.
- Identify and characterize $MgCl_2$ solutions and corrosion-inhibiting additives.
- Perform accelerated corrosion testing and corrosion characterization of heavy vehicle materials.
- Evaluate brake shoe failures to identify aggressive corrosion species and extent of corrosion.
- Determine the thermo-elastic and mechanical properties of the lining material, brake shoe table, and corrosion products.
- Incorporate the mechanical properties of the lining material, brake shoe, and corrosion products into computer-aided engineering (CAE) codes to predict the stresses associated with swelling of oxides on the shoe/lining interface.

- Identify more desirable ice-clearing chemical formulations and application methods.
- Generate "best practice" recommendations for reduced vehicle corrosion and improved safety.

Accomplishments

- Established an advisory/steering committee consisting of representatives from the American Trucking Association, industry, and the Montana Department of Transportation (MDT). (MDT is also a member of the Pacific Northwest Snowfighters Association).
- Surveyed and assessed materials, components, and safety-related systems affected by anti-icing and deicing treatments.
- Conducted a literature survey of past and current ice-clearing chemical corrosion investigations to (1) assess the status of ice-clearing chemicals on heavy vehicle corrosion and (2) assess appropriate corrosion test methods.
- Acquired commercial ice-clearing chemical products prevalently used in the northwestern states for evaluation.
- Acquired test equipment to evaluate and characterize the corrosion potential and corrosion rates of the ice-clearing chemical products.
- Completed indentation tests to determine the mechanical properties of the brake shoe metal and oxide.
- Began tests to determine the mechanical and thermal properties of the brake pads.
- Measured the as-machined surface roughness on each brake shoe metal test disc.

Future Direction

- Evaluate and characterize $MgCl_2$ anti-icing/deicing solutions and other ice-clearing chemical products ($CaCl_2$-based and nonchloride solutions).
- Conduct accelerated corrosion testing of heavy vehicle materials.
- Conduct in-service field evaluation (coupons will be attached to selected trucks in the field that are exposed to regions that use only one method of snow and ice control (i.e., $MgCl_2$ applications, rock salt).
- Conduct forensic analysis of failed brake shoes.
- Determine the remainder of the thermal and mechanical properties of the brakes.
- Develop a finite element model and incorporate the material property data.
- Determine the stresses that arise from the growth of corrosion products between the pads and the table.

Introduction

In recent years, many states have introduced anti-ice liquid treatments, particularly $MgCl_2$ road treatments, to prevent the bonding of ice and snow before the onset of a winter storm. Spraying the treatment on roads before the onset of a storm potentially can expose vehicles to concentrated solutions for longer periods of time because the solution is not immediately diluted by snow or water. Increased corrosion damage on heavy truck components has been reported by truck fleets and owner/operators. Vehicle safety concerns have arisen, based on the observation of accelerated corrosion damage in heavy

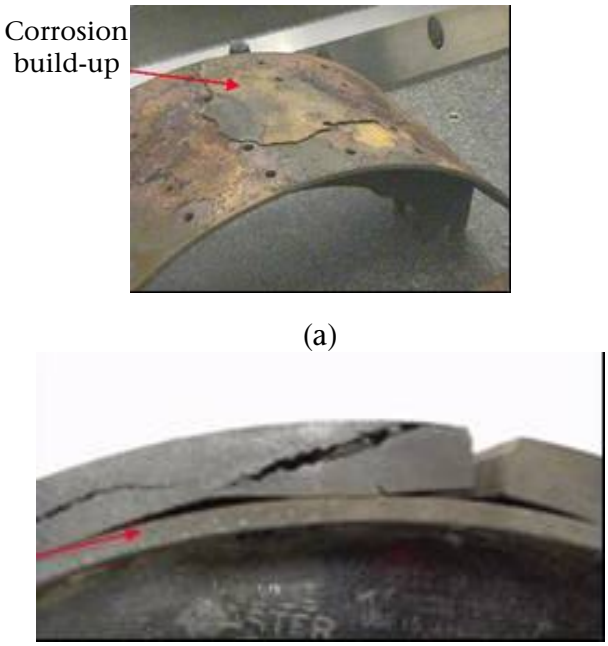

Figure 1. An illustration of rust jacking: (a) corrosion product buildup on the brake shoe table displaces the brake lining; (b) shoe table/friction liner interface.

truck brake systems, also known as "rust jacking" (Figure 1).

Although there is a strongly voiced opinion within the trucking community suggesting that accelerated damage is being caused by $MgCl_2$ road treatments, there is a lack of significant data to quantify the role of various $MgCl_2$ treatments on heavy truck component corrosion.

In May 2003, Pacific Northwest National Laboratory and Oak Ridge National Laboratory began collaboration on a two-year research effort focused on developing a more fundamental understanding of the interaction of these chemicals with representative heavy vehicle materials and structures. The project consists of six tasks, with the first two primarily focused on establishing a steering committee to ensure unity among the trucking industry and to assess the heavy truck corrosion damage that may be associated with the application of anti-icing/deicing treatments on roadways. Following is a description of the remainder of the four project tasks.

Characterization of $MgCl_2$ Solutions and Corrosion-Inhibiting Additives

The purpose of this task is to identify the commonly used $MgCl_2$ treatments and application methods, characterize the corrosive behavior of the various formulations, and establish appropriate accelerated corrosion test methods. Based on a state-by-state survey of operating highway departments, the project will identify the commonly used $MgCl_2$ treatments. In addition, the project will evaluate the methods by which $MgCl_2$ treatments are applied and how $MgCl_2$ is used in conjunction with deicing treatments.

Selected $MgCl_2$ treatments will be characterized chemically, and corrosion inhibitors will be identified for each of the selected $MgCl_2$ solutions. Analysis of the $MgCl_2$ treatments and the exposure conditions will be used to establish subsequent materials test methods. Other ice-clearing chemical products will also be investigated for a comparison.

Corrosion Testing and Corrosion Characterization

Using the information generated on ice-clearing chemical compositions and corrosion potential, a selected series of accelerated corrosion tests using representative heavy-vehicle materials will be conducted. A principal objective of this task will be to determine the effects of various accelerated test parameters and to help specify meaningful accelerated test methods for use by the heavy-vehicle manufacturers. To this end, tests will be conducted at selected temperatures to determine the effects of realistic winter temperatures on corrosion behavior. The parametric variables are solution composition, test temperature, and time of wetness.

Simple coupon specimens, stress corrosion cracking specimens, and selected

advanced materials (such as metal matrix composites and magnesium castings) will be included in the accelerated corrosion tests.

In-service vehicle testing will also be conducted during the 2003 winter season to compare with the laboratory test results. Coupons will be attached to selected trucks that operate in regions that are exposed to only one method of snow and ice control (i.e., $MgCl_2$ applications, rock salt) as well as to selected trucks that are exposed to many methods. Half of the coupons will be examined at the end of the winter season and the remainder at the end of summer 2004.

At the end of the corrosion tests, detailed surface examinations (microscopy and scanning electron microscopy) will be conducted to characterize the type of corrosion damage that is occurring (such as general corrosion, pitting corrosion, and stress corrosion cracking) and to identify the corrosive species.

Brake Shoe Evaluation

Forensic analyses of failed brake shoes will be performed to assess the extent of corrosion and to identify the aggressive species that were incorporated into the corrosion product. Optical metallography and back-scattered electron imaging and X-ray microanalysis in scanning electron microscopes will be used to characterize these failed parts.

Samples of the present materials used in construction of the brake shoe table, as well as appropriately chosen materials that would be economically viable replacements, will be included in the accelerated corrosion testing. The data generated will allow for selection of appropriate materials for future brake shoe manufacture and comparison of the effect of various anti-icing/deicing compounds on corrosion rates.

An initial forensic evaluation of a failed brake system showed that corrosion is nonuniform (as is to be expected for plain carbon steel) in chloride environments. Banding of the oxide scale was observed. This may reflect the changing corrosion conditions to which the brakes are exposed. Variations in composition and concentration of anti-icing and deicing salts, pH, moisture, temperature, and frequency and pressure of braking could all impact the corrosion rate and resultant products. Salt composition and concentration and pH, which affect the corrosion potential of the plain carbon steel, are the major contributors to the banding. A small change in salt composition and/or concentration, with or without a slight change in pH, can result in shifts between Fe_3O_4 and Fe_2O_4 phase fields.

The recently introduced anti-icing and deicing compounds result in increased “time of wetness” and hence increased corrosion. Cracking, porosity, and localized spalling of the scale would provide new pathways for water ingress and exposure of fresh metal to the corrosive environment. However, this initial analysis found no evidence of calcium and magnesium chlorides, which are the newly introduced deicing and anti-icing compounds and are less soluble in water than the chlorides of sodium and potassium that were identified in the scale. This may be a result of nonexposure of the examined brake table to calcium and magnesium chloride. The mechanisms for the increased failure rate are postulated as being an increased rate of corrosion due to positive shifts in the corrosion potential, as well as an increased amount of corrosion due to an increased time of wetness that results from the presence of hygroscopic salts.

Modeling of Brake Lining Failure

A model is being developed of the lining material fracture phenomenon caused by the forces produced by the growth of corrosion products at the shoe table/lining interface. This model will require information on the mechanical properties of the constituents, namely, elastic properties for the lining material and shoe, and the corrosion products that exert a force on the lining

surface, as well as flexural strength of the lining material. The mechanical properties of the lining material and oxides will then be incorporated into CAE codes to predict the stresses associated with swelling of oxides on the shoe/lining interface.

Elastic Property Indentation Tests

Instrumented indentation tests were performed on brake pad material (new and worn) and on the brake table (including oxide layer) to determine the elastic modulus of these materials.

Indentation tests on the metal from the worn brakes were done in two locations. These tests were performed around the rivet holes, away from the rivet holes, and through the oxide layer. The results of the modulus data from these tests show that the modulus of elasticity in the metal, away from the oxide layer and the rivet holes, is about 170 GPa. There is some variation in the modulus depending on whether the indentation is in a grain. The modulus of the metal is slightly higher in the grain. The average modulus for the indentations in the material grain is about 194 GPa.

In the region of the oxide layer, the modulus is significantly reduced. There is some variation for the oxide layer, depending on whether it is right on the surface. The average modulus of elasticity for the oxide on the surface is about 63 GPa. Indentation tests on the oxide away from the surface show the average modulus for the oxide is about 125 GPa, which may be higher as a result of less porosity.

The results of the indentation tests on the worn brake pad material show that the modulus is affected by the location of the indentation. The brake pads are a mixture of several different materials, and the indentation test yields the modulus of the individual material at the location of the indentation. The modulus in the brake pads varies from an average of 11.4 GPa in one area to an average of 89.4 GPa in another area. The average of all the indentation tests in the worn brake pads is 37 GPa. Similar variations were obtained for new brake pads, and the overall average modulus of elasticity determined was 20.6 GPa.

Flexure Tests

Two flexure tests have been completed on the brake pad material at room temperature. The results of the completed tests are shown in the graph in Figure 2. Future flexure tests will be conducted at elevated temperatures.

SPECIMEN	CONDITIONS	B=IN	H=IN	LOAD(LBS)	STR(LBS)*	STR(MPA)	STDEV	AVG.STR
B1	ROOM TEMP	0.5030	0.3750	352.42	5884.05	40.56	3.15	38.34
B2	ROOM TEMP	0.5000	0.3800	320.28	5238.88	36.12		

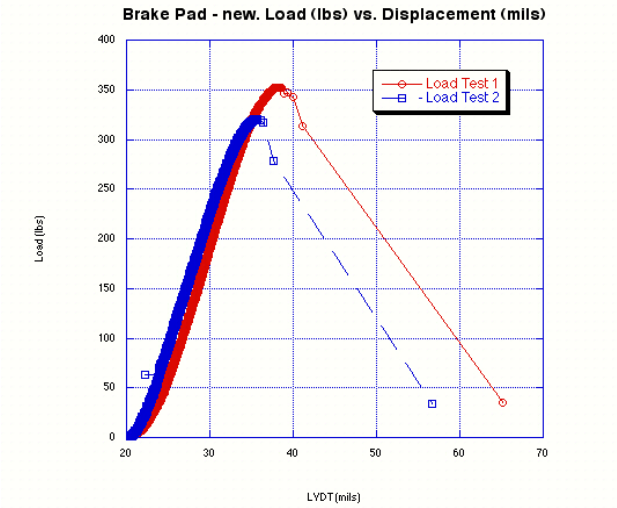

Figure 2. Flexure test results.

Thermal Diffusivity Tests

Tests have been completed to determine the thermal diffusivity of the brake pads. Tests were conducted on three different pad specimens at temperatures ranging from 103 to 508°C. Figure 3 is a plot of the average values of diffusivity for each of the specimens tested vs. temperature.

Thermal Expansion Tests

Two 25-mm-long samples with 3 × 4 mm cross sections were heated and cooled at 3˚C/min to 400˚C in a dilatometer to

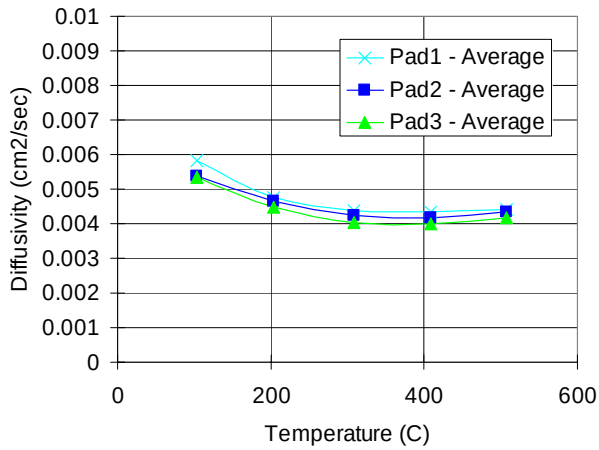

Figure 3. Diffusivity test results.

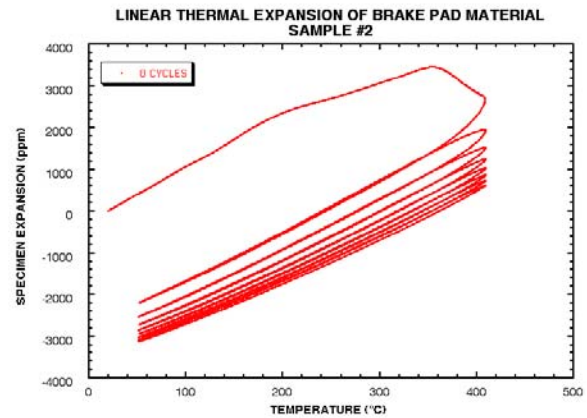

Figure 4. Linear thermal expansion of sample 2.

determine the thermal expansion of the brake pad material. The test results of the second sample are shown in Figure 4. During the initial heating and cooling cycle, both samples exhibited a permanent shrinkage of about 2500 ppm or 0.25%. Most of this change in length occurred during an event that starts at around 360°C. Repeated cycling of the samples indicated that the sample was still changing after as many as eight cycles. The coefficient of thermal expansion (CTE) of the materials was also determined. The mean or average CTE was calculated. This is the expansion at a given temperature divided by the temperature interval between 20°C and that given temperature.

Modeling Efforts

The modeling effort to determine the stresses that arise from the growth of corrosion products between the brake pads and brake shoe table interface has begun. Figure 5 shows a worn brake and a sketch of the interface of the brake pad and shoe table containing a corrosion product. A two-dimensional (2D) model is being developed. The 2D model will be used to gather some basic information about the problem and to assist in understanding how variations in temperature and model geometry affect the problem. After the 2D calculations are complete, a 3D model will be developed that

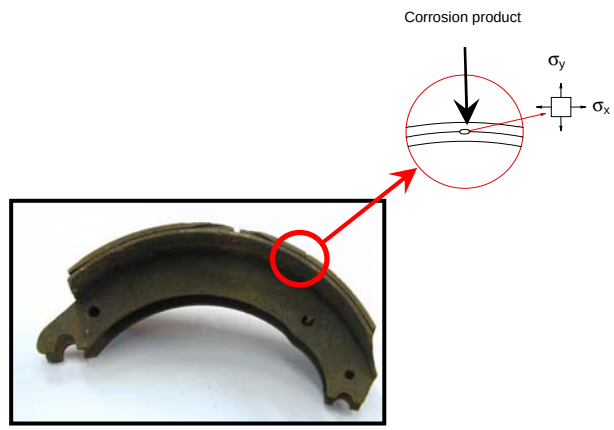

Figure 5. Worn brake pad and brake shoe table.

accounts for the nonsymmetric features of the brake pad and brake shoe table.

Deliverables

Project deliverables will include the following:

- A numerical ranking of the corrosion potential of various ice-clearing chemicals, with emphasis on the newer magnesium-chloride formulations.
- Specification of a recommended accelerated corrosion test method for use by the truck original equipment manufacturers.

- A listing of existing material corrosion potential and corrosion rates, with recommended alternative materials (where appropriate).
- A list of recommended "best practices" for use by the truck-operating fleets and owners.
- A detailed report including the forensic analyses of failed brake tables, the corrosion types and rates of chosen brake materials in various anti-icing/deicing solutions, and recommendations of viable materials.
- An initial model of rust jacking
- A final report at the conclusion of the project.

Appendix A
ACRONYMS AND ABBREVIATIONS

ACS	advanced squeeze casting
AFS	aluminum foam sandwich
ALM	automotive lightweighting materials
ANG	adsorbed natural gas
ANL	Argonne National Laboratory
ARC	Albany Research Center
ASME	American Society of Mechanical Engineers
ASTM	American Society for Testing and Materials
CAE	computer-aided engineering
CMM	coordinate measurement machine
CRADA	cooperative research and development agreements
CSEM	commerically available test rig
CTE	coefficient of thermal expansion
DFMEA	design failure modes effects and analysis
DOE	U.S. Department of Energy
DSC	dynamic scanning calorimetry
EBSD	electron backscatter diffraction
EC	engine conditioned
ECAE	equal channel angular extrusion
EMTA	Eshelby-Mori-Tanka approach
EPC	evaporative pattern casting
FE	finite element
FEA	fiite element analysis
FEM	finite element method
FSJ	friction stir joining
FSP	friction stir processing
FSW	friction stir welding
HSWR	high-strength weight reduction
INEEL	Idaho National Engineering and Environmental Laboratory
INS	inelastic neutron scattering
LANL	Los Alamos National Laboratory
LSP	laser shot-peening
LST	laser surface texturing
MA	mechanical alloying
MATA	methane adsorption test apparatus
MDT	Montana Department of Transportation
MEL	Magnesium Elektron
MMC	metal matrix composites
NATT	Northwest Alliance for Transportation Technologies
NCC	National Composites Center
NFC	near-frictionless carbon
NGF	next-generation frame
NIST	National Institute of Standards and Technology
NRCAN	Natural Resources of Canada
NSF	National Science Foundation

NVH	noise, vibration, and harshness
ODS	oxide dispersion strengthened
OEM	original equipment manufacturer
OFCVT	Office of FreedomCAR and Vehicle Technologies
OHVT	Office of Heavy Vehicle Technologies
OM	optical microscopy
ORNL	Oak Ridge National Laboratory
PAN	polyacrylonitrile
PNNL	Pacific Northwest National Laboratory
PPAP	production part approval process
PU	pickup
R&D	research and development
RDF	radial distribution function
RMC	reverse Monte Carlo
RTM	resin transfer mold
SANS	small-angle neutron scattering
SDSMT	South Dakota School of Mines and Technology
SEM	scanning electron microscopy
SMC	sheet molding compound
SSBT	subscale brake tester
SUV	sport utility vehicle
TEM	transmission electron microscopy
ULC	ultra-large thin-wall structural castings
USAMP	U.S. Automotive Materials Partnership
UT	University of Tennessee
UW	ultrasonic welding
VAVE	value analysis/falue engineering
YSZ	yttria-stabilized zirconia